2017

Inhibition of Oxidative and Conjugative Metabolism of Buprenorphine Using Generally Recognized As Safe (GRAS) Compounds or Components of Dietary Supplements

Neha V. Maharao

Inhibition of Oxidative and Conjugative Metabolism of Buprenorphine Using *Generally Recognized As Safe* (GRAS) Compounds or Components of Dietary Supplements

A dissertation submitted in partial fulfillment of the requirements for the degree of Doctor of Philosophy at Virginia Commonwealth University

By Neha Maharao
Bachelor of Pharmacy, Mumbai University, India

Advisor: Phillip M. Gerk, Pharm.D., PhD
Associate Professor, Department of Pharmaceutics

Virginia Commonwealth University
Richmond, Virginia
May 2017

Acknowledgments

The last four years have been a period of intense learning – both on a professional and personal level. For the first time in my life, I was continents away from my home, family & friends and completely out of my comfort zone. From the moment I landed in Richmond for the first time till today, life has been an amazing journey with all its bitter-sweet surprises and ups and downs. I would like to take this opportunity to reflect on the people who have supported and helped me so much throughout this period.

Without a doubt, Dr. Phillip M. Gerk has been an awesome, kind, patient and supportive advisor I could ever ask for. His guidance on all the fronts – research, coursework and TA duties has been immensely helpful. Dr. Gerk has always fostered independent thinking and encouraged me to look at obstacles as "learning opportunities". His kind words of encouragement always bring out the best in me. His generous, honest and helpful approach towards everyone always inspires me. Thank you for giving me an opportunity to be a part of the VCU family!

I would also like to thank Dr. Jürgen Venitz, whose passion for science, for teaching and for helping students always motivates me. I owe the entire idea of performing IVIVE to Dr. Venitz because it was his written comprehensive exam that inspired this idea. Despite his busy schedule, he has always gone above and beyond to help us with our research. Every discussion I have had with Dr. Venitz has been intellectually stimulating and has inspired me to be the best version of myself.

I would like to thank Dr. Joseph Ritter for helping me with all the enzyme kinetic studies. Thank you for letting me stop by your office multiple times on short notice and guiding me on several topics. I would also like to thank Dr. Matthew Halquist for providing helpful guidance on the analytical method development of buprenorphine and

naloxone and Dr. MaryPeace McRae for several helpful discussions. I would like to thank all the committee members for their valuable suggestions to guide and shape my research. I would also like to thank Dr. Anand Joshi for teaching me several techniques including Caco-2 cell culturing and transport studies, PAMPA, oxidative metabolism studies, analytical method development and for his guidance on my research.

A special shout out to Deblina Biswas and Sneha Dhapare – Thanks for always being there for me whenever I needed you guys, for comforting me through difficult times and for all the fun moments. I would also like to thank all my lab mates and friends at VCU and back home for their help and support.

Last but not the least, a special thanks goes to my beautiful family – Mauli, Ujwal-aai, Anagha and Vidyesh Maharao and Veena Joshi. Words simply lack the power to express my love and gratitude for all of you. Everything I could accomplish so far is because of your unconditional love and support. You have given me the strength to face adversities with courage, learning through the mistakes, to look at life as a journey of self-discovery, to never give up and to always believe in myself. I thank the Lord Almighty everyday for blessing me with such a wonderful family.

I would also like to thank coffee and their makers - Au Bon Pain's morning blend, Einstein Bros. café latte, Starbucks' salted caramel mocha and Maxwell's medium roast coffee. Thank you for powering me through the late nights and sleep deprived days!

Table of Contents

List of Figures

List of Tables

List of Abbreviations

A-B - apical to basolateral

A-SF - allosteric scaling factor

ACAT - advanced compartmental and absorption transit

ACN - acetonitrile

AUC - area under the curve

B-A - basolateral to apical

BBB - blood brain barrier

BCS - biopharmaceutics classification system

BSA - bovine serum albumin

BUP - buprenorphine

BUPG - buprenorphine glucuronide

Cl_{hep} - hepatic clearance

CL_{int} - intrinsic clearance

Cl_{perm} - permeability clearance

Cl_{tot} - total clearance

CYP - cytochrome P450

DMEM - Dulbecco's modified Eagle's medium

DMSO - dimethyl sulfoxide

DS - dietary supplement

E-SF - empirical scaling factor

EAF - everything added to food

EHC - enterohepatic recirculation

F_a - fraction absorbed

FaSSGF - fasted state simulated gastric fluid

FaSSIF - fasted state simulated intestinal fluid

FBS - fetal bovine serum

FeSSGF - fed state simulated gastric fluid

FeSSIF - fed state simulated intestinal fluid

F_g - intestinal availability

F_h - hepatic availability

F_{oral} - oral bioavailability

fu_G - fraction unbound in gut

fu_p - fraction unbound in plasma

GI - gastrointestinal

GIT - gastrointestinal tract

GRAS - generally recognized as safe

HBSS - Hank's balanced salt solution

HCl - hydrochloride

HIM - human intestinal microsomes

HLM - human liver microsomes

HPLC - high performance liquid chromatography

IVIVE - *in vitro in vivo* extrapolation

LPV - lopinavir

LY - lucifer yellow

MCS - Monte Carlo simulations

$MgCl_2$ - magnesium chloride

MM - Michaelis Menten

NaCl - sodium chloride

NaOH - sodium hydroxide

NBUP - norbuprenorphine

NBUPG - norbuprenorphine glucuronide

NX - naloxone

P-gp - P-glycoprotein

P_{app} - apparent permeability

PB-SF - physiologically based scaling factor

PBD-SF - physiologically and drug based scaling factor

PBPK - physiologically based pharmacokinetics

PSA - polar surface area

Q_{hep} - liver blood flow

Q_{villi} - intestinal villous blood flow

RAF - relative activity factor

RED - rapid equilibrium dialysis

RH 123 - rhodamine 123

RTV - ritonavir

TEER - transepithelial electrical resistance

UDPGA - uridine diphosphoglucuronic acid

Abstract

This dissertation aimed at developing an inhibitor strategy to improve the oral bioavailability (F_{oral}) and systemic exposure (AUC_{∞}) of buprenorphine (BUP) as well as reduce the variability associated with them. Twenty-seven generally recognized as safe (GRAS) compounds or dietary substances were evaluated for their potential to inhibit the oxidative and conjugative metabolism of BUP, using pooled human intestinal and liver microsomes. Using IVIVE, the extraction ratio of BUP in the intestine and liver was predicted to be 91% and 71%, respectively. In both the organs, oxidation appeared to be the major metabolic pathway with a 6 fold (intestine) and 4 fold (liver) higher intrinsic clearance than glucuronidation. Buprenorphine was predicted to show low and variable F_{oral} (3±2%), AUC_{∞} (344±327 ng*min/ml) and a large total clearance (CL_{tot} = 1050±126 ml/min). The biorelevant solubilities of 5 preferred inhibitors (α-mangostin, chrysin, ginger extract, pterostilbene and silybin) were incorporated in the final model. Of the preferred inhibitors, pterostilbene appeared to be most effective in improving the mean predicted F_{oral} (74.8%) and AUC_{∞} (36,130 ng*min/ml). A ten fold lower concentration of pterostilbene appeared to be more effective in reducing the variability (by 2 fold) in the mean predicted AUC_{∞} of BUP. An equipotent combination of pterostilbene and ginger extract was tested and it inhibited the oxidative and conjugative metabolism of BUP in an additive manner. These results demonstrate the feasibility of the approach of using GRAS or dietary compounds to inhibit the presystemic metabolism of buprenorphine and thus improve its oral bioavailability. This inhibitor strategy has promising applicability to a variety of drugs suffering from low and variable oral bioavailability due to extensive presystemic oxidative and conjugative metabolism.

Chapter 1: Introduction

1.1 Buprenorphine

1.1.1 Mechanism of action

Opioid dependence continues to be a serious health problem throughout the world [1]. Buprenorphine or combination of buprenorphine and naloxone is one of the widely used therapeutic alternatives for treatment of opioid addiction as well as pain management [2]. Buprenorphine is a semisynthetic thebaine derivative belonging to morphinan class of opioids [3]. It was approved by the US FDA in 1981 for severe pain management and in 2002 for opioid addiction. Buprenorphine is the first medication to treat opioid dependence that can be prescribed in various settings such as offices, community hospitals, correctional facilities etc. by qualified physicians [4]. Buprenorphine possess a unique pharmacology characterized by partial agonism at the μ opioid receptors because of which it has lower potential of producing side effects such as respiratory depression, addiction and withdrawal symptoms [3-6]. Being a partial agonist, it exhibits high affinity but low intrinsic activity than the full agonists at the μ opioid receptor thus blocking access of abused opioids for prolonged period of time (Fig 1.1) [4, 6]. It has a long receptor fixation half-life, which is responsible for its longer duration of action making alternate day dosing possible [3, 4, 6]. Buprenorphine has a better safety profile than other opioids because even at higher than normal doses it rarely produces significant respiratory depression ('ceiling effect') [3-5]. However, care must be taken to avoid co-administration of CNS depressants like alcohol or benzodiazepines with buprenorphine [3].

Figure 1.1: Buprenorphine - a partial agonist at μ opioid receptors [4]

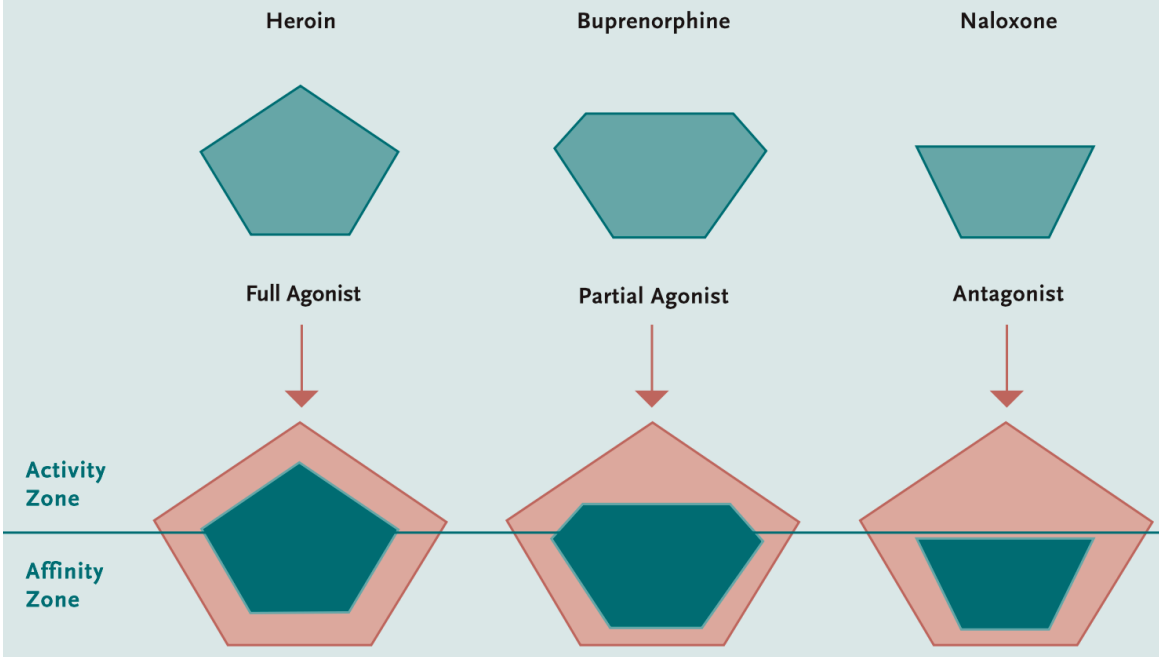

1.1.2 Pharmacokinetics of buprenorphine

BUP suffers from poor oral bioavailability but given sublingually it achieves 33 – 55% bioavailability [3, 7, 8]. It is highly lipophilic because of which it exhibits a large volume of distribution estimated to be around 188–335L after IV administration [3]. Buprenorphine is highly plasma protein bound (96%) mainly to α and β globulins [3]. Despite having good GI solubility and permeability, it shows poor oral bioavailability due to extensive presystemic metabolism [3, 8-10]. It undergoes CYP mediated oxidation (CYP 3A4, 2C8, 2C9) [11, 12] to form norbuprenorphine (NBUP) and UGT mediated glucuronidation (UGT 1A1, 1A3 and 2B7) [13-15] to form buprenorphine glucuronide (BUPG) (Fig 1.2). NBUP further undergoes glucuronidation (UGT 1A1 and 1A3) [14, 15] to from norbuprenorphine glucuronide (NBUPG) (Fig 1.2). Picard et al. studied the contribution of various CYP450 enzymes to NBUP formation and also to BUP consumption [12]. CYP3A4 was reported to be the major CYP450 enzyme involved in

producing maximum NBUP formation [12]. Two approaches were used for testing the contribution of CYP3A4 to NBUP formation namely relative activity factor (RAF) approach and chemical inhibition. The relative activity factor approach is one of the techniques used for quantitative reaction phenotyping and helps in scaling the enzymatic activities obtained using recombinant enzymes to liver or intestinal microsomes [12]. Using an RAF value of 0.284 for recombinant CYP3A4 (obtained from BD Gentest), the relative contribution of CYP3A4 to BUP metabolism in liver microsomes was estimated by Picard et al. to be 73% [12]. Based on the chemical inhibition of CYP3A4 using ketoconazole (0.25 – 1.5 μM), CYP3A4 accounts for approximately 65% of NBUP formation in liver [12]. These results are in agreement with the inhibition experiments conducted by Iribarne et al. using ketoconazole (about 75% inhibition) or the CYP3A mechanism-based inhibitors troleandomycin, gestodene, and erythral (about 70% inhibition) [11]. Rouguieg et al. investigated the individual contribution of the hepatic UGT isoforms to glucuronidation of BUP [14]. The RAF approach was used which as explained earlier involves use of selective substrates such as etoposide and azido-thymidine for UGT1A1 and UGT2B7, respectively to scale the isoform specific clearances in recombinant enzymes to human liver microsomes [14]. The study reports UGT1A3 to be the major contributor (50%) followed by UGT2B7 (40%) and UGT1A1 (10%) [14]. Despite being the major contributor, the contribution of UGT1A3 was determined indirectly i.e. without calculating the RAF value using a selective UGT1A3 substrate. However, a study by Chang and Moody confirms involvement of recombinant UGTs 1A1, 2B7, 1A3 in conjugating BUP, granting support to the results of the Rouguieg et al. study [13]. Among the metabolites, NBUP is the only active metabolite

having about one-fiftieth of analgesic potency of its parent drug [3]. On the other hand, the glucuronide metabolites do not exhibit any of the therapeutic effects of BUP [3], similar to morphine-3 glucuronide (inactive) but unlike morphine-6-glucuronide (active).

Figure 1.2: Metabolic pathways of Buprenorphine

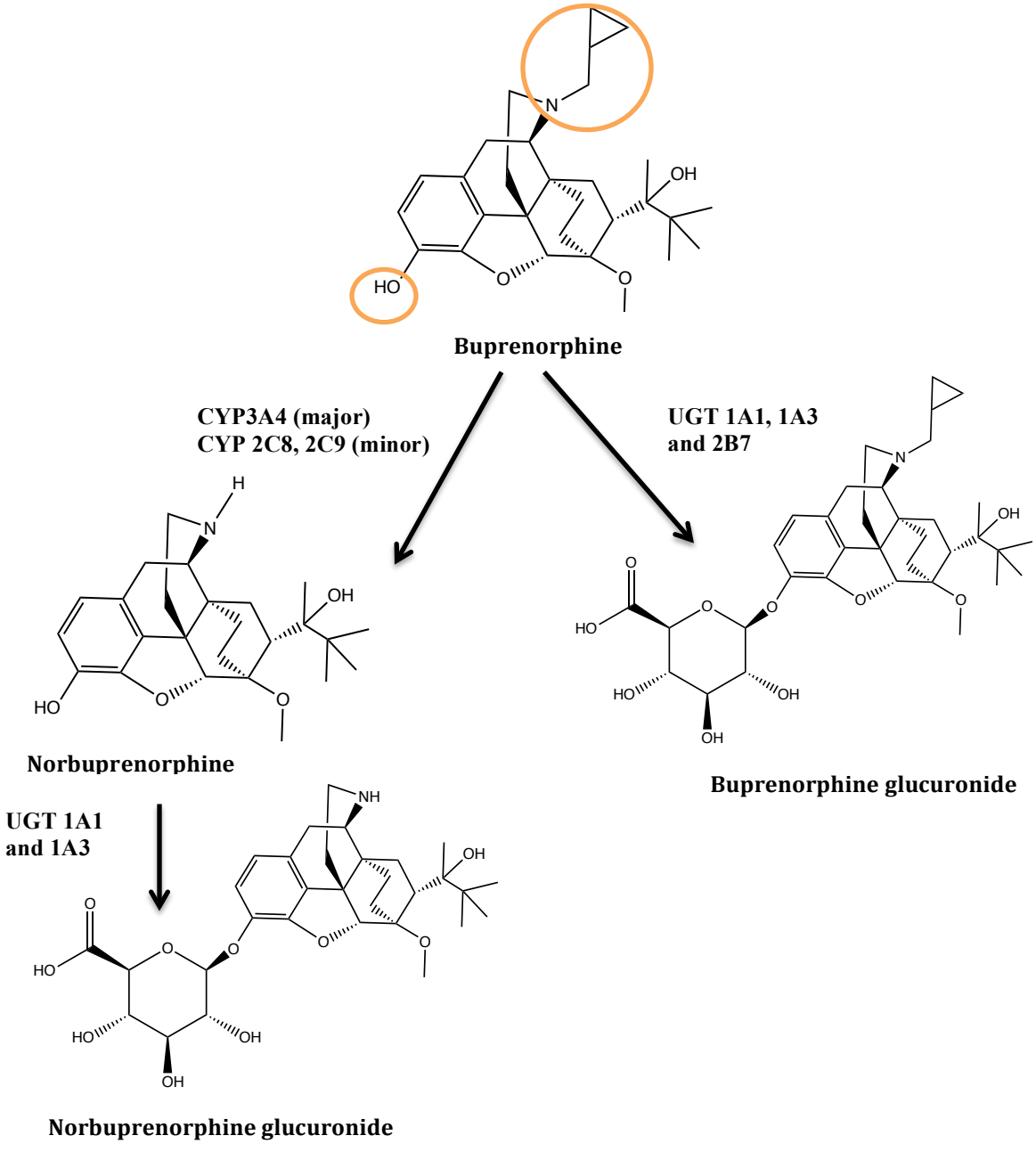

BUP is highly extracted in the liver, which is evident from plasma clearances in healthy human volunteers ranging from 1042 to 1280 mL/min [3]. Assuming a liver blood flow of 1500 ml/min, these plasma clearances result in hepatic extraction ratio ranging from 0.7 – 0.9, making BUP a high extraction ratio drug [3]. BUP appears to have a long elimination half-life, however the half-life estimates (24 – 69 hours) vary significantly from amongst the published reports [3]. One of the probable reasons includes differences in the sensitivity of analytical methods used for detection of BUP and its metabolites, especially when lower doses of the parent drug are administered [3]. In addition, differences in the duration for which plasma samples are collected can influence the final elimination half-life estimates [3]. The route of administration also influences the elimination half-life, which is evident from the longer half-life following sublingual administration of BUP as compared to IV dosing [3]. As per the product monograph, sublingual BUP shows a mean elimination half-life of about 37 hours [3, 7]. Following IV administration, ~70% of the dose is eliminated in feces mostly as BUP and NBUP while ~30% dose appears in urine mainly as glucuronide conjugates [3, 10]. Buprenorphine, norbuprenorphine and their glucuronide metabolites have also been reported to undergo enterohepatic recirculation, which can further prolong their elimination half-life [3, 10]. Sublingual BUP has been proposed to exhibit enhanced sequestration in adipose tissue and oral mucosa, which can contribute to its long half-life [3, 10]. Kuhlman and colleagues have proposed a three-compartment model to incorporate the absorption component from the reservoir in the oral mucosa to the systemic circulation [16]. The absorption rate constant from the reservoir in oral mucosa to the plasma compartment appears to be slower than the elimination rate constant [16].

Thus, following sublingual administration, BUP shows larger volume of distribution than after IV administration. The tight binding to and slow dissociation from the opioid receptors coupled with extended elimination half-life are responsible for the longer duration of action shown by BUP [3].

Limited information is available on pharmacokinetics of BUP following oral administration. To the best of our knowledge, we could find only two references that discuss metabolic disposition of BUP after oral administration in humans:

Reference 1 - Review paper by Walter and Inturrisi (1995)[10]

Walter and Inturrisi have discussed a collection of studies evaluating ADME of BUP in humans following administration through various routes like IV, IM, sublingual, SC and oral [10]. The amount of BUP and its metabolites excreted in feces and urine have been quantified using radiolabelled HPLC methods or Gas phase liquid chromatography (GPLC). The following results were generated by subjecting methanolic extracts of the feces to chromatographic analysis [10].

Table 1.1: BUP and its metabolites excreted in human urine and feces

Route	Dose (µg/kg)	Method	Collection period (days)	% Dose		
				Urine	Feces	Total
IM	2	^{3}H	7	27.0	67.5	94.5
PO	15	^{3}H	7	15.3	70.7	86.0
PO	20	^{3}H	15	16.5	62.7	79.2
PO	20	^{3}H	15	10.3	49.6	59.9

Adapted from Walter and Inturrisi review [10]

About 10 – 15% radioactivity following oral dose of BUP was detected in urine mainly in the form of polar glucuronide metabolites NBUPG and BUPG [10]. The

majority of the radioactivity was detected in feces (50 – 70%), most of which was BUP with a relatively minor presence of NBUP [10]. The exact % composition of BUP and NBUP in feces is not reported. The number of healthy human subjects used in these studies was also not reported. Another study conducted by Cone et al. has been discussed in this review. The quantification of BUP and the metabolites in feces and urine was performed using GC-MS [10, 17]. In this study, about 12% of the oral dose was excreted in urine: 7-8% as NBUPG, 2-3% as NBUP and about 1.5 – 3% as BUPG [10, 17]. Unconjugated BUP and NBUP were not detected in urine and feces in this study. The results of the fecal analysis performed by Cone et al. were presented in a convoluted manner and hence are difficult to interpret [17]. However, from the discussion presented by the author, it can be inferred that both conjugated and unconjugated BUP and NBUP were detected in the feces [17]. However, unconjugated BUP and NBUP were clearly the major components in feces, with reported % higher for BUP than NBUP [17].

Reference 2 – Jeffcoat et al. taken from NIDA research monograph 132 (1993) [8]

This research monograph discusses study performed after oral administration of 0.63 μg/kg body weight dose of [^{3}H] BUP in 4 young adult subjects. The observed average plasma C_{max} of BUP, NBUP, BUPG and NBUPG was 7 pg/ml, 8 pg/ml, 8 pg/ml and 10 pg/ml [8]. 11% of the administered dose was detected in urine and 72% in feces (in agreement with the results of studies reported in the Walter and Inturrisi review paper) [8, 10]. The oral bioavailability of BUP observed in this study was reported to be <15% [8]. However, this monograph lacks description of the methods employed to obtain the aforementioned results. Hence, it is difficult to assess the appropriateness of the techniques used to perform this study and lowers the confidence in their reported

findings. Also, such similar mean C_{max} values for BUP and its metabolites after oral administration are surprising.

Based on the published in vitro studies as well as in vivo studies, we know that BUP is extensively metabolized [10, 18-20]. Thus, it is difficult to believe that ~ 50 - 70% of BUP is excreted unchanged in feces. A more logical explanation would be conjugated BUP, after being subjected to hydrolysis by β-glucuronidase (in lower gut), gets converted to BUP and appears in feces. Thus, it is difficult to determine the exact percentage of BUP excreted unchanged in feces versus the fraction of BUP that was hydrolyzed from BUPG. BUP and NBUP are also reported to undergo enterohepatic circulation, which can further alter the fraction of BUP converted to BUPG and NBUP. In addition, the contribution of oxidation versus glucuronidation as well as the contribution of intestine versus liver to the overall presystemic metabolism of BUP still remains to be determined.

1.1.3 Need for oral buprenorphine

Currently, BUP is available for various routes of administration such as sublingual, transdermal, buccal, intravenous and intramuscular administration. Sublingual BUP appears to be one of the widely used routes of administration. However it suffers from several disadvantages such as longer dissolution time, variable sublingual retention times between different patients, interference with daily activities such as drinking, eating, talking, inability to mask bitter taste etc. [2] These disadvantages can lead to a certain degree of patient non-compliance [2]. Oral BUP can address these issues and would be expected to be associated with higher patient compliance. However, an oral formulation of BUP is not yet available because after oral administration it would suffer

from poor and variable oral bioavailability due to extensive presystemic metabolism [9, 10, 17, 18]. Administering a higher oral dose of BUP to improve its systemic availability would not be an ideal strategy because the higher dose would still be expected to show variable F_{oral} and systemic exposure. Increasing the dose will also result in exponential elevation in the price of this already expensive drug product ($581/g of BUP (Medisca) and $348 for 30 Suboxone films of 8/2 mg strength), which would be undesirable. Hence, there is a need for developing an effective and economical strategy to inhibit the metabolism of BUP and achieve adequate bioavailability following oral administration.

1.2 Inhibitor strategy using GRAS compounds and dietary constituents

Several *generally recognized as safe* (GRAS) compounds and dietary constituents have been reported in the literature to interact with CYP and UGT enzymes [21-26]. Thus, it appears logical to co-administer suitable dietary components with BUP to achieve pharmaco-enhancement of BUP through inhibition of its presystemic metabolism. A classic example of pharmaco-enhancement achieved by combining two agents includes the lopinavir-ritonavir (Kaletra) combination [27, 28]. Lopinavir (LPV) suffers from poor oral bioavailability due to its low oral uptake and extensive presystemic metabolism by CYP3A4, thus limiting its use as an independent anti-retroviral agent [27, 28]. However, co-administration of a small dose of ritonavir (RTV) produces drastic improvement in the systemic concentrations of LPV making it a therapeutically effective protease inhibitor [27, 28]. RTV is a potent CYP3A4 inhibitor (IC_{50} = 0.073 μM in human liver microsomes) and it significantly inhibits the hepatic CYP3A4 mediated metabolism of LPV and might also inhibit its P-gp mediated intestinal efflux [27-29]. Thus, RTV boosts the oral bioavailability and systemic exposure of LPV making it a successful pharmaco-enhancer. Thus, we propose to utilize the GRAS compounds or

dietary constituents as pharmaco-enhancers to achieve sufficiently high and less variable oral bioavailability and systemic exposure of BUP.

We evaluated twenty-seven dietary compounds that appeared to be likely candidates to inhibit UGT and CYP enzymes, based on their structural characteristics as well as published studies [30]. Various criteria were considered while selecting the test compounds such as their regulatory status (FDA-GRAS compounds, dietary supplements, everything added to food (EAF)), maximum daily doses in humans, potential for safe clinical use, favorable physicochemical features. Most of these compounds are lipophilic, unsaturated or bicyclic with phenol or alkyl catechol groups making them structurally favorable to interact with conjugating enzyme systems such as UGT and phase I enzyme systems like CYP. The list of compounds tested included α-mangostin, *t*-anethole, iso-borneol, carvacrol, chrysin, *t*-cinnamaldehyde, curcumin, ethyl cinnamate, geraniol, geranyl acetate, ginger extract, 6-gingerol, grapeseed oil, hesperitin, D-limonene, linalool, linalyl acetate, magnolol, menthol, menthyl acetate, naringin, pterostilbene, pulegone, quercetin, resveratrol, silybin and thymol (Fig 1.3, structures drawn using ChemDraw v15.1). Most of these putative inhibitors are single compounds with the exception of ginger extract and grapeseed oil. Linoleic acid appears to be the major fatty acid component of grapeseed oil [31]. Ginger extract is a mixture composed of four main constituents namely 6-gingerol, 8-gingerol, 10-gingerol and 6-shogaol [32-34]. 6-Gingerol is reported be the most abundant component of ginger extract, hence it was also tested individually for its potential to inhibit the metabolism of BUP.

Figure 1.3: Structures of putative inhibitors

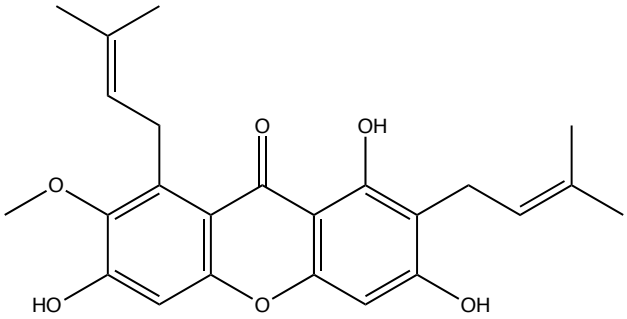

a-mangostin

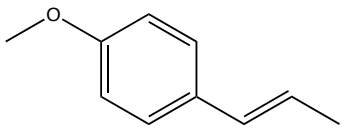

trans-anethole

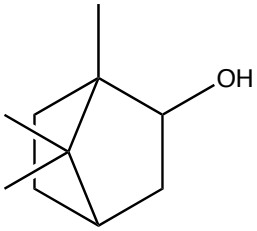

iso-borneol

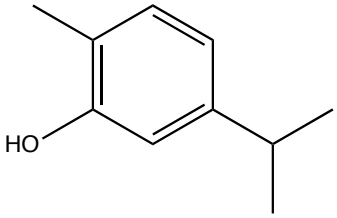

carvacrol

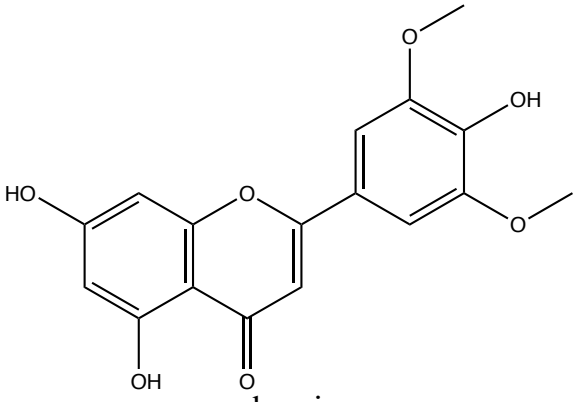

chrysin

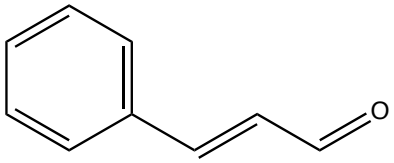

trans-cinnamaldehyde

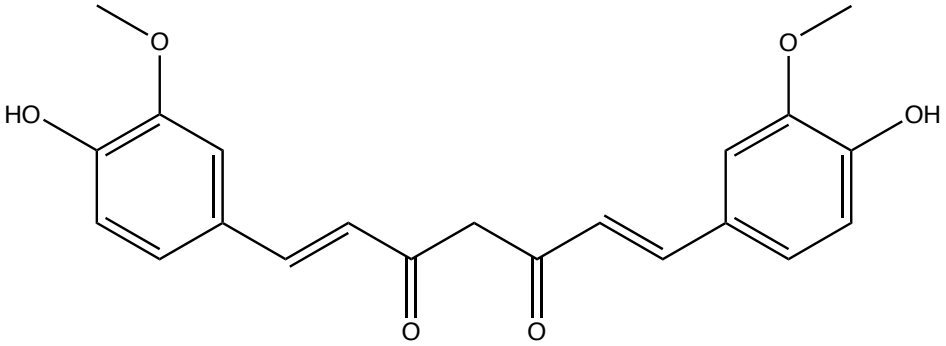

curcumin

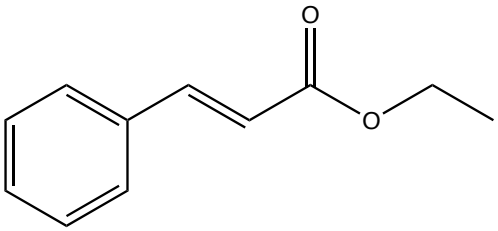

ethyl cinnamate

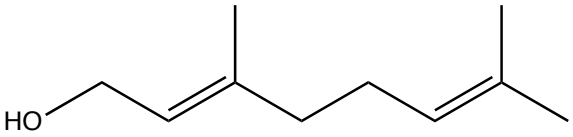

geraniol

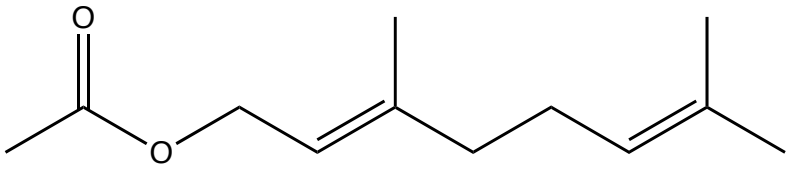

geranyl acetate

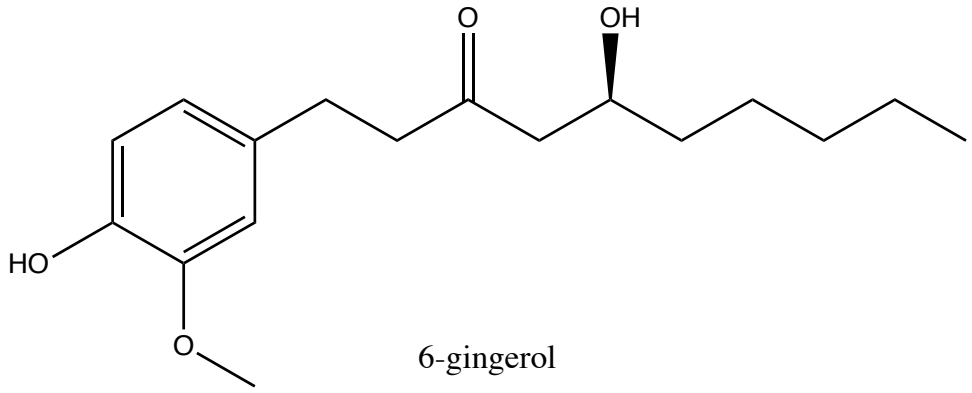

6-gingerol

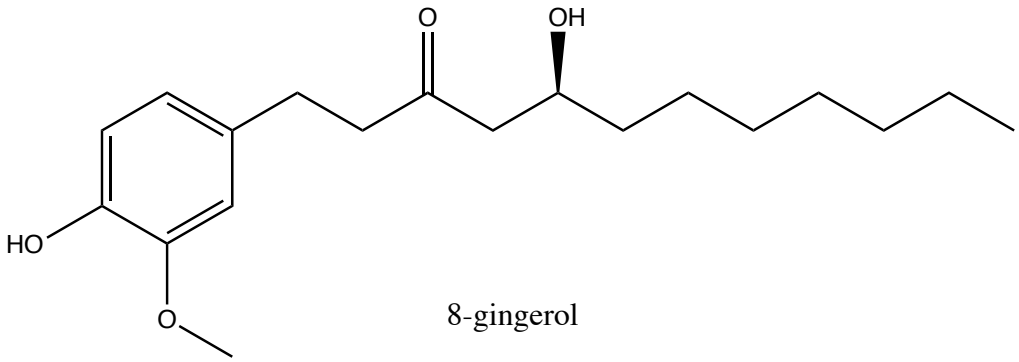

8-gingerol

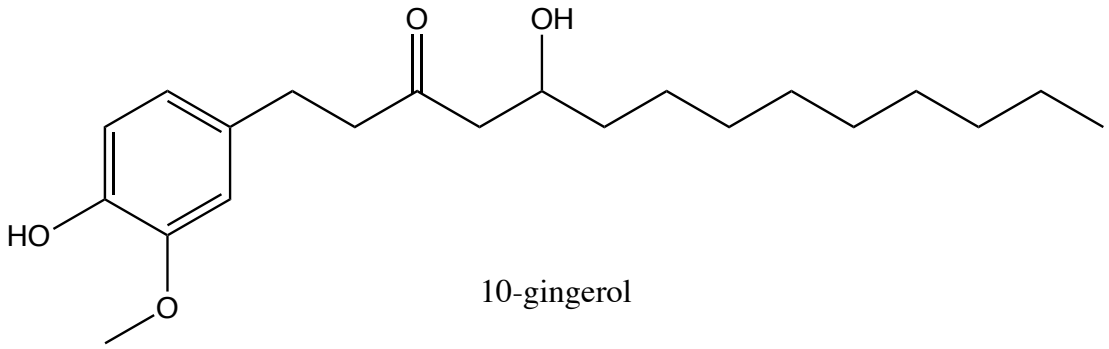

10-gingerol

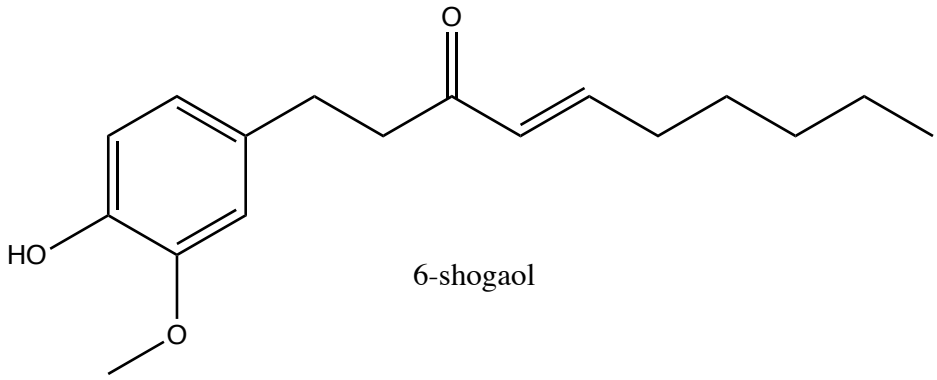

6-shogaol

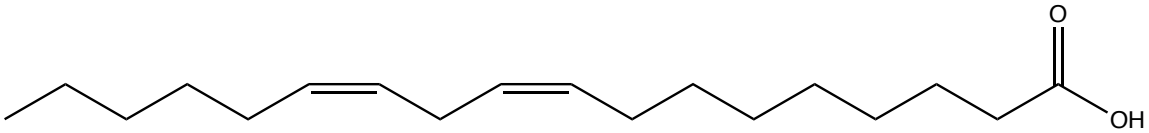

linoleic acid

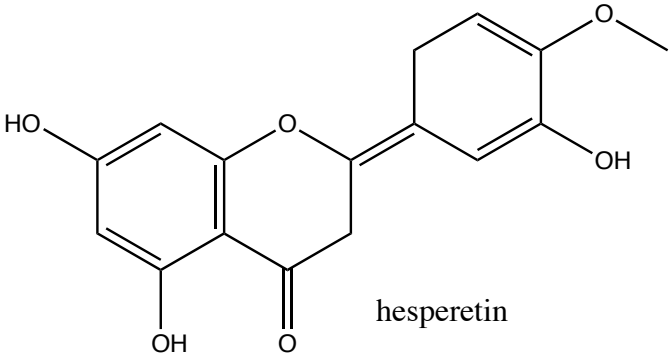

hesperetin

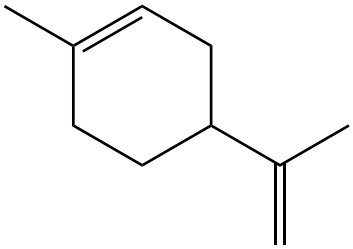

D-limonene

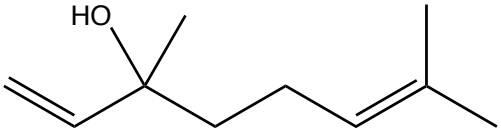

linalool

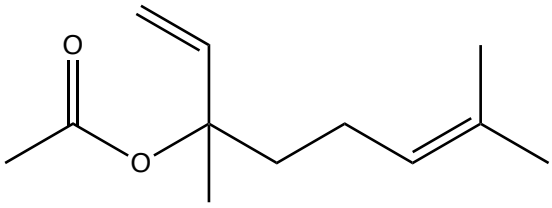

linalyl acetate

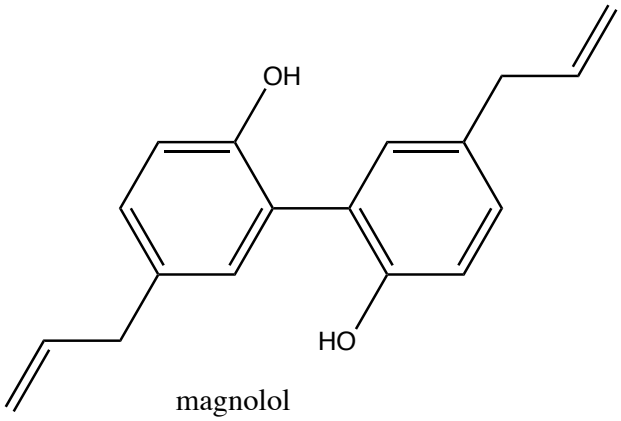

magnolol

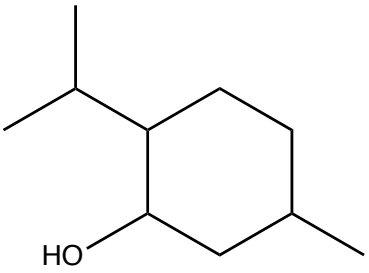

menthol

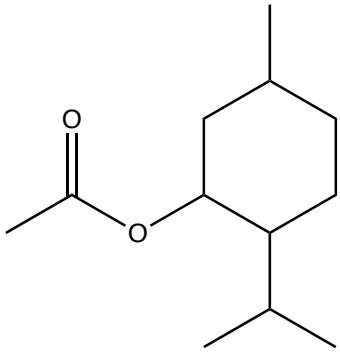

menthyl acetate

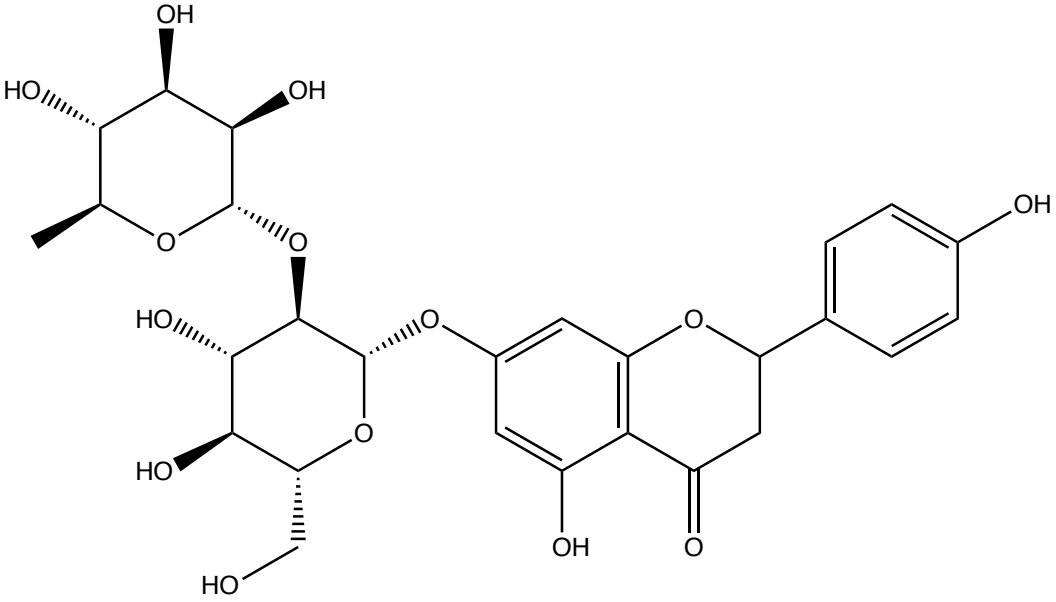

naringin

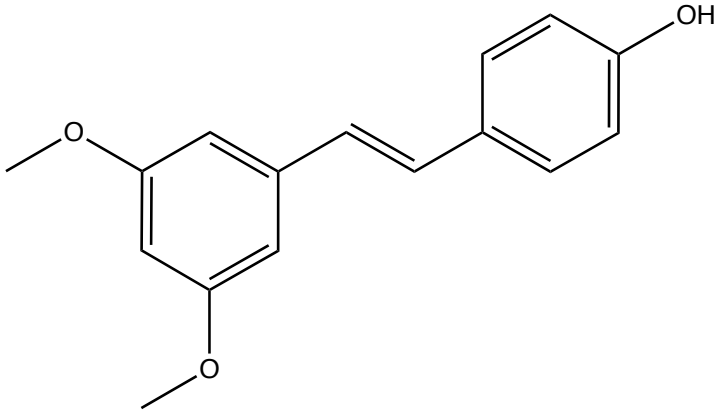

pterostilbene

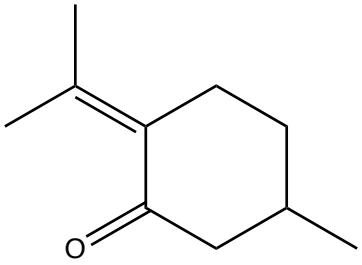

pulegone

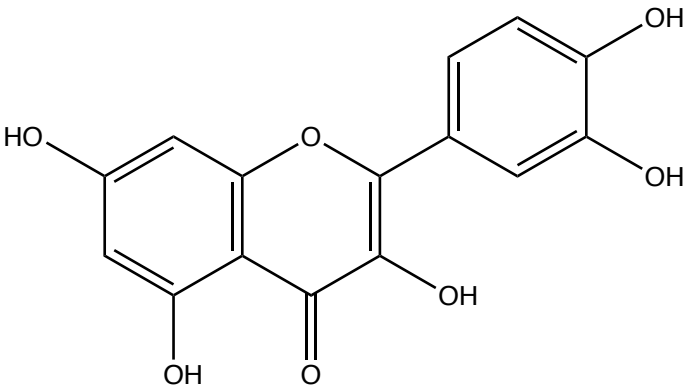

quercetin

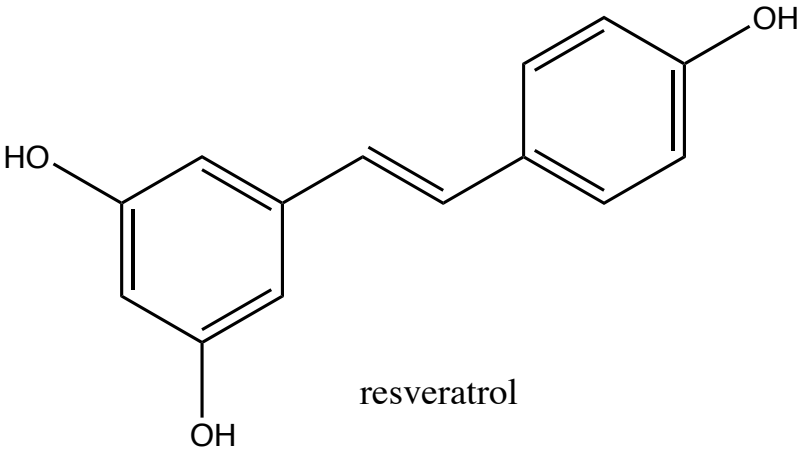

resveratrol

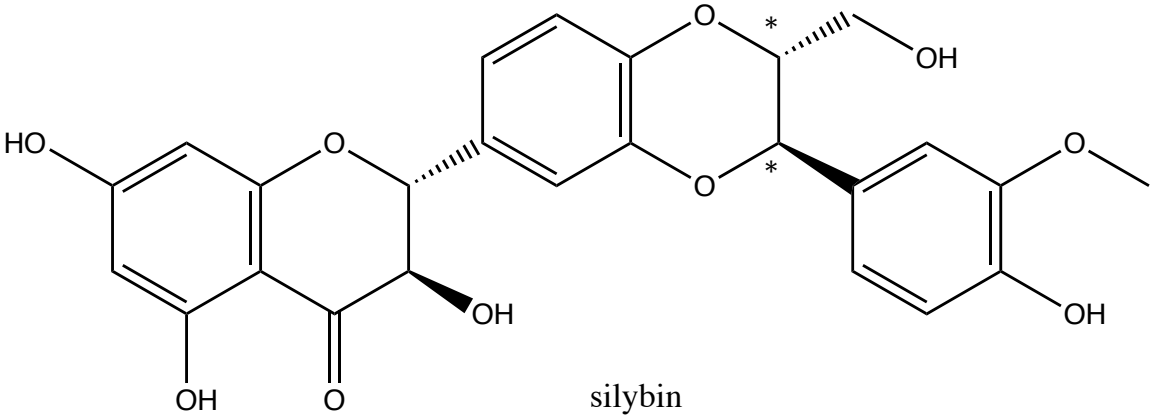

silybin

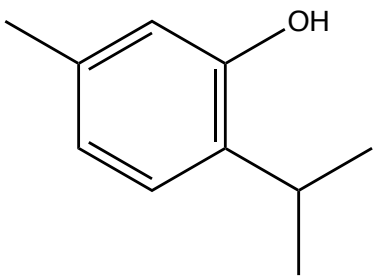

thymol

1.3 Biorelevant solubility

The aqueous solubility of a compound is one of the key factors influencing its oral absorption from the gastrointestinal tract (GIT) [35, 36]. Several studies focusing on the computational prediction of aqueous solubility of compounds with distinct physicochemical profiles have been performed with varying degrees of success [35-39]. These publications emphasize the importance of determining solubilites in a biorelevant medium instead of aqueous buffers to improve the predictive power of the computational models [35-39]. A biorelevant medium is an artificial medium that mimics the physicochemical properties of the corresponding physiological fluid with regards to its buffer capacity, pH, composition of surfactants, osmolarity etc. [40, 41] The biorelevant media are especially helpful in determining the solubility of poorly soluble drugs [41, 42]. Dressman and colleagues were the first research group to propose and design the biorelevant media and revealed marked superiority of the biorelevant media over the traditional aqueous media for studying the physiochemical characteristics of diverse chemical entities [43]. Several media mimicking various physiological fluids have been developed such as simulated human physiological fluids such as body fluid, blood plasma, synovial fluid, gastric fluid, intestinal fluid, colonic fluid, saliva, lung fluid, vaginal fluid, semen, lacrimal fluid (tears), sweat etc. [42] These simulated fluids have

proven extremely helpful in evaluating solubility and dissolution characteristics of dosage forms and predicting their *in vivo* performance at the site where maximum drug absorption takes place [38-42]. Their application can be extended to include various conventional and non-conventional routes of administration such as oral, parenteral, sublingual, buccal, pulmonary, ocular, vaginal, rectal, dermal (skin), organ-targeted drug delivery etc. [42] The composition of some of the aforementioned biorelevant medium can be modified to simulate fasted or fed conditions [38-42]. This can be crucial for drugs whose rate and extent of absorption is drastically affected by presence or absence of food.

Biorelevant media simulating the human intestinal fluid have found widespread use for determination of solubility, dissolution and permeability profiles of novel compounds during drug development [38-42]. Several publications in the past few years have highlighted the differences in solubility exhibited by a compound in aqueous buffers versus in a biorelevant medium [38-42]. The dissimilarity becomes readily apparent in case of poorly soluble drugs predominantly because of the drastic disparity in the wettability of the compounds in the two mediums. While aqueous buffers like phosphate, acetate, bicarbonate, phosphate buffered saline etc. can capture the effect of ionization on solubility at various pH, they are devoid of the surfactants such as sodium taurocholate and lecithin present in the human intestinal fluid [40, 41]. These surfactants possess the potential to significantly improve the solubility of compounds showing poor solubility in aqueous buffers. Fasted state simulated intestinal fluid (FaSSIF) and FaSSIF-V2 are widely used simulated intestinal fluids for dissolution and solubility testing under fasted condition [38-42]. The two formulations differ in their lecithin content, which is about

four fold higher in FaSSIF. The composition and properties of the two buffers are as shown in Table 1.2.[42]

Table 1.2: Composition of human simulated intestinal medium [42]

Component	FaSSIF (mM)	FaSSIF-V2 (mM)
Sodium taurocholate	3.5	3.5
Lecithin	0.75	0.2
Sodium hydroxide	10.5	34.8
Sodium chloride	105.85	68.62
Sodium dihydrogen phosphate	28.65	-
Maleic acid	-	19.12
Properties		
pH	6.5	6.5
Buffer capacity (mmol/L/pH)	270 ± 10	180 ± 10
Osmolality (mOsm/kg)	12	10

For the purpose of this dissertation, the biorelevant solubility determination was performed to better predict concentrations of inhibitors in the gut lumen following oral administration under fasted conditions. The equilibrium solubility of four shortlisted inhibitors (α-mangostin, chrysin, pterostilbene and silybin) was determined using FaSSIF. To supplement our empirical solubility values, biorelevant solubility of these compounds was also predicted using ADMET predictor™ v8.1 (Simulation Plus, Lancaster, CA).

1.4 *In vitro in vivo* extrapolation (IVIVE)

In vitro (Latin: in glass) studies refer to the experiments conducted in a controlled

environment in lieu of a natural setting or within a living organism. *In vivo* (Latin: in living) studies represent the represent the studies carried out in whole living organisms instead of partial or dead organisms. *In vitro* to *in vivo extrapolation* allows qualitative or quantitative transposition of *in vitro* observations to predict phenomena *in vivo* [44]. One of the key aims of drug discovery and development studies is the ability to predict the *in vivo* clearance of a novel entity from *in vitro* studies [45-52]. Several methods have been proposed to predict *in vivo* clearances from kinetic parameters determined using *in vitro* systems like hepatocytes, microsomes, cell-lines etc. [45-52] Ito and Houston compared five different methods to predict *in vivo* hepatic intrinsic clearance ($CL_{int,hep}$) namely physiologically based scaling factor (PB-SF), physiologically based and drug specific scaling factor (PBD-SF), rat intrinsic clearance, empirical scaling factor (E-SF) method and allometric scaling (A-SF) method [53]. The PB-SF method was based on using a scaling factor based on hepatic microsomal recovery from whole liver. Intrinsic clearance data from human microsomes scaled using PB-SF showed strongest positive correlation (r^2= 0.82) with the predicted *in vivo* intrinsic clearance [53]. However, this method showed a general trend of underpredicting the hepatic $CL_{int,hep}$ probably due to incomplete recovery of microsomes from the human liver samples. This underprediction appeared to improve when an empirical scaling factor (E-SF) (6.2 g protein/kg body weight) or a drug based physiological scaling factor (PBD-SF) based on *in vivo* and *in vitro* $CL_{int,hep}$ obtained in rats was introduced [53]. Using the rat intrinsic clearance, the predicted *in vivo* $CL_{int,hep}$ showed negligible bias. Similar observation was made when an allometric scaling factor (A-SF) was used [53]. However, the A-SF method exhibited poorest precision of all the methods [53].

The hepatic clearance (CL_{hep}) can be predicted from $CL_{int,hep}$ using traditional models such as well-stirred model and parallel tube model or some newer methods such as Berezhkovskiy et al. method and Poulin et al. method [53-56]. The well-stirred and parallel tube model have contradictory assumptions about the distribution of the enzyme [55]. The well-stirred model assumes uniform distribution of enzymes within the liver and exposure to a well-mixed concentration of drug within the liver cells [55]. On the other hand, parallel tube model (Eq. 1) assumes that the enzyme is distributed along uniform series of parallel tubes and there is an exponential concentration gradient across the liver sinusoids [55]. The extraction ratios predicted using the two methods differ significantly for drugs showing intrinsic clearances that exceed liver blood flow (i.e. highly extracted drugs) [55]. The well-stirred model was used in this dissertation and will be discussed in detail further.

$$E_{hep} = 1 - e^{-fu \times \frac{CL_{int,u}}{Q_{hep}}} \quad (1)$$

where E_{hep} = hepatic extraction ratio, Q_{hep} = liver blood flow (1500 ml/min), fu = fraction unbound, CLint, u = unbound intrinsic clearance.

Berezhkovskiy et al. (Eq. 2-4) method accounts for the ionization of unbound drug after exposure to varying pH in the extracellular and intracellular spaces of hepatocytes [54, 56].

$$CL_{hep} = \frac{Q_{hep} \times R_{bp} \times CL_{int,in\ vivo,hep} \times \frac{fu-app}{f_{u,inc}}}{Q_{hep} + R_{bp} \times CL_{int,in\ vivo,hep} \times \frac{fu-app}{f_{u,inc}}} \quad (2)$$

$$F_{up-app} = in\ vitro\ fu_p \times F_I \quad (3)$$

$$F_I = \frac{f_{unionized,plasma}}{f_{unionized,intracellular\ water}} \quad (4)$$

where R_{bp} = blood to plasma ratio, $f_{u\text{-}app}$ = unbound fraction corrected for ionization, $F_I = f_u$ of drugs unionized between extracellular plasma ($f_{unionized,plasma}$) and intracellular tissue ($f_{unionized,intracellular\ water}$).

Poulin et al. proposed modification of the well-stirred model to incorporate the protein-facilitated metabolism and uptake resulting from ionic interactions between surface of the liver cells and extracellular protein-drug complex (Eq. 5-6) [54]. This method replaces fu_p with fu_{liver} to take into account liver specific drug distribution and protein binding [54].

$$CL_{hep} = \frac{Q_{hep} \times R_{bp} \times CL_{int,in\ vivo,hep} \times \frac{f_{u,liver}}{f_{u,inc}}}{Q_{hep} + R_{bp} \times CL_{int,in\ vivo,hep} \times \frac{f_{u,liver}}{f_{u,inc}}} \quad (5)$$

$$f_{u,liver} = \frac{PLR \times fu_{p-app}}{1+(PLR-1)\times fu_{p-app}} \quad (6)$$

where fu,liver = unbound fraction of drug in liver and PLR = plasma-to whole-liver concentration ratio

Of the three methods, the well-stirred model is the simplest method that requires less information [53, 54, 56]. However, it shows a general trend of underpredicting the hepatic clearance probably because the model assumes that the extent of protein binding shown by a drug in plasma in similar to binding in liver cells [53, 54, 56]. Thus, it fails to incorporate the effects of pH gradient, protein binding and distribution with respect to the hepatocytes, which is accounted for by the remaining two methods. The Poulin et al. method appears to show least error in accuracy and precision especially for drugs with extensive albumin binding [54].

The IVIVE methods for predicting intestinal clearance are gaining prominence because numerous publications have highlighted the role of intestine as an important drug-metabolizing organ [14, 45-47, 50, 57-64]. Three models namely well-stirred, Q_{gut}, and ACAT models are commonly used for prediction of *in vivo* intestinal clearances.

The intestinal well-stirred model is similar to the hepatic well-stirred model and was used in this dissertation for predicting intestinal availability (explained on page 25-26). The Q_{gut} model (Eq. 7-8) slightly modifies the well-stirred model to incorporate permeability characteristics of the drug while estimating its intestinal extraction [65]. The parameter Q_{gut} represents a hybrid of both the permeability clearance (Cl_{perm}) of a compound and the villus blood flow (300 ml/min) [65]. The Cl_{perm} can be calculated (Eq. 9) based on the effective permeability of the test compound determined using *in vitro* systems such as Caco-2 cells, MDCK cells, PAMPA, or using physiochemical properties of the drug like polar surface area or number of hydrogen bond donors [65].

$$F_g = \frac{Q_{gut}}{Q_{gut} + f_{u_G} \times \ in\ vitro\ Cl_{int}} \quad (7)$$

$$Q_{gut} = \frac{Cl_{perm} \times Q_{villi}}{Cl_{perm} + Q_{villi}} \quad (8)$$

$$Cl_{perm} = P_{eff} \times A \quad (9)$$

where fu_G = fraction unbound in gut (generally assumed to be 1), in vitro Clint – intrinsic clearance determined using in vitro systems like cell lines or microsomes, Cl_{perm} = permeability clearance, Q_{villi} = villous blood flow (300 ml/min), P_{eff} = effective permeability determined using *in vivo* jejuonal perfusion and A = intestinal surface area (0.66 m^2, assuming average length and radius of the small intestine = 6 m and a1.75 cm, respectively.)

Yang et al. compared the performance of the two minimal models i.e. the well-stirred and the Q_{gut} model by using a dataset of 16 drugs predominantly metabolized by CYP3A [65]. Of the two models, the Q_{gut} model was associated with the least mean prediction error (best accuracy) and mean squared prediction error (best precision) [65].

The advanced compartmental and absorption transit or ACAT model (Fig 1.4) is a complex dynamic compartmental PBPK model which includes linear and nonlinear transport and metabolism kinetics and depicts the absorption of drug through nine distinct physiological compartments i.e. stomach, seven segments of small intestine, and colon

[65, 66]. The model allows incorporation of physicochemical properties (pKa, solubility, particle size and density, lipophilicity, permeability), physiological features (intestinal transit time, gastric emptying, presystemic metabolism and intestinal transport) as well as formulation/dosage factors (dosage form and dose) to better predict the oral absorption of drugs [66]. Although this model gives a comprehensive prediction of oral absorption and bioavailability of compounds, its requires extensive information about the drug, exhaustive characterization of the metabolic fate of the test compound in the enterocytes, its GI transit as well as the effect of various gradients of enzymes and transporters (such as pH, fluid and blood flow) while passing through different sections of the GI tract.

Figure 1.4: ACAT model

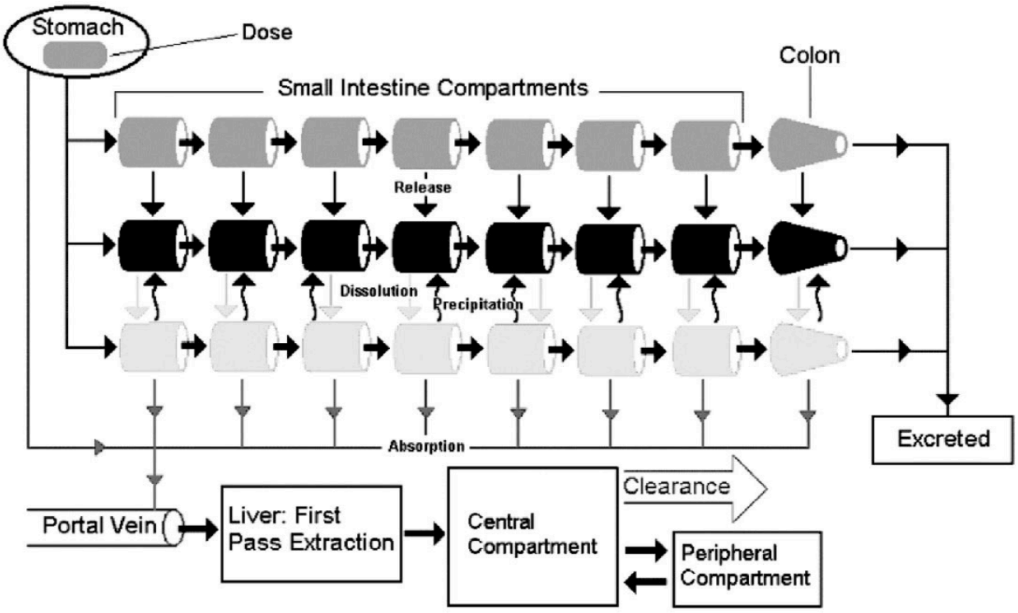

Several in vitro and in vivo studies focusing on metabolism of BUP have been published [9, 10, 12, 14, 20, 67]. However, these studies do not reveal any information on the contribution of the two metabolic pathways (CYP and UGT) as well as the overall extraction of BUP in intestine versus liver. Hence, the intrinsic metabolic clearances from our microsomal studies were extrapolated using the well-stirred model to predict

intestinal (F_g) and hepatic availability (F_h) [65, 68, 69]. In the intestinal well-stirred model (Eq. 10), Q_{villi} (300 ml/min) indicates intestinal villous blood flow, f_{u_G} represents the unbound fraction of BUP in the enterocytes and *in vitro* Cl_{int} is the total intrinsic clearance in the pooled intestinal microsomes scaled to physiological level using two scaling factors i.e. 20.5 mg microsomal protein/g intestinal mucosa (SF_1) and 11.16 g intestinal mucosa/kg (SF_2) [65]. In addition to the well-stirred model, F_g was also predicted using the Q_{gut} model. However for a highly permeable drug like BUP, the Q_{gut} term is expected to be similar to the villous blood flow (Q_{villi}). Thus, F_g predicted using the two models did not differ drastically (~ 2 fold difference) and hence the well-stirred model was chosen.

$$F_g = \frac{Q_{villi}}{Q_{villi} + f_{u_G} \times \ in\ vitro\ Cl_{int} \times SF_1 \times SF_2} \quad (10)$$

Similarly in the hepatic well-stirred model (Eq. 11), Q_{hep} (20.7 ml/min/kg) represents hepatic blood flow, fu_p is the fraction of unbound BUP in plasma and *in vitro* Cl_{int} is the total intrinsic clearance in pooled liver microsomes physiologically scaled using two scaling factors i.e. 40 mg microsomal protein/g liver (SF_1) and 21.4 g liver/kg (SF_2) [68, 69].

$$F_h = \frac{Q_{hep}}{Q_{hep} + f_{u_p} \times \ in\ vitro\ Cl_{int} \times SF_1 \times SF_2} \quad (11)$$

The intestinal and hepatic availabilities were used to predict the systemic availability of BUP using equation 12 [70]. Since BUP hydrochloride is highly soluble and highly permeable drug expected to exhibit almost complete absorption, the fraction

absorbed (F_a) was assumed to be 1.

$$F_{oral} = F_a \times F_g \times F_h \times 100 \quad (12)$$

1.5 Predicting the effect of inhibitor treatments on variability in PK parameters

A drug undergoing extensive presystemic metabolism is often associated with poor and highly variable systemic bioavailability and exposure values [55]. Huge variability in the PK parameters can be detrimental to the efficacy and safety of a drug, limiting its administration in humans [55]. Understanding the biochemical and physiological mechanisms responsible for the interindividual variability in the magnitude of presystemic metabolism is extremely pivotal for optimization of drug therapy [71]. Although CYP3A enzymes are expressed profusely in the human livers, they have been observed to show a high degree of interindividual variability (>100 fold) [71]. Of special importance is the variability in CYP3A4 metabolism because it is the most dominant of all CYP450 enzymes expressed in the intestine and liver and is reported to be involved in the metabolism of a majority of the currently marketed drugs [64]. Numerous factors influencing the expression and function of CYP3A enzymes [71] have been identified such as epigenetic factors (DNA methylation, histone modification, impact of microRNAs) [72], host specific factors (gender, age, body weight, organ blood flow especially liver perfusion, protein binding and expression of transporters and enzymes, disease states etc. [73-79] and to a smaller extent genetic polymorphisms. In addition, drug-drug, drug-food or disease state mediated interactions can also contribute to the variability in CYP3A metabolism by inducing or inhibiting the enzyme expression and function [55]. Using a sample set of 52 human livers, Cubitt et al. observed about 41%

variability in the hepatic CYP3A4 abundance [46]. A variability of 33% in CYP3A4 content was reported by Kato et al. based on an in silico study using 43 diverse CYP3A substrates [60]. While the variability in hepatic CYP3A4 has been studied considerably, the interindividual variability in intestinal CYP3A4 content still remains significantly understudied [46, 55, 61]. The intestinal CYP3A4 accounts for 70 to 80% of the total CYP450 content and has been identified as an important organ involved in the first pass metabolism of drugs [46, 55, 61]. Midazolam, a CYP3A substrate was reported to show significantly higher variability in the intestinal extraction ratio (mean- 0.43±0.24, range- 0 to 0.77) over the hepatic extraction ratio (mean- 0.44±0.14, range- 0.24 to 0.76) [80]. A study by Paine et al. performed using six human intestinal samples revealed a 60% interindividual variability in CYP3A4 abundance [61], while the in silico study by Kato et al. reported an 81% variability in the intestinal intrinsic clearance corrected for permeability [60]. Intestine represents a highly heterogeneous biological tissue with significant intra-organ variability, contrary to the liver [61, 80]. Hence, it is not surprising that a higher interindividual variability was observed in the intestine as compared to the liver.

In addition to predicting the F_{oral} of BUP, the scope of this dissertation also included determining the effect of inhibitors on the variability associated F_{oral} and systemic exposures (AUC_{∞}) of BUP. Hence, a simulated population dataset was generated using Monte Carlo simulations (MCS). @RISK (Palisade Corporation, Ithaca, NY) software was used to perform MCS. The sampling technique used in MCS involves random sampling of numbers from a given probability distribution. The values chosen through MCS are completely random and can fall anywhere within the specified range of

distribution of the input variables [81]. MCS gives an opportunity to define the variability in input variables and integrate them in to the prediction of output variables [82]. It is recommended to have adequate number of iterations in a simulation to avoid the problem of clustering while generating input distributions [81]. Thus, using MCS a large simulated population of 10,000 individuals was generated and the effect on input variables on the mean and variability in the mean of the output variables was evaluated in this dissertation. Another crucial aspect while setting up MCS is selecting appropriate distributions for the input variables [82]. For the purpose of our analysis, all the input variables were assigned normal distribution with a minimum possible value of zero (non-negative). In our model, F_{oral}, AUC_{∞} and Cl_{tot} were the desired output variables while the intrinsic hepatic and intestinal clearances for the CYP and UGT pathway represent the input variables. In presence of inhibitors, the model included additional variables i.e. predicted inhibitor concentrations in the gut lumen and the portal vein. Also, the potency of inhibition i.e. K_i for each pathway in the intestine and liver determined from *in vitro* inhibition studies was included in the model. In order to investigate the effect of input variables on the output variables, a sensitivity analysis was performed. Spearman rank correlation coefficient was used to describe the magnitude and direction of the effect of the input variables on output parameters. Spearman rank correlation coefficient was chosen because it does not assume linear relationship between the input and output variables and is less sensitive to the effect of outliers in the simulated population.

1.6 Previous work from our lab

The preliminary inhibition studies on several dietary compounds including the ones listed earlier were performed in LS180 cells (intestinal human colon adenocarcinoma cell line). The LS180 cells were treated with calcitriol (5 μM) to induce

CYP3A4 expression confirmed by the CYP glow assay (using selective CYP3A4 fluorescent probe). After induction (72 - 96 hours), the cells were exposed to BUP (10 μM) alone or along with certain putative inhibitors (24 μM, chosen based on prior studies in our lab) for two hours. The incubation time was optimized by monitoring formation of the metabolites (NBUP, BUPG) at various time points till 2 hours. One-way ANOVA with Dunnett's post-hoc test was used to determine significant inhibition of NBUP or BUPG formation ($\alpha = 0.05$; Prism v6.0). In addition, an *in vivo* study in rats was conducted in our laboratory to determine the effect of certain dietary components on F_{oral} of BUP [83]. A cocktail of eugenol (20 mg/kg), isoeugenol (16 mg/kg), ethyl vanillin (20 mg/kg), vanillin (20 mg/kg), curcumin (5 mg/kg), silybin (5 mg/kg), α-mangostin (5 mg/kg), resveratrol (20 mg/kg), propyl gallate (12 mg/kg) and naringin hydrate (60 mg/kg) was co-administered with BUP (10 mg/kg) and naloxone (2.5 mg/kg) using oral gavage. [83]. A 2-fold increase in the oral bioavailability of buprenorphine in presence of inhibitors was observed in this study. [83]. These *in vitro* and *in vivo* studies provide proof of concept that these dietary compounds can be utilized to inhibit the oxidative and conjugative metabolism of BUP and thereby improve its systemic availability. Thus, the compounds showing statistically significant inhibition in the LS180 cell studies and some compounds from the inhibitor cocktail used in rat studies were further studied in pooled human intestinal and liver microsomes as discussed in the succeeding chapters.

1.7 Hypothesis and specific aims

1.7.1 Hypothesis:

a) GRAS compounds or components of dietary supplements can be utilized to inhibit the presystemic metabolism of buprenorphine and significantly improve its oral bioavailability and systemic exposure.

b) GRAS or dietary compounds can also produce significant reduction in the variability associated with oral bioavailability and systemic exposure of buprenorphine.

1.7.2 Specific aims

Following are the specific aims and objectives of the research performed in this dissertation:

Specific aim 1:

Determine the transport of buprenorphine using Caco-2 cells and investigate if it suffers from intestinal permeability limitations.

Specific aim 2:

Identify the potential inhibitors of oxidative and conjugative metabolism of buprenorphine from a set of twenty-seven GRAS or dietary compounds using pooled human intestinal and liver microsomes.

Specific aim 3

Determine the potency of inhibition (IC_{50}) of oxidation and conjugation metabolism of buprenorphine for five shortlisted inhibitor candidates in pooled human intestinal and liver microsomes.

Specific aim 4

Determine the biorelevant solubilites of the shortlisted inhibitor candidates using fasted state simulated intestinal fluid (FaSSIF).

Specific aim 5

a) Predict the oral bioavailability (F_{oral}), systemic exposure (AUC_{∞}) and total clearance (CL_{tot}) of BUP with and without inhibitor treatments.

b) Predict the effect of inhibitor treatments on the variability in the mean predicted F_{oral}, AUC_{∞} and CL_{tot} of BUP.

c) Perform sensitivity analysis and identify the most sensitive input variable showing strong influence on F_{oral}, AUC_{∞} and CL_{tot} of BUP in presence and absence of inhibitor treatments.

Chapter 2 – Transport of buprenorphine across Caco-2 cells

Partially drawn from manuscript published Biopharmaceutics and Drug Disposition (January 2017, 38: 139-154)

2.1 Introduction

The factors governing oral bioavailability of a drug include gastrointestinal (GI) solubility, GI permeability and presystemic metabolism in intestine and/or liver. Published literature provides strong evidence on contribution of presystemic metabolism to the poor oral bioavailability of BUP. However, limited information is available on the impact of efflux transporters on the intestinal absorption of BUP. Contradictory evidence exists in the literature on the status of BUP as a P-glycoprotein (P-gp) substrate. Certain *in vivo* and *in vitro* studies indicate involvement of P-gp in mediating efflux of BUP at the blood brain barrier (BBB) [84]. On the other hand, studies in *in vitro* systems like Caco-2 monolayers and P-gp ATPase assay suggest that BUP does not appear to be a P-gp substrate [85]. It was of interest to determine if BUP undergoes efflux at the GI lumen resulting in reduced absorption following an oral dose.

The Caco-2 cell monolayers are a well characterized and widely used *in vitro* model to study the intestinal absorption of test compounds and evaluate the transport mechanisms involved [86-88]. The apparent permeability values determined from this *in vitro* model show a high degree of correlation with observed in vivo absorption in humans [86, 87, 89]. Hence, in the present study the transport of BUP was studied using Caco-2 cell monolayers. If the results indicate involvement of efflux transporters like P-gp in the transport of BUP, then the potential of GRAS or dietary compounds to inhibit the GI efflux of BUP will be investigated as a strategy to improve oral bioavailability of BUP.

2.2 Materials and Methods

2.2.1 Biological materials

The Caco-2 cells were purchased from American Type Culture Collection (Manassas, VA). Dulbecco's modified Eagle's medium (DMEM) and non-essential amino acids were obtained from Gibco (Grand Island, NY) and fetal bovine serum (FBS) was obtained from Atlanta Biologicals (Lawrenceville, GA). Penicillin and streptomycin were purchased from Quality Biological (Gaithersburg, MD).

2.2.2 Chemicals and reagents

Hanks balanced salt solution (HBSS), lucifer yellow (LY) and caffeine were purchased from Sigma-Aldrich (St Louis, MO), and polycarbonate transwell filters and polystyrene plates were obtained from Costar (Corning, NY). Rhodamine 123 (RH-123) was purchased from MP Biomedicals (Solon, OH) and haloperidol from Wako Chemicals (Richmond, VA).

2.2.3 Caco-2 cell culture

The Caco-2 cells (passage 10–16) were grown in a humidified incubator at 37 °C under 5% CO_2 in air in DMEM containing 10% v/v heat inactivated FBS, 0.1 mM nonessential amino acids, 2 mM L-glutamine, 100 U/ml penicillin and 100 μg/ml streptomycin. The Caco-2 cells were seeded on polycarbonate transwells (0.4 μM pore size, 12 mm diameter, Costar #3401) at a density of 3×10^5 cells/cm^2 and grown for 21 days. Cell culture media was replaced within 12 h of seeding, and thereafter every other day for the initial 7 days, and subsequently every day until day 21.

2.2.4 Transport of buprenorphine in Caco-2 cells

The integrity of the cell monolayers was evaluated by a low paracellular permeability marker lucifer yellow (100 μM) and transepithelial electrical resistance measurements (TEER) measured 21–24 days after seeding. The TEER values were corrected for background values due to the filters. The transport of RH-123 (10 μM, a P-gp substrate) in the presence or absence of P-gp inhibitor haloperidol (50 μM) was evaluated to confirm the functionality of P-gp in the Caco-2 cells. The filters containing cell monolayers were incubated in HBSS + HEPES (25 mM, pH 7.4) (apical side volume 0.5 ml and basolateral side volume 1.0 ml) and allowed to equilibrate for 10 min in an incubator- orbital shaker at 37 °C and 100 rpm. To study the transport of buprenorphine in the basolateral to apical (B-A) direction, the donor solution containing 10 μM buprenorphine was placed on the basolateral side and the aliquots were taken from the apical side. For transport in apical to basolateral (A-B) direction, aliquots were taken from the basolateral side. The transport experiment was performed in triplicate for 120 min with aliquots (200 μl) taken at 5, 15, 30, 45, 60, 90 and 120 min. At every time point, the 200 μl aliquot was replenished by an equal amount of HBSS + HEPES to maintain constant volume. Aliquots were taken before beginning the transport study to serve as blanks, and at the end of the experiments for determining the recovery and mass balance in the system. The lucifer yellow transport was performed simultaneously with the buprenorphine transport experiment in separate wells to determine monolayer integrity. Lucifer yellow transport was also performed for 1 h subsequent to the buprenorphine transport experiment in the buprenorphine treated wells to investigate the effect of buprenorphine on the monolayer integrity. The apparent permeability coefficients (P_{app})

and efflux ratios were determined at sink conditions using equations 1 and 2, respectively [85].

$$P_{app} = \frac{dQ}{dt*A*Co} \quad (1)$$

where dQ/dt is the linear appearance rate of mass in the receiver compartment, A is the surface area of the membrane filter, and C_o is the initial concentration in the donor compartment.

$$Efflux\ ratio = \frac{P_{app_{B-A}}}{P_{app_{A-B}}} \quad (2)$$

Transport of high transcellular permeability standard caffeine was also performed simultaneously in separate wells. Lucifer yellow and rhodamine-123 were quantitated using a Synergy 2 plate reader (Biotek, Inc; Winooski, VT) at $\lambda_{excitation}$ = 485 nm and $\lambda_{emission}$ = 528nm. Quantification of caffeine was performed on a Waters 2695 HPLC system with a 2487 dual wavelength UV-Vis detector (280 nm), using Altima C18 column (4.6x100mm, 3µm). The HPLC method comprised a mobile phase flow (1 ml/ min) of 10% acetonitrile (Solvent A) and 90% water (Solvent B) from 1 min (0 to 1 min) followed by a Solvent A gradient from 10% to 40% over 4 min (1 to 4 min) with a subsequent ramping of Solvent A from 40 to 90% over 0.5 min (4 to 4.5 min) followed by maintaining 90% Solvent A for 1 min (4.5 to 5.5 min) and returning to 10% Solvent A over 1.5 min (5.5 to 7 min).

2.2.5 Sample analysis

Buprenorphine concentrations were analyzed using a previously validated method consisting of reversed phase HPLC coupled with Acquity QDa mass spectrometric detection (as described in chapter 3) [90]. Linear calibration curves were obtained for buprenorphine (single ion recording of BUP - 468.6).

2.3 Results

2.3.1 Transport of buprenorphine in Caco-2 cells

The net TEER values at 37°C were greater than 200 $\Omega.cm^2$, the apparent permeability (P_{app}) of $\leq 1\times10^{-6}$ cm/s for Lucifer yellow confirmed the presence of tight junctions in the Caco-2 cell monolayers. The high transcellular permeability standard caffeine displayed a permeability of 45×10^{-6} cm/s, which is comparable to the values previously reported [89, 91]. The efflux ratio of 23.5 of RH-123 was reduced to 7.5 in the presence of the P-gp inhibitor haloperidol confirming the functionality of P-gp in Caco-2 cells (Table 2.1). RH-123 has also been reported to be a BCRP substrate [92, 93]. Thus, lack of BCRP inhibition by haloperidol might account for the efflux ratio being greater than 2. The mean apparent permeability of buprenorphine (n = 2) in A-B direction was $34\times10^{-6} \pm 14\times10^{-6}$ cm/s while the mean B-A permeability was $39\times10^{-6} \pm 20\times10^{-6}$ cm/s. Different passages of the Caco-2 cells (passages 10 and 13) were used for the BUP transport studies and the cells were not protein normalized which might explain the differences between the apparent A-B and B-A permeability values in the two experiments. The observed efflux ratio was 1.2 suggesting lack of efflux of buprenorphine in the GI lumen [88].

Table 2.1: Apparent permeability of RH-123 and BUP in Caco-2 cells

Test compound	P_{app} (A – B) (x 10^{-6} cm/s)	P_{app} (B – A) (x 10^{-6} cm/s)	Efflux ratio
RH-123	0.2 ± 0.01	5.5 ± 0.2	23
RH-123 + Haloperidol	0.2 ± 0.03	1.5 ± 0.2	7.5
BUP	34 ± 15	39 ± 20	1.2

Figure 2.1: A-B transport of BUP in Caco-2 cells

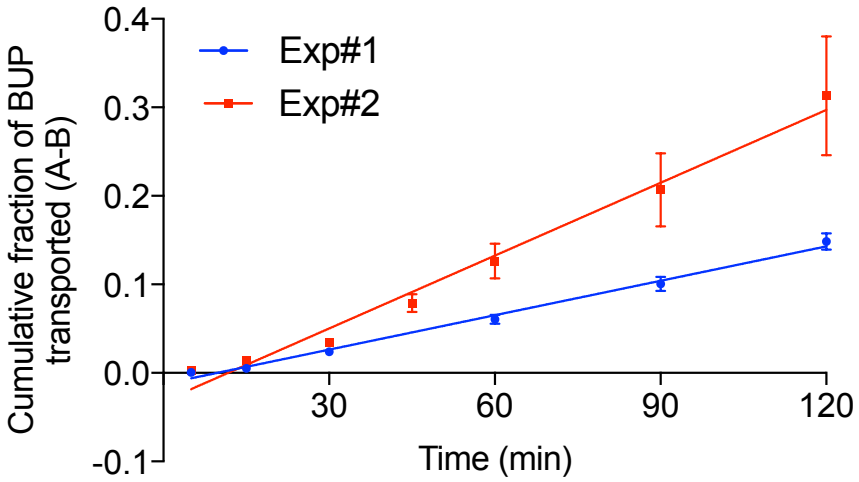

Fig 2.1: Apical to basolateral transport of BUP in Caco-2 cells
All determinations were made in triplicate. Date represents mean ± SD of the cumulative fraction transported at various time points from 5 to 120 mins. Mean apparent A-B permeabilities in expt#1 and exp#2 were 22 ± 0.1 x 10^{-6} cm/s and 46 ± 0.1 x 10^{-6} cm/s.

Figure 2.2: B-A Transport of BUP in Caco-2 cells

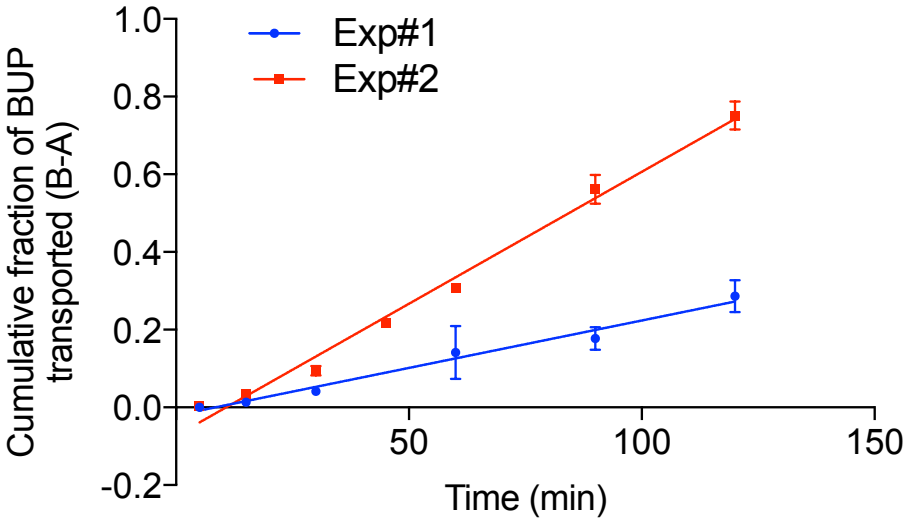

Fig 2.2: Basolateral to apical transport of BUP in Caco-2 cells
All determinations were made in triplicate. Date represents mean ± SD of the cumulative fraction transported at various time points from 5 to 120 mins. Mean apparent B-A permeabilities in expt#1 and exp#2 were 21 ± 0.4 x 10^{-6} cm/s and 58 ± 0.2 x 10^{-6} cm/s.

2.4 Discussion and conclusions

The integrity of Caco-2 monolayers was established by TEER measurements, lucifer yellow and caffeine transport. The transport of RH-123 from basolateral to apical side was significantly higher than the absorptive transport, as would be expected for a P-gp substrate. Treatment with haloperidol (50 μM), a selective P-gp inhibitor drastically reduced the efflux ratio of RH-123. Thus, the functionality of P-gp protein in the Caco-2 cells was established. The bidirectional transport studies of BUP in the Caco-2 cells indicate that BUP is highly permeable drug. The ratio of B-A and A-B permeabilities of BUP was less than 2, indicating BUP does not undergo efflux transport by transporters like P-gp and BCRP in the Caco-2 cells. Poor GI solubility, poor GI permeability and extensive presystemic metabolism could result in poor oral bioavailability. However, BUP shows high permeability and high solubility indicating that its extensive presystemic metabolism is likely responsible for its low oral bioavailability. Hence, future studies will focus on investigating the potential of GRAS or dietary compounds to inhibit the oxidative and conjugative metabolism of BUP.

Chapter 3: Screening Study To Identify Potential Inhibitors Of Oxidative And Conjugative Metabolism Of Buprenorphine

Partially drawn from manuscript published Biopharmaceutics and Drug Disposition (January 2017, 38: 139-154)

3.1 Introduction

Opiate addiction is a severe health problem in the United States and throughout the world [1]. In 2014, 1.9 million people in the USA suffered from substance use disorders related to prescription opioid pain medicines and 586,000 suffered from a heroin use disorder [1]. Therapeutic regimens or treating opiate addiction have met varying degrees of success and failures. However, a growing need for new products and strategies still exists.

Currently, buprenorphine (BUP) in combination with naloxone (NX) is a preferred treatment for maintenance of opioid dependence. It is available as a sublingual (SL) tablet and film. A sublingual tablet or film containing buprenorphine and naloxone exhibits bitter taste/aftertaste [2]. Sublingual buprenorphine is reported to suffer from certain limitations such as a longer dissolution time, variability in the sublingual retention time, inability to mask the bitter taste, interference with common activities – talking, drinking and eating; these issues lead to a certain degree of patient non-compliance [2]. According to a survey conducted by Reckitt Benckiser Pharmaceuticals, a high percentage of patients reported problems with the sublingual dissolution time of the Suboxone tablet as well as its taste [7]. Oral administration of buprenorphine could help in mitigating these issues, thus providing a better drug product with lesser variability and comparable or higher efficacy. However, buprenorphine exhibits poor oral bioavailability due to extensive presystemic metabolism by both oxidation (primarily by cytochrome P450 (CYP) 3A4 and minor contributions by CYP2C8 and CYP2C9) to form

norbuprenorphine (NBUP) and glucuronidation (mainly by glucuronosyltransferases (UGTs) – 1A1, 1A3 and 2B7) to form buprenorphine glucuronide (BUPG) [8, 12, 14]. Norbuprenorphine is then conjugated to form norbuprenorphine glucuronide (NBUPG) [14]. Due to the extensive presystemic metabolism and accompanying low and variable bioavailability, an oral formulation of buprenorphine is currently not available in the market.

Limited information is available on the pharmacokinetics of buprenorphine after oral administration in humans. Published in vivo studies indicate that the majority (~70%) of the oral dose is eliminated via feces with minor (~10–15%) renal elimination [8, 10]. In the feces, unchanged buprenorphine is reported to be the major component with unchanged norbuprenorphine as the minor component [8, 10]. However, the unchanged buprenorphine in feces is contaminated with buprenorphine obtained following hydrolysis of buprenorphine glucuronide by β-glucuronidase in the gut wall. In the urine, norbuprenorphine glucuronide (8–10%) and buprenorphine glucuronide (2–3%) form the major components with trace amounts of unchanged buprenorphine and norbuprenorphine [94]. However, the above data do not distinguish between the intestinal vs hepatic as well as the CYP vs UGT contributions to the overall presystemic metabolism of buprenorphine.

There are numerous reports on the effects of dietary components on drug metabolism [21-26]. Therefore it would seem reasonable to create a strategy in which selected dietary and/or GRAS substances could be combined to inhibit the presystemic metabolism of drugs such as buprenorphine (which are extensively metabolized). Such a strategy would need to be established considering many aspects of the dietary or GRAS

substances as inhibitors: target enzyme inhibition, solubility, permeability, systemic bioavailability, clinically feasible doses, regulatory status, potential for side effects/toxicity and potential for undesired interactions with other medications. A recent study conducted in rats in our laboratory demonstrated a 2-fold increase in the oral bioavailability of buprenorphine following co-administration of buprenorphine with a cocktail of GRAS /dietary supplements [83]. The focus of this chapter will be the inhibition of the target enzyme pathways.

The present study consists of two objectives: (1) the prediction of the contribution of CYP and UGT to overall presystemic metabolism of buprenorphine in intestine and liver using well-stirred model, (2) inhibition of oxidative and conjugative metabolism of buprenorphine (individually) using GRAS compounds and dietary supplements or components (referred to as 'inhibitors' hereafter).

3.2 Materials and Methods

3.2.1 Chemicals and reagents

Curcumin, geraniol, geranyl acetate, linalool, naringin and thymol were purchased from Alfa Aesar (Ward Hill, MA). Ginger extract, 6-gingerol, menthyl acetate, pulegone, tris hydrochloride (Tris-HCl), UDP-glucuronic acid (UDPGA) were obtained from Sigma Aldrich (St Louis, MO). Trans-anethole was obtained from Oxchem Corporation (Irwindale, CA), iso-borneol and D-limonene from MP Biomedicals LLC (Solon, OH), carvacrol from TCI America (Portland, OR), chrysin from Hawkins Pharmaceutical Group (Minneapolis, MN), trans-cinnamaldehyde and linalyl acetate from Acros (NJ), hesperitin and silybin from Cayman Chemical Co. (Ann Arbor, MI), α-mangostin from Indofine Chemical Company (Hillsborough, NJ), menthol from Humco (Texarkana, TX), resveratrol and magnolol from Ark Pharm Inc. (Libertyville, IL),

saccharolactone from Calbiochem (La Jolla, CA), magnesium chloride ($MgCl_2$), dimethyl sulfoxide (DMSO) from Fisher Scientific (Fairlawn, NJ) and alamethicin from Enzo Life Sciences (Farmingdale, NY). Buprenorphine HCl and naloxone HCl were purchased from Medisca (Plattsburgh, NY), norbuprenorphine and buprenorphine glucuronide from Cerilliant (Round Rock, TX). All the solvents were high-performance liquid chromatography (HPLC) grade and were obtained from VWR (Radnor, PA). Quercetin was purchased from ChemImpex (Wood Dale, IL), pterostilbene from AK Scientific, (Union City, CA) and ethyl cinnamate from Beantown Chemical (Hudson, NH). NADPH was obtained from Akron Biotech (Boca Raton, FL) and bovine serum albumin (BSA) from Calbiochem (San Diego, CA). Human plasma from a healthy adult male was obtained under approval from the VCU IRB. Pooled human liver microsomes (HLM) (pool of 200 donors; lot no: 1210347 and 1410230) and human intestinal microsomes (HIM) (pool of 10 donors; lot no: 1410074 and pool of 13 donors; lot no: 1310173) were obtained from Xenotech, LLC (Lenexa, KS).

3.2.2 General assay procedure with pooled microsomes

The incubation mixture (100 µl) contained 0.1–0.33 mg/ml of pooled HIM or HLM. Depending on the enzyme of interest (CYPs or UGTs), the incubation mixture comprised 1 mM of NADPH or 2.5 mM UDPGA (respectively) and 5 or 10 µM buprenorphine. The CYP mediated reactions were carried out in 0.1 M potassium phosphate buffer (pH 7.4) containing 0.05% BSA, 3.3 mM $MgCl_2$, while the UGT mediated reactions were carried out in 100 mM Tris.HCl buffer (pH 7.4) containing 0.05% BSA, 12.5 mM $MgCl_2$, 31.25 µg/ml of alamethicin and 8 mM saccharolactone. The UGT mediated reactions were preactivated with alamethicin for 20 min on ice and 5

min at 37°C. Regardless of the enzyme, all reactions were carried out at 37°C and in the case of CYPs, the reactions were exposed to an atmosphere saturated with humidity. Following 10 to 30 min incubation, depending on the enzyme (see Table 3.1), the reactions were stopped by the addition of an equal volume of cold acetonitrile (ACN) containing naloxone (1 μM) as the internal standard. Samples were subsequently centrifuged at 12,500 × g for 5 min at 4°C to precipitate protein. The supernatant was stored at 20°C until further analysis. Control incubations without the cofactors, substrate or the enzyme were also performed. All incubations were performed in triplicate.

Table 3.1: Experimental conditions

Test condition	HLM		HIM	
	CYP	UGT	CYP	UGT
Incubation time (min)	15	11	15	30
Protein concentration (mg/mL)	0.1	0.1	0.33	0.2

3.2.3 Determination of binding of buprenorphine to human plasma, BSA and microsomes

Rapid equilibrium dialysis (RED; Thermo Scientific Pierce, Rockford, IL) was used to determine the binding of buprenorphine to human plasma, 0.05% bovine serum albumin (BSA) and pooled microsomes. The protein solution (200 μl) containing varying concentrations of buprenorphine was added to the sample compartment and appropriate buffer solution (350 μl) was added to the buffer compartment (Table 3.2). The Teflon base plate containing the inserts was sealed and incubated at 37°C on an orbital shaker at 100 rpm for a suitable time (Table 3.2) chosen from prior optimization experiments (see

Fig 3.1). The fraction unbound was calculated using equation 1. All determinations were made in triplicates.

$$\%\ unbound = \frac{Concentration\ in\ buffer\ compartment}{Concentration\ in\ sample\ compartment} \times 100 \quad (1)$$

Table 3.2: Test conditions for binding studies using RED

Binding to	Sample compartment	Buffer compartment	Incubation time (hours)	BUP test concentrations (µM)
Plasma proteins	Human plasma	Phosphate buffered saline	8	4.1, 32, 98
0.05% BSA	Phosphate buffer (pH 7.4) containing 0.05% BSA	Phosphate buffer (pH 7.4)	2	3.5, 29, 69
Microsomes	Start solution[a] containing HLM (0.1 mg/mL) or HIM (0.2 mg/mL)	Start solution[a]	4	2.8, 27, 106

a – start solution comprises of 12.5 mM $MgCl_2$, 31.25 µg/ml of alamethicin and 8 mM saccharolactone in 100 mM phosphate buffer (pH 7.4)

3.2.4 Determination of kinetic parameters in pooled microsomes

In preliminary experiments with pooled microsomes, the linearity of metabolite formation (buprenorphine glucuronide or norbuprenorphine) with incubation time (5–60 min) was established. Kinetic experiments were then performed by incubating increasing concentrations of buprenorphine (1 µM–160 µM) with either the liver or intestinal microsomes (0.1–0.33 mg/ml) for 10–30 min depending on the enzyme of interest. The Michaelis-Menten or Hill equation was fitted to the resulting kinetic data, and kinetic parameters were calculated by nonlinear regression analysis using Prism v6.0 (GraphPad Software, Inc.; La Jolla, CA). Intrinsic clearances (Cl_{int}) were estimated using Equation 2

when the Michaelis-Menten equation was chosen and Equation 3 [95] when the Hill equation was used.

$$\mathrm{Cl}_{int} = \frac{V_{max}}{K_m} \quad (2)$$

$$\mathrm{Cl}_{int} = \frac{V_{max}}{K_m} \times \frac{h-1}{h(h-1)^{1/h}} \quad (3)$$

where V_{max} is the maximal velocity rate, K_m is the substrate concentration at 50% of V_{max}, and h is the Hill coefficient.

The $Cl_{int,CYP}$ and $Cl_{int,UGT}$ were corrected for nonspecific microsomal binding as well as binding to BSA to determine the total unbound intrinsic clearance ($Cl_{u_{int}}$). In the pooled HIM, the $Clu_{int,\ CYP}$ and $Clu_{int,UGT}$ were scaled to an in vivo level using intestinal scaling factors of 20.5 mg microsomal protein/g intestinal mucosa (SF_1) and 11.16 g intestinal mucosa/kg (SF_2) [67, 96]. The $Clu_{int,CYP}$ and $Clu_{int,UGT}$ determined using HLM were scaled to an in vivo level using hepatic scaling factors of 40 mg microsomal protein/g liver and 21.4 g liver/kg [67, 96]. The total scaled in vitro Cl_{int} (ml/min/kg) in both HLM and HIM was calculated by addition of scaled $Clu_{int,CYP}$ and $Clu_{int,UGT}$ of buprenorphine, respectively.

3.2.5 Prediction of intestinal availability (F_g)

The well-stirred model (Eq. 4) was used to predict the intestinal availability (F_g) of buprenorphine [65, 97]. Q_{villi} (300 ml/min) is the intestinal villous blood flow, f_{u_G} indicates the unbound fraction of the substrate in the enterocytes and *in vitro* Cl_{int} is the total intrinsic clearance in HIM scaled using scaling factors 20.5 mg microsomal protein/g intestinal mucosa (SF_1) and 11.16 g intestinal mucosa/kg (SF_2)[65].

$$F_g = \frac{Q_{villi}}{Q_{villi} + f_{u_G} \times \ in\ vitro\ Cl_{int} \times SF_1 \times SF_2} \quad (4)$$

The following assumptions were made:

(a) fu_G was assumed to be 1. Yang et al. have shown that equating fu_G with fu in plasma or blood instead of using $fu_G = 1$ led to a loss of successful prediction of F_g. The resultant F_G values (when $fu_G \neq 1$) for a wide variety of drugs were reported to approach 1. Models with fu_G set to unity showed lowest mean prediction error (accuracy) and the mean squared prediction error (precision) [65].

(b) Linear PK (i.e. gut concentrations of buprenorphine < K_m) conditions were achieved enabling addition of the $Cl_{int,CYP}$ and $Cl_{int,UGT}$ (estimated separately) in the HIM to determine the total Cl_{int} in the intestine. The oral doses of 0.63 μg/kg, 15 μg/kg and 20 μg/kg of buprenorphine reported in the literature result in gut concentrations almost equal to or less than the K_m values (determined from the present in vitro studies) supporting the assumption of linear PK conditions [8, 10].

3.2.6 Prediction of hepatic availability (F_h)

The hepatic well-stirred model (Eq. 5) was utilized for determining hepatic availability (F_h) of buprenorphine [68, 69]. Q_{hep} (20.7 ml/min/kg) is the human hepatic blood flow, fu_p indicates fraction of unbound drug in plasma and *in vitro* Cl_{int} is the total intrinsic clearance in HLM scaled using scaling factors 40 mg microsomal protein/g liver (SF_1) and 21.4 g liver/kg (SF_2). Linear PK conditions were assumed as with the intestinal well-stirred model.

$$F_h = \frac{Q_{hep}}{Q_{hep} + f_{u_p} \times \ in\ vitro\ Cl_{int} \times SF_1 \times SF_2} \quad (5)$$

3.2.7 Prediction of oral bioavailability (F_{oral})

The oral bioavailability of buprenorphine was predicted based on the above-determined F_g and F_h values using Eq. 6. [70]. The F_a (fraction absorbed) was assumed to be 1 since buprenorphine hydrochloride is expected to show near complete absorption being a highly soluble and highly permeable drug [3, 10, 67].

$$F_{oral} = F_a \times F_g \times F_h \times 100 \quad (6)$$

3.2.8 Inhibition studies in HLM and HIM

Inhibition studies were performed using the same experimental method as described above for microsomes, although studies were carried out in the presence of inhibitors. Inhibitor solutions (final concentration: 25 μM) were prepared from DMSO stock solutions (100 mM) for all pure compounds based upon their molecular weights as usual. However, since ginger extract is a mixture of mainly 6-, 8- and 10-gingerols and 6-shogaol [32], the molecular mass of 8-gingerol was chosen as an approximate representative of the mixture, and stock solutions of ginger extract were prepared to provide a final total concentration of 25 μM. Buprenorphine (5 or 10 μM) was incubated with or without 25 μM of inhibitors for 10–30 min with 0.1–0.33 mg/ml HLM and HIM, depending on the metabolic pathway being tested (Table 3.1). Control reactions were carried out in the absence of inhibitors (solvent control). Significant inhibition was tested by comparing the % inhibition of norbuprenorphine or buprenorphine glucuronide formation to control reactions (no inhibition) using one-way ANOVA with Dunnett's post-hoc test ($\alpha = 0.05$; Prism v6.0).

3.2.9 Sample analysis

Quantification of buprenorphine and its metabolites buprenorphine glucuronide and norbuprenorphine was performed using a previously validated method [90]. Briefly, the HPLC method comprised a mobile phase flow (1 ml/ min) of 1% acetonitrile (Solvent A) and 99% of 90% aqueous 25 mM ammonium acetate (pH 6.6, adjusted with 5 µl glacial acetic acid) in 10% acetonitrile (Solvent B) from 1 min (0 to 1 min) followed by a Solvent A gradient from 1% to 50% over 1.5 min (1 to 2.5 min) with a subsequent ramping of Solvent A from 50 to 90% over 0.5 min (2.5 to 3 min) and followed by maintaining 90% Solvent A for 3 min (3 to 6 min). The column (Alltima HP C18, 4.6 × 100 mm, 3 µm; Grace- Davison Discovery Sciences, Columbia, MD) was re-equilibrated to 1% Solvent A for 1.5 min (6 to 7.5 min). The column and sample temperatures were 30 °C and 5 °C, respectively. The initial effluent (3 min) was diverted to the waste. Detection consisted of an Acquity QDa mass spectrometer (Waters, Milford, MA), with the capillary positive voltage set at 0.8 kV and the probe temperature set to 600 °C. Instrument control, acquisition and data processing were performed using Empower 3 software (Waters). The single ion recording (m/z ratio) for the four analytes and the internal standard (IS) are as follows: norbuprenorphine glucuronide 590.6, norbuprenorphine 414.5, buprenorphine glucuronide 644.7, buprenorphine 468.6 and naloxone 328.4. Linear calibration curves were obtained from 25–4000 ng/ml for norbuprenorphine and buprenorphine and from 100–4000 ng/ml for norbuprenorphine glucuronide and buprenorphine glucuronide. Buprenorphine concentrations from the enzymatic assays that were outside the calibration curve of buprenorphine on the QDa mass detector were quantified by UV detection (Waters 2487) at 220 nm.

3.3 Results

3.3.1 Binding of buprenorphine to plasma proteins, BSA and microsomes

Incubation time of 8 hours and 2 hours was chosen for plasma and BSA binding studies, respectively. Beyond these time points a pattern of reduction in the fraction of bound buprenorphine was observed (Fig 3.1 a-b). Buprenorphine exhibited 48 ± 14% binding to 0.05% BSA. The microsomal binding of buprenorphine was determined to be 72 ± 3% in pooled HIM (0.2 mg/ml) and 78 ± 3% in pooled HLM (0.1 mg/ml). The plasma protein binding of buprenorphine was determined to be 97 ± 1%, which is in good agreement with the published values [3, 10].

Figure 3.1: Optimization of incubation time for binding studies of buprenorphine in (a) plasma and (b) 0.05% BSA.

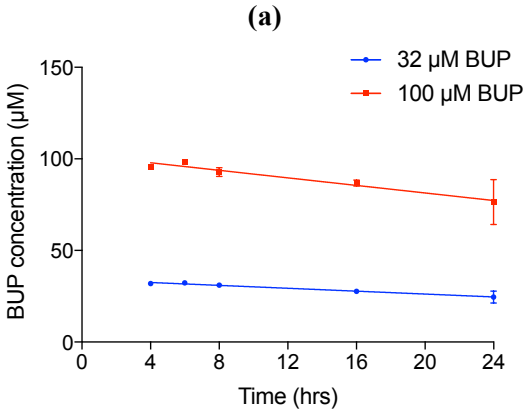

Fig 3.1 (a) Optimization of incubation time for binding studies of buprenorphine in plasma: BUP (32 and 100 µM) was added to the plasma compartment and appropriate buffer solution (350 µl) was added to the buffer compartment (PBS) and incubated at 37 °C on an orbital shaker at 100 rpm. Data represents BUP concentrations (mean ± SD) in plasma compartment at various time points till 24 hours. All determinations were made in triplicate.

(b)

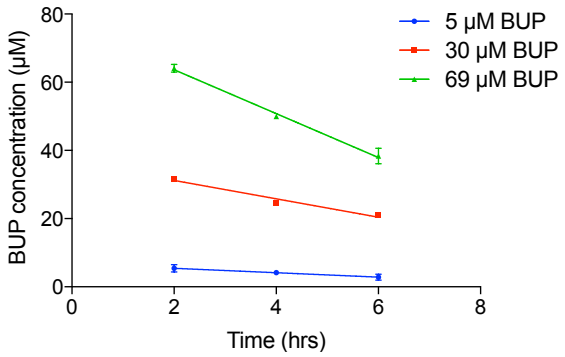

Fig 3.1 (b) Optimization of incubation time for binding studies of buprenorphine in 0.05% BSA: BUP (32 and 100 µM) was added to the sample compartment and appropriate buffer solution (350 µl) was added to the buffer compartment (100 mM phosphate buffer) and incubated at 37 °C on an orbital shaker at 100 rpm. Data represents BUP concentrations (mean ± SD) in the sample compartment at various time points till 6 hours. All determinations were made in triplicate.

3.3.2 Kinetics of buprenorphine in HLM and HIM

In both HLM and HIM, the disappearance of buprenorphine translated into formation of metabolite (NBUP or BUPG). Metabolite formation (BUPG and NBUP) was linear in pooled HIM and HLM till 60 min (Fig 3.2). Under the final experimental conditions (Table 3.1), saturable formation of buprenorphine glucuronide and norbuprenorphine was observed in the microsomes (Table 3.3, Fig 3.3). In the HIM, the contribution of oxidation (unbound $Cl_{int,\ CYP}$ = 21.4 µl/min/mg protein) to the total intestinal clearance of buprenorphine was about 6 fold higher than glucuronidation ($Cl_{int,\ UGT}$ = 3.43 µl/min/mg protein), indicating CYP to be the major metabolic pathway for buprenorphine in the intestine (Table 3.3). CYP appeared to be the major pathway in liver microsomes as well with about 4 fold higher Cl_{int} ($Cl_{int,\ CYP}$ = 183 µl/min/mg protein) than glucuronidation ($Cl_{int,\ UGT}$ = 47.4 µl/min/mg protein). These intrinsic clearances were corrected for binding to 0.05% BSA and microsomes and then scaled using intestinal and hepatic scaling factors to determine F_g and F_h, respectively.

Figure 3.2: Linearity of metabolite formation in pooled HIM and HLM

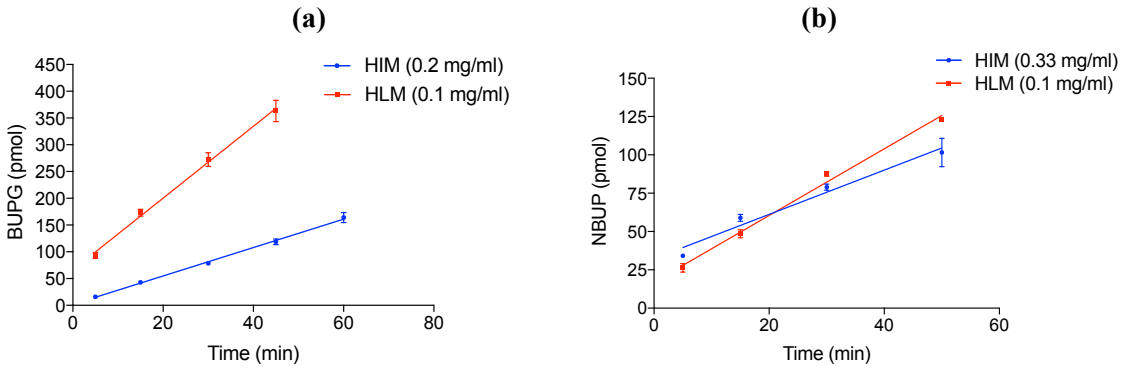

Fig 3.2 Linearity of BUPG and NBUP formation in pooled HIM and HLM.
All the determinations were performed in triplicates. Data represent mean ± SD.
a: BUPG formation in pooled HIM (slope = 2.65 ± 0.1 pmol/min, R^2 = 0.99, 10 µM BUP, Lot 1310173) and HLM (slope = 6.70 ± 0.2 pmol/min, R^2 = 0.99, 10 µM BUP, Lot 1410230)
b: NBUP formation in pooled HIM (slope =1.44 ± 0.15 pmol/min, R^2 = 0.95, BUP, Lot 1410074) and HLM (slope = 2.17 ± 0.1 pmol/min, R^2 = 0.99, 5 µM BUP, Lot 1210347)

Figure 3.3: Saturation of BUPG and NBUP formation in pooled HIM and HLM

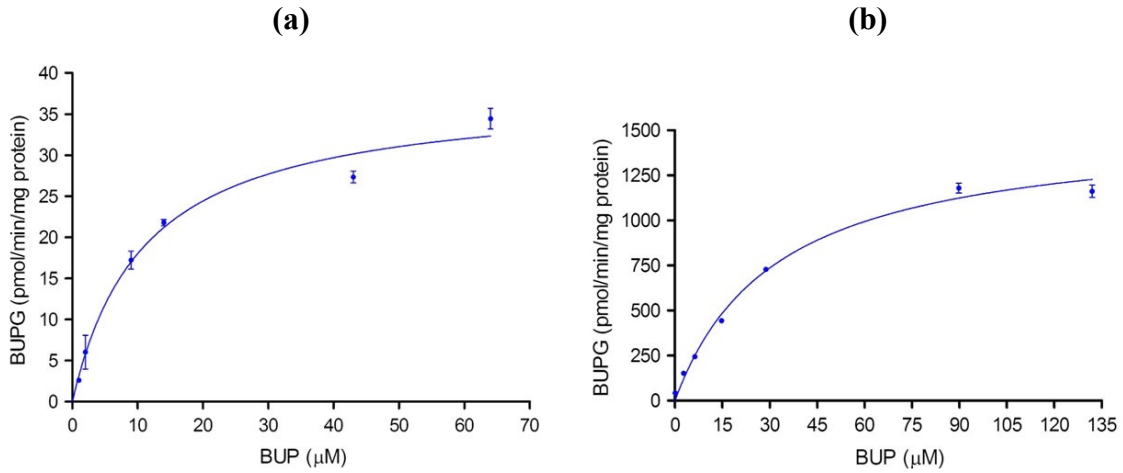

Fig 3.3: Saturation of buprenorphine glucuronide formation in pooled HIM and HLM.
All the determinations were performed in triplicates. Data represent mean ± SD. Curves represent best fit of Michaelis–Menten curve. (a) Buprenorphine glucuronide (BUPG) formation in pooled HIM (0.2 mg/ml, 30 min incubation, buprenorphine (BUP) concentrations: 1– 64 µM; Lot 1310173), V_{max} = 37.9 ± 1.5 pmol/min/mg protein; K_m = 11.1 ± 1.4 µM. (b) Buprenorphine glucuronide formation in pooled HLM (0.1 mg/ml, 11 min incubation, buprenorphine concentrations: 0.1–132 µM; Lot 1410230), V_{max} = 1527 ± 46 pmol/min/mg protein; K_m = 32.2 ± 2.6 µM

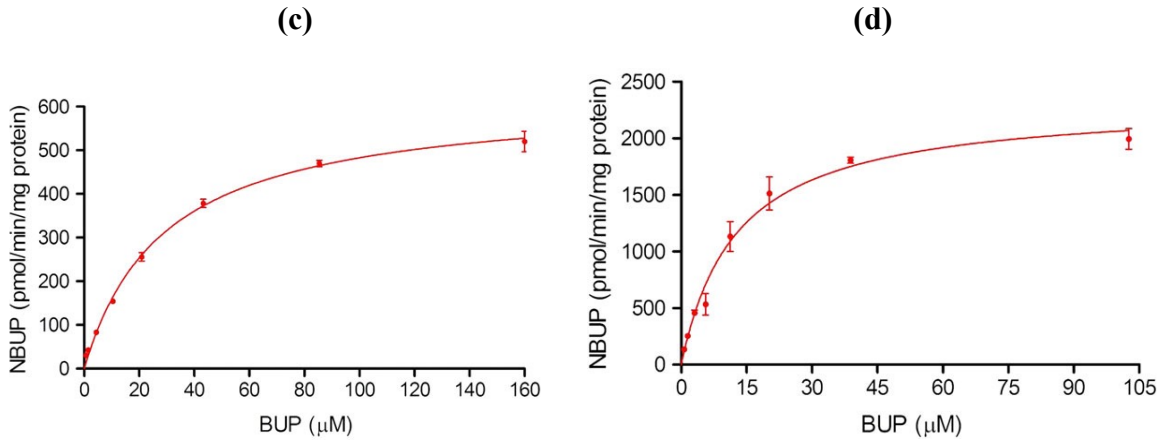

Fig 3.3: Saturation of norbuprenorphine formation in pooled HIM and HLM. All the determinations were performed in triplicate. Data represent mean ± SD. Curves represent best fit of Michaelis–Menten curve. (c) Norbuprenorphine (NBUP) formation in pooled HIM (0.33 mg/ml, 15 min incubation, buprenorphine (BUP) concentrations: 0.68–160 μM; Lot 1410074), V_{max} = 624 ± 11 pmol/min/mg protein; K_m = 29.2 ± 1.6 μM. (d) Norbuprenorphine formation in pooled HLM (0.1 mg/ml, 15 min incubation, buprenorphine concentrations: 0.68–103 μM; Lot 1210347), V_{max} = 2323 ± 80 pmol/ min/mg protein; K_m = 12.7 ±1.3 μM

Table 3.3: Saturation assay in pooled HIM and HLM

Parameter	HIM		HLM	
	CYP	UGT	CYP	UGT
V_{max} (pmol/min/mg protein)	624±11	37.9±1.5	2323±80	1527±46
K_m (μM)	29.2±1.6	11.1±1.4	12.7±1.3	32.2±2.6
R^2	1.00	0.98	0.98	0.99
Hill slope (h)	1	1	1	1
Cl_{int} (μL/min/mg protein)	21.4	3.43	183	47.4
Clu_{int} (mL/min/ mg protein)[a]	0.15	0.02	1.6	0.41
scaled Clu_{int} (μL/min/kg)	33.6[b]	5.39[b]	1370[c]	355[c]

a- Cl_{int} corrected for nonspecific binding to 0.05% BSA ($f_{u,BSA}$ = 0.52) and microsomes ($f_{u,mic}$ = 0.28 for HIM and 0.22 for HLM).
b- scaled using intestinal scaling factors 20.5 mg protein/g intestinal mucosa and 11.2 g intestinal mucosa/kg body weight.
c- scaled using hepatic scaling factors 40 mg protein/g liver and 21.4 g liver/kg body weight.

3.3.3 Prediction of intestinal availability (F_g)

Using the well-stirred model, F_g was estimated to be 0.095, indicating 90.5% intestinal extraction of buprenorphine. Based on these results, we would expect a significant contribution of intestinal metabolism to the first-pass clearance of buprenorphine when given orally. Of the total predicted fraction of buprenorphine metabolized, 86% was attributed to oxidation and 14% to glucuronidation indicating CYP to be the major metabolic pathway in the gut wall.

3.3.4 Prediction of hepatic availability (F_h)

Using the hepatic well-stirred model, F_h was estimated to be 0.29 indicating 71% hepatic extraction of buprenorphine. In the liver, while the CYP contribution was 79%, glucuronidation contributed to 21% of the hepatic metabolism. Thus, when given orally buprenorphine would be expected to undergo extensive presystemic metabolism in both intestine and liver.

3.3.5 Prediction of oral bioavailability (F_{oral})

Based on the predicted F_g of 0.095, F_h of 0.29 and assuming $F_a = 1$, the F_{oral} was predicted to be 2.75% (Eq. 6). Assuming the F_{oral} of buprenorphine to be 2.75%, inhibition of 75% of intestinal extraction and 50% of hepatic extraction by the GRAS compounds or dietary constituents or their combinations would result in a bioavailability of 49.7%. F_{oral} of 49.7% is comparable to the bioavailability of the sublingual buprenorphine (30–55%) [16, 98, 99], indicating the feasibility of an oral swallowed formulation.

3.3.6 Inhibition study in pooled HLM and HIM

Of the 28 inhibitors tested in the microsomes, 14 inhibitors in HIM and 15 inhibitors in HLM significantly inhibited buprenorphine glucuronide formation (Fig 3.4 a-b). Chrysin, curcumin, ginger extract and silybin produced an impressive inhibition of glucuronidation in both HIM and HLM. With regard to oxidation (norbuprenorphine formation), five compounds showed statistically significant inhibition in HIM, but 11 compounds in HLM (Fig 3.4 c-d).

Ginger extract inhibited oxidation as well as glucuronidation in both the microsomes. Chrysin and pterostilbene inhibited norbuprenorphine formation in HLM as well as HIM while curcumin was effective in inhibiting glucuronidation in both the microsomes. Also, curcumin and resveratrol produced effective inhibition of oxidation in the HLM and HIM. Overall, most of the tested compounds exhibited better inhibition of glucuronidation than oxidation of buprenorphine.

Some inhibitors such t-anethole, iso-borneol, t-cinnamaldehyde, ethyl cinnamate, geraniol, geranyl acetate, D-limonene, linalool, linalyl acetate, menthol, menthyl acetate, pulegone and thymol appeared significantly to promote buprenorphine glucuronide formation in HIM or HLM. Also, six compounds (hesperitin, cinnamaldehyde, ethyl cinnamate, geraniol acetate, linalyl acetate, D-limonene) showed apparent stimulation of norbuprenorphine formation in HLM, but not in HIM.

Figure 3.4: Metabolite formation in presence of inhibitors in pooled HIM and HLM

(a)

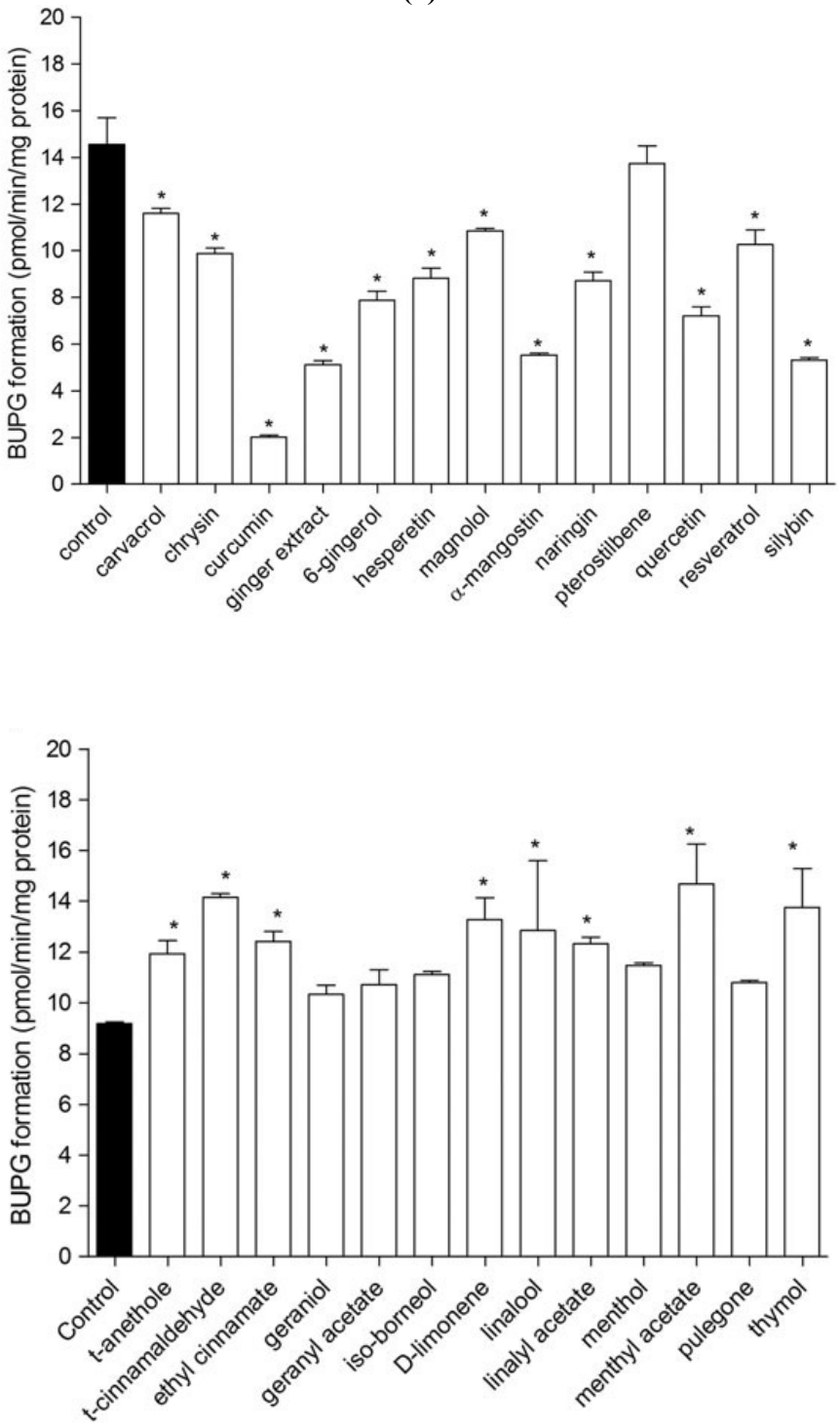

Fig 3.4 (a): Buprenorphine glucuronide (BUPG) formation with and without inhibitors in pooled HIM; Lot 1310173. Data represent mean ± SD of buprenorphine glucuronide or norbuprenorphine formation rate. All the determinations were performed in triplicate. Panels represent separate experiments. Asterisk indicates $p < 0.05$

(b)

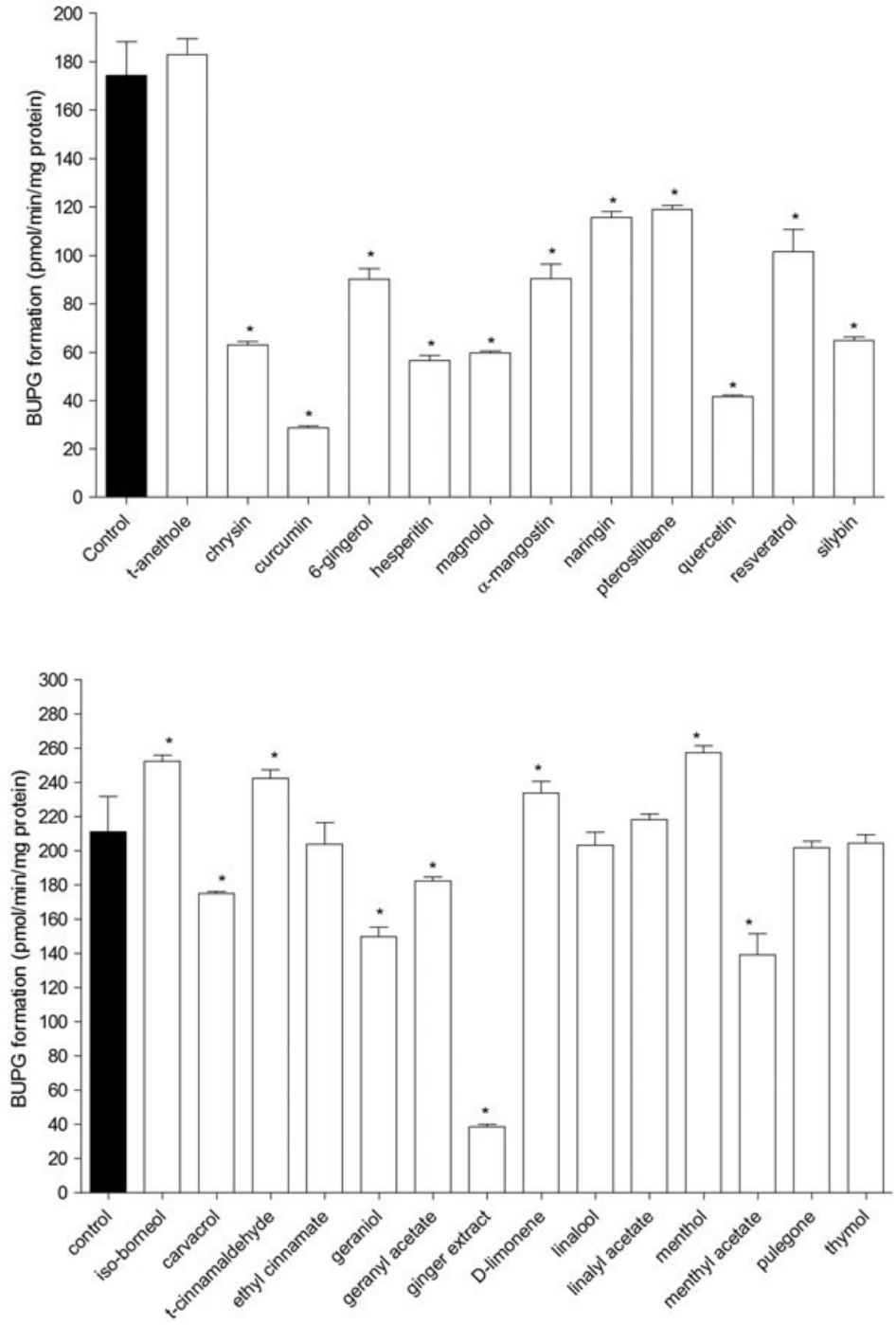

Fig 3.4 (b): Buprenorphine glucuronide (BUPG) formation with and without inhibitors in pooled HLM; Lot 1410230. Data represent mean ± SD of buprenorphine glucuronide or norbuprenorphine formation rate. All the determinations were performed in triplicate, except iso-borneol (n = 2). Panels represent separate experiments. Asterisk indicates $p < 0.05$

(c)

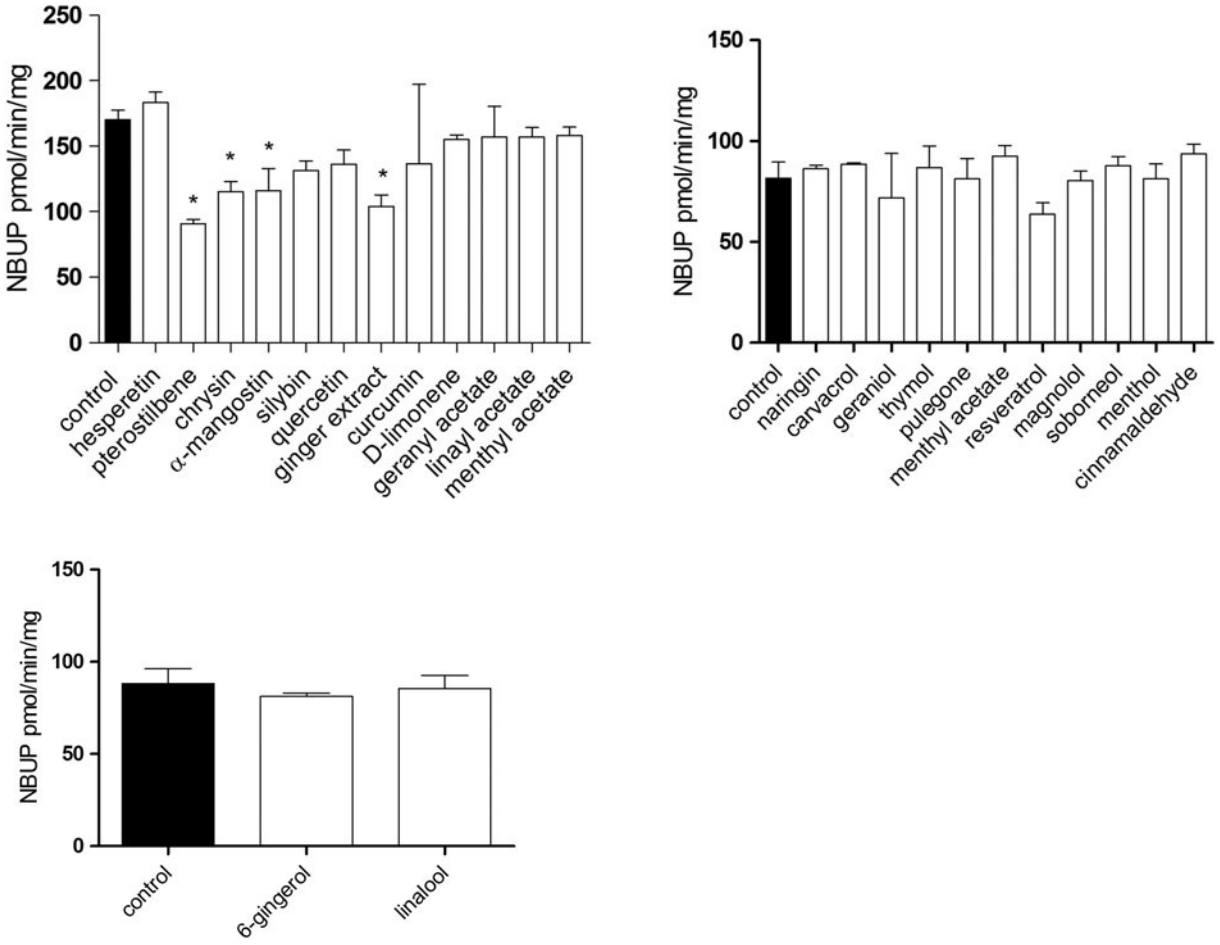

Fig 3.4 (c): Norbuprenorphine (NBUP) formation with and without inhibitors in pooled HIM; Lot 1410074. Data represent mean ± SD of buprenorphine glucuronide or norbuprenorphine formation rate. All the determinations were performed in triplicate, except menthol and carvacrol (n = 2). Panels represent separate experiments. Asterisk indicates $p < 0.05$. t-Anethole was also tested (n = 2) but did not appear different from the control

(d)

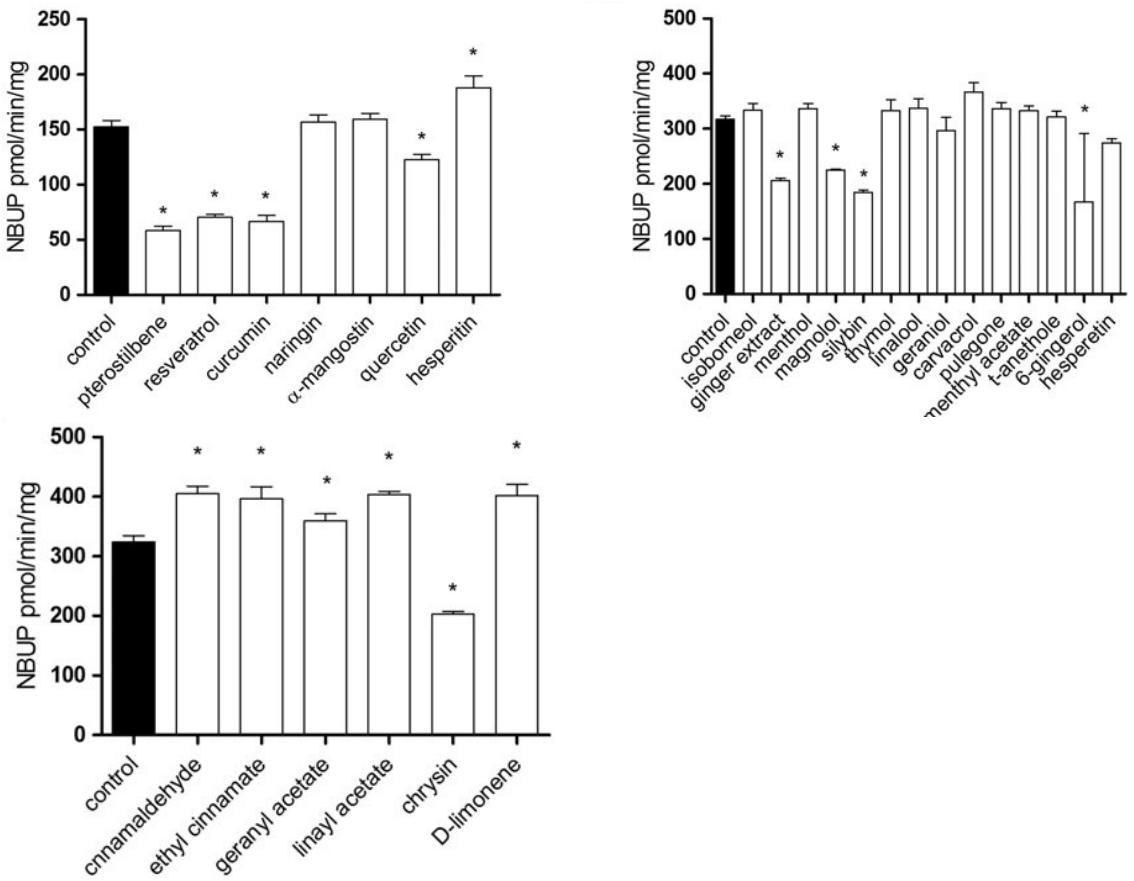

Fig 3.4 (d): Norbuprenorphine (NBUP) formation with and without inhibitors in pooled HLM; Lot 1210347. Data represent mean ± SD of buprenorphine glucuronide or norbuprenorphine formation rate. All the determinations were performed in triplicate. Panels represent separate experiments. Asterisk indicates $p < 0.05$

3.4 Discussion

Oxidative and conjugative metabolism of buprenorphine has been extensively studied in several in vitro and in vivo systems [9, 10, 12, 14, 20, 67]. However, the contribution of the CYP vs the UGT pathway in the intestine and liver as well as the contribution of the two organs to the presystemic metabolism of buprenorphine has not been well studied. Cubitt et al. reported that the intestinal oxidation of buprenorphine was significantly higher than the hepatic oxidation and liver was reported to be the major site for buprenorphine glucuronidation [67]. Our *in vitro* results and corresponding extrapolations are in agreement with the Cubitt et al. study [67]. Oxidation appears to be the dominant pathway in both the gut wall and liver with a 6-fold greater hepatic intrinsic clearance and 3-fold higher intestinal intrinsic clearance over glucuronidation. Furthermore, Rouguieg et al. reported a norbuprenorphine glucuronide formation rate in HLM of 51.8 pmol/mg/min at 5 μM norbuprenorphine; they also reported sigmoidal kinetic parameters for buprenorphine glucuronide formation in HLM [14]. From the latter, a rate of buprenorphine glucuronide formation at 5 μM is calculated to be 247 pmol/mg/min; thus, the norbuprenorphine glucuronide formation rate is substantially lower than the buprenorphine glucuronide formation rate, which is also less than the norbuprenorphine formation rate [14]. Using well-stirred model, the intestinal extraction was predicted to be 90.5% and the hepatic extraction to be 71%, resulting in a predicted F_{oral} of 2.75%. Thus, buprenorphine given orally would be expected to undergo significant presystemic metabolism in both the intestine as well as in the liver. Previous oral studies in humans indicate buprenorphine displays an F_{oral} of <15%, which is consistent with our results [8, 10, 16]. However, most of these studies do not provide a

detailed description of how the determination of F_{oral} was made. Also, buprenorphine was administered to a limited number (< 4) of healthy volunteers in these studies. Hence, our IVIVE predictions cannot be validated accurately due to lack of robust *in vivo* information on oral bioavailability of buprenorphine.

Increasing the dose to improve the oral bioavailability of BUP does not appear to be a feasible strategy. 8mg of sublingually administered BUP is reported to exhibit about 42% bioavailability [7]. Assuming an F_{oral} of 3%, the sublingual dose (8 mg) would have to be increased to 107 mg to achieve an oral bioavailability similar to the sublingual bioavailability. One gram of USP grade BUP hydrochloride (from Medisca) costs about $581 [100]. 30 units of Suboxone comprising 8 mg BUP (and 2 mg naloxone) cost about $348 [101]. Thus, a formulation with 107 mg BUP would increase the price exponentially (by atleast 13 fold), making it an economically unviable strategy. In addition, administering a higher oral dose would not address the issue of the large variability in the systemic availability and exposure shown by a highly extracted drug like BUP. On the other hand, co-administering herbal (i.e. GRAS or dietary compounds) inhibitors as bioenhancers of BUP affords an economical strategy to not only improve the PK properties of BUP but also reduce the variability associated with them.

From these screening studies, chrysin, curcumin, ginger extract, hesperetin, 6-gingerol, α-mangostin, magnolol, quercetin, pterostilbene, resveratrol and silybin were identified as preferred inhibitors. These inhibitors (at 25 μM concentration) produced ≥50% UGT and/or ≥30% CYP inhibition (Table 3.4).

Table 3.4: List of preferred inhibitors

Inhibitor	Formation (% of control) in pooled HIM		Formation (% of control) in pooled HLM		FDA status[a]	Maximum human dose (mg)[b]
	CYP	UGT	CYP	UGT		1000
Chrysin	67.7±7.5	67.6±8.2	62.5±4.0	36.1±8.4	DS	500
Curcumin	80.1±44	13.9±8.6	43.6±9.4	16.5±8.7	DS	600
Ginger extract	61.1±9.2	35.1±8.4	65.1±2.6	18.2±10	F, DS	38[c]
6-gingerol	92.0±9.3	53.9±9.3	52.6±75	51.7±9.3	DS	1000
Hesperitin	108±5.6	60.4±9.3	123±6.9	32.4±8.8	DS	150
α- Mangostin	68.1±15	37.9±7.9	104±5.2	51.8±10	DS	1200
Pterostilbene	53.3±3.5	94.0±9.6	38.2±7.9	68.2±8.2	G, DS	2000
Quercetin	79.9±8.7	49.3±9.5	80.6±5.4	23.8±8.1	G, DS	500
Resveratrol	78.1±13	70.3±10	46.1±5.4	58.2±12	G, DS	480
Silybin	77.1±6.6	36.5±8.0	58.3±2.9	37.2±8.3	DS	1000

a: G – GRAS, F – food additive (EAFUS), DS – dietary supplement
b: Doses taken from FDA-approved use as GRAS substance or food additive, or current usage as dietary supplement, whichever is higher.
c: assuming 6.3% 6-gingerol content in ginger extract [102]

The apparent stimulation of glucuronidation and/or oxidation by certain compounds is curious. Being a microsomal system, the regulation of expression is obviously impossible, while any detergent-based or pore-forming activity of the compounds would be overwhelmed by our use of alamethicin. Similarly, gefitinib was reported to activate CYP3A in mouse and human hepatic microsomes [103]. One of the possible reasons explaining the apparent stimulation of UGT and/or CYP metabolism by certain compounds such as D-limonene could be a cooperative interaction between CYP/CYP or UGT/UGT enzymes. Several studies have reported that certain UGT isoforms such as UGT1A1, 1A3, 1A9, 2B7 etc. undergo oligomerization and can possibly act as cooperative ligand-binding multisubunit enzymes [104, 105]. Such oligomerization can result in conformational changes leading to stimulation of the glucuronidation activity and enhancement of substrate affinity [105]. Recent studies have also reported that CYP–CYP interactions can occur among the same (homo-oligomer) and different

(hetero-oligomer) CYP isoforms [106]. This can significantly affect the functional capacity of the CYP enzymes and the substrate specificity. Also, some CYP3A4 substrates do not follow Michaelis-Menten kinetics instead exhibiting positive cooperativity or simultaneous activation of the enzyme by a second substrate [95]. Hosea et al. has shown that the CYP3A4 active site is large enough to allow binding of more than one substrate molecule [107]. Thus, the observed stimulation of norbuprenorphine or buprenorphine glucuronide formation could also be due to allosteric effects. However, the interactions between buprenorphine and the putative inhibitors are difficult to predict given the current understanding of the enzyme structures as well as the occurrence of conflicting effects such as simultaneous inhibition and activation of the enzymes. Thus, further studies would be needed to elucidate the exact mechanism by which these compounds stimulate metabolite formation.

The approach of using GRAS or dietary compounds as inhibitors of presystemic metabolism would preferably only inhibit intestinal and hepatic enzymes during absorption, and would preferably not affect systemic clearance. In that case, undesirable pharmacokinetic interactions with other medications could easily be avoided. This would depend upon the chosen compounds resulting in low systemic exposure. In fact, this is reasonably well supported by several published studies. For example, following doses of 2 g of ginger, 6-gingerol was undetectable (< 0.1 μg/ ml; 0.34 μM) in human plasma [34]. Next, in human subjects receiving 5g oral resveratrol, peak plasma concentrations reached only 2.4 μM [108]. Also, patients receiving up to 8 g oral curcumin had serum concentrations up to 3.6 μM [109]. Additionally, the peak plasma concentration of quercetin following a 50 mg oral dose was 0.29 μM [110]. Finally, in a separate study, on

day 7 of dosing with quercetin 150 mg orally, the median peak plasma concentration of quercetin was 0.43 μM [111]. While a comprehensive review of human PK of all of the compounds used in the present study is outside the scope, these and other published data suggest that these compounds generally reach low circulating plasma concentrations and are thus unlikely to have significant effects on systemic clearance mechanisms.

Furthermore, the approach would depend upon the ability of the inhibitors to be clinically administered to humans in doses that would be effective at inhibiting presystemic intestinal and hepatic metabolism, while not causing toxicities. Table 3.4 lists the top inhibitors (as discussed previously), residual metabolite formation activity, their FDA regulatory status and their current maximum dose. All the compounds are able to be taken by humans as either GRAS or dietary components. Maximal intestinal concentrations of inhibitors will depend upon their dose, solubility, and absorption rate. For example, dose will likely be concentration limiting for 6-gingerol (38 mg/ 250 ml ~ 500 μM), while solubility will be concentration-limiting for curcumin (potentially enhanced by lipid formulations) [112].

These results demonstrate the feasibility of our research hypothesis of using GRAS or dietary compounds to inhibit the presystemic metabolism of buprenorphine and thus improve its oral bioavailability. Inhibition of at least 50% of hepatic extraction and 75% of intestinal metabolism would lead to a predicted F_{oral} equivalent to sublingual buprenorphine. Thus, an oral formulation of buprenorphine and these inhibitor treatments or their combinations has promising potential to serve as an efficacious alternative to sublingual buprenorphine.

Based on the published data (mainly animal; limited human data), buprenorphine

as well as its metabolites appear to undergo enterohepatic recirculation (EHC) following oral administration [9, 113]. The route of administration is reported to have a significant influence on the magnitude of enterohepatic recirculation. Brewster et al. reported that the intrahepatoportal route was associated with greater enterohepatic recirculation (91%) in comparison with intraduodenal (46%) or sublingual administration of buprenorphine in rats [9]. Most of the inhibitors are extensively metabolized via conjugation by UGTs and SULTs in the gut wall and liver [114-119]. The available literature in animal models and/or humans suggests that the parent compounds as well as their conjugates can undergo enterohepatic recirculation to varying extents [114-118]. Although limited information is available on the elimination half-lives in humans for several of the tested inhibitors, most of these are reported to exhibit relatively short to intermediate elimination half-lives in rats compared with buprenorphine [9, 114-118]. Hence, while the inhibitors could potentially affect the enterohepatic recirculation of buprenorphine, the effect might not be clinically significant because of the relatively short residence times of inhibitors compared with that of buprenorphine. However, it is possible that the buprenorphine + inhibitor(s) combination might exhibit different enterohepatic recirculation characteristics, which may not be predicted from their individual enterohepatic recirculation patterns. Further *in vivo* studies following the co-administration of buprenorphine and inhibitors would be required to evaluate the effect on enterohepatic recirculation of buprenorphine.

Future studies will also focus on determining the potency of the top inhibitors determined from this screening study. Various combinations of these inhibitor treatments will also be evaluated to investigate the nature of interaction (synergistic, additive or

antagonistic) between them. Isoform-specific investigations will also be helpful to avoid undesirable interactions. The intrinsic clearance of buprenorphine in the presence of these inhibitors or their combinations will be determined to predict the oral bioavailability of buprenorphine. These studies will further help to optimize an oral formulation of buprenorphine with reduced variability and comparable or higher bioavailability.

3.5 Conclusion

These results affirm our proposed approach of using GRAS or dietary compounds to inhibit the presystemic metabolism of buprenorphine and thus improve its oral bioavailability. Our IVIVE studies indicated that both liver and intestine contributed extensively to the presystemic metabolism of buprenorphine and oxidation was the predominant pathway over glucuronidation in both liver and the intestine. Selected inhibitors displayed inhibitions of greater than 30% and 50% for oxidation and glucuronidation, respectively. These inhibitors exhibit the potential to improve the low oral bioavailability of buprenorphine and would aid in reducing the in vivo variability associated with it. The results from the present study will aid in the selection of inhibitors or their combinations to effectively reduce intestinal and hepatic presystemic metabolism of buprenorphine. An oral formulation of buprenorphine and these inhibitors or their combinations has potential to substitute for sublingual buprenorphine to improve patient compliance, acceptability and therapeutic outcomes. Future studies will focus on defining feasible effective doses and combinations of the top inhibitors.

Chapter 4: Determination of Potency of Inhibition of α-Mangostin, Chrysin, Ginger Extract, Pterostilbene and Silybin Towards Oxidative and Conjugative Metabolism of Buprenorphine Using Intestinal and Liver Microsomes

4.1 Introduction

About 73% of the top 200 drugs are cleared by metabolism, of which the members of the cytochrome P450 (CYP) superfamily account for about 75%, with CYP3A family being the major (46%) contributor [64]. Among the phase II metabolic pathways, UGTs play a crucial role in metabolism of 20-30% of currently marketed drugs [120] and are responsible for 40-70% of all drugs metabolized through conjugation reactions [121-124]. The UGTs occupy second position after CYPs as the primary metabolic pathway, accounting for metabolism of 10% of the top 200 drugs [64, 125]. Both the enzyme families significantly contribute to the presystemic metabolism of drugs resulting in poor and variable oral bioavailability. Buprenorphine (BUP) serves as an apt example because it suffers from poor and variable oral bioavailability due to extensive presystemic metabolism by CYPs (CYP3A4 – major, CYPs 2C8, 2C9 - minor) to form norbuprenorphine (NBUP) [12] and UGTs (1A1, 1A3 and 2B7) to form buprenorphine glucuronide (BUPG) [3, 14]. The primary oxidative metabolite NBUP further undergoes glucuronidation (UGTs – 1A1 and 1A3) to form norbuprenorphine glucuronide (NBUPG) [3, 14]. Previous studies using pooled human intestinal (HIM) and liver (HLM) microsomes suggest oxidation to be the major metabolic pathway for BUP in both intestine and liver [30, 67, 126].

As discussed in the previous chapter, several *generally recognized as safe* (GRAS) compounds, dietary supplements and dietary constituents have been reported to

enhance bioavailability of orally administered drugs [21-26]. The mechanisms hypothesized to be responsible for this bioenhancement include but are not limited to i) improved GI solubility ii) delayed GI transit and emptying time iii) reduction in gastric acid secretion iv) increased intestinal permeation by modification of GI membrane v) increased intestinal perfusion vi) reduction in intestinal motility vi) inhibition of presystemic intestinal and hepatic metabolism vii) increased bile flow from liver [127, 128]. Our research hypothesis is based on the bioenhancement achieved through metabolic inhibition of CYP and UGT enzymes.

Chapter 3 evaluated the potential of 27 compounds to inhibit the oxidative and conjugative metabolism of BUP in pooled human intestinal (HIM) and liver microsomes (HLM). A retrospective filter was applied to the results where compounds exhibiting ≥ 50% inhibition of BUPG formation and/or ≥ 30% inhibition of NBUP formation were identified as preferred inhibitors. The purpose of this retrospective filter was to identify the potential inhibitor candidates from rest of the test compounds. Chrysin, curcumin, ginger extract, 6-gingerol, hesperitin, α–mangostin, pterostilbene, quercetin, resveratrol and silybin appeared to be the preferred inhibitors of BUP metabolism in intestinal and/or liver microsomes [30]. The next step was to further isolate and shortlist 5 inhibitor candidates to study their potency of inhibition towards the oxidative and conjugative metabolism of BUP.

On the basis of our IVIVE predictions and previous publications, the contribution of the gut wall to the presystemic metabolism of BUP appears to be significant [30, 67, 126]. Hence, it was pivotal that the shortlisted compounds inhibit the major metabolic pathway i.e. CYP metabolism of BUP, ideally in both intestinal and liver microsomes. In

addition, intestine represents the first major biological site of metabolism for orally administered compounds. Thus, preference was given to the candidates inhibiting CYP metabolism of BUP in the HIM. Most of the test compounds show poor aqueous solubility and extensive metabolism by conjugative enzymes resulting in low to intermediate oral bioavailability [34, 108, 110, 114-119, 129-131]. Hence, most of these inhibitors have a higher probability of inhibiting the intestinal metabolism of BUP as compared to its hepatic metabolism. The second factor considered in the screening process was inhibition of BUPG formation, ideally in both HIM and HLM. Due to the reasons explained earlier, preference was given to candidates inhibiting glucuronidation of BUP in HIM. The physicochemical characteristics of the inhibitors influencing their GI solubility and permeability were also evaluated. The Biopharmaceutics Classification System (BCS) was used to compare their solubility and permeability characteristics [132]. A BCS class of I (i.e. high solubility and high permeability) was highly preferable. However, since most of the compounds showed poor aqueous solubility, they appeared to be BCS class II or IV compounds, with the exception of 6-gingerol, which belonged to BCS class I [131]. Lastly, the maximum daily dose allowed in humans was also considered while shortlisting the inhibitors. An inhibitor with a higher daily dose was preferred, as this would maximize the probability of achieving higher local and systemic inhibitor concentrations and subsequently help in achieving greater inhibition of the metabolism of BUP in the intestine and liver. The pharmacokinetic characteristics of these inhibitors in animals and/or humans were also studied using previous publications [34, 108, 110, 114-119, 129, 130, 133-135]. However, most of these compounds except pterostilbene are reported to exhibit low oral bioavailability [34, 108, 110, 114-119, 129,

130, 133-135]. Also, limited information is available on the oral disposition of these compounds in humans. Hence, oral bioavailability or pharmacokinetic features of the inhibitors could not be used as a distinguishing criterion in the selection process. Thus, based on the aforementioned factors (inhibition of CYP and UGT metabolism in HIM and HLM, BCS class and maximum daily dose in humans), α-mangostin chrysin, ginger extract, pterostilbene and silybin were shortlisted for further studies (Table 4.1). This chapter aims at determination of the potency of inhibition (i.e. IC_{50}) of CYP and UGT metabolism of BUP by these five inhibitor candidates in pooled HIM and HLM.

Table 4.1: Factors considered to shortlist inhibitors for further study

Inhibitors	HIM		HLM		BCS class	Maximum human dose[b] (mg/day)
	CYP	UGT	CYP	UGT		
chrysin	✓	✗	✓	✓	**II**	**1000**
curcumin	✗	✓	✓	✓	IV	500
ginger extract	✓	✓	✓	✓	**II**	**600**
6-gingerol	✗	✓	✓	✗	I	38[c]
hesperetin	✗	✗	✗	✓	II	1000
α-mangostin	✓	✓	✗	✗	**IV[a]**	**150**
pterostilbene	✓	✗	✓	✗	**II[a]**	**1800**
quercetin	✗	✓	✗	✓	II	2000
resveratrol	✗	✓	✓	✗	II	500
silybin	✗	✓	✓	✓	**II**	**480**

Inhibitors highlighted in orange were identified as preferred inhibitors.
[a]Estimated from solubility and permeability data [129, 136-140]
[b]Doses taken from FDA-approved use as GRAS substance or food additive, or current usage as dietary supplement, whichever is higher.
[c]Assuming 6.3% 6-gingerol content in ginger extract [102]

4.2 Materials and Methods

4.2.1 Chemicals and Reagents

Ginger extract, tris hydrochloride, acetic acid and UDPGA were obtained from Sigma Aldrich (St. Louis, MO), chrysin from Hawkins Pharmaceutical Group

(Minneapoils, MN), silybin from Cayman Chemical Company (Ann Arbor, MI), pterostilbene from AK Scientific (Union City, CA) and α–mangostin from Indofine Chemical Company (Hillsborough, NJ). Saccharolactone was purchased from Calbiochem (La Jolla, CA), magnesium chloride ($MgCl_2$) and dimethyl sulfoxide (DMSO) from Fisher Scientific (Fairlawn, NJ). Alamethicin was obtained from Enzo Life sciences (Farmingdale, NY), potassium monophosphate and dibasic potassium phosphate from J.T. Baker (Center Valley, PA). Buprenorphine HCl and naloxone HCl were purchased from Medisca (Plattsburgh, NY), NBUP and BUPG from Cerilliant (Round Rock, TX), NADPH from Akron Biotech (Boca Raton, FL). All the solvents used were of high-performance liquid chromatography (HPLC) grade and were purchased from VWR (Radnor, PA). Pooled human liver (pool of 200 donors, Lot 1410230) and intestinal microsomes (pool of 10 donors, Lot 1417004) were obtained from Xenotech LLC (Lenexa, KS).

4.2.2 Inhibition studies in pooled microsomes

The oxidative and conjugative metabolism of BUP was studied individually in pooled HIM and HLM as described in Chapter 3. The inhibitory potency i.e. IC_{50} was determined by incubating BUP (11 μM) with 0.1 mg/ml HLM (Lot: 1410230) or 0.4 mg/ml HIM (Lot: 1417004) for 15 min (CYP) or 30 min (UGT) in presence of a wide concentration range of inhibitors (as shown in Figs. 4.1 to 4.10). Linearity of metabolite formation with time was established as described in Chapter 3. The oxidative inhibition studies were repeated thrice and conjugative studies twice to ensure reproducibility of the IC_{50} values. Duplicate measurements were performed for each inhibitor concentration on

each inhibition curve. The resulting data was fit to the following standard four-parameter equation using Prism v7.0 (GraphPad, La Jolla, CA):

$$Y = Bottom + \frac{(Top - Bottom)}{1 + \frac{X^h}{IC_{50}^h}} \quad (1)$$

where Y = Metabolite formation (expressed as % of control), X = inhibitor concentration (μM), IC_{50} = inhibitor concentration producing 50% inhibition of metabolite formation, h = Hill slope of the inhibition curve and Top & Bottom = Metabolite formation at lowest and highest inhibitor concentration, respectively. Initially, two models with Bottom = 0 versus bottom ≠ 0 were compared using Akaike Information Criterion (AIC). The model chosen statistically was then modified to compare Hill slope = 1 versus Hill slope ≠ 1. The statistically preferred model was chosen and corresponding results for the 4 parameters i.e. IC_{50}, Hill slope, Top and Bottom were noted.

4.2.3 Analysis of the combination of Pterostilbene and Ginger extract

The effect of equipotent combination of pterostilbene and ginger extract on CYP and UGT pathways was studied individually in HIM (BUP=11μM). These inhibitors were combined in an equipotent manner (as a ratio of their IC_{50}) and a wide range of concentrations was studied to determine the inhibitor ratio i.e. IR_{50}. IR_{50} represents the concentration of the combination that produces 50% inhibition of metabolite formation. As with earlier inhibition studies, these combination treatments were evaluated three times for their potential to inhibit oxidative metabolism and twice for inhibition of glucuronidation of BUP in pooled HIM. The nature of interaction in the combination was determined using the curve shift analysis method as previously described [141]. Briefly, the average inhibition curves of pterostilbene, ginger extract and their equipotent combination were plotted on the same graph; where X axis (I/IC_{50}) represents the IC_{50}

normalized concentrations of the inhibitors and Y axis indicates the metabolite formation (NBUP or BUPG) expressed as % of control. A leftward shift in the curve of the combination with respect to the individual inhibitors would indicate a synergistic interaction whereas a rightward shift would indicate an antagonistic interaction. No significant shift in the combination curve with respect to the curves of the individual inhibitors would indicate additive interactions in the combination.

4.2.4 Sample analysis

BUP and its metabolites BUPG and NBUP were quantified using a previously validated method as described in Chapter 3 [90]. The same HPLC method was also used for quantification of chrysin, α–mangostin, pterostilbene and silybin using UV spectrometric detection. Silybin, chrysin, pterostilbene and α-mangostin eluted at 4.4 min, 4.97 min, 5.1 min and 6.1 min, respectively. Linear standard curves with $R^2 \geq 0.99$ were obtained from 0.75-48 μg/ml for silybin, 0.40-25 μg/ml for chrysin, 0.40-26 μg/ml for pterostilbene and 0.64–41 μg/ml for α-mangostin. Components of the ginger extract could not be quantified using this analytical method.

4.3 Results

4.3.1 Inhibition studies in pooled microsomes

The apparent IC_{50} values of α-mangostin, chrysin, ginger extract, pterostilbene and silybin in HIM and HLM are as shown in Tables 4.1 – 4.4 and figures 4.1 to 4.10. Pterostilbene appeared to the most potent inhibitor of NBUP formation in both HIM (IC_{50} = 1.30 ± 0.89 μM) and HLM (IC_{50} = 0.79 ± 0.10 μM). Ginger extract exhibited moderate potency towards inhibition of NBUP and BUPG formation in HIM and HLM with apparent IC_{50} values between 10 – 27 μM. Similarly, α-mangostin, chrysin and silybin

appeared to be moderately potent towards inhibition of NBUP formation in HIM and HLM. However, α-mangostin in HIM (IC_{50} = 5.57 ± 1.00 μM) and silybin in HLM (IC_{50} = 1.21 ± 0.34 μM) appeared to be most potent in inhibiting the glucuronidation of BUP. Most inhibitor treatments were able to achieve complete inhibition of oxidation and glucuronidation of BUP except pterostilbene, chrysin in HIM and silybin in HLM. Pterostilbene (bottom = 28.0 ± 6.4%) and chrysin (bottom = 29.8 ± 2.1%) could achieve maximum inhibition of 72% and 70% respectively for NBUP formation in HIM and silybin showed 56% maximum inhibition of BUPG formation in HLM. The IC_{50} and Hill slope values for all the inhibitor treatments were fairly reproducible with < 2 fold difference between different experiments and with acceptable R^2 values, typically >0.95.

Figure 4.1: Inhibition of NBUP formation by α-mangostin

(a)

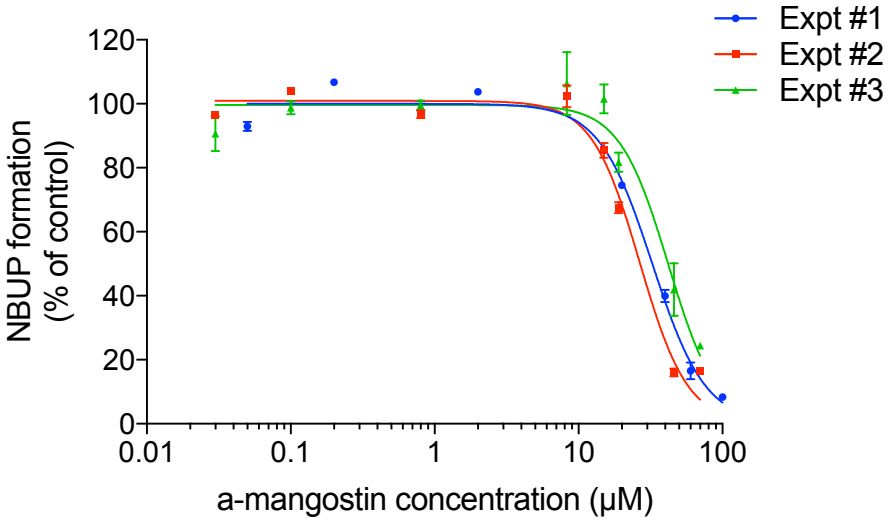

Fig 4.1 (a): Inhibition of NBUP formation by α-mangostin in pooled HIM. Data represent mean ± SD of NBUP formation rate expressed as % of control. All the determinations were performed in duplicate. Each curve represents a separate experiment. In experiments 1, 2 and 3, the NBUP formation in control was 125 ± 2.75, 156 ± 3.08 and 88.6 ± 2.14 pmol/min/mg protein and R^2 value was 0.99, 0.98 and 0.94, respectively.

(b)

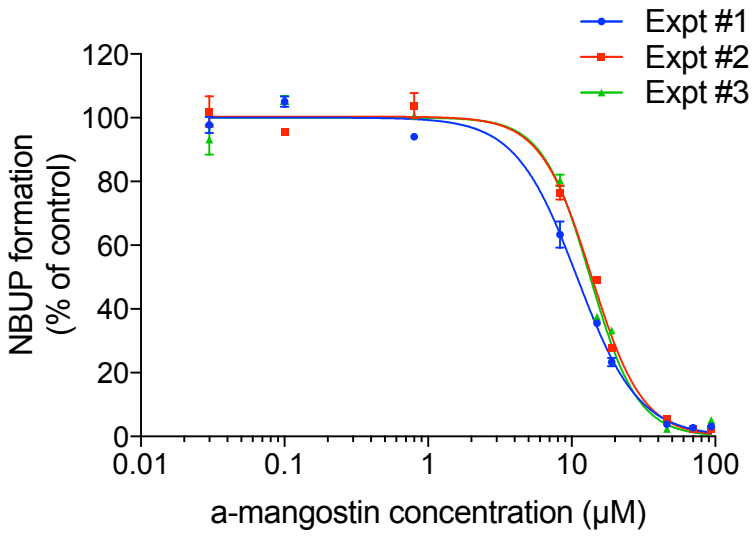

Fig 4.1 (b): Inhibition of NBUP formation by α-mangostin in pooled HLM. Data represent mean ± SD of NBUP formation rate expressed as % of control. All the determinations were performed in duplicate. Each curve represents a separate experiment. In experiments 1, 2 and 3, the NBUP formation in control was 346 ± 6.00, 439 ± 6.85 and 348 ± 8.61 pmol/min/mg protein and R^2 value was 1.00, 0.99 and 0.99, respectively.

Figure 4.2: Inhibition of BUPG formation by α-mangostin

(a)

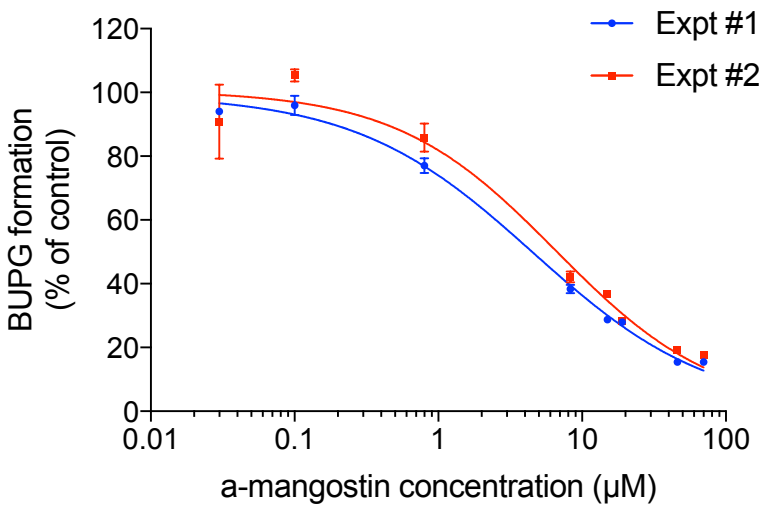

Fig 4.2 (a): Inhibition of BUPG formation by α-mangostin in pooled HIM. Data represent mean ± SD of BUPG formation rate expressed as % of control. All the determinations were performed in duplicate. Each curve represents a separate experiment. In experiments 1 and 2, the BUPG formation in control was 9.15 ± 0.19, and 9.01 ± 0.35 pmol/min/mg protein and R^2 value was 1.00 and 0.97, respectively.

(b)

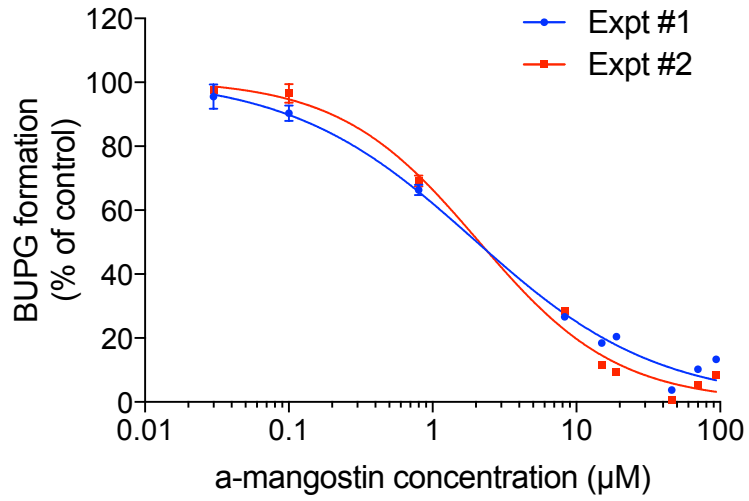

Fig 4.2 (b): Inhibition of BUPG formation by α-mangostin in pooled HLM. Data represent mean ± SD of BUPG formation rate expressed as % of control. All the determinations were performed in duplicate. Each curve represents a separate experiment. In experiments 1 and 2, the BUPG formation in control was 288 ± 10.8, and 270 ± 6.67 pmol/min/mg protein and R^2 value was 0.99 and 0.99, respectively.

Figure 4.3: Inhibition of NBUP formation by chrysin

(a)

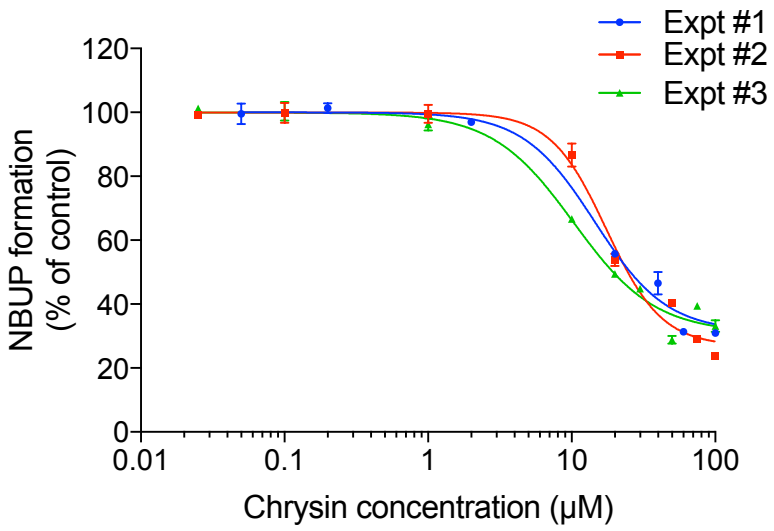

Fig 4.3 (a): Inhibition of NBUP formation by chrysin in pooled HIM. Data represent mean ± SD of NBUP formation rate expressed as % of control. All the determinations were performed in duplicate. Each curve represents a separate experiment. In experiments 1, 2 and 3, the NBUP formation in control was 111 ± 2.06, 134 ± 2.44 and 119 ± 2.12 pmol/min/mg protein and R^2 value was 0.99, 0.98 and 0.98, respectively.

(b)

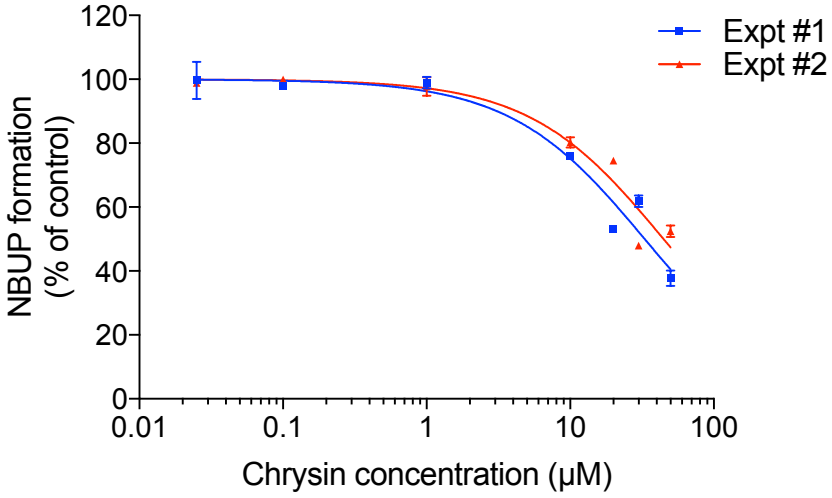

Fig 4.3 (b): Inhibition of NBUP formation by chrysin in pooled HLM. Data represent mean ± SD of NBUP formation rate expressed as % of control. All the determinations were performed in duplicate. Each curve represents a separate experiment. In experiments 1 and 2, the NBUP formation in control was 342 ± 9.96 and 285 ± 8.13 pmol/min/mg protein and R^2 value was 0.95 and 0.93 respectively.

Figure 4.4: Inhibition of BUPG formation by chrysin

(a)

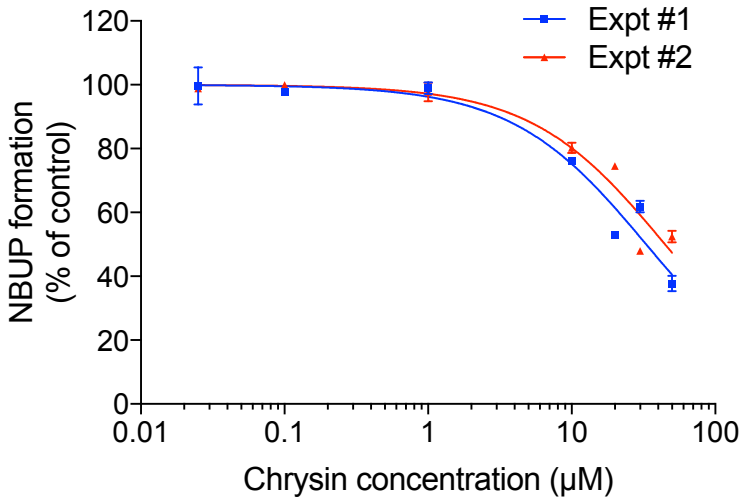

Fig 4.4 (a): Inhibition of BUPG formation by chrysin in pooled HIM. Data represent mean ± SD of BUPG formation rate expressed as % of control. All the determinations were performed in duplicate. Each curve represents a separate experiment. In experiments 1 and 2, the BUPG formation in control was 17.6 ± 0.59, and 16.2 ± 0.54 pmol/min/mg protein and R^2 value was 0.96 and 0.96, respectively.

(b)

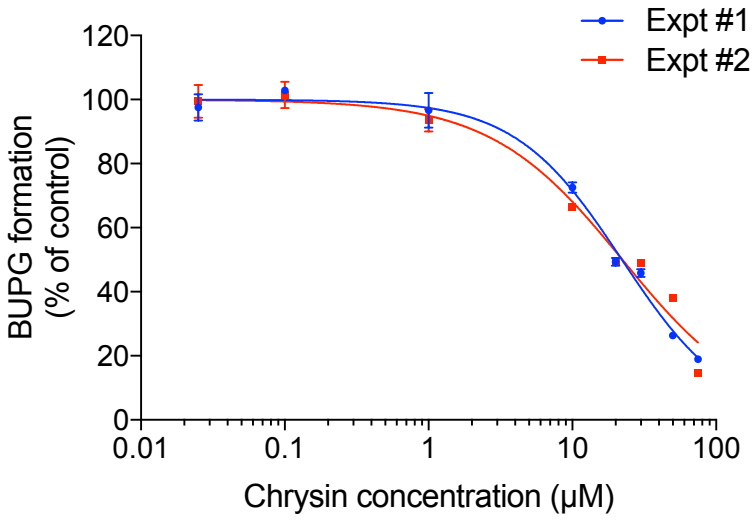

Fig 4.4 (b): Inhibition of BUPG formation by chrysin in pooled HLM. Data represent mean ± SD of BUPG formation rate expressed as % of control. All the determinations were performed in duplicate. Each curve represents a separate experiment. In experiments 1 and 2, the BUPG formation in control was 279 ± 4.31, and 263 ± 7.14 pmol/min/mg protein and R^2 value was 0.99 and 0.97, respectively.

Figure 4.5: Inhibition of NBUP formation by ginger extract

(a)

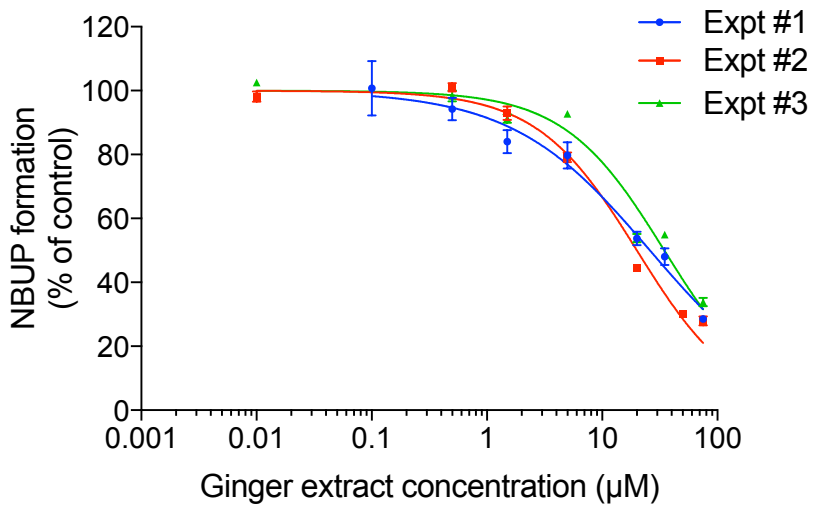

Fig 4.5 (a): Inhibition of NBUP formation by ginger extract in pooled HIM. Data represent mean ± SD of NBUP formation rate expressed as % of control. All the determinations were performed in duplicate. Each curve represents a separate experiment. In experiments 1, 2 and 3, the NBUP formation in control was 149 ± 5.20, 106 ± 3.17 and 140 ± 3.15 pmol/min/mg protein and R^2 value was 0.97, 0.98 and 0.96, respectively.

(b)

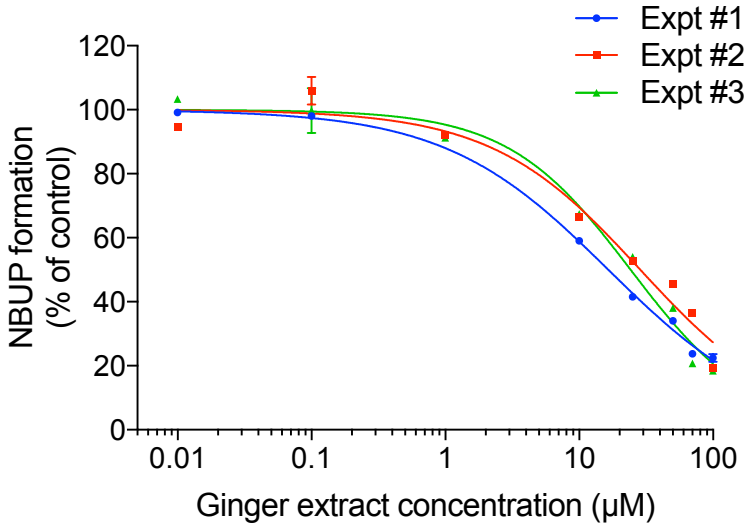

Fig 4.5 (b): Inhibition of NBUP formation by ginger extract in pooled HLM. Data represent mean ± SD of NBUP formation rate expressed as % of control. All the determinations were performed in duplicate. Each curve represents a separate experiment. In experiments 1 and 2, the NBUP formation in control was 488 ± 5.84, 405 ± 11.8 and 416 ± 9.16 pmol/min/mg protein and R^2 value was 1.00, 0.97 and 0.98 respectively.

Figure 4.6: Inhibition of BUPG formation by ginger extract

(a)

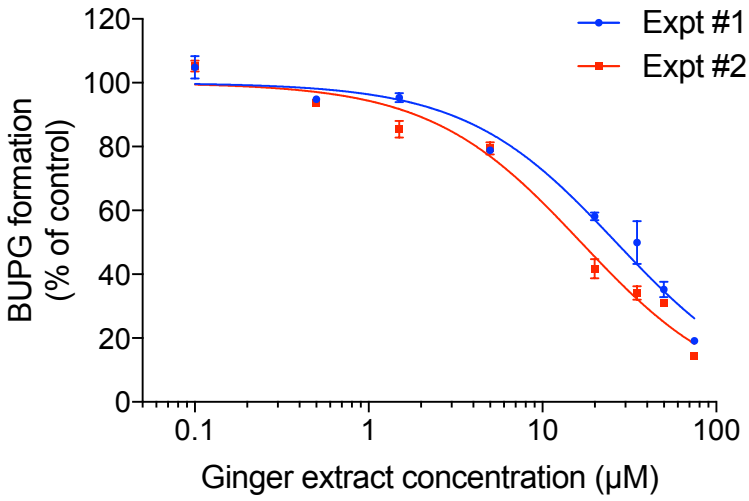

Fig 4.6 (a): Inhibition of BUPG formation by ginger extract in pooled HIM. Data represent mean ± SD of BUPG formation rate expressed as % of control. All the determinations were performed in duplicate. Each curve represents a separate experiment. In experiments 1 and 2, the BUPG formation in control was 8.36 ± 0.18, and 10.2 ± 0.25 pmol/min/mg protein and R^2 value was 0.97 and 0.98, respectively.

(b)

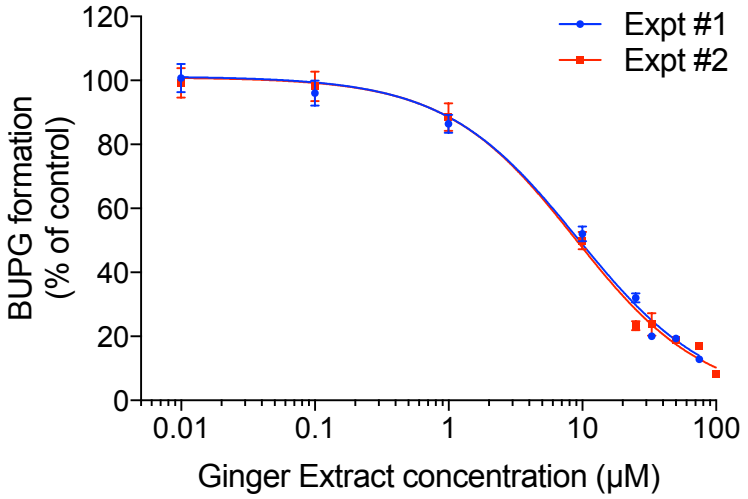

Fig 4.6 (b): Inhibition of BUPG formation by ginger extract in pooled HLM. Data represent mean ± SD of BUPG formation rate expressed as % of control. All the determinations were performed in duplicate. Each curve represents a separate experiment. In experiments 1 and 2, the BUPG formation in control was 236 ± 3.62, and 251 ± 3.82 pmol/min/mg protein and R^2 value was 0.99 and 0.99, respectively.

Figure 4.7: Inhibition of NBUP formation by pterostilbene

(a)

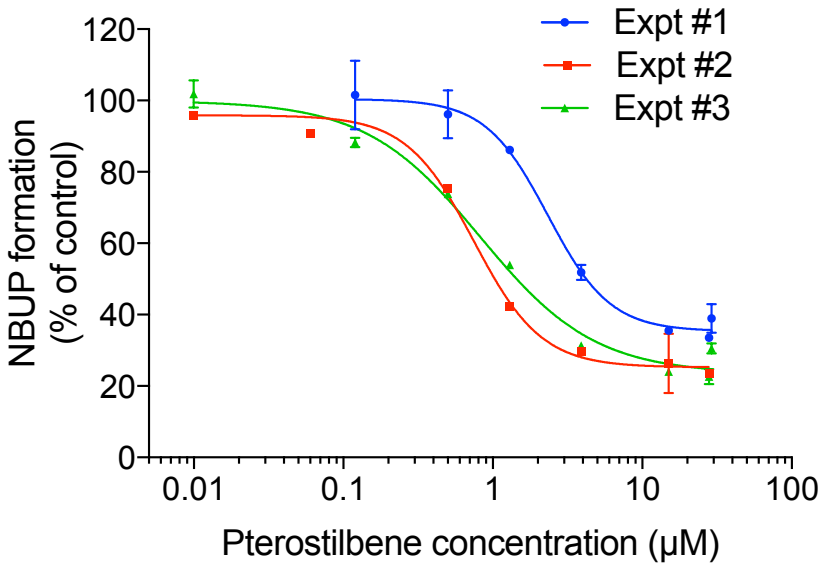

Fig 4.7 (a): Inhibition of NBUP formation by pterostilbene in pooled HIM. Data represent mean ± SD of NBUP formation rate expressed as % of control. All the determinations were performed in duplicate. Each curve represents a separate experiment. In experiments 1, 2 and 3, the NBUP formation in control was 93.5 ± 2.60, 156 ± 2.61 and 124 ± 1.79 pmol/min/mg protein and R^2 value was 0.98, 0.99 and 0.99, respectively.

(b)

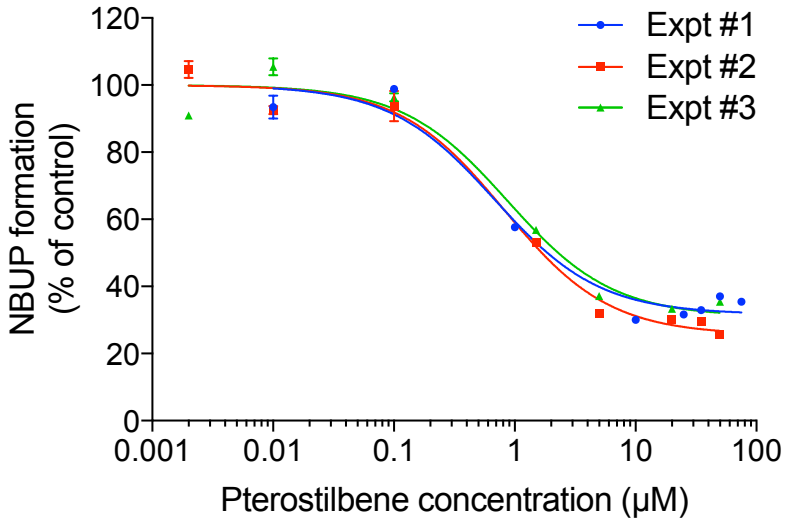

Fig 4.7 (b): Inhibition of NBUP formation by pterostilbene in pooled HLM. Data represent mean ± SD of NBUP formation rate expressed as % of control. All the determinations were performed in duplicate. Each curve represents a separate experiment. In experiments 1, 2 and 3, the NBUP formation in control was 389 ± 12.4, 420 ± 8.04 and 382 ± 9.50 pmol/min/mg protein and R^2 value was 0.97, 0.99 and 0.97, respectively.

Figure 4.8: Inhibition of BUPG formation by pterostilbene

(a)

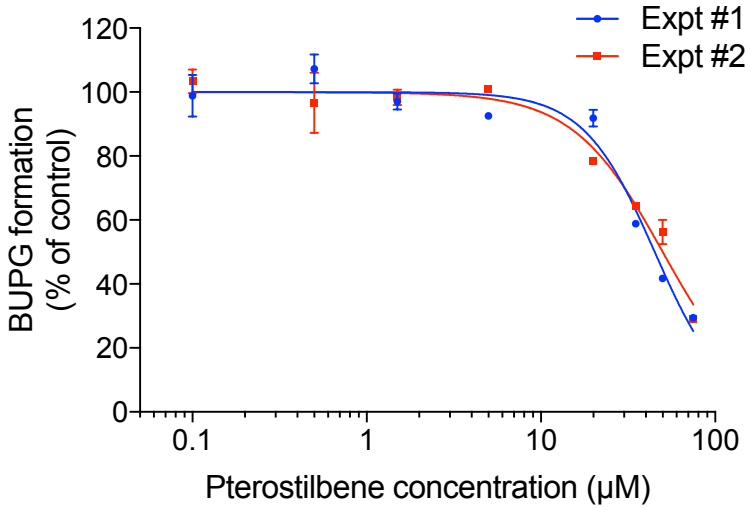

Fig 4.8 (a): Inhibition of BUPG formation by pterostilbene in pooled HIM. Data represent mean ± SD of BUPG formation rate expressed as % of control. All the determinations were performed in duplicate. Each curve represents a separate experiment. In experiments 1 and 2, the BUPG formation in control was 9.80 ± 0.21, and 10.7 ± 0.20 pmol/min/mg protein and R^2 value was 0.96 and 0.97, respectively.

(b)

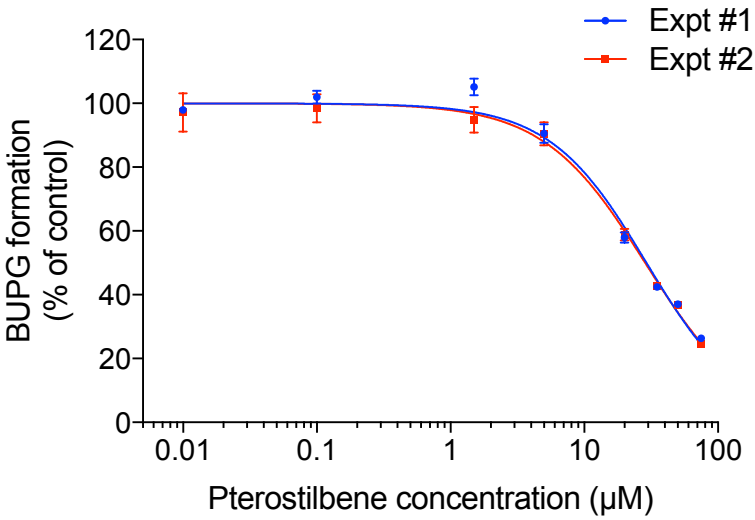

Fig 4.8 (b): Inhibition of BUPG formation by pterostilbene in pooled HLM. Data represent mean ± SD of BUPG formation rate expressed as % of control. All the determinations were performed in duplicate. Each curve represents a separate experiment. In experiments 1 and 2, the BUPG formation in control was 202 ± 3.54, and 240 ± 3.43 pmol/min/mg protein and R^2 value was 0.98 and 0.99, respectively

Figure 4.9: Inhibition of NBUP formation by silybin

(a)

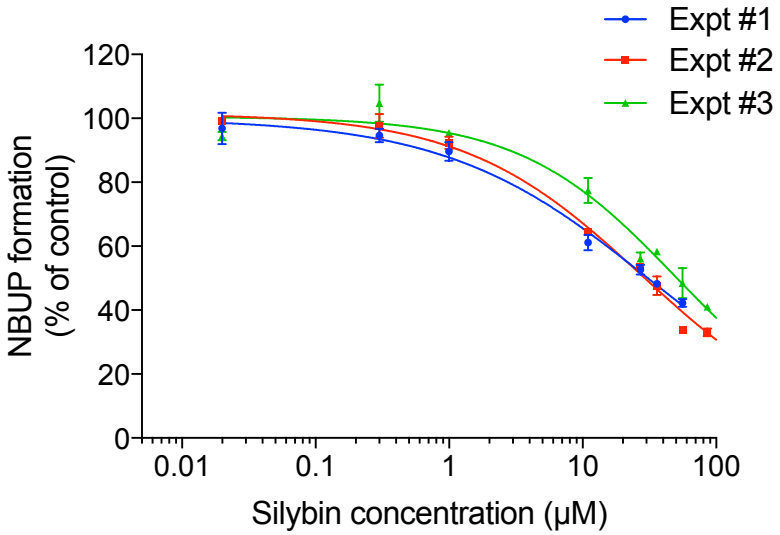

Fig 4.9 (a): Inhibition of NBUP formation by silybin in pooled HIM. Data represent mean ± SD of NBUP formation rate expressed as % of control. All the determinations were performed in duplicate. Each curve represents a separate experiment. In experiments 1, 2 and 3, the NBUP formation in control was 142 ± 3.76, 151 ± 2.44 and 199 ± 4.46 pmol/min/mg protein and R^2 value was 0.99, 0.99 and 0.97, respectively.

(b)

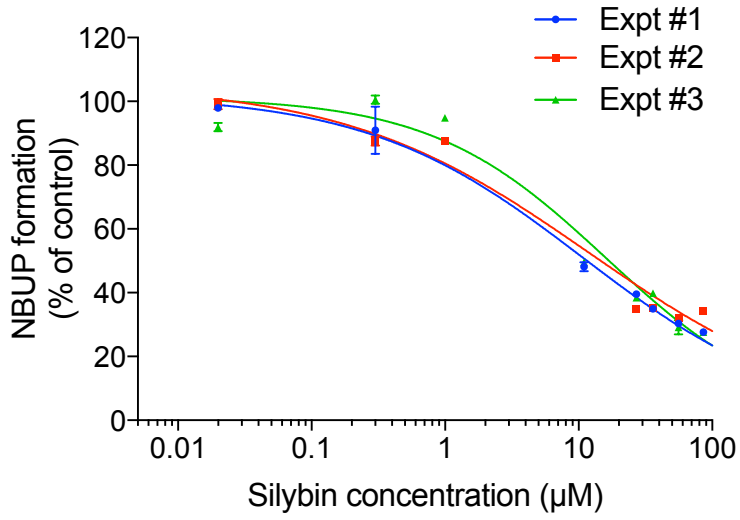

Fig 4.9 (b): Inhibition of NBUP formation by silybin in pooled HLM. Data represent mean ± SD of NBUP formation rate expressed as % of control. All the determinations were performed in duplicate. Each curve represents a separate experiment. In experiments 1, 2 and 3, the NBUP formation in control was 390 ± 10.7, 291 ± 14.0 and 295 ± 10.4 pmol/min/mg protein and R^2 value was 0.99, 0.97 and 0.96, respectively.

Figure 4.10: Inhibition of BUPG formation by silybin

(a)

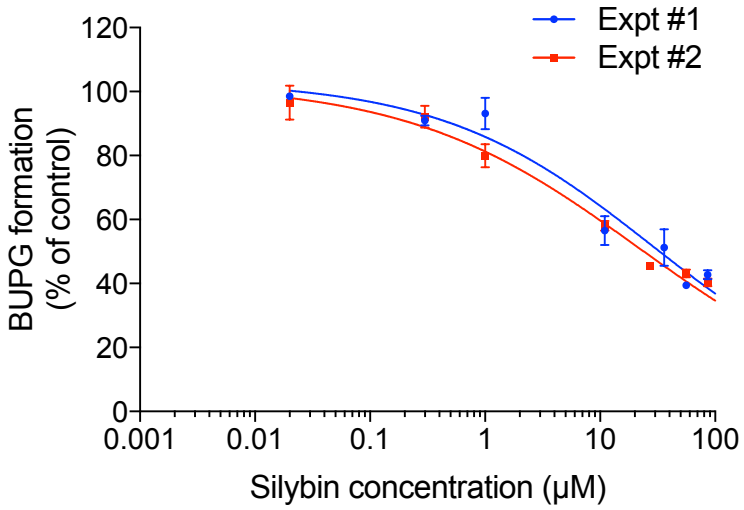

Fig 4.10 (a): Inhibition of BUPG formation by silybin in pooled HIM. Data represent mean ± SD of BUPG formation rate expressed as % of control. All the determinations were performed in duplicate. Each curve represents a separate experiment. In experiments 1 and 2, the BUPG formation in control was 14.3 ± 0.68, and 9.83 ± 0.56 pmol/min/mg protein and R^2 value was 0.96 and 0.98, respectively.

(b)

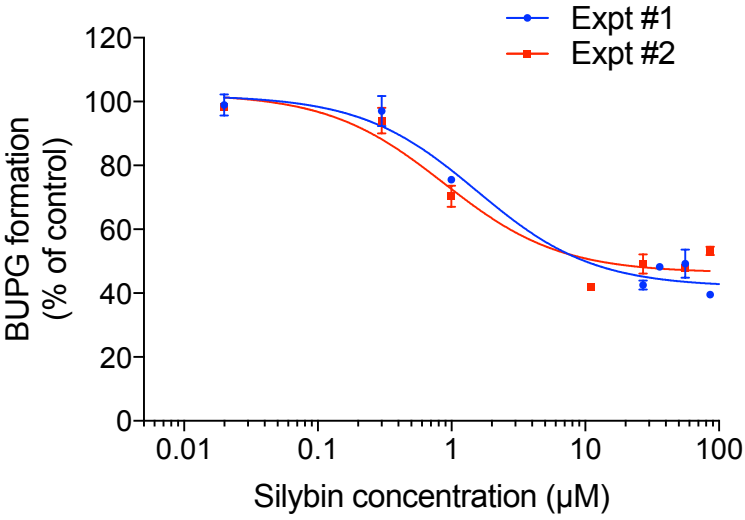

Fig 4.10 (b): Inhibition of BUPG formation by silybin in pooled HLM. Data represent mean ± SD of BUPG formation rate expressed as % of control. All the determinations were performed in duplicate. Each curve represents a separate experiment. In experiments 1 and 2, the BUPG formation in control was 211 ± 4.95 and 224 ± 6.80 pmol/min/mg protein and R^2 value was 0.97 and 0.94, respectively.

Table 4.2: Inhibition of NBUP formation in pooled HIM

Inhibitor	Inhibition of NBUP formation in pooled HIM		
	IC_{50} (μM)	Hill slope	Bottom (% of control)
α-mangostin	33.8 ±6.4	2.51 ± 0.1	0
Chrysin	14.1 ± 2.9	1.84 ± 0.3	29.8 ± 2.1
Ginger extract	26.9 ± 6.0	0.91 ± 0.1	0
Pterostilbene	1.30 ± 0.9	1.71 ± 0.5	28.0 ± 6.4
Silybin	36.2 ± 9.9	0.66 ± 0.1	0

Data represents mean ± SD of IC_{50}, Hill slope and bottom values observed from three separate inhibition experiments. All the determinations were performed in duplicate.

Table 4.3: Inhibition of NBUP formation in pooled HLM

Inhibitor	Inhibition of NBUP formation in pooled HLM		
	IC_{50} (μM)	Hill slope	Bottom (% of control)
α-mangostin	12.7 ± 1.3	2.37 ± 0.2	0
Chrysin	38.9 ± 5.8	0.93 ± 0.002	0
Ginger extract	23.1 ± 5.0	0.81 ± 0.1	0
Pterostilbene	0.79 ± 0.1	1	29.4 ± 3.3
Silybin	12.9 ± 2.4	0.56 ± 0.1	0

Data represents mean ± SD of IC_{50}, Hill slope and bottom values observed from three separate inhibition experiments (except two experiments for chrysin). All the determinations were performed in duplicate.

Table 4.4: Inhibition of BUPG formation in pooled HIM

Inhibitor	Inhibition of BUPG formation in pooled HIM		
	IC_{50} (μM)	Hill slope	Bottom (% of control)
α-mangostin	5.57 ± 1.0	0.74 ± 0.04	0
Chrysin	19.2 ± 0.1	1.18 ± 0.003	0
Ginger extract	21.6 ± 4.0	1	0
Pterostilbene	47.5 ± 3.6	1.91 ± 0.3	0
Silybin	24.9 ± 5.1	0.45 ± 0.03	0

Data represents mean ± SD of IC_{50}, Hill slope and bottom values observed from two separate inhibition experiments. All the determinations were performed in duplicate.

Table 4.5: Inhibition of BUPG formation in pooled HLM

Inhibitor	Inhibition of BUPG formation in pooled HLM		
	IC_{50} (μM)	Hill slope	Bottom (% of control)
α-mangostin	2.00± 0.1	0.79 ± 0.1	0
Chrysin	22.2 ±0.1	1.06 ± 0.1	0
Ginger extract	9.04 ± 0.2	0.89 ± 0.01	0
Pterostilbene	28.9 ± 0.5	1.17 ± 0.04	0
Silybin	1.21 ± 0.3	1	44.2 ± 2.2

Data represents mean ± SD of IC_{50}, Hill slope and bottom values observed from three separate inhibition experiments. All the determinations were performed in duplicate.

4.3.2 Inhibition by the equipotent combination of Pterostilbene and Ginger extract

The ratio of IC_{50}s of pterostilbene and ginger extract for inhibition of NBUP formation appeared to be between 1:15 and 1:25. However, practically these ratios could not be achieved due to solubility issues. The highest achievable ratio of pterostilbene: ginger extract was 1:11, which is biased towards pterostilbene in its composition. For inhibition of BUPG formation, the mean ratio of IC_{50}s of pterostilbene and ginger extract was 2:1. Reproducible IC_{50} and Hill slope values were achieved for the combination treatment for inhibition of CYP and UGT metabolism of BUP in pooled HIM with R^2 values ≥ 0.98 (Table 4.5 and Fig 4.11). For both the pathways, the combination curve appeared to be similar to the curve of the individual inhibitor treatments, indicating additive interactions in the combination (Fig. 4.12).

Table 4.6: Inhibition by combination of pterostilbene and ginger extract

Pathway	Effect of pterostilbene and ginger extract combination		
	IR_{50} (μM)	Hill slope	Bottom (% of control)
Oxidation	1.72 ± 0.3	0.65 ± 0.1	0
Glucuronidation	1.46 ± 0.1	1.05 ± 0.01	0

Data represents mean ± SD of IR_{50}, Hill slope and bottom values observed from separate inhibition experiments. All the determinations were performed in duplicate.

Figure 4.11: Inhibition of NBUP formation by pterostilbene and ginger extract combination

(a)

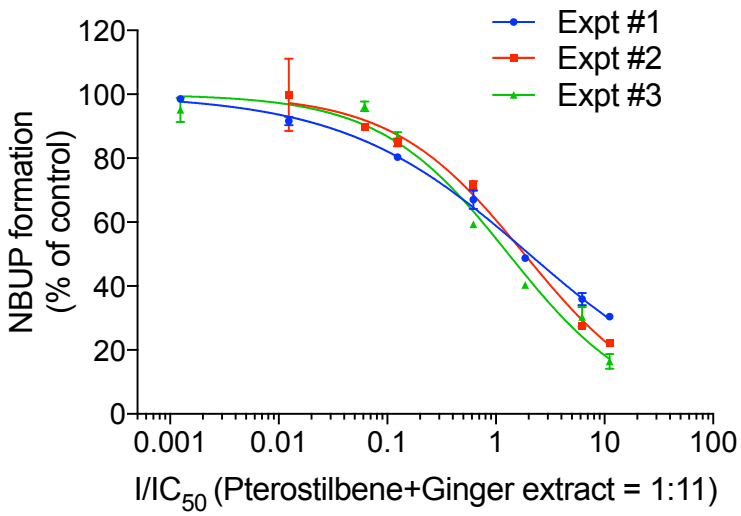

Fig 4.11 (a): Inhibition of NBUP formation by pterostilbene and ginger extract (1:11) combination in pooled HIM. Data represent mean ± SD of NBUP formation rate expressed as % of control. All the determinations were performed in duplicate. Each curve represents a separate experiment. In experiments 1, 2 and 3, the NBUP formation in control was 136 ± 2.17, 129 ± 5.00 and 126 ± 4.27 pmol/min/mg protein and R^2 value was 0.99, 0.98 and 0.98, respectively.

(b)

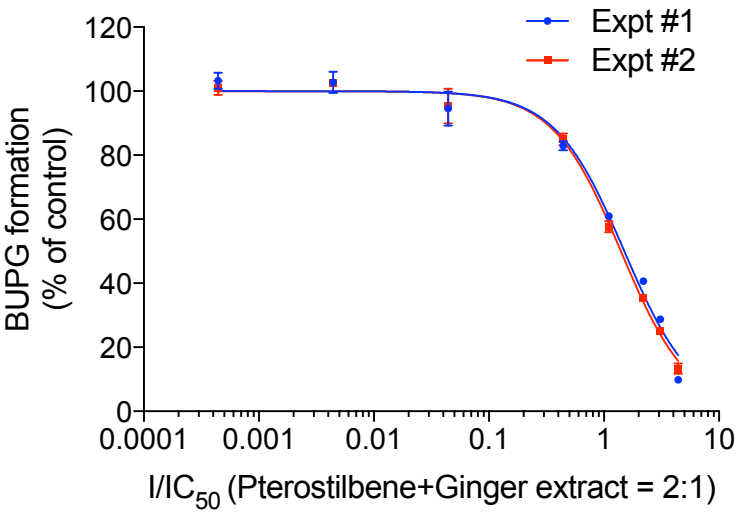

Fig 4.11 (b): Inhibition of BUPG formation by pterostilbene and ginger extract combination (2:1) in pooled HIM. Data represent mean ± SD of BUPG formation rate expressed as % of control. All the determinations were performed in duplicate. Each curve represents a separate experiment. In experiments 1 and 2, the NBUP formation in control was 9.33 ± 0.19 and 8.89 ± 0.11 pmol/min/mg protein and R^2 value was 0.98 and 0.99, respectively.

Figure 4.12: Curve shift analysis for effect on NBUP and BUPG formation in HIM

(a)

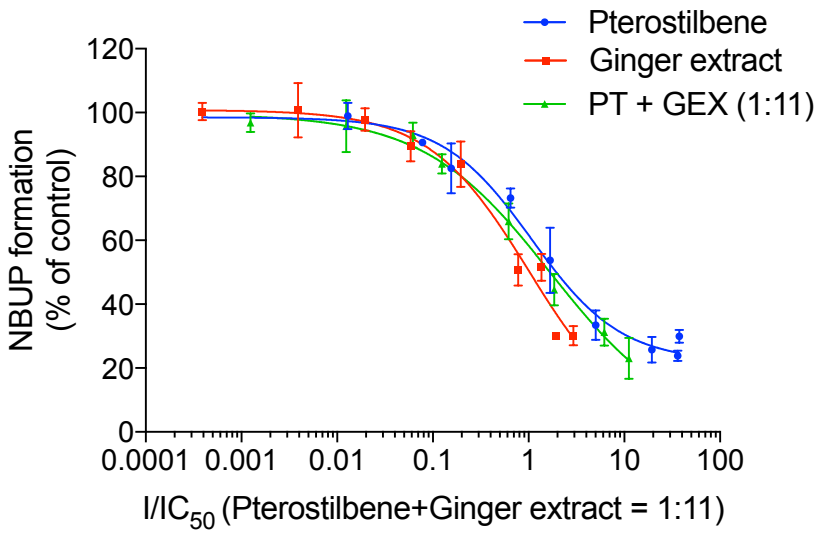

Fig 4.12 (a): Curve shift analysis for effect on NBUP formation in HIM. The curves represent average of three different curves for each inhibitor treatment. Data represent mean ± SD of NBUP formation rate expressed as % of control. Pterostilbene and ginger extract are combined in 1:11 ratio. No significant shift in the combination curve indicates additive interaction.

(b)

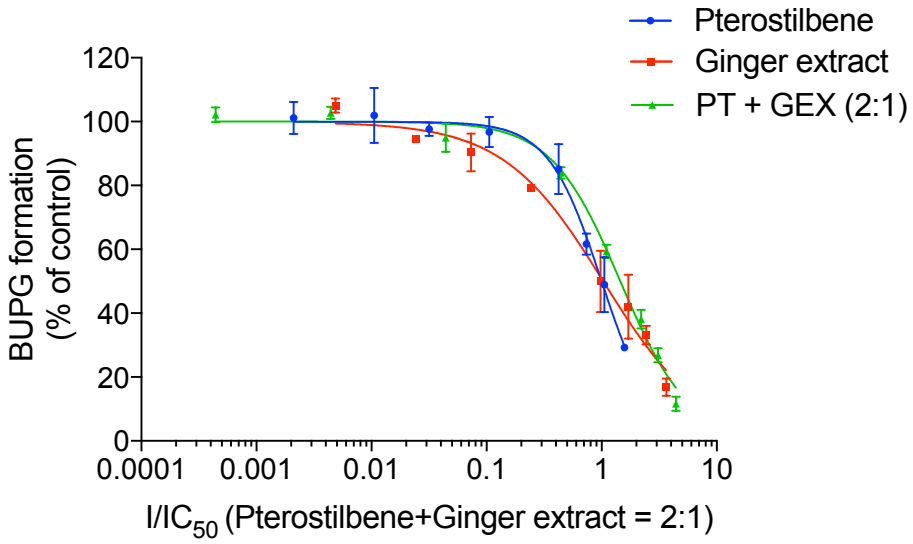

Fig 4.12 (b): Curve shift analysis for effect on BUPG formation in HIM. The curves represent average of two different curves for each inhibitor treatment. Data represent mean ± SD of NBUP formation rate expressed as % of control. Pterostilbene and ginger extract are combined in 2:1 ratio. No significant shift in the combination curve indicates additive interaction.

4.4 Discussion

CYPs and UGTs represent major drug metabolizing enzyme families responsible for clearance of majority of the current top 200 drugs [64, 120-125]. BUP is an example of such a compound that is oxidized (CYP 3A4 2C8, 2C9) to form norbuprenorphine and glucuronidated (UGT 1A1, 1A3 and 2B7) to form buprenorphine glucuronide [3, 12, 14, 67, 126]. Theoretically, inhibition of the presystemic metabolism of buprenorphine can be expected to significantly improve its systemic availability following oral administration. This is evident from several clinical studies where systemic exposures of sublingual BUP increased drastically when co-administered with CYP3A inhibitors like ritonavir, atazanavir, delaviridine, ketoconazole, voriconazole etc. [142-146] These studies support our hypothesis of improving oral bioavailability of BUP by co-administering GRAS or dietary compounds to inhibit the oxidative and conjugative metabolism of BUP.

Several herbal compounds have been reported in the literature to produce bioenhancement by employing various mechanisms to improve GI solubility, permeability and reduce the first pass clearance of poorly bioavailable drugs [21-26, 127, 128]. From the list of 28 putative inhibitors evaluated in Chapter 3, α-mangostin, chrysin, ginger extract, pterostilbene and silybin were shortlisted for further studies because of their favorable physiochemical properties, BCS class, potency of inhibition, oral PK in humans and/or animals and the maximum daily dose in humans [30]. Pterostilbene appeared to be most potent inhibitor of oxidative metabolism of BUP with IC_{50} values of ≤1 μM in HIM and HLM whereas α-mangostin and silybin were most potent in inhibiting glucuronidation of BUP in the intestinal and liver microsomes, respectively. Pterostilbene showed incomplete inhibition of oxidation in HIM and HLM. Among the

CYP isoforms responsible for oxidation of BUP, CYP3A4 accounts for 70-80% with minor contributions from CYP 2C8 and 2C9 [11, 12]. It is possible that pterostilbene can only inhibit CYP3A4 mediated NBUP formation with minimal to no effect on other CYP isoforms. This might explain the ~70% inhibition (bottom = 28.0 ± 6.4% in HIM and 29.4 ± 3.3% in HLM) of oxidation shown by pterostilbene in both HIM and HLM. However, above reasoning does not explain the incomplete inhibition of NBUP formation shown by chrysin in HIM (bottom = 29.4 ± 6.4%) but not in the HLM. Further studies on the effect of chrysin on other CYP isoforms in the liver microsomes, metabolism of chrysin and the effect of the metabolite(s) on the inhibitory action of chrysin etc. need to be performed. The IC_{50} and Hill slope values for inhibition of NBUP formation in HIM and HLM were in good agreement for pterostilbene and ginger extract and in fair agreement with < 3 fold difference for α-mangostin, chrysin and silybin.

Most of the inhibitors showed complete inhibition of glucuronidation of BUP except silybin in HLM. Silybin exhibited about 56% inhibition of BUPG formation in pooled HLM but it was able to achieve complete inhibition of glucuronidation in pooled HIM. As explained earlier, one of the probable reasons includes differential effect of silybin on UGT enzymes involved in conjugating BUP. The major isoforms responsible for glucuronidation of BUP in liver include UGT 1A1, 1A3 and 2B7. Using the relative activity factor approach, Rouguieg et al. reported that UGT1A3 accounts for about 50% of the glucuronidation of BUP in HLM followed by UGT2B7 (~40%) and minor contribution of UGT1A1 (~10%) [14]. However, despite being the major isoform, the contribution of UGT1A3 was determined indirectly without using a selective UGT1A3 substrate. Chang and Moody performed a similar study using insect cell cDNA-expressed

human UGT supersomes to identify the UGT isoforms involved in glucuronidation of BUP [13]. The results of this study are in agreement with the Rouguieg et al. study for the most part except Chang and Moody observed that UGT2B17 can also cause glucuronidation of BUP [13]. However, the relative expression of UGT2B17 in liver is reported to be about 5% of UGT2B7 suggesting minor contribution towards conjugation of BUP [147, 148]. There is minimal to no expression of UGT1A3 in the intestine [15, 148, 149]. Thus, it is logical to expect higher contribution from UGT 1A1, 2B7 and possibly UGT2B17 in the intestinal conjugation of BUP. Thus, if silybin inhibits only UGT 1A1 and 2B7 [150] with minimal to no effect on UGT1A3, this could possibly explain complete inhibition of BUPG formation in HIM but not in HLM . This differential effect on UGT isoforms might also explain the 21 fold difference in the IC_{50} of silybin in intestinal and liver microsomes. The IC_{50} and Hill slope values of rest of the inhibitors for inhibition of BUPG formation in pooled HIM and HLM were in fair agreement.

The equipotent combination of pterostilbene and ginger extract was tested to investigate possible synergistic interactions in the combination. The combination (pterostilbene: ginger extract = 1:11) tested for inhibition of oxidation of BUP was biased towards pterostilbene in its composition. Although pterostilbene alone showed incomplete inhibition of NBUP formation in pooled HIM, the combination produced complete inhibition (Fig 4.11 (a) and table 4.5) of oxidation. No significant shift was observed for the combination curve with respect to the individual inhibitor curves indicating additive interactions in the combination (Fig 4.12a). Similarly, the equipotent combination of pterostilbene and ginger extract (2:1) showed additive interactions

towards inhibition of BUPG formation in pooled HIM (Fig 4.12b). Since the combination failed to show any synergistic interactions in HIM, further combination studies in HLM were not performed.

Amongst the five inhibitor treatments, pterostilbene appears to be the most promising candidate. It can be safely dosed up to 1800 mg/day in humans (Dose taken from FDA-approved use as GRAS substance or food additive). Pterostilbene has been reported to show dose dependent bioavailability in rodents ranging from 12% to 80%, which is significantly higher than its structural analogue resveratrol [133-135]. It is highly permeable and is reported to show an aqueous solubility of 80 μM [138, 139]. The biorelevant solubility of pterostilbene is expected to be higher than its aqueous solubility due to the presence of surfactants such as lecithin and sodium taurocholate in the biorelevant medium. Thus, pterostilbene has fair potential to achieve sufficiently higher local (gut lumen) and systemic concentrations to produce a clinically relevant enhancement in the systemic exposures of orally administered BUP. However, pterostilbene does not exhibit a significant inhibitory effect on the glucuronidation pathway and shows incomplete inhibition of the CYP metabolism of BUP. Hence, to achieve maximal inhibition of both the metabolic pathways, a combination strategy can also be considered. Future studies will focus on extrapolating the effect of these inhibitor treatments on the predicted oral bioavailability and the variability associated with oral bioavailability and AUC_{∞} of BUP.

Chapter 5 – Determination of biorelevant solubilites of α-mangostin, chrysin, pterostilbene and silybin

5.1 Introduction

Aqueous solubility is an important molecular property influencing the oral absorption of drugs from GIT [35, 36]. Compounds suffering from poor aqueous solubility often exhibit incomplete GI absorption, variable systemic concentrations, significant food effects, formulation challenges etc. [35, 37]. Potent inhibitors with high GI solubility can provide high concentration that drives the inhibition of various drug metabolizing enzymes and transporters. Significant efforts have been made to develop computational models to predict solubilites of novel entities [37, 38]. However, so far these methods are not yet robust enough to accurately predict solubilites. One probable reason for this could be the shortage of large sets of empirical solubility measurements for a wide range of compounds under identical test conditions [37, 38]. Recent published studies have underlined the importance of performing solubility measurements in biorelevant media like fasted or fed state simulated intestinal fluid (FaSSIF or FeSSIF), fasted or fed state simulated gastric fluid (FaSSGF or FeSSGF) etc. [35, 37, 38]. Solubility measurements made using biorelevant media in lieu of aqueous buffers seem to improve the predictions of physiologically based PK models [35, 37, 38]. This chapter aims at determining the equilibrium solubilities of four inhibitor candidates, namely α-mangostin, chrysin, pterostilbene and silybin using FaSSIF (Fig 5.1, structures drawn using ChemDraw v15.1). Silybin used in these studies comprises a mixture of the diastereoisomers silybin A and B (1:1). In addition, the solubilities of these compounds in FaSSIF will be predicted using ADMET predictor v8.1.

Figure 5.1: Structures of test compounds

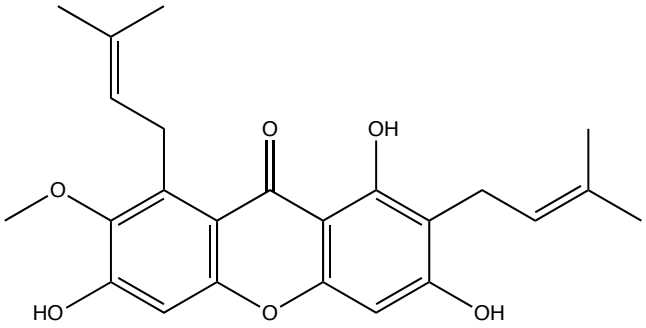

a-mangostin

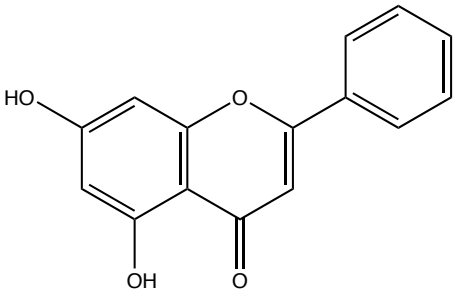

chrysin

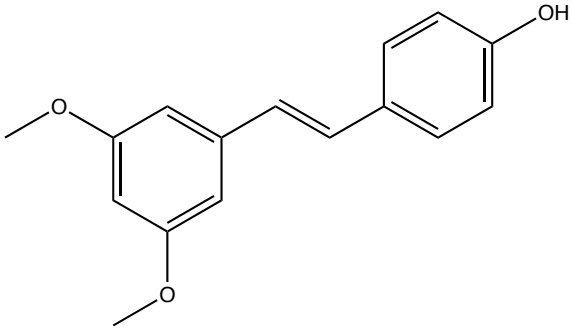

pterostilbene

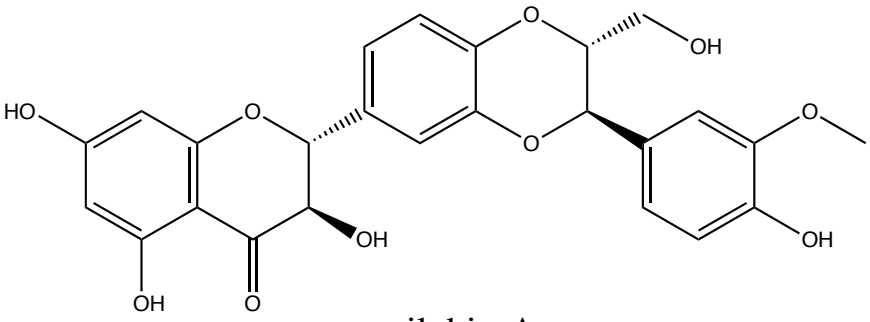

silybin-A

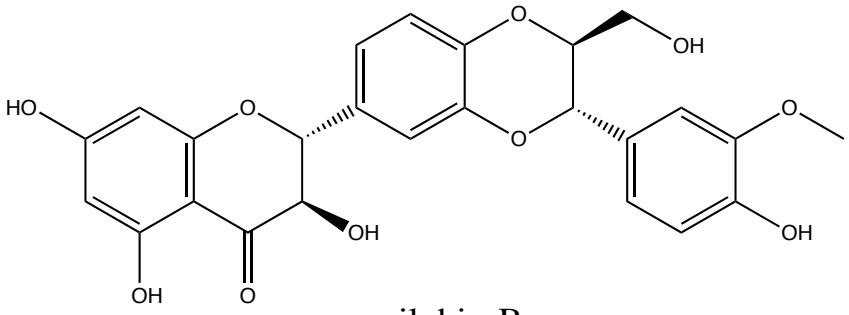

silybin-B

5.2 Materials and Methods

5.2.1 Chemicals and Reagents

α-Mangostin obtained from Indofine Chemical Company (Hillsborough, NJ), silybin from Cayman Chemical Co. (Ann Arbor, MI), chrysin from Hawkins Pharmaceutical Group (Minneapolis, MN) and pterostilbene from AK Scientific, (Union City, CA). Sodium chloride (NaCl) and sodium hydroxide (NaOH) were purchased from Fischer Scientific (Fairlawn, NJ), sodium phosphate monobasic monohydrate ($NaH_2PO_4 \bullet H_2O$) from J.T. Baker (Center Valley, PA) and FaSSIF powder from biorelevant.com.

5.2.2 Preparation of FaSSIF medium

The FaSSIF medium was prepared freshly on the day of the experiment according to the manufacturer's protocol (www.biorelevant.com). A blank buffer (250 ml) comprising of 0.1 g of NaOH pellets, 0.99 g of $NaH_2PO_4 \bullet H_2O$ and 1.55 g of NaCl was prepared and the pH was adjusted to 6.5 using 1N NaOH. This was followed by addition of 0.56g of the FaSSIF powder to the blank buffer (250 ml). The medium was then equilibrated for 2 hours at room temperature before using it for the experiment. The final medium contained 3 mM sodium taurocholate and 0.75 mM lecithin.

5.2.3 Determination of equilibrium solubility

Compounds (10.25 mg, 6.35 mg, 2.5 mg or 13 mg of α-mangostin, chrysin, pterostilbene or silybin) were added to 25 ml of FaSSIF medium in 50 ml tubes to attain a maximum potential solubility of 1mM. The tubes were then rotated end over end in an air incubator maintained at 37°C. The incubation was carried out for 24 hours in order to achieve a presumptive thermodynamic equilibrium. At the end of this incubation period, the tubes were centrifuged at 6000g for 10 min at 4°C. Subsequently, the supernatant was passed through a 0.2 micron syringe filter and the resulting solution was then subjected to HPLC-UV analysis (see sample analysis section).

5.2.4 Predicting FaSSIF solubility using ADMET predictor

ADMET predictor v8.1 by Simulation Plus (Lancaster, CA) was used to predict the solubility of the four test compounds. In addition, other physicochemical properties of the four herbal compounds (pKa, log P, aqueous solubility and number of freely rotatable bonds) were also predicted using ADMET predictor v8.1.

5.2.4 Sample analysis

The HPLC method comprised a mobile phase flow (1 ml/min) of 1% acetonitrile (solvent A) and 99% of 90% aqueous 25 mM ammonium acetate (pH 6.6, adjusted with 5 µl glacial acetic acid) in 10% acetonitrile (solvent B) from 1 min (0 to 1 min) followed by a solvent A gradient from 1% to 50% over 1.5 min (1 to 2.5 min) with a subsequent ramping of solvent A from 50 to 90% over 0.5 min (2.5 to 3 min) and followed by maintaining 90% solvent A for 3 min (3 to 6 min). The column (Alltima HP C18, 4.6 × 100 mm, 3 µm; Grace- Davison Discovery Sciences, Columbia, MD) was re-equilibrated to 1% solvent A for 1.5 min (6 to 7.5 min). The column and sample temperatures were 30

°C and 5 °C, respectively. The initial effluent (3 min) was diverted to the waste. UV detection (Waters 2487) at 220 nm was used. Silybin, chrysin, pterostilbene and α-mangostin eluted at 4.4 min, 4.97 min, 5.1 min and 6.1 min, respectively. Linear standard curves with $R^2 \geq 0.99$ were obtained from 0.75-48 µg/ml for silybin, 0.40-25 µg/ml for chrysin, 0.40-26 µg/ml for pterostilbene and 0.64–41 µg/ml for α-mangostin. This analytical method did not distinguish between the diastereoisomers of silybin and thus total silybin (silybin-A + silybin-B) was detected.

5.3 Results

5.3.1 Determination of equilibrium solubility in FaSSIF medium

The measured and predicted equilibrium solubilites of the four test compounds are as shown in Table 5.1. Pterostilbene showed the highest equilibrium solubility of 83 µg/ml followed by α-mangostin with solubility of 66 µg/ml. Chrysin and silybin exhibited significantly lower biorelevant solubilites of 2.0 µg/ml and 0.62 µg/ml, respectively. The predicted and measured FaSSIF solubilites were fairly agreeable for α-mangostin and pterostilbene but differed significantly for chrysin and silybin.

Table 5.1: Observed vs. predicted solubility in FaSSIF medium

Compound	Predicted FaSSIF solubility (µg/ml)	Observed FaSSIF solubility (µg/ml)*
α-mangostin	50	66.1 ± 0.10
chrysin	103	2.02 ± 0.01
pterostilbene	55	83.2 ± 0.07
silybin (total)	160	0.66 ± 0.01

*Data represents mean ± SD.

5.4 Discussion and conclusions

It is well known that poor solubility is a limiting factor for absorption of drug and can result in significantly lower systemic concentrations and subsequent loss of therapeutic effect [35]. Biorelevant medium such as FaSSIF are extremely useful as they mimic the characteristics of human intestinal fluids and aid in predicting the solubility of new chemical entities [37, 38]. Incorporation of biorelevant solubilites in computational models has been reported to improve their predictive power [37, 38].

In the present study, solubility of four herbal compounds in FaSSIF medium was determined and compared to the solubilites predicted using ADMET predictor. As indicated in Table 5.1, pterostilbene exhibited highest observed solubility of 83 μg/ml followed by α-mangostin (66 μg/ml), chrysin (2 μg/ml) and silybin (0.66 μg/ml). The observed and predicted solubilites of pterostilbene and α-mangostin were in fair agreement with less than 2 fold difference. However, a 52 fold and 242 fold difference was observed in the predicted and measured solubilites of chrysin and silybin, respectively.

Several physiochemical properties listed in Table 5.2 below influence the solubility of a molecule in the FaSSIF medium.

Table 5.2: Predicted physicochemical properties of the test compounds

Compound	Mol. Wt.	Acidic pk_a	Log P	PSA*	# free rotatable bonds	Aqueous Solubility (μg/ml)	FaSSIF solubility (μg/ml)
α-mangostin	410.5	pka_1=9.95 pka_2=8.87 pka_3=7.91	4.50	96.2	5	10	50
chrysin	254.2	pka_1=12.4 pka_2=7.48	3.5	66.8	1	39	103
pterostilbene	256.3	9.67	4.15	38.7	4	27	55
silybin	482.4	pka_1=9.83 pka_2=9.13 pka_3=7.84	1.79	155	4	189	160

*PSA – polar surface area was determined using ChemSpider. All the other properties were generated using ADMET predictor

There appears to be a disagreement in the literature about the impact of these physicochemical properties on solubility in biorelevant media such as FaSSIF. Depending on the size of the datasets and the physiochemical nature of compounds being tested, Mithani et al. and Fagerberg et al. have reported increase in solubilization with increased lipophilicity (log P) [38, 39]. Ottaviani et al. indicates surface activity properties especially critical micelle concentrations to be significant predictor of solubility in FaSSIF [151]. The FaSSIF solubility predictions of the ADMET predictor v8.1 are based on a dataset of diverse 160 drug-like compounds in FaSSIF-V2. One of the possible reasons for the discrepancy in measured and predicted solubilites of chrysin and silybin could be the difference in composition of the biorelevant medium. FaSSIF–v2 possess lower lecithin content (0.2 mM) than FaSSIF (0.75 mM). The difference in bile

salt: lecithin ratio between the two preparations can result in variations in micelle formation affecting drug solubility. For instance, a study by Yu et al. reports enhancement in solubility of silybin to 10 mg/ml by using sodium cholate and phospholipid [152]. The ratio of silybin: sodium cholate: phospholipid in the final formulation was 0.22: 0.33: 0.44, respectively [152]. Solubility of 10 mg/ml is significantly higher than our measured FaSSIF solubility (6.4×10^{-4} mg/ml) as well as the predicted solubility (0.160 mg/ml). This further suggests that differences in surfactant ratios can result in significant differences in the observed solubility of compounds. Another possible reason for the disagreement between observed and predicted FaSSIF solubilites could be related to the physicochemical nature and structural aspects of the 160 drug-like compounds included in the ADMET predictor v8.1 dataset. Since the properties of compounds included in this dataset are not known, it is impossible to verify if the dataset included compounds that structurally resemble chrysin and silybin. Also, the dataset of 160 compounds is not sufficiently large enough which can diminish the predictive power of the software.

The purpose of determining biorelevant solubilites for the four candidates was to improve the confidence in the inhibitor concentration values in gut lumen to be used in the final inhibition model. However, the impact of these solubility values on the overall inhibition shown by these compounds also depends on the potency of inhibition (IC_{50} or K_i) of the inhibitor candidates. To be thorough in our analysis, both the measured and predicted biorelevant solubilites of chrysin and silybin will be tested in the inhibition model in Chapter 6.

Chapter 6: Predicting The Effect Of Inhibitor Treatments on the Oral Bioavailability, Systemic Exposure and Total Clearance of Buprenorphine Using *In Vitro In Vivo* Extrapolation

6.1 Introduction

In vitro systems like human liver and intestinal microsomes, cryopreserved human hepatocytes, immortalized human hepatocarcinoma cell lines, human embryonic stem cells etc. have been successfully used in evaluating the metabolic stability of several compounds [45-52, 153]. One of the key objectives during drug discovery and development studies is to accurately predict the *in vivo* clearance of compounds using relatively simple *in vitro* assays [45-52, 153]. The intrinsic clearances determined using *in vitro* models could be extrapolated to predict the intestinal (F_g) and hepatic (F_h) availabilities and consequently the oral bioavailability (F_{oral}) of compounds. Numerous methods to predict *in vivo* clearance from *in vitro* data have been proposed and described, and have met with varying degree of success [49, 57, 59, 62, 65, 154, 155].

As discussed in chapter 3, the well-stirred model was used to predict the F_g, F_h and ultimately F_{oral} of buprenorphine (BUP) [30]. Of the 27 test compounds, the potency and equilibrium solubilities of five shortlisted inhibitor candidates (α-mangostin, chrysin, ginger extract, pterostilbene and silybin) were determined, as discussed in Chapters 4 and 5 respectively. The next logical step was to extrapolate the intrinsic clearance of BUP in the presence of these inhibitor treatments to predict the resultant F_{oral} of BUP. A highly extracted drug like BUP is likely to show poor and variable systemic availability and exposure. Hence, it was also of interest to predict the effect of these inhibitor treatments on the variability associated with F_{oral}, systemic exposure (AUC_∞) and total clearance (CL_{total}) of BUP. BUP is metabolized by CYP (mainly CYP3A4) and UGT enzymes

(mainly UGT 1A1, 1A3 and 2B7) [11-14]. Both CYP and UGT enzyme families are reported to be associated with high interindividual variability [49, 61, 156, 157]. Studies conducted by Cubitt et al. and Kato et al. have reported 33 – 41% interindividual variability in the hepatic metabolism of CYP3A substrates [46, 60]. The variability in the intestinal CYP3A metabolism appears to be relatively understudied [46, 60]. A small study conducted on six human intestinal tissue samples by Paine et al. [61] and another in silico study conducted by Kato et al. [60] revealed 60 – 81% interindividual variability in intestinal CYP3A metabolism, which is significantly higher than the 40% variability generally observed in clinical DDI parameters [158]. Oxidative metabolism by CYPs (CYP3A4) appears to be the major metabolic pathway of BUP in intestine and liver [11, 12, 30]. The UGT pathway appears to be a minor pathway for BUP metabolism and is considerably understudied with respect to the interindividual variability in the intestinal and hepatic UGT metabolism [30, 67]. Hence, % variability values reported for intestinal and hepatic CYP3A metabolism were used in our studies.

This chapter focuses on predicting the effect of inhibitor treatments on the a) mean F_{oral}, AUC_{∞} and CL_{total} of BUP using well-stirred models b) variability in the predicted mean F_{oral}, AUC_{∞} and CL_{total} of BUP by generating simulated population datasets through Monte Carlo simulations using @RISK software (an add-on linked to Microsoft Excel). In addition, a sensitivity analysis study was performed to identify the parameters significantly influencing the predicted F_{oral}, AUC_{∞} and CL_{total} values of BUP with and without inhibitors.

6.2 Materials and methods

6.2.1 Model description:

The intestinal availability (F_g), hepatic availability (F_h) and F_{oral} of BUP were extrapolated using the well-stirred model as explained in chapter 3 [30]. Five inhibitor candidates, namely α-mangostin, chrysin, ginger extract, pterostilbene and silybin, were subjected to *in vitro in vivo* extrapolation (IVIVE) to study their effect on predicted F_{oral} of BUP. The following assumptions were made:

a) Linear PK (BUP concentrations ≤ K_m).

The oral doses of 0.63 μg/kg, 15 μg/kg and 20 μg/kg of BUP reported in the literature, result in gut concentrations almost equal to or less than the K_m values (determined from our in vitro metabolic studies) supporting the assumption of linear PK conditions [8, 10].

b) The inhibitor exhibits reversible competitive or non-competitive inhibition; thus K_i value can be calculated from the IC_{50} value using Cheng-Prussof equation [159].

Several publications have reported that phenolic or polyphenolic compounds (including some of the shortlisted inhibitors or their close structural analogues) show competitive (or in minor cases – mixed or non-competitive) type of inhibition of CYP and UGT enzymes lending some support to the above assumption [24, 160-167]. For instance, the inhibition of various CYP isoforms by components on mangosteen extract was studied in liver miscrosomes and recombinant CYP enzymes. α-Mangostin exhibited competitive inhibition of CYP3A enzyme.

c) Equilibrium biorelevant solubility of the inhibitor (determined based on the experiments in Chapter 5) represents its predicted *in vivo* concentrations in the gut lumen,

d) Portal vein concentrations will be predicted using the most conservative (lowest) estimate of F_{oral} of the inhibitors (in humans and/or animals) available in the literature and

e) CL_{tot} of BUP is equal to the total hepatic clearance (CL_{hep}) of BUP (negligible contribution of non-hepatic pathways)

After oral administration of BUP in healthy human volunteers, about 10 – 15% of the dose was eliminated in urine, mostly as glucuronide conjugates with negligible/no presence of unchanged BUP [10, 17]. This indicates that biliary excretion appears to be the major route of elimination for BUP, thus supporting our assumption.

6.2.2 Steps involved in the extrapolation in presence of inhibitors

Following is the description of the steps involved in the IVIVE study of BUP in presence of inhibitor treatments:

i) Assuming reversible competitive/non-competitive inhibition, the IC_{50} of each inhibitor treatment for the CYP and UGT pathway was converted to K_i using the Cheng-Prussof equation [159] stated below:

$$K_i = \frac{IC_{50}}{1+\frac{S}{K_m}} \quad (1)$$

ii) Intrinsic clearance of BUP in presence of inhibitor was determined as follows [64]:

$$Cl_{int}^{I} = \frac{Cl_{int,BUP}}{1+\frac{I}{K_i}} \quad (2)$$

where Cl_{int}^{I}= intrinsic clearance of BUP in presence of inhibitor treatment, $Cl_{int,\ BUP}$ = unbound intrinsic clearance of BUP and I = inhibitor concentration.

iii) The F_g and F_h values of BUP in presence of inhibitor (i.e. F_g^I and F_h^I, respectively) were predicted by extrapolating the Cl_{int}^{I} values using well-stirred model equations (Eq. 3 and 4) given below [65, 68]:

$$F_g^I = \frac{Q_{villi}}{Q_{villi} + fu_G \times \text{in vitro } Cl_{int,GW}^{I} \times SF_1 \times SF_2} \quad (3)$$

where Q_{villi} is villous blood flow = 4.1 ml/min/kg, fu_G is fraction of BUP unbound in the enterocytes (assumed to be 1) and in vitro $Cl_{int,GW}^{I}$ is the Cl_{int}^{I} in pooled HIM scaled to physiological levels using scaling factors SF_1 (20.5 mg microsomal protein/g intestinal mucosa) and SF_2 (11.16 g intestinal mucosa/kg) [65].

$$F_h^I = \frac{Q_{hep}}{Q_{hep} + fu_p \times \text{in vitro } Cl_{int,hep}^{I} \times SF_1 \times SF_2} \quad (4)$$

where Q_{hep} is hepatic blood flow = 20.7 mL/min/kg, fu_p indicates fraction of unbound drug (BUP) in plasma = 0.03 [30] and $in\ vitro\ Cl_{int,hep}^{I}$ is the Cl_{int}^{I} in pooled HLM scaled using scaling factors - SF_1 (20.5 mg microsomal protein/g hepatic mucosa) and SF_2 (11.16 g hepatic mucosa/kg) [68].

iii) The F_{oral} of BUP in presence of the inhibitor (F_{oral}^{I}) was determined using the following equation [70]:

$$F_{oral}^{I} = F_a \times F_g^I \times F_h^I \times 100 \quad (5)$$

where F_a is the fraction absorbed, assumed to be 1 since BUP is a highly soluble (relative to dose) and highly permeable drug.

The total hepatic clearance in absence (CL_{hep}) or presence (CL_{hep}^{I}) of inhibitor treatments and was calculated as follows [70]:

$$CL_{hep}\ or\ CL_{hep}^{I} = Q_{hep} \times (1 - F_h\ or\ F_h^I) \quad (6)$$

The AUC_∞ values of BUP with or without inhibitor treatments was predicted using Eq. 7 [70]:

$$AUC_\infty^{PO} = \frac{F_{oral} \times Dose}{CL_{tot}} \text{ or } AUC_\infty^{PO,I} = \frac{F_{oral}^{I} \times Dose}{CL_{tot}^{I}} \quad (7)$$

where AUC_∞^{PO} or $AUC_\infty^{PO,I}$ and CL_{tot} or CL_{tot}^{I} indicates the predicted AUC_∞ and CL_{tot} of BUP in absence or presence of inhibitor treatments, respectively and dose represents the oral dose of BUP assumed to be 10 mg (falls in the dosing range of sublingual BUP, 4-24 mg). As per the Suboxone monograph, BUP HCl exhibits an aqueous solubility of 17 mg/ml [168]. Thus, it would be logical to expect that an oral dose of 10 mg of BUP would be show near complete solubility.

6.2.3 Predicting inhibitor concentrations in gut lumen and portal vein

As discussed in Chapter 5, the equilibrium solubilities of α-mangostin, chrysin, pterostilbene and silybin were experimentally determined in a fasted simulated intestinal fluid (FaSSIF) as well as predicted using ADMET predictor (Simulation Plus, Lancaster, CA). The experimental and predicted solubilities of α-mangostin and pterostilbene appeared to be in good agreement, but differed significantly for chrysin and silybin. For thoroughness of analysis, both the experimental and predicted equilibrium solubilities of chrysin and silybin were tested. Several studies have analyzed the composition of ginger extract and observed that 6-gingerol (most abundant), 8-gingerol, 10-gingerol and 6-shogaol appear to be the major components [34, 102, 131]. Although the solubility of ginger extract was not experimentally determined, the predicted solubilities of the aforementioned major components of ginger extract were used in our study [131]. The relative composition of the four components in the ginger extract used for the inhibition studies was not known. Hence, an average of the predicted solubilities of the four

components was assumed to represent the solubility of the extract. As stated earlier, these observed or predicted solubilities were assumed to represent the gut lumen concentrations i.e. I (GW) following oral administration of the inhibitors. A literature search was performed to determine the most conservative (lowest) estimates of F_{oral} of the inhibitors in humans and/or animals. Pharmacokinetic studies of ginger extract or major components of ginger extract in humans and animals did not report % F_{oral}. Following oral administration of several doses up to 2.0 g in humans, no free 6-gingerol, 8-gingerol, 10-gingerol or 6-shogaol could be detected in plasma (LLOQ-5 ng/ml) [32-34, 102]. Thus, despite showing good oral absorption, these ginger components suffered from poor oral bioavailability due to extensive presystemic conjugation by UGT and SULT enzyme families [32-34, 102]. Pfeiffer et al. have shown that 6-gingerol undergoes significant glucuronidation in both intestinal and liver microsomes [169]. However, the relative contribution of the intestine versus liver to the overall presystemic metabolism of the gingerols has not been reported. Hence, for the purpose our analysis it was assumed that 10% of the oral dose of ginger extract in gut lumen survives intestinal metabolism and appears in portal vein to undergo further metabolism in liver. The portal vein concentrations i.e. I (hep) for the rest of the inhibitor treatments were calculated as follows:

$$I\ (hep) = F_{oral} \times I\ (GW) \tag{8}$$

where F_{oral} is the bioavailable fraction after oral administration and I (GW) represents the gut lumen concentrations of the inhibitors. The reason behind using this method to predict I (hep) was to be as conservative as possible in our predictions, since I (hep) was not experimentally determined (using animal models) in our lab. The FDA guidance on

drug-drug interactions recommends the use of Eq. 8 to determine hepatic inhibitor concentrations [170]. However, this equation could not be used for our study because most of the parameters of like fraction unbound ($f_{u,b}$), maximum steady state plasma concentrations $[I]_{max}$, absorption rate constant (k_a) and F_a were unknown for the all the test compounds. Also, the $\%F_{oral}$ of most of the inhibitors except pterostilbene and ginger extract was less than 1%, which would lead to extremely low values of I (hep) irrespective of the equation used to predict them. The predicted I (GW) and I (hep) values of all the inhibitor treatments are summarized in Table 6.1.

$$I\ (hep) = \frac{f_{u,b} \times [I]_{max,b} + F_a \times K_a \times Dose}{Q_h} \quad (9)$$

Table 6.1: Predicted inhibitor concentrations in the gut lumen and portal vein

Inhibitor	I (GW) (µM)	% F_{oral}	I (hep) (µM)
α-mangostin	161	0.4[a]	0.64
chrysin (exp. sol)*	7.97	0.02[b]	0.002
chrysin (pred. sol)*	405	0.02[b]	0.08
ginger extract	176	NA**	17.6
pterostilbene	325	12.5[c]	40.6
silybin (exp. sol)	2.57	0.95[d]	0.02
silybin (pred. sol)	629	0.95[d]	5.98

* exp. sol and pred. sol indicate experimental and predicted solubility, respectively.

** Not available, assumed to be 10%

a- Orozco et al. (2013) [171] and Li et al. (2013) [117], b- Walle et al. (2001) [129], c- Lin et al. (2009) [135] and d- Wu et al. (2009)[172]

6.2.4 Predicting the effect on variability in F_{oral}, CL_{total} and AUC_{∞}

@RISK (Palisade Corporation, Ithaca, NY) was used to perform Monte Carlo simulations for generation of simulated population. This technique involves sampling random numbers from a given probability distribution. A single simulation comprising of 10,000 iterations was used to generate a simulated population dataset. All the input variables were assumed to exhibit normal distribution with a minimum possible value of zero. For BUP alone, the model had four input variables i.e. CLint, (GW,CYP), CLint, (GW,UGT), CLint, (hep,CYP) and CLint, (hep,UGT) and three output parameters i.e F_{oral}, CL_{tot} and AUC_{∞} (Table 6.2). The model comprising BUP with the inhibitor treatment had two additional input variables i.e. I (GW) and I (hep) leading to a total of six input variables and same three output parameters stated earlier. An inhibitor can exhibit distinct potency of inhibition (K_i) of the CYP versus UGT pathway, which can result in different extent of inhibition of the two pathways in the intestine and liver. Hence, the input variables I (GW) and I (hep) were further categorized as I (GW,CYP), I (GW,UGT), I (hep,CYP) and I (hep,UGT) to distinguish the contribution of inhibitor concentrations (with reference to their K_i) to % inhibition for each individual pathway in the intestine and liver. A larger value for inhibitor concentrations and a smaller K_i value for a particular metabolic pathway will result in higher % inhibition for that pathway.

The following two conditions with different % variability in the intestinal and hepatic clearances were tested:

a) Scenario #1 - 60% variability in intestinal and 41% variability in hepatic intrinsic clearances

b) Scenario #2 - 40% variability in intestinal and 25% variability in hepatic intrinsic clearances

For the higher variability scenario #1, 41% variability was applied to the hepatic intrinsic clearances [CLint, (hep,CYP) and CLint, (hep,UGT)], based on previously published studies [46, 60]. Paine et al. and Kato et al. have reported 60% and 81% interindividual variability in intestinal clearances [60, 61]. Hence, a variability of 60% (case 1) and 81% (case 2) in the intestinal intrinsic clearances was tested for this scenario. If no significant difference is observed in the resultant standard deviation of the predicted mean of the three output variables, then a variability of 60% in the intestinal intrinsic clearances would be used for further extrapolation in scenario #1. To assess the effect of variability in inhibitor concentrations in the gut lumen and portal vein on output parameters, a variability of 25% and 20% was applied to I (GW) and I (hep), respectively. The results are reported as mean ± SD of the three output variables in presence of different inhibitor treatments under scenarios #1 and 2.

A sensitivity analysis was performed to identify the input variables that strongly influence the output variables i.e. F_{oral}, CL_{tot} and AUC_{∞} of BUP. The results of the sensitivity analysis will be reported using tornado graphs with input variables on Y-axis and spearman rank correlation coefficient (r) on X-axis. The correlation co-efficient conveys the magnitude as well as direction of the effect of the input variables on output parameters. The intrinsic clearances are expected to exhibit negative or inverse correlation with F_{oral} and AUC_{∞} and positive correlation with CL_{tot}, while inhibitor concentrations are likely to show positive correlation with F_{oral} and AUC_{∞} and negative correlation with CL_{tot}.

Table 6.2: Description of input variables of the model

Input variables	Description	Units
CLint (GW,CYP)	scaled intrinsic clearance for the CYP pathway in intestinal microsomes	ml/min
CLint (GW,UGT)	scaled intrinsic clearance for the UGT pathway in intestinal microsomes	ml/min
CLint (hep,CYP)	scaled intrinsic clearance for the CYP pathway in liver microsomes	ml/min
CLint (hep,UGT)	scaled intrinsic clearance for the UGT pathway in liver microsomes	ml/min
I (GW,CYP)	Inhibitor concentration in gut lumen available for inhibition of intestinal CYP metabolism of BUP	μM
I (GW,UGT)	Inhibitor concentration in gut lumen available for inhibition of intestinal UGT metabolism of BUP	μM
I (hep, CYP)	Inhibitor concentration in portal vein available for inhibition of hepatic CYP metabolism of BUP	μM
I (hep, UGT)	Inhibitor concentration in portal vein available for inhibition of hepatic UGT metabolism of BUP	μM

6.3 Results

6.3.1 Effect of inhibitor treatments on predicted F_{oral}, AUC_{∞} and CL_{tot} of BUP

As stated in the methods section, two scenarios comprising distinct % variability in the intrinsic clearances were evaluated. Based on the predictions of the IVIVE study under both scenarios, BUP exhibited a poor and variable oral bioavailability of 3 ± 2% (Tables 6.3 and 6.4). The CL_{tot} of BUP was predicted to be ~ 1050 to 1060 ml/min yielding an extraction ratio of 0.7 (assuming liver blood flow of 1500 ml/min [68]). The F-test for equality of variances (α=0.025) was used to detect significant differences in the variance of mean predicted F_{oral}, AUC_{∞} and CL_{tot} between the 60% variability (case 1) and 80% variability (case 2) group. For all the output variables, the critical F-value (F_{oral} = 1.2, AUC_{∞} = 1.2 and CL_{tot} = 1.1) was greater than 1.0 (F-value from the F-distribution table for ∞ degrees of freedom) indicating significant difference between the two groups. However, the statistical difference did not seem scientifically meaningful hence a variability of 60% in CLint (GW) was used in all studies in scenario #1.

Regarding the output, first let's consider means; the effect of inhibitor treatments on the mean of all output variables appeared to be similar under the conditions of scenarios #1 and 2. Pterostilbene appeared to be the most potent inhibitor that significantly improved the mean F_{oral} and AUC_{∞} by 22 to 24 fold and 105 fold, respectively with 4 fold reduction in CL_{tot} of BUP. The extrapolations made using experimental versus predicted solubilites of silybin generated significantly distinct results. IVIVE based on its predicted solubility made silybin the second most potent inhibitor after pterostilbene, producing an 11 fold and 15 to 16 fold increase in the mean F_{oral} and AUC_{∞} of BUP, respectively and minor reduction (2 fold) in the mean CL_{tot} of BUP. In contrast, the extrapolations based on its experimental solubility indicate that

silybin does not have a significant effect on systemic availability, exposure and clearance of BUP. Similarly, chrysin appeared to drastically improve the predicted mean F_{oral} and AUC_{∞} of BUP, only when the extrapolations were performed using its predicted solubility. Ginger extract produced 8 to 9 fold and 13 fold increase in the predicted mean F_{oral} and AUC_{∞} of BUP, respectively and a minor decrease (1.5 fold) in the predicted Cl_{tot} of BUP. On the other hand α-mangostin improved the mean F_{oral} and AUC_{∞} by 5 fold with no significant effect on the predicted Cl_{tot} of BUP.

Next, lets consider the effect of inhibitors on variability associated with mean. The variability around the mean of output variables was higher under scenario #1 than scenario #2 due to larger % variability in the intrinsic clearances in scenario #1. Pterostilbene showed highest reduction in the variability around mean F_{oral} (8 to 9 fold) while a 2 to 3 fold reduction was achieved by α-mangostin, ginger extract as well as chrysin and silybin (IVIVE using predicted solubilities). No significant change in variability in the predicted mean Cl_{tot} was observed for all the inhibitors except pterostilbene, which exhibited 22 to 30 fold increase. About 2 fold reduction was observed in the variability associated with AUC_{∞} after treatment with pterostilbene as well as chrysin and silybin (IVIVE using predicted solubilities), while rest of the inhibitor treatments did not strongly affect the variability in AUC_{∞}. The results for all the treatment groups are summarized in Tables 6.3 and 6.4.

Table 6.3: Effect of inhibitors on F_{oral}, AUC_{∞} and CL_{tot} of BUP (scenario #1)

Treatment	Foral (%)		AUC_{∞} (ng*min/ml)		CLtot (ml/min)	
	Mean ± SD	% CV	Mean ± SD	% CV	Mean ± SD	% CV
BUP (case 1)*	3.39 ± 2.24	66	344 ± 327	95	1050 ± 126	12
BUP (case 2)*	3.32 ± 2.48	75	336 ± 302	90	1050 ± 122	12
BUP + a-M	16.5 ± 6.62	40	1780 ± 1160	65	1000 ± 133	13
BUP + CHR (exp. sol)**	5.45 ± 3.25	60	553 ± 447	81	1050 ± 123	12
BUP + CHR (pred. sol)**	24.5 ± 6.96	28	2490 ± 1390	56	1050 ± 122	12
BUP + GEX	28.3 ± 8.60	30	4429 ± 3020	68	715 ± 141	20
BUP + PT	74.8 ± 5.60	7.5	36,130 ± 25,460	70	247 ± 75.3	30
BUP + SIL (exp. sol)**	3.78 ± 2.56	68	384 ± 324	84	1050 ± 122	12
BUP + SIL (pred. sol)**	36.1 ± 9.28	26	5450 ± 4790	88	769 ± 160	21

* case 1 and case 2 represent 60% and 81% variability in the CLint (GW). Above results were obtained after applying 60% variability in the intestinal clearances and 41% variability in the hepatic clearances. ** exp. sol and pred. sol indicate experimental and predicted solubility, respectively.

Table 6.4: Effect of inhibitors on F_{oral}, AUC_{∞} and CL_{tot} of BUP (scenario #2)

Treatment	F_{oral} (%)		AUC_{∞} (ng*min/ml)		CL_{tot} (ml/min)	
	Mean ± SD	% CV	Mean ± SD	% CV	Mean ± SD	% CV
BUP (case 3)*	3.14 ± 1.46	46	300 ± 151	50	1060 ± 69.2	6.5
BUP + a-M	15.7 ± 4.67	30	1579 ± 579	37	1020 ± 75.9	7.4
BUP + CHR (exp. sol)**	5.08 ± 2.12	42	486 ± 225	46	1060 ± 69.2	6.5
BUP + CHR (pred. sol)**	23.6 ± 4.21	18	2262 ± 582	26	1060 ± 68.9	6.5
BUP + GEX	27.4 ± 6.54	24	3900 ± 1384	35	729 ± 93.1	13
BUP + PT	74.4 ± 4.55	6.1	31,538 ± 10,086	32	251 ± 54.0	22
BUP + SIL (exp. sol)**	3.46 ± 1.61	47	332 ± 168	51	1060 ± 69.5	6.5
BUP + SIL (pred. sol)**	35.0 ± 6.44	18	4622 ± 1587	34	787 ± 99.5	13

*case 3 represents 40% variability in the CLint (GW). Above results were obtained after applying 40% variability in the intestinal clearances and 25% variability in the hepatic clearances.
** exp. sol and pred. sol indicate experimental and predicted solubility, respectively.

Despite showing significant enhancement of predicted AUC_{∞} in scenarios #1 and 2, pterostilbene exhibited a large variability of 70% under scenario #1. Hence, scenario #1 was subjected to further analysis using five additional doses of pterostilbene (Figs. 6.1 – 6.3). Based on the results of this study, a ten fold lower dose (I (GW) = 32.5 μM and I (hep) = 4.06 μM) was further studied under the conditions of scenarios #1 and 2. In addition, the effect of introduction of higher variability (60%) in I (hep) was also investigated and the results are as summarized in Table 6.4. Reducing the concentration of pterostilbene to 32.5 μM not only improved F_{oral} and AUC_{∞} of BUP but also lowered

the variability in AUC_{∞} from 95% to 49% in scenario #1 and from 50% to 28% in scenario #2. Increasing the variability in I (hep) to 60% resulted in a minor increase in the variability around AUC_{∞} for both scenarios.

Figure 6.1: Effect of different concentrations of pterostilbene on predicted $\%F_{oral}$

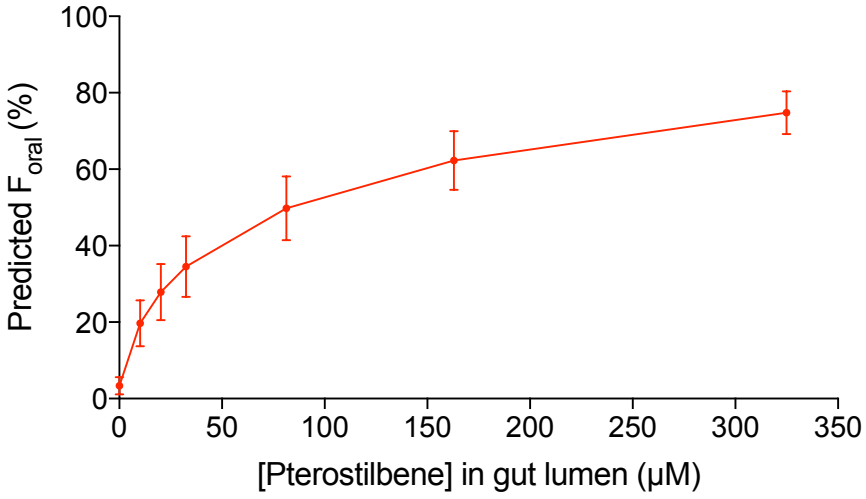

Figure 6.2: Effect of different concentrations of pterostilbene on predicted CL_{tot}

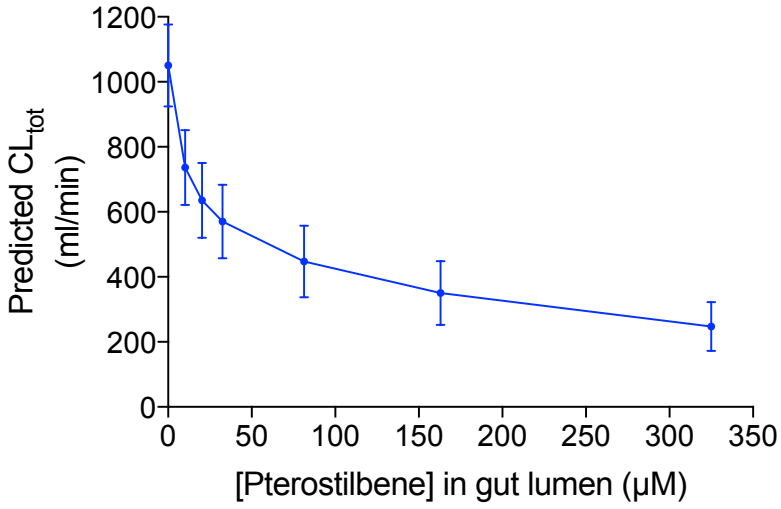

Figure 6.3: Effect of different concentrations of pterostilbene on predicted AUC_{∞}

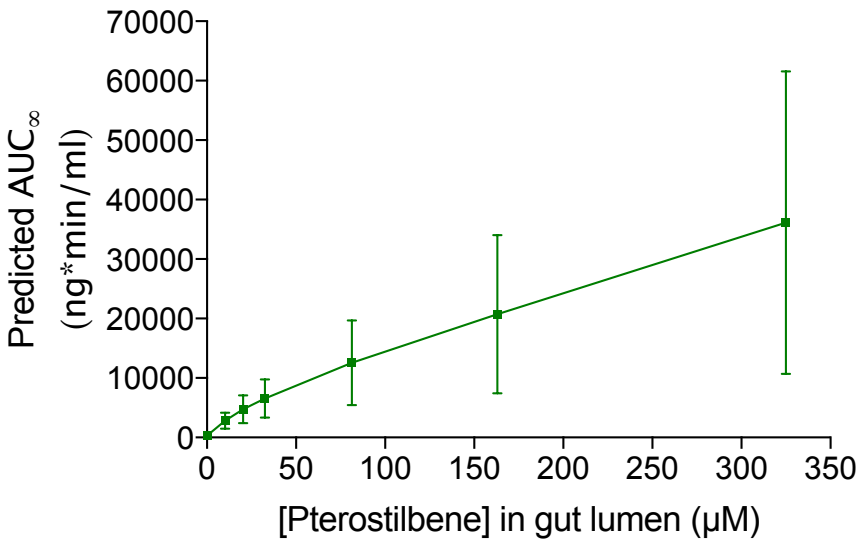

Table 6.5: Effect of ten fold lower dose of pterostilbene on output variables

Test condition	F_{oral} (%)		AUC_{∞} (ng*min/ml)		CL_{tot} (ml/min)	
	Mean ± SD	% CV	Mean ± SD	% CV	Mean ± SD	% CV
Scenario #1						
A	34.5 ± 7.93	23	6584 ± 3225	49	570 ± 113	20
B	33.9 ± 8.50	25	6486 ± 3722	57	588 ± 143	24
Scenario #2						
C	34.7 ± 5.92	17	6217 ± 1718	28	574 ± 72.5	13
D	34.0 ± 6.62	20	6067 ± 2070	34	593 ± 112	19

Test conditions A and C represent variability of 20% in I (hep) same as before
Test conditions B and D represent 60% variability in I (hep)

6.3.2 Sensitivity analysis

In scenario #1, the results of the sensitivity analysis of BUP for case 1 with 60% (Fig 6.4) or case 2 with 81% (Fig 6.5) variability in the intestinal clearances were in agreement with previous predictions (discussed in chapter 3) that CYP pathway appears to be the dominant metabolic pathway for BUP. The intestinal CYP intrinsic clearance (CLint (GW,CYP)) was predicted to be the most sensitive input variable in both cases with a negative correlation to F_{oral} (r = -0.85 or -0.88) and AUC_{∞} (r = -0.75 or -0.79) whereas hepatic CYP clearance showed a strong positive relationship with CL_{tot} (r =0.97). The intestinal clearances exhibit no impact on CL_{tot} because the model assumes that total clearance is similar to the hepatic clearance of BUP. The results of the sensitivity analysis in scenario #1 were in agreement with the results of scenario #2; hence tornado plots of only scenario #1 are shown below.

Figure 6.4: Tornado plot for BUP (case 1)

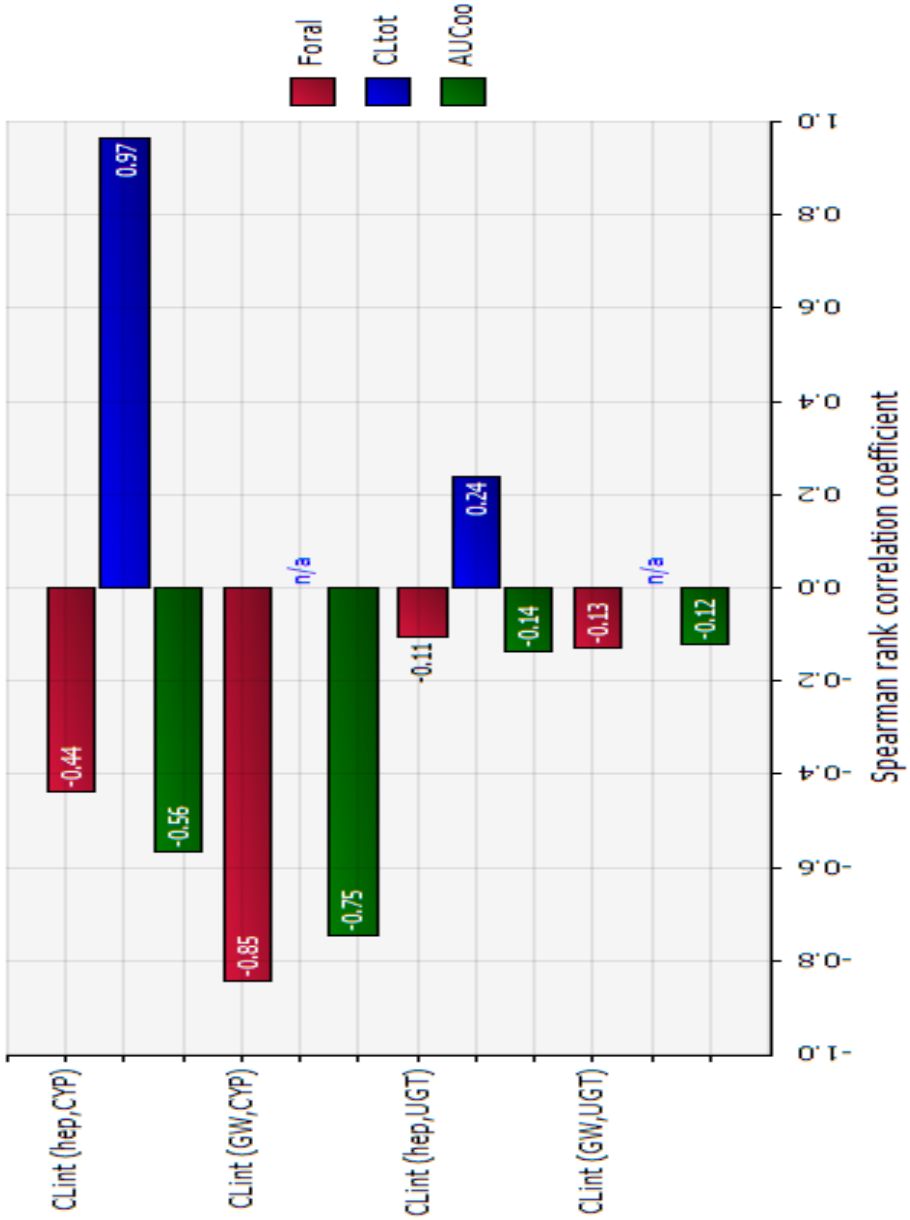

Figure 6.5: Tornado plot of BUP (case 2)

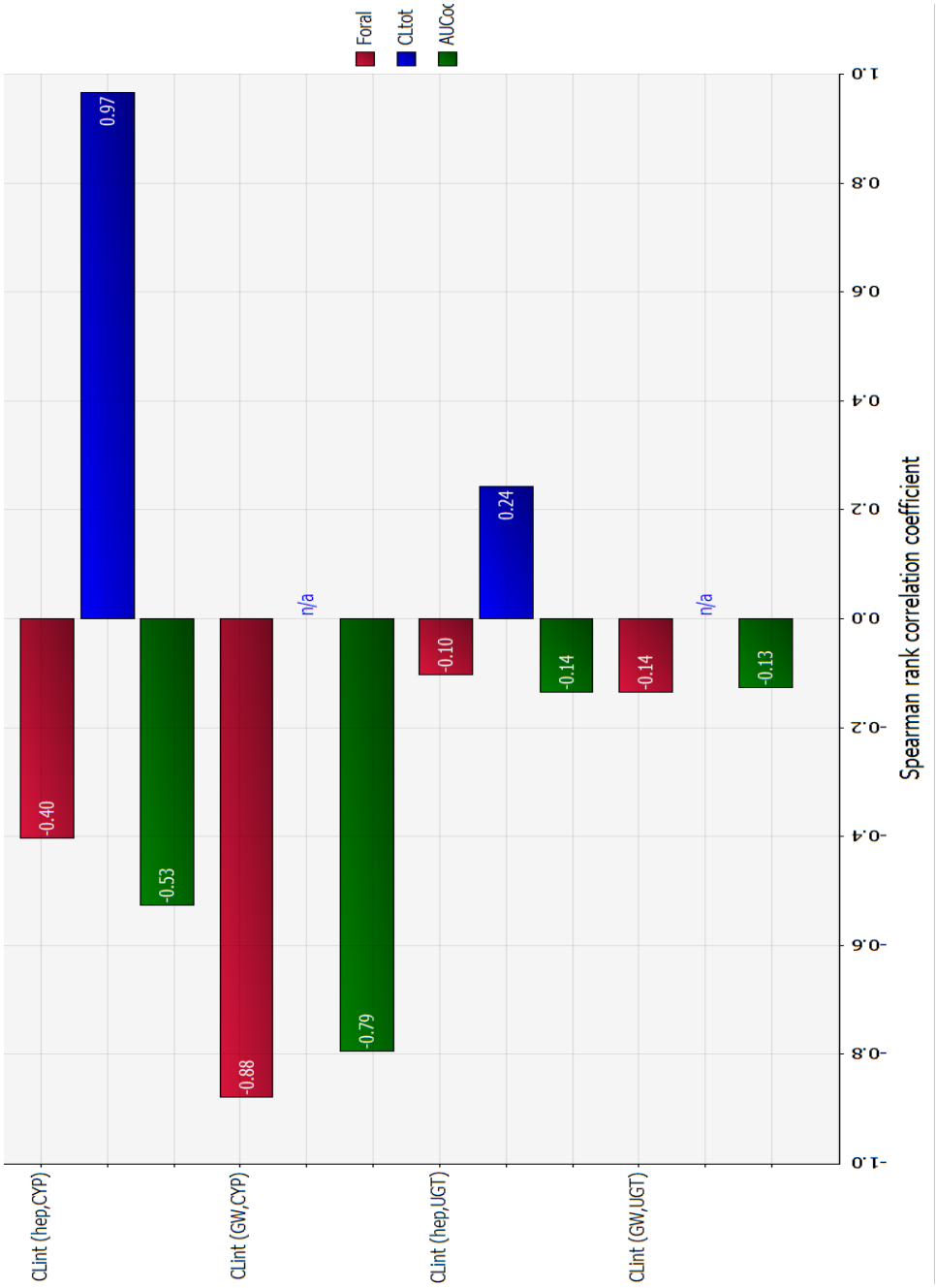

CLint (GW,CYP) and CLint (hep,CYP) appeared to be the most sensitive input variables influencing F_{oral} and AUC_{∞} of BUP for all the inhibitor treatments except pterostilbene. The rank order of the input variables (with reference to the magnitude and direction of their effect on output variables) appeared to be in excellent agreement under the test conditions of scenarios #1 and #2. Hence, the results of only one scenario i.e. scenario #1 will be discussed. Among the variables impacting F_{oral} of BUP, CLint (GW,CYP) appeared to be the most sensitive input variable showing strong negative correlation in presence of α-mangostin (r = -0.70), chrysin and silybin (IVIVE using experimental solubility, r = -0.82 and -0.8, respectively) and ginger extract (r = -0.73) (Figs. 6.6 – 6.12), while CLint (hep,CYP) exhibited strong negative relationship with F_{oral} for chrysin (r = -0.88) and silybin based on extrapolations using predicted solubility (r = -0.77). AUC_{∞} of BUP was strongly and negatively influenced by CLint (GW,CYP) after treatment with chrysin and silybin (IVIVE using experimental solubility, r = -0.73 and – 0.76, respectively) and by CLint (hep,CYP) in presence of α-mangostin, chrysin and silybin (IVIVE using predicted solubility, r = -0.92 and -0.89 ,respectively) and ginger extract (r = -0.76), respectively (Figs. 6.6 – 6.12). As expected CLint (hep,CYP) showed a strong positive correlation with CL_{tot} of BUP for all the inhibitor treatments except pterostilbene. In presence of pterostilbene, CLint (hep,UGT) was the most sensitive input variable exhibiting strong negative correlation with F_{oral} (r = -70)and AUC_{∞} (r = -0.92) and strong positive correlation with CL_{tot} (r = 0.93) of BUP. For all the inhibitor treatments, intestinal and hepatic inhibitor concentrations showed weak positive correlations with F_{oral}, AUC_{∞} and negative correlation with CL_{tot}. The inhibitor concentrations appeared to have a relatively stronger effect on output variables in

scenario#2 than scenario #1. However, even in scenario #2 their correlation coefficient values were $\leq$ 0.41 indicating weak effect on output parameters (data not shown). Amongst the four inhibitor concentration variables, I (GW,CYP) appeared to be most sensitive to F_{oral} and AUC_{∞} in presence of all inhibitor treatments except pterostilbene which had I (hep,UGT) as the most sensitive variable.

Figure 6.6 Tornado plot for α-mangostin

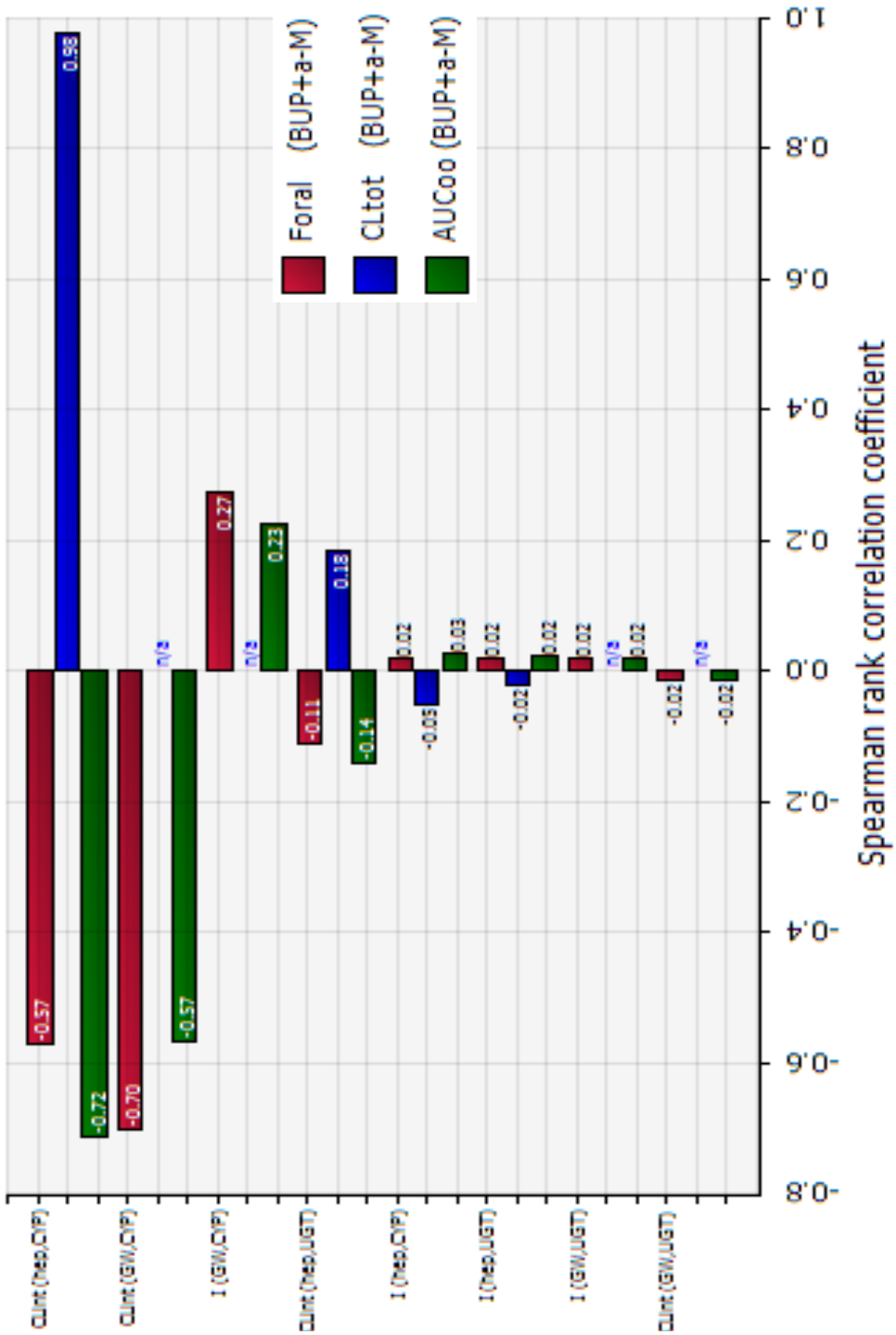

Figure 6.7: Tornado plot for chrysin (using experimental solubility)

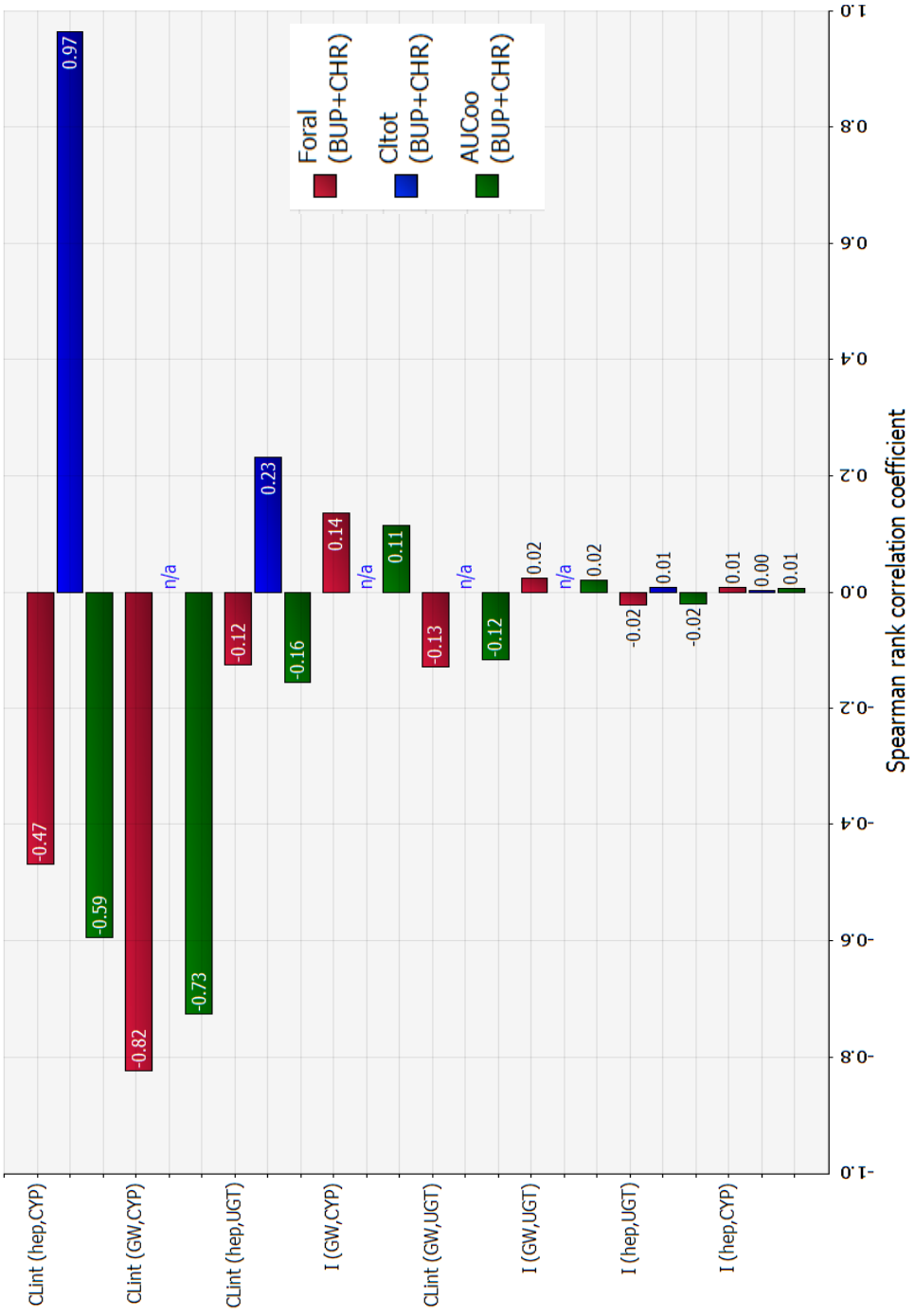

Figure 6.8: Tornado plot for chrysin (using predicted solubility)

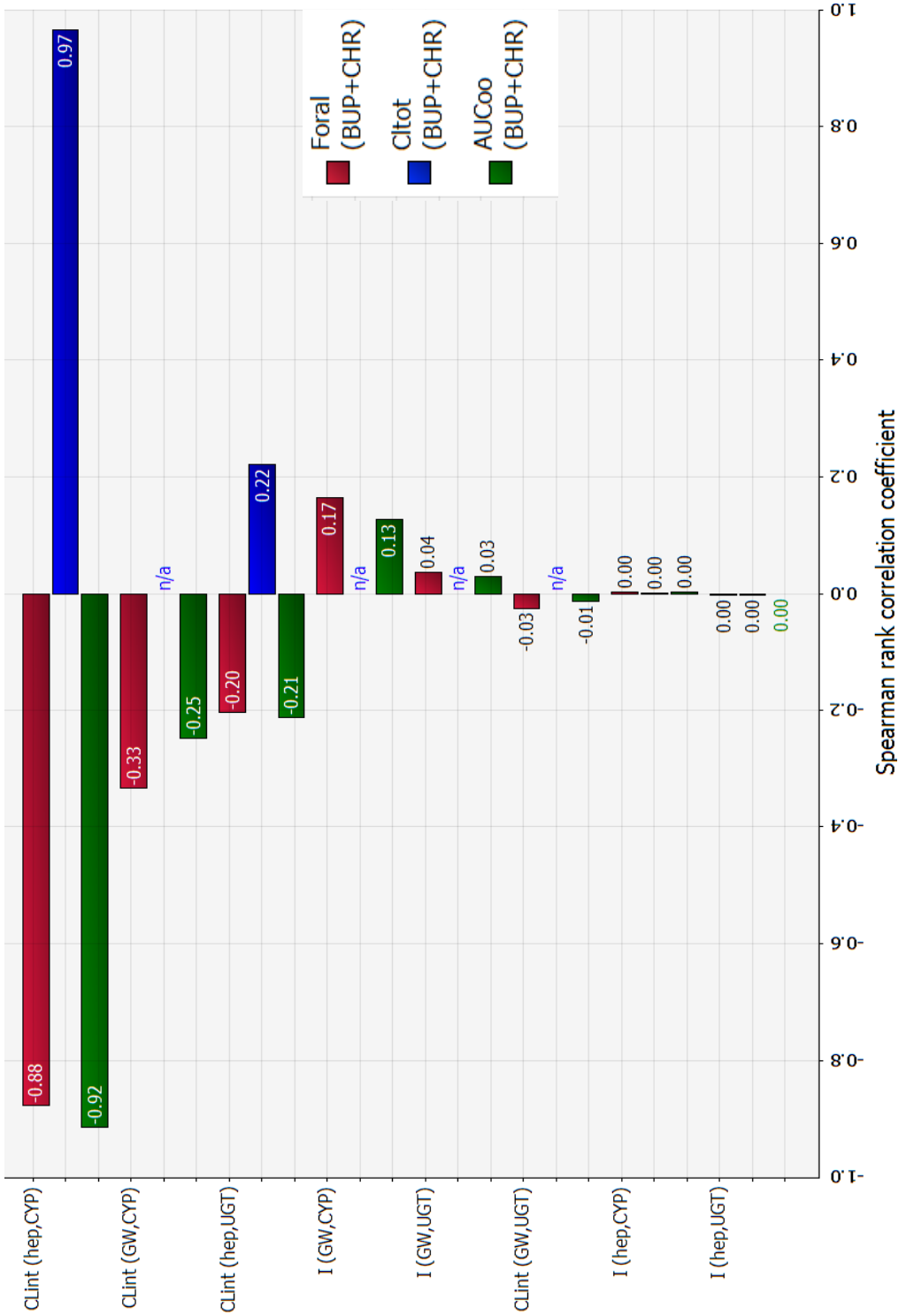

Figure 6.9: Tornado plot for ginger extract

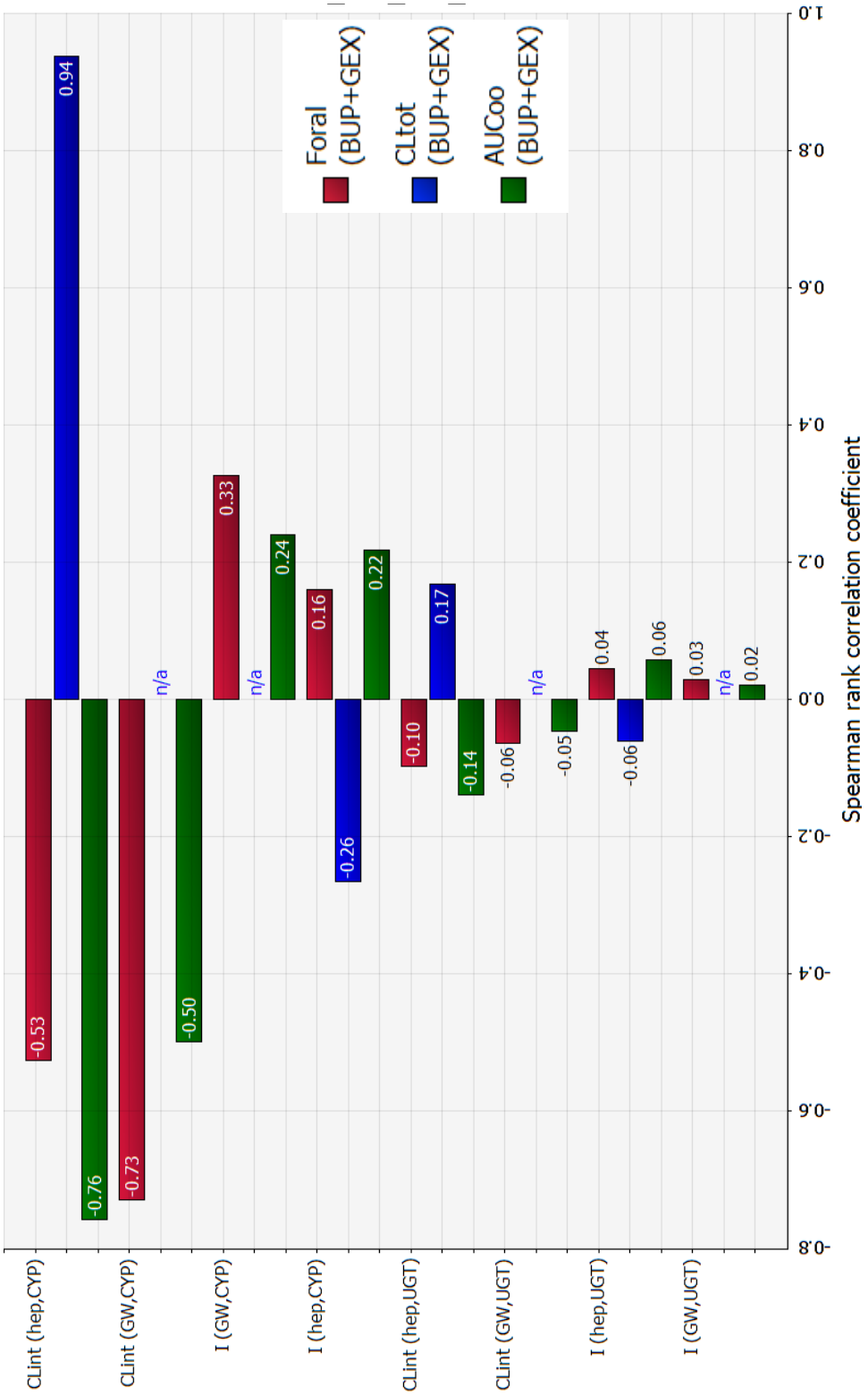

Figure 6.10: Tornado plot for pterostilbene

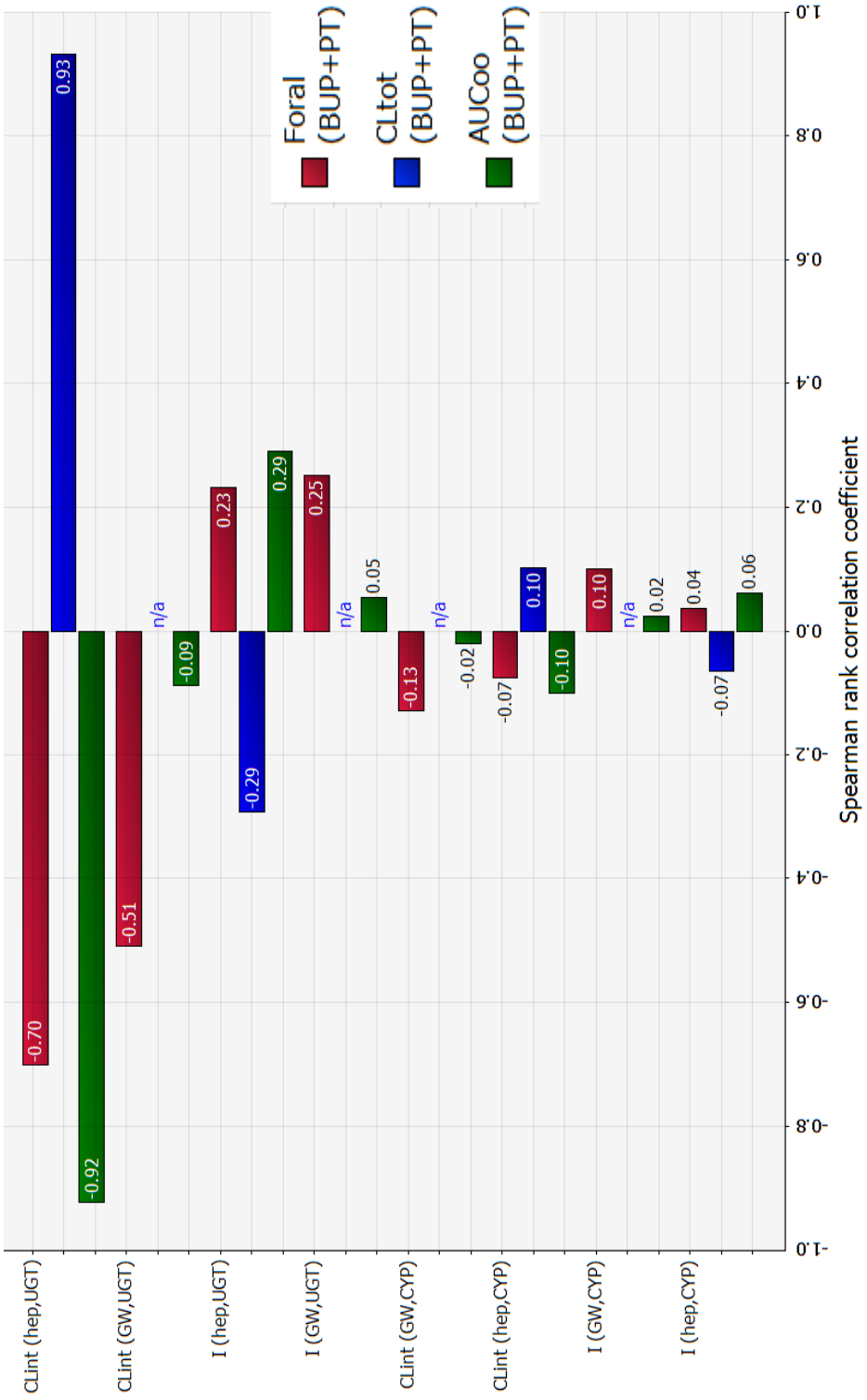

Figure 6.11: Tornado plot for silybin (using experimental solubility)

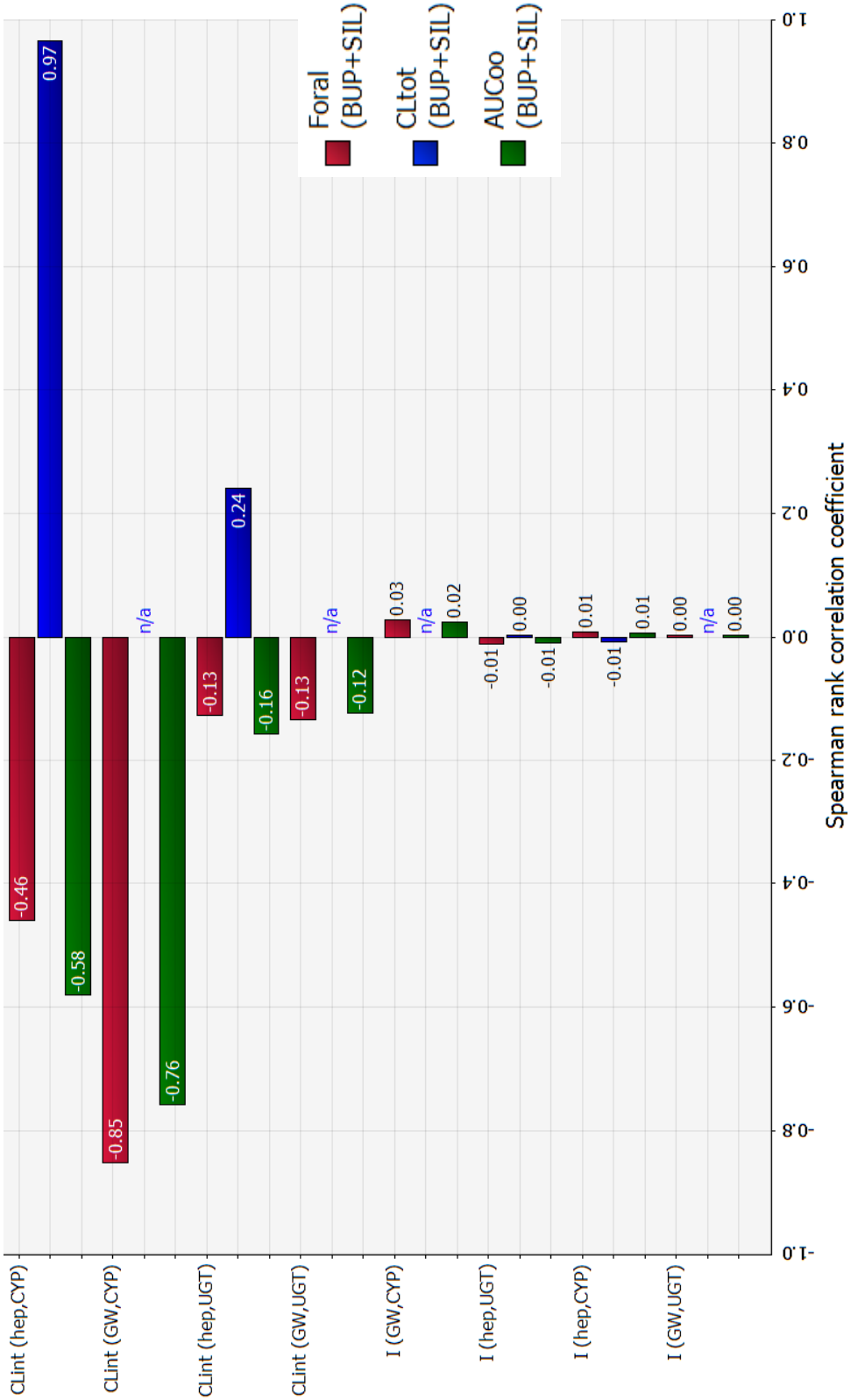

Figure 6.12: Tornado plot for silybin (using predicted solubility)

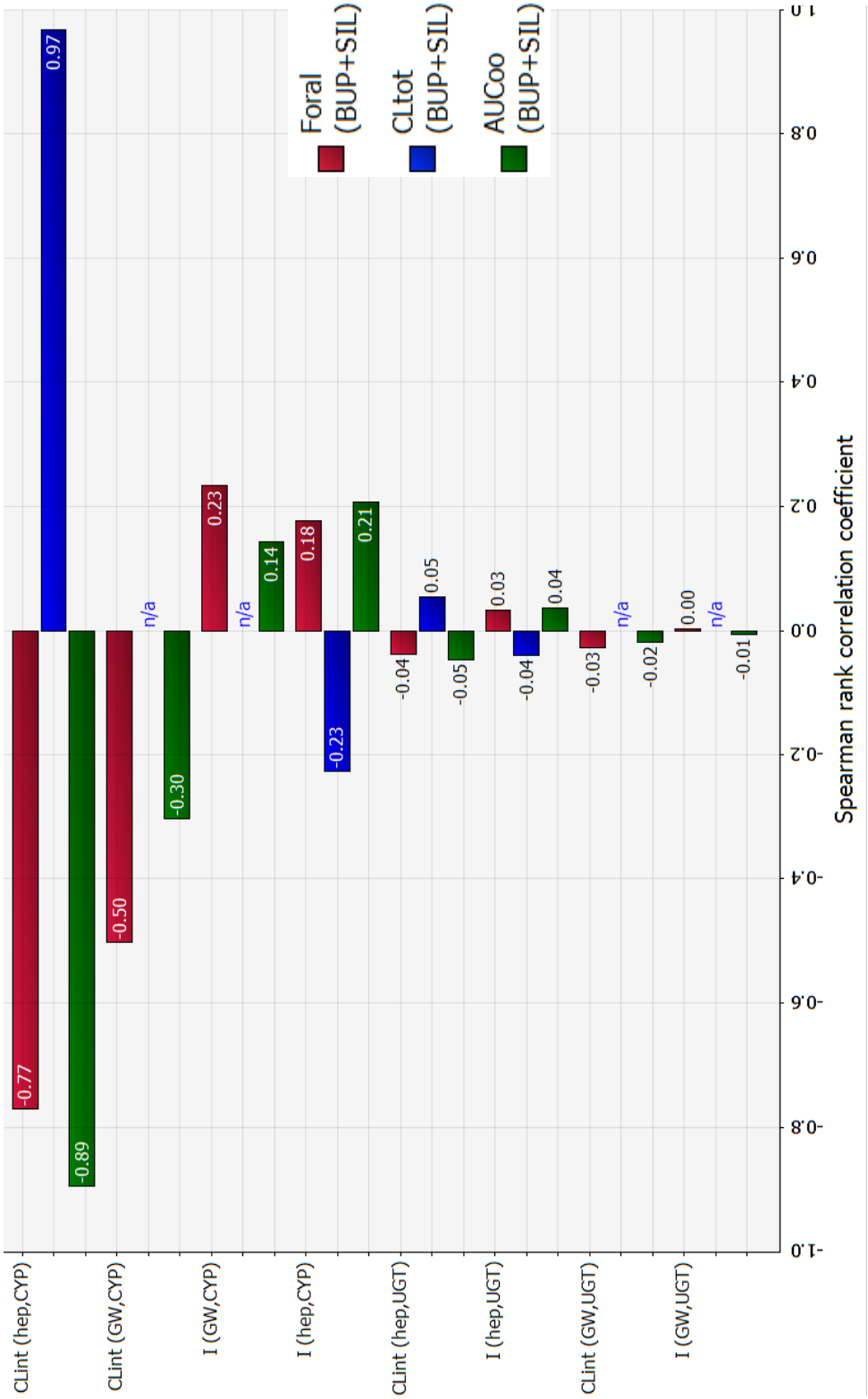

6.4 Discussion

Oral bioavailability is one of the most important PK properties for an orally administered drug [173, 174]. For a drug to reach systemic circulation in an unchanged form, it has to first get absorbed, survive metabolism while passing through the gut wall and finally avoid extraction by liver either through enzymatic metabolism or via biliary excretion [175, 176]. Measuring oral bioavailability *in vivo* especially in humans can be quite expensive, laborious and possibly yield results with huge variability [173-176]. Hence, in silico methods of predicting PK parameters such as F_{oral}, clearance, systemic exposure, presystemic intestinal and hepatic extraction using results from relatively simple in vitro systems can prove very helpful during the process of drug discovery and development. *In vitro* to *in vivo* extrapolations can also help in predicting PK parameters when clinical data are not available [48, 50, 57, 173-176]. As discussed in Chapter 3, limited information is available on pharmacokinetic features of BUP after oral administration in humans. Hence, a minimal model (i.e. well-stirred model) was used to predict the pharmacokinetic properties of BUP such as F_{oral} AUC_{∞} and CL_{tot}. Intrinsic oxidative and conjugative clearances in pooled intestinal and hepatic microsomes were extrapolated using the well-stirred model to make predictions on oral PK characteristics of BUP. The well-stirred model assumes that the metabolic enzymes are distributed uniformly within the organ and have access to a well-stirred concentration of drug [55]. As is evident from the mathematical formula, the model links the unbound intrinsic clearance to the extraction efficiency of the organ [55].

CYP3A4 is reported to be the major CYP isoform responsible for oxidation of BUP [11, 12]. Historically, it was believed that liver represents the major site for metabolism of drugs by CYP3A4 [61, 63]. However, within the last few decades

numerous studies emphasizing the contribution of intestine to CYP3A4 metabolism have been published [45-47, 50, 57-60, 62, 64, 156]. Drugs metabolized by CYP3A4 have been reported to exhibit a high degree of interindividual variability [45-47, 50, 57-60, 62, 64, 156]. One of the major factors responsible for this appears to be the high variability in the metabolic activity of hepatic and intestinal CYP3A4 [45-47, 50, 57-60, 62, 64, 156]. Numerous sources of variability have been proposed and studied such as genetic polymorphism, epigenetic factors, non-genetic factors like age, gender, body weight, liver blood flow, expression of drug metabolizing enzymes and transporters, disease states, enzyme induction or inhibition etc. [71] Cubitt et al. conducted a study to estimate the interindividual variability in hepatic CYP3A4 abundance (using three CYP3A substrates i.e. alprazolam, triazolam and midazolam) to improve estimation of variability in the predicted *in vivo* clearance [46]. The variability in CYP3A4 abundance in 52 livers was studied and the interindividual variability was estimated to be 41% [46]. Kato et al. performed an *in silico* study to predict the factors contributing to interindividual variability in PK parameters (AUC, total and oral clearance, intestinal and hepatic extraction) in humans. They identified hepatic CYP3A4 content as the most sensitive parameter affecting the variability in AUC_{dose} of test substrate [60]. This study reported % CV of 33% and 81% for hepatic CYP3A4 content and intrinsic intestinal clearance corrected for permeability, respectively [60]. Another study conducted by Paine et al. using six human intestines reported 60% variability in the intestinal CYP3A4 content [61]. However, the 60% and 81% variability reported in both the studies likely accounts for both experimental and true interindividual variability [46]. Since the true interindividual variability in clearance of BUP after oral administration in humans is not

yet known, two scenarios with distinct variability in intestinal and hepatic intrinsic clearances were evaluated. Scenario #1 represents the least favorable condition with higher variability while scenario #2 represents a more favorable condition with lower variability in intrinsic clearances. Based on the interindividual variability estimates for CYP3A4 abundance, scenario #1 comprised 41% variability in the hepatic intrinsic clearances and a variability of 60% in the intestinal clearances. In addition, a variability of 81% in the intestinal clearances was also tested, but no significant difference was observed in the variability around mean of the output variables (F_{oral} AUC_{∞} and CL_{tot}) for 60% versus 81% variability. Hence, %CV for intestinal clearances was set at 61% under scenario #1. On the other hand, scenario #2 comprised almost half the variability in scenario 1 i.e. of 40% variability in the intestinal intrinsic clearances and a variability of 25% in the hepatic clearances. Both the scenarios exhibited similar mean values for all the output variables as well as similar ranking of input variables in the results of the sensitivity analysis. However, as expected the variability in the mean values of the output variables was much higher under conditions of scenario #1 than #2.

BUP was predicted to exhibit poor F_{oral} and AUC_{∞} with 46 to 66% and 50 to 95% variability, respectively as well as a huge CL_{tot} (1050 to 1060 ml/min) in both scenarios. The results of the sensitivity analysis predict CLint (GW,CYP) to be the most sensitive input variable affecting F_{oral} and AUC_{∞} of BUP while CL_{tot} was most sensitive to CLint (hep,CYP). These results are consistent with our IVIVE predictions showing higher contribution of oxidation (6 fold in intestine and 4 fold in liver) over glucuronidation to the overall metabolism of BUP [30]. The results of the *in vitro* studies performed by Cubitt et al. reporting 70% and 66% contribution of the CYP pathway to the metabolism

of BUP in the liver and intestinal microsomes, respectively; appear to be in good agreement with our predictions [67].

Treatment with α-mangostin, improved the predicted F_{oral} and AUC_{∞} of BUP by 5 fold with a ~2 fold reduction in their variability and a negligible effect on CL_{tot} of BUP. CLint (hep,CYP) showed the strongest influence on AUC_{∞} and CL_{tot} while F_{oral} was most sensitive to CLint (GW,CYP). These results seem logical because α-mangostin exhibited poor inhibition (9%) of hepatic oxidation and glucuronidation (30%) but was more effective in inhibiting intestinal oxidation (87%) and conjugation (98%) of BUP. Despite showing higher potency in inhibiting oxidation (K_i = 6.8 μM-liver, 24.6 μM -intestine) and glucuronidation (K_i = 1.5 μM-liver, 2.8 μM -intestine) in liver, the overall % inhibition was higher in the intestine due to significantly higher predicted concentrations in the gut lumen (161 μM) as compared to the portal vein (0.6 μM).

The effect of chrysin using both experimental (7.97 μM) and predicted (405 μM) equilibrium solubilities (as gut lumen concentrations) was tested for thoroughness of analysis. The extrapolations made using experimental solubility show negligible/no effect of chrysin on all the output variables, while the use of predicted solubility values results in a 7 to 8 fold increase in the predicted mean F_{oral} and AUC_{∞} as well as 2 to 3 fold reduction in their variability. No significant effect on CL_{tot} of BUP was observed for both treatment groups. Since extrapolated results of chrysin using experimental solubility show negligible inhibition of BUP metabolism, the sensitivity analysis yields similar results as BUP alone. On the other hand, predictions based on predicted solubility of chrysin show that CLint (hep, CYP) has the strongest influence on all the output variables. This is most likely due to higher predicted gut lumen concentrations coupled

with about 2 fold higher potency of CYP and UGT inhibition in intestine than liver resulting in 98% inhibition of intestinal metabolism and negligible/no inhibition of hepatic metabolism of BUP.

In presence of ginger extract, the mean F_{oral} and AUC_{∞} increased and CL_{tot} decreased by 8, 13 and 1.5 fold, respectively. In addition, a 2 fold and 1.4 fold reduction in the variability in F_{oral} and AUC_{∞} of BUP was observed, respectively after treatment with ginger extract. CLint (GW,CYP) influenced F_{oral} strongly while AUC_{∞} and CL_{tot} appeared to be most sensitive to CLint (hep,CYP). This is likely explained by lower % inhibition of the hepatic metabolism in comparison to the intestinal metabolism. Despite showing similar potencies in inhibiting oxidation (K_i = 19.6 μM- intestine, 12.3 μM - liver) and glucuronidation (K_i = 11.0 μM- intestine, 6.7 μM - liver) of BUP in the intestine and liver, the total % inhibition of intestinal metabolism was higher due to significantly higher predicted concentrations in the gut lumen (176 μM) than the portal vein (17.6 μM).

Similar to chrysin, the effect of both experimental (2.57 μM) and predicted (629 μM) equilibrium solubilities of silybin was tested for thoroughness of analysis. The extrapolations made using experimental solubility show negligible effect on the mean and the variability of all output variables due to very low solubility values. On the other hand, extrapolations made using predicted solubility exhibit improvement in the mean F_{oral} and AUC_{∞} by 11 and 15 to 16 fold, respectively with minor (1.4 fold) reduction in CL_{tot} of BUP. A 3 fold reduction of variability in F_{oral}, 2 fold increase in variability in CL_{tot} and negligible effect (1.1 fold) on variability in AUC_{∞} was observed. The CL_{tot} value indicates significant reduction in the hepatic extraction ratio of BUP from 0.70 to 0.51

(assuming liver blood flow = 1500 ml/min) in presence of silybin. Collectively, these results suggest that silybin might have the potential to inhibit systemic clearance of BUP. As expected, the sensitivity analysis results using observed solubility of silybin are similar to the results of BUP with no inhibitor. However, the sensitivity analysis performed using predicted solubility shows CLint (hep,CYP) to be the most sensitive input variable strongly influencing all the output variables. This is consistent with a low % inhibition (46%) of hepatic CYP metabolism shown by silybin. Silybin exhibits higher potency in inhibiting hepatic oxidation (K_i = 26.3 μM- intestine, 6.9 μM - liver) and hepatic glucuronidation (K_i = 12.5 μM- intestine, 0.9 μM - liver). However, the drastic difference in the predicted gut lumen (629 μM) versus portal vein concentrations (6 μM) is likely responsible for higher % inhibition of intestinal metabolism. Hoh et al. observed a 60 fold higher concentration of silibinin in the intestinal tissue (140 ± 170 μM) over the hepatic tissue (2.5 ± 2.4 μM) in cancer patients following oral administration of silibinin (1.4 g/day) [177].

In the presence of pterostilbene, CLint (hep,UGT) was predicted to be the most sensitive input variable that strongly influences all the output variables. This is expected because of the weak inhibition of glucuronidation and extremely potent inhibition of oxidation of BUP shown by pterostilbene in both intestine and liver. Pterostilbene appeared to be the most potent of all the inhibitors showing 22 to 24 fold increase in mean predicted F_{oral}, 105 fold enhancement in mean AUC_{∞} and 4 fold reduction in mean CL_{tot} of BUP. It was also effective in reducing the variability in the predicted mean F_{oral} of BUP. However as seen with other inhibitors, the % variability in AUC_{∞} after treatment with pterostilbene was very large especially in scenario #1 where 70% variability was

observed which would be clinically significant and highly undesirable. The likely cause of the higher variability in AUC_{∞} is the strong inhibition of CL_{tot} of BUP by pterostilbene, which converts a highly extracted drug like BUP in to a low extraction ratio drug. Thus, it is reasonable to expect that inhibitor concentration in the portal vein is extremely crucial in case of pterostilbene because it has a direct effect on the CL_{tot}. Of all the inhibitor treatments, pterostilbene had the highest portal vein concentration of 40.6 μM predicted assuming an oral bioavailability of 12.5%. To assess the effect of lower portal vein concentrations of pterostilbene, a dose – effect study was performed using 5 additional doses of pterostilbene, as shown in Figs. 6.1 – 6.3. A ten fold lower dose i.e. with I (GW) = 32.5 μM and I (hep) = 4.06 μM that could still achieve predicted F_{oral} closer to sublingual bioavailability of BUP (~33%) was chosen for further analysis. Published studies report a wide variability in F_{oral} of pterostilbene in rats ranging from 12.5 to 80% [133-135, 138], depending on the dose administered. Thus, an additional 60% variability was introduced in I (hep) and the effect of this lower dose on the output variables was investigated. As reported in Table 6.5, the variability in AUC_{∞} of BUP reduced by almost 50% in scenario #1 (from 95 % to 49%) and # 2 (from 50 % to 28%). Increasing the variability in I (hep) from 20% to 60% resulted in a minor increase in the variability around the mean of the output variables (Table 6.5). Thus, a lower dose of pterostilbene exhibited significant improvement in systemic availability of BUP to achieve an F_{oral} similar to the sublingual availability (~33%) of currently marketed BUP formulations. In addition, there was also a significant improvement in the predicted mean AUC_{∞} and modest reduction in the variability associated with the mean AUC_{∞} of BUP under both scenarios making pterostilbene the most favored candidate of all the inhibitors.

Cubitt et al. conducted a study quite similar to the initial part of our IVIVE analysis, to evaluate the contribution of the intestinal and hepatic - oxidation as well as glucuronidation to the metabolism of BUP (among other compounds) and predict its *in vivo* clearance after IV and oral administration [67]. The conclusions of their study about CYP being the dominant metabolic pathway (in both organs) and that intestinal oxidation exceeds hepatic oxidation (after correction for CYP3A abundance) support our results [67]. In addition, the F_g, F_h and F_{oral} values extrapolated using the *in vitro* intrinsic clearances of the Cubitt et al. study appear to be in fair agreement with our predicted estimates [67]. However, the study omits prediction of *in vivo* intrinsic clearance of BUP following oral administration due to lack of adequate information on PK of orally dosed BUP in humans. Using a simple static model i.e. well-stirred model and under a set of assumptions, we could predict the *in vivo* intrinsic clearance as well as the total systemic clearance of BUP in addition to F_{oral} [30]. Unfortunately, our predictions could not be validated due to lack of published clinical studies reporting these parameters for orally administered BUP in humans. Several published studies have tried to identify the factors responsible for the high degree of inter-individual variability in the systemic availabilities and exposures of CYP3A substrates among other CYP substrates [46, 55, 60, 61, 63, 158]. Significant research has been conducted on the use of various herbal compounds as bio-enhancers acting via inhibition of the most prevalent drug metabolizing enzymes such as CYP (especially CYP3A4) and UGTs [21-26, 46, 55, 60, 61, 63, 158, 160, 178]. Their application to improve the oral bioavailability of therapeutic agents has also been proposed, studied using *in vitro* systems and modeled using diverse *in silico* systems and PBPK models [21-26, 46, 55, 60, 61, 63, 158, 160, 178]. However, to the best of our

knowledge we did not come across combinatorial studies such as ours, that investigated the effect of such herbal/dietary agents to not only improve the pharmacokinetic properties of a drug but also reduce the variability associated with them.

6.5 Conclusion

The potential of five GRAS or dietary compounds (α-mangostin, chrysin, ginger extract, pterostilbene and silybin) to improve the oral bioavailability and systemic exposure and to reduce the variability associated with them was evaluated. Using the well-stirred model, the *in vitro* clearances of BUP in presence and absence of inhibitor treatments were extrapolated to predict their effect on F_{oral}, AUC_{∞} and CL_{tot} under physiological conditions. Of the five inhibitors, only pterostilbene and silybin could achieve an F_{oral} similar to the marketed sublingual products but with lower variability. However, these inhibitors exhibited an undesirable high variability in the systemic exposure of BUP under both higher (#1) and relatively lower (#2) variability scenarios. However, a ten fold lower concentration of pterostilbene (32.5 μM or 8.3 μg/ml) appeared to be the most effective in improving F_{oral} and AUC_{∞} considerably lowering their variability. These results provide strong support to our strategy of co-administering GRAS or dietary compounds like pterostilbene with BUP to inhibit its oxidative and conjugative metabolism and achieve sufficiently high oral availability and systemic exposure to produce its intended therapeutic effects. Future studies will focus on evaluating the effect of pterostilbene *in vivo* using animal models such as dogs to identify the effective clinical doses, study the PK profile of BUP in presence of the various doses of pterostilbene and to design a suitable dosing regimen for the oral administration of BUP + pterostilbene combination.

Chapter 7: Conclusions and Future Directions

Drug addiction including misuse of prescription pain opioid medications or use of illicit substances like heroin is a grave problem throughout the world [1]. Buprenorphine (BUP) alone or in combination with naloxone is a widely used therapeutic agent for treatment of opioid dependence as well as for pain management. It is available for several routes of administration (sublingual, buccal, intravenous, intramuscular, transdermal etc.) except the traditional oral route. The sublingual route suffers from disadvantages like inability to mask bitter taste, interference with daily activities, high interindividual variability in systemic availability & exposure due to factors such as inconsistencies in sublingual retention time, rate and extent of absorption from oral mucosa, loss of drug via swallowing etc. [2, 7] However, the extensive presystemic metabolism of BUP through oxidation and conjugation in intestine and liver significantly lowers its systemic availability, hindering its successful oral administration [11-14]. Hence, the main objective of this dissertation was to improve the oral bioavailability (F_{oral}) of BUP and reduce the variability associated with its bioavailability and systemic exposure (AUC_{∞}). An inhibitor strategy was proposed which includes use of *generally recognized as safe* (GRAS) compounds or components of dietary supplements to inhibit the oxidative and conjugative metabolism of BUP. *In vitro* to *in vivo* extrapolations (IVIVE) were performed to predict the F_{oral}, AUC_{∞} and total clearance (CL_{tot}) of BUP in presence and absence of five promising inhibitor candidates (α-mangostin, chrysin, ginger extract, pterostilbene and silybin). The overall conclusions based on the experiments conducted in each chapter are as discussed below:

7.1 Evaluating the intestinal permeability of BUP

One of the factors influencing the oral bioavailability of a compound is its gastrointestinal (GI) permeability. The intestinal permeability of BUP was evaluated using the well-characterized Caco-2 cell model, which involves studying the bidirectional transport of a test substrate through the tight monolayers of the Caco-2 cells plated on Transwell filters [86-88]. It was also of interest to determine if BUP undergoes efflux through intestinal efflux transporters such as P-gp, BCRP etc. As would be expected from a small lipophilic molecule, BUP appeared to be a highly permeable drug with an apparent absorptive permeability of 32 x 10^{-6} cm/s. The transport of BUP in basolateral to apical direction was quite similar to its transport from apical to basolateral direction resulting in an efflux ratio of ~1. Thus, the results of this study indicated that BUP is a highly permeable drug that does not undergo efflux transport by transporters like P-gp and BCRP in the Caco-2 cells. It was also inferred that since BUP was highly soluble and highly permeable, its poor oral bioavailability is most likely an outcome of its extensive presystemic metabolism.

7.2 Predicting the oral bioavailability of BUP

As presystemic metabolism was identified as the likely factor responsible for the poor oral bioavailability of BUP, its metabolism was closely studied in pooled human intestinal and liver microsomes. The intrinsic CYP and UGT clearances of BUP in pooled human intestinal and liver microsomes were extrapolated using a simple physiological model (i.e. well-stirred model) to predict intestinal (F_g) and hepatic (F_h) availabilities and ultimately F_{oral} of BUP. BUP was predicted to show 91% intestinal extraction (F_g = 0.09) and 71% hepatic extraction (F_h = 0.29) resulting in a mean predicted F_{oral} of 2.7%. The intrinsic CYP clearances were six and four fold higher than the UGT clearances in the

intestine and liver, respectively. Taken together, these results indicate significant contribution of the intestine to the overall presystemic metabolism of BUP and that CYP appears to be the dominant metabolic pathway for BUP in both intestine and liver. Our results appeared to be in good agreement with previous publications evaluating the contribution of hepatic and intestinal – oxidation and glucuronidation to the metabolism of BUP [67, 126].

7.3 Screening study to identify potential inhibitors

Several GRAS or dietary compounds have been studied for their effect on drug metabolizing enzymes like CYP, UGT, SULT etc. [21-26] Compounds with functional groups such as phenol, catechol, stilbene, flavanol etc. are ideal candidates for interacting with conjugating enzymes (UGT, SULT). Hence, 27 such compounds were evaluated for their potential to inhibit the oxidative and conjugative metabolism of BUP. The effect of these inhibitors (25 μM) on the formation of oxidative metabolite i.e. norbuprenorphine (NBUP) and conjugative metabolite i.e. buprenorphine glucuronide (BUPG) was monitored individually in the pooled human intestinal and liver microsomes. The results were subjected to a retrospective filter i.e. compounds inhibiting ≥50% of BUPG formation and/or ≥30% of NBUP formation, were identified as preferred inhibitors. Using this selection criterion, ten preferred inhibitors were identified, namely: chrysin, curcumin, ginger extract, 6-gingerol, hesperitin, α-mangostin, pterostilbene, quercetin, resveratrol and silybin.

7.4 Determination of potency of inhibition (IC_{50}) of the preferred candidates

The ten preferred inhibitors identified on the basis of the screening study were further scrutinized using factors such as favorable physiochemical properties, BCS class,

oral PK in humans and/or animals and the maximum daily dose in humans and further shortlisted to five promising inhibitors i.e. α-mangostin, chrysin, ginger extract, pterostilbene and silybin. The inhibitory potency (IC_{50}) of these five inhibitors towards each metabolic pathway was individually studied in pooled human intestinal and liver microsomes. Of the five compounds, pterostilbene appeared to be the most potent inhibitor ($IC_{50} \leq 1$ μM) of CYP metabolism in both intestine and liver while α-mangostin in intestine and silybin in liver were the most potent inhibitors of UGT metabolism of BUP. Ginger extract and chrysin exhibited moderate to low potency of inhibition for both the pathways in the intestinal and liver microsomes. An equipotent combination of pterostilbene and ginger extract was also tested for its potential to inhibit the metabolism of BUP in the intestinal microsomes. The results of the curve shift analysis indicate that the combination showed additive interactions for inhibition of both the metabolic pathways.

7.5 Determination of biorelevant solubility of the inhibitor candidates

The next logical step after studying the metabolism of BUP and identifying promising inhibitor candidates was to extrapolate the *in vitro* results to physiological levels and predict the F_{oral}, AUC_{∞} and CL_{tot} of BUP with and without inhibitor treatments. To improve the predictive power of the well-stirred model, an appropriate selection of inhibitor concentrations in the GI lumen was very critical. To aid in predicting the inhibitor concentrations in the gut lumen, the equilibrium solubilites of the shortlisted candidates (except ginger extract) were determined using a biorelevant medium (FaSSIF; fasted state simulated intestinal fluid). It was assumed that the equilibrium solubilites represent the concentration of the inhibitors in the GI lumen following oral administration. In addition to experimental determination, the equilibrium

solubilities of the four inhibitors were also predicted using ADMET predictor (Simulation Plus, CA). Pterostilbene and α-mangostin showed experimental biorelevant solubilites of 83.2 ± 0.07 µg/ml and 66.1 ± 0.01 µg/ml, respectively in good agreement with their predicted solubilities (55 and 50 µg/ml). On the other hand, chrysin and silybin exhibited biorelevant solubilities of 2.02 ± 0.01 µg/ml and 0.66 ± 0.01 µg/ml, respectively with a 52 and 242 fold difference in their respective predicted solubilites. For thoroughness in analysis, the extrapolations were performed using both experimental and predicted solubilities of chrysin and silybin. Irrespective of being experimentally determined or predicted, the equilibrium solubilities indicate that the four inhibitors show poor aqueous solubilites that might possibly lower their oral bioavailability.

7.6 *In vitro in vivo* extrapolation to predict the effect of inhibitors on F_{oral}, AUC_{∞} and CL_{tot} of BUP

To assess the effect of inhibitors on the variability associated with F_{oral}, AUC_{∞} and CL_{tot} of BUP, a simulated population dataset of 10,000 patients was generated using Monte Carlo simulations. BUP was predicted to show a poor and variable oral bioavailability (3 ± 2%) and systemic exposure (334 ± 327 ng*min/ml) with huge total clearance (1050 ml/min). Being the most potent inhibitor of the dominant CYP pathway, pterostilbene showed the highest improvement in mean predicted F_{oral} (22 fold) and AUC_{∞} (105 fold) and drastic reduction in CL_{tot} (4 fold) of BUP. Silybin appeared to be the second most effective inhibitor based on the extrapolations using its predicted solubility, showing an 11 and 16 fold increase in F_{oral} and AUC_{∞} of BUP, respectively. All the rest of the inhibitor treatments were not effective in achieving the F_{oral} equal to or more than the sublingual bioavailability of BUP (~33%). Despite showing significant enhancement of mean predicted F_{oral} and AUC_{∞} as well reduction of variability in mean

F_{oral}, both pterostilbene and silybin failed to reduce the variability in the mean AUC_{∞} of BUP. Hence, a concentration-effect study was performed using a wide range of pterostilbene concentrations (0 – 325 μM) and a concentration of 32.5 μM was chosen for further analysis. At this lower concentration, pterostilbene was still able to achieve an F_{oral} similar to sublingual bioavailability of BUP but also exhibited considerable reduction in the variability associated with the mean predicted AUC_{∞} of BUP. Increasing the variability in the portal vein inhibitor concentrations of pterostilbene (to 60%) did not produce significant increase in the variability in F_{oral} or AUC_{∞} at this lower dose. Pterostilbene exhibits potential to inhibit the systemic clearance of BUP in addition to its presystemic metabolism. Inhibition of systemic clearance can influence the elimination half-life of BUP, which might necessitate dose adjustment or alteration of the dosing regimen of BUP. Due to limited availability of clinical data after oral administration of BUP in humans, it was not possible to validate our predictions. Also due to limited clinical data on both BUP and the inhibitors, our model was built on several assumptions that may or may not be true. All these factors can have a significant effect on our predictions depending on the extent to which the assumptions deviate from clinical observations.

7.7 Overall conclusions

In conclusion, the overall results demonstrate feasibility of the proposed approach of co-administering GRAS inhibitors such as pterostilbene with BUP to inhibit its oxidative and conjugative metabolism and achieve sufficiently high F_{oral} & AUC_{∞} to produce its intended pharmacological effect. These results support the potential of developing an efficacious oral formulation of BUP with greater patient compliance to serve as a better alternative to sublingual BUP. The GRAS inhibitor strategy has

promising applicability to a wide variety of drugs suffering from low and variable oral bioavailability due to extensive presystemic metabolism.

7.8 Future directions

Future studies will focus on further characterizing the effect of pterostilbene on oral PK properties of BUP *in vivo* using animal models such as beagle dogs. Dogs appear to exhibit similarities in several PK properties (absorption, oral bioavailability, route of elimination and contribution of CYP vs. UGT metabolic pathways) to humans [10, 20]. The use of rats as an animal model for BUP is not recommended because this species strongly favors glucuronidation over oxidation, which contradicts the metabolic pattern of BUP observed in humans [9, 18, 19, 179]. Such *in vivo* studies can help in determining safe and effective doses of pterostilbene as well as an optimal dosing regimen for the BUP+pterostilbene oral formulation. The mechanism of inhibition of pterostilbene and possible time-dependent inhibition can be studied using *in vitro* systems like pooled microsomes, primary hepatocytes, intestinal cell lines etc. The metabolism of pterostilbene can be studied in the aforementioned *in vitro* systems to predict the extent of its metabolism *in vivo* and possible effects of the metabolites on the inhibition efficiency of pterostilbene. Using the Caco-2 cell monolayers, the permeability and possible efflux of pterostilbene at the GI lumen can be evaluated. On the basis of the collective results from all these *in vitro* studies, a more comprehensive physiologically based dynamic PK model can be developed to better predict the effect of inhibitors such as pterostilbene on the pharmacokinetics of BUP after oral administration in humans. Such a model is likely to be superior in its predictive power than the minimal model used in this dissertation. Combinations of pterostilbene with other GRAS or dietary compounds can also be tested to investigate any potential synergistic interactions, which

might help in reducing the overall dose of inhibitors to be co-administered with BUP. Formulation studies to develop nanoparticles or liposomes for the oral formulation of BUP and inhibitor(s) might prove helpful in overcoming the solubility issues of the inhibitors.

References

1. United States Department of Health HS. Substance A, Mental Health Services Administration. Center for Behavioral Health Services and Quality. National Survey on Drug Use and Health. *Inter-univeristy Consortium for Political and Social Reasearch (ICSPR)* 2014
2. Fischer A, Jonsson M and Hjelmstrom P. Pharmaceutical and pharmacokinetic characterization of a novel sublingual buprenorphine/naloxone tablet formulation in healthy volunteers. *Drug Dev Ind Pharm* 2015; 41: 79-84. DOI: 10.3109/03639045.2013.846365
3. Elkader A and Sproule B. Buprenorphine: clinical pharmacokinetics in the treatment of opioid dependence. *Clin Pharmacokinet* 2005; 44: 661-80. DOI: 10.2165/00003088-200544070-00001
4. Jones HE. Practical considerations for the clinical use of buprenorphine. *Sci Pract Perspect* 2004; 2: 4-20
5. Lutfy K and Cowan A. Buprenorphine: a unique drug with complex pharmacology. *Curr Neuropharmacol* 2004; 2: 395-402. DOI: 10.2174/1570159043359477
6. Ohtani M. Basic pharmacology of buprenorphine. *European Journal of Pain Supplements* 2007; 1: 69-73. DOI: 10.1016/S1754-3207(08)60017-6
7. Webpage. SC. Reckett Benckiser Inc. http://www.suboxone.com/; http://www. suboxone.com/hcp/about_suboxone/treatment_ evolution.aspx [Accessed 1 June 2013].
8. Jeffcoat ARea. Human Disposition of Intravenous, Oral and Sublingual [3H]-Buprenorphine. In *Problems of Drug Dependence, 1992:Proceeding of the 54th Annual Scientific Meeting The College on Problems of Drug Dependence,Inc NIDA research monograph 132*, Harris L (ed): Keystone, Colorado, 1992; 98.
9. Brewster D, Humphrey MJ and McLeavy MA. Biliary excretion, metabolism and enterohepatic circulation of buprenorphine. *Xenobiotica* 1981; 11: 189-96
10. Walter DaI, C. Absorption, Distribution, Metabolism, and Excretion of Buprenorphine in Animals and Humans. In *Buprenorphine: Combatting Drug Abuse With a Unique Opiod*, Cowan A, and Lewis, J. (ed). Wiley-Liss: NewYork, 1995; 113-135.
11. Iribarne C, Picart D, Dreano Y, Bail JP and Berthou F. Involvement of cytochrome P450 3A4 in N-dealkylation of buprenorphine in human liver microsomes. *Life Sci* 1997; 60: 1953-64
12. Picard N, Cresteil T, Djebli N and Marquet P. In vitro metabolism study of buprenorphine: evidence for new metabolic pathways. *Drug metabolism and disposition: the biological fate of chemicals* 2005; 33: 689-95. DOI: 10.1124/dmd.105.003681
13. Chang Y and Moody DE. Glucuronidation of buprenorphine and norbuprenorphine by human liver microsomes and UDP-glucuronosyltransferases. *Drug Metab Lett* 2009; 3: 101-7

14. Rouguieg K, Picard N, Sauvage FL, Gaulier JM and Marquet P. Contribution of the different UDP-glucuronosyltransferase (UGT) isoforms to buprenorphine and norbuprenorphine metabolism and relationship with the main UGT polymorphisms in a bank of human liver microsomes. *Drug metabolism and disposition: the biological fate of chemicals* 2010; 38: 40-5. DOI: 10.1124/dmd.109.029546
15. Seo KA, Kim HJ, Jeong ES, Abdalla N, Choi CS, Kim DH and Shin JG. In vitro assay of six UDP-glucuronosyltransferase isoforms in human liver microsomes, using cocktails of probe substrates and liquid chromatography-tandem mass spectrometry. *Drug metabolism and disposition: the biological fate of chemicals* 2014; 42: 1803-10. DOI: 10.1124/dmd.114.058818
16. Kuhlman JJ, Jr., Lalani S, Magluilo J, Jr., Levine B and Darwin WD. Human pharmacokinetics of intravenous, sublingual, and buccal buprenorphine. *J Anal Toxicol* 1996; 20: 369-78
17. Cone EJ, Gorodetzky CW, Yousefnejad D, Buchwald WF and Johnson RE. The metabolism and excretion of buprenorphine in humans. *Drug metabolism and disposition: the biological fate of chemicals* 1984; 12: 577-81
18. Brewster D, Humphrey MJ and McLeavy MA. The systemic bioavailability of buprenorphine by various routes of administration. *J Pharm Pharmacol* 1981; 33: 500-6
19. Furukawa T, Nakamori F, Tetsuka K, Naritomi Y, Moriguchi H, Yamano K, Terashita S and Teramura T. Quantitative prediction of intestinal glucuronidation of drugs in rats using in vitro metabolic clearance data. *Drug Metab Pharmacokinet* 2012; 27: 171-80
20. Furukawa T, Naritomi Y, Tetsuka K, Nakamori F, Moriguchi H, Yamano K, Terashita S, Tabata K and Teramura T. Species differences in intestinal glucuronidation activities between humans, rats, dogs and monkeys. *Xenobiotica* 2014; 44: 205-16. DOI: 10.3109/00498254.2013.828362
21. Appiah-Opong R, Commandeur JN, van Vugt-Lussenburg B and Vermeulen NP. Inhibition of human recombinant cytochrome P450s by curcumin and curcumin decomposition products. *Toxicology* 2007; 235: 83-91. DOI: 10.1016/j.tox.2007.03.007
22. Bhardwaj RK, Glaeser H, Becquemont L, Klotz U, Gupta SK and Fromm MF. Piperine, a major constituent of black pepper, inhibits human P-glycoprotein and CYP3A4. *J Pharmacol Exp Ther* 2002; 302: 645-50. DOI: 10.1124/jpet.102.034728
23. Custodio JM, Wu CY and Benet LZ. Predicting drug disposition, absorption/elimination/transporter interplay and the role of food on drug absorption. *Adv Drug Deliv Rev* 2008; 60: 717-33. DOI: 10.1016/j.addr.2007.08.043
24. Foti RS, Wahlstrom JL and Wienkers LC. The in vitro drug interaction potential of dietary supplements containing multiple herbal components. *Drug metabolism and disposition: the biological fate of chemicals* 2007; 35: 185-8. DOI: 10.1124/dmd.106.012724
25. Gufford BT, Chen G, Lazarus P, Graf TN, Oberlies NH and Paine MF. Identification of diet-derived constituents as potent inhibitors of intestinal

glucuronidation. *Drug metabolism and disposition: the biological fate of chemicals* 2014; 42: 1675-83. DOI: 10.1124/dmd.114.059451
26. Mandlekar S, Hong JL and Kong AN. Modulation of metabolic enzymes by dietary phytochemicals: a review of mechanisms underlying beneficial versus unfavorable effects. *Curr Drug Metab* 2006; 7: 661-75
27. Crommentuyn KM, Kappelhoff BS, Mulder JW, Mairuhu AT, van Gorp EC, Meenhorst PL, Huitema AD and Beijnen JH. Population pharmacokinetics of lopinavir in combination with ritonavir in HIV-1-infected patients. *Br J Clin Pharmacol* 2005; 60: 378-89. DOI: 10.1111/j.1365-2125.2005.02455.x
28. Molto J, Barbanoj MJ, Miranda C, Blanco A, Santos JR, Negredo E, Costa J, Domingo P, Clotet B and Valle M. Simultaneous population pharmacokinetic model for lopinavir and ritonavir in HIV-infected adults. *Clin Pharmacokinet* 2008; 47: 681-92. DOI: 10.2165/00003088-200847100-00005
29. Sham HL, Kempf DJ, Molla A, Marsh KC, Kumar GN, Chen CM, Kati W, Stewart K, Lal R, Hsu A, Betebenner D, Korneyeva M, Vasavanonda S, McDonald E, Saldivar A, Wideburg N, Chen X, Niu P, Park C, Jayanti V, Grabowski B, Granneman GR, Sun E, Japour AJ, Leonard JM, Plattner JJ and Norbeck DW. ABT-378, a highly potent inhibitor of the human immunodeficiency virus protease. *Antimicrob Agents Chemother* 1998; 42: 3218-24
30. Maharao NV, Joshi AA and Gerk PM. Inhibition of Glucuronidation and Oxidative Metabolism of Buprenorphine Using GRAS Compounds or Dietary Constituents/Supplements: In Vitro Proof of Concept. *Biopharm Drug Dispos* 2016. DOI: 10.1002/bdd.2050
31. Garavaglia J, Markoski MM, Oliveira A and Marcadenti A. Grape Seed Oil Compounds: Biological and Chemical Actions for Health. *Nutr Metab Insights* 2016; 9: 59-64. DOI: 10.4137/NMI.S32910
32. Shao X, Lv L, Parks T, Wu H, Ho CT and Sang S. Quantitative analysis of ginger components in commercial products using liquid chromatography with electrochemical array detection. *J Agric Food Chem* 2010; 58: 12608-14. DOI: 10.1021/jf1029256
33. Yu Y, Zick S, Li X, Zou P, Wright B and Sun D. Examination of the pharmacokinetics of active ingredients of ginger in humans. *AAPS J* 2011; 13: 417-26. DOI: 10.1208/s12248-011-9286-5
34. Zick SM, Djuric Z, Ruffin MT, Litzinger AJ, Normolle DP, Alrawi S, Feng MR and Brenner DE. Pharmacokinetics of 6-gingerol, 8-gingerol, 10-gingerol, and 6-shogaol and conjugate metabolites in healthy human subjects. *Cancer Epidemiol Biomarkers Prev* 2008; 17: 1930-6. DOI: 10.1158/1055-9965.EPI-07-2934
35. Colclough N, Ruston, L. and Tam, K. Aqueous Solubility in Drug Discovery Chemistry, DMPK, and Biological Assays. In *Estimation of Solubility, Permeability, Absorption and Bioavailability*, Testa HvdWaB (ed). Wiley-VCH Verlag GmbH & Co. KGaA: Weinheim, Germany, 2008.
36. Schwebel HJ, van Hoogevest P, Leigh ML and Kuentz M. The apparent solubilizing capacity of simulated intestinal fluids for poorly water-soluble drugs. *Pharm Dev Technol* 2011; 16: 278-86. DOI: 10.3109/10837451003664099

37. Davis AMaB, P. . In Silico Prediction of Solubility. In *Drug Bioavailability: Estimation of Solubility, Permeability, Absorption and Bioavailability*, Testa HvdWaB (ed). Wiley-VCH Verlag GmbH & Co. KGaA: Weinheim, Germany, 2008.
38. Fagerberg JH, Karlsson E, Ulander J, Hanisch G and Bergstrom CA. Computational prediction of drug solubility in fasted simulated and aspirated human intestinal fluid. *Pharm Res* 2015; 32: 578-89. DOI: 10.1007/s11095-014-1487-z
39. Mithani SD, Bakatselou V, TenHoor CN and Dressman JB. Estimation of the increase in solubility of drugs as a function of bile salt concentration. *Pharm Res* 1996; 13: 163-7
40. Klein S. The use of biorelevant dissolution media to forecast the in vivo performance of a drug. *AAPS J* 2010; 12: 397-406. DOI: 10.1208/s12248-010-9203-3
41. Takacs-Novak K, Szoke V, Volgyi G, Horvath P, Ambrus R and Szabo-Revesz P. Biorelevant solubility of poorly soluble drugs: rivaroxaban, furosemide, papaverine and niflumic acid. *J Pharm Biomed Anal* 2013; 83: 279-85. DOI: 10.1016/j.jpba.2013.05.011
42. Marques M, Lobenberg, R. and Almukainzi, M. Simulated Biological Fluids with Possible Application in Dissolution Testing. *Dissolution Technologies* 2011
43. Galia E, Nicolaides E, Horter D, Lobenberg R, Reppas C and Dressman JB. Evaluation of various dissolution media for predicting in vivo performance of class I and II drugs. *Pharm Res* 1998; 15: 698-705
44. Heikkinen AT, Fowler S, Gray L, Li J, Peng Y, Yadava P, Railkar A and Parrott N. In vitro to in vivo extrapolation and physiologically based modeling of cytochrome P450 mediated metabolism in beagle dog gut wall and liver. *Mol Pharm* 2013; 10: 1388-99. DOI: 10.1021/mp300692k
45. Cubitt HE, Houston JB and Galetin A. Prediction of human drug clearance by multiple metabolic pathways: integration of hepatic and intestinal microsomal and cytosolic data. *Drug metabolism and disposition: the biological fate of chemicals* 2011; 39: 864-73. DOI: 10.1124/dmd.110.036566
46. Cubitt HE, Yeo KR, Howgate EM, Rostami-Hodjegan A and Barter ZE. Sources of interindividual variability in IVIVE of clearance: an investigation into the prediction of benzodiazepine clearance using a mechanistic population-based pharmacokinetic model. *Xenobiotica* 2011; 41: 623-38. DOI: 10.3109/00498254.2011.560294
47. Darnell M, Ulvestad M, Ellis E, Weidolf L and Andersson TB. In vitro evaluation of major in vivo drug metabolic pathways using primary human hepatocytes and HepaRG cells in suspension and a dynamic three-dimensional bioreactor system. *J Pharmacol Exp Ther* 2012; 343: 134-44. DOI: 10.1124/jpet.112.195834
48. Galetin A. Rationalizing underprediction of drug clearance from enzyme and transporter kinetic data: from in vitro tools to mechanistic modeling. *Methods Mol Biol* 2014; 1113: 255-88. DOI: 10.1007/978-1-62703-758-7_13

49. Galetin A and Houston JB. Intestinal and hepatic metabolic activity of five cytochrome P450 enzymes: impact on prediction of first-pass metabolism. *J Pharmacol Exp Ther* 2006; 318: 1220-9. DOI: 10.1124/jpet.106.106013
50. Gertz M, Harrison A, Houston JB and Galetin A. Prediction of human intestinal first-pass metabolism of 25 CYP3A substrates from in vitro clearance and permeability data. *Drug metabolism and disposition: the biological fate of chemicals* 2010; 38: 1147-58. DOI: 10.1124/dmd.110.032649
51. Gill KL, Houston JB and Galetin A. Characterization of in vitro glucuronidation clearance of a range of drugs in human kidney microsomes: comparison with liver and intestinal glucuronidation and impact of albumin. *Drug metabolism and disposition: the biological fate of chemicals* 2012; 40: 825-35. DOI: 10.1124/dmd.111.043984
52. Ulvestad M, Darnell M, Molden E, Ellis E, Asberg A and Andersson TB. Evaluation of organic anion-transporting polypeptide 1B1 and CYP3A4 activities in primary human hepatocytes and HepaRG cells cultured in a dynamic three-dimensional bioreactor system. *J Pharmacol Exp Ther* 2012; 343: 145-56. DOI: 10.1124/jpet.112.195750
53. Ito K and Houston JB. Prediction of human drug clearance from in vitro and preclinical data using physiologically based and empirical approaches. *Pharm Res* 2005; 22: 103-12
54. Poulin P, Kenny JR, Hop CE and Haddad S. In vitro-in vivo extrapolation of clearance: modeling hepatic metabolic clearance of highly bound drugs and comparative assessment with existing calculation methods. *J Pharm Sci* 2012; 101: 838-51. DOI: 10.1002/jps.22792
55. Shen DD, Kunze KL and Thummel KE. Enzyme-catalyzed processes of first-pass hepatic and intestinal drug extraction. *Adv Drug Deliv Rev* 1997; 27: 99-127
56. Berezhkovskiy LM. The corrected traditional equations for calculation of hepatic clearance that account for the difference in drug ionization in extracellular and intracellular tissue water and the corresponding corrected PBPK equation. *J Pharm Sci* 2011; 100: 1167-83
57. Hallifax D, Foster JA and Houston JB. Prediction of human metabolic clearance from in vitro systems: retrospective analysis and prospective view. *Pharm Res* 2010; 27: 2150-61. DOI: 10.1007/s11095-010-0218-3
58. Houston JB and Galetin A. Methods for predicting in vivo pharmacokinetics using data from in vitro assays. *Curr Drug Metab* 2008; 9: 940-51
59. Howgate EM, Rowland Yeo K, Proctor NJ, Tucker GT and Rostami-Hodjegan A. Prediction of in vivo drug clearance from in vitro data. I: impact of inter-individual variability. *Xenobiotica* 2006; 36: 473-97. DOI: 10.1080/00498250600683197
60. Kato M, Chiba K, Ito T, Koue T and Sugiyama Y. Prediction of interindividual variability in pharmacokinetics for CYP3A4 substrates in humans. *Drug Metab Pharmacokinet* 2010; 25: 367-78
61. Paine MF, Khalighi M, Fisher JM, Shen DD, Kunze KL, Marsh CL, Perkins JD and Thummel KE. Characterization of interintestinal and intraintestinal

variations in human CYP3A-dependent metabolism. *J Pharmacol Exp Ther* 1997; 283: 1552-62
62. Shiran MR, Proctor NJ, Howgate EM, Rowland-Yeo K, Tucker GT and Rostami-Hodjegan A. Prediction of metabolic drug clearance in humans: in vitro-in vivo extrapolation vs allometric scaling. *Xenobiotica* 2006; 36: 567-80. DOI: 10.1080/00498250600761662
63. Thummel KE. Gut instincts: CYP3A4 and intestinal drug metabolism. *J Clin Invest* 2007; 117: 3173-6. DOI: 10.1172/JCI34007
64. Wienkers LC and Heath TG. Predicting in vivo drug interactions from in vitro drug discovery data. *Nat Rev Drug Discov* 2005; 4: 825-33. DOI: 10.1038/nrd1851
65. Yang J, Jamei M, Yeo KR, Tucker GT and Rostami-Hodjegan A. Prediction of intestinal first-pass drug metabolism. *Curr Drug Metab* 2007; 8: 676-84
66. Huang W, Lee SL and Yu LX. Mechanistic approaches to predicting oral drug absorption. *AAPS J* 2009; 11: 217-24. DOI: 10.1208/s12248-009-9098-z
67. Cubitt HE, Houston JB and Galetin A. Relative importance of intestinal and hepatic glucuronidation-impact on the prediction of drug clearance. *Pharm Res* 2009; 26: 1073-83. DOI: 10.1007/s11095-008-9823-9
68. Pang KS and Rowland M. Hepatic clearance of drugs. I. Theoretical considerations of a "well-stirred" model and a "parallel tube" model. Influence of hepatic blood flow, plasma and blood cell binding, and the hepatocellular enzymatic activity on hepatic drug clearance. *Journal of Pharmacokinetics and Biopharmaceutics* 1977; 5: 625-653. DOI: 10.1007/bf01059688
69. Rowland M, Benet LZ and Graham GG. Clearance concepts in pharmacokinetics. *Journal of Pharmacokinetics and Biopharmaceutics* 1973; 1: 123-136. DOI: 10.1007/bf01059626
70. Pang KS and Gillette JR. Theoretical relationships between area under the curve and route of administration of drugs and their precursors for evaluating sites and pathways of metabolism. *Journal of Pharmaceutical Sciences* 1978; 67: 703-704. DOI: 10.1002/jps.2600670536
71. Zanger UM and Schwab M. Cytochrome P450 enzymes in drug metabolism: regulation of gene expression, enzyme activities, and impact of genetic variation. *Pharmacol Ther* 2013; 138: 103-41. DOI: 10.1016/j.pharmthera.2012.12.007
72. Dannenberg LO and Edenberg HJ. Epigenetics of gene expression in human hepatoma cells: expression profiling the response to inhibition of DNA methylation and histone deacetylation. *BMC Genomics* 2006; 7: 181. DOI: 10.1186/1471-2164-7-181
73. Beierle I, Meibohm B and Derendorf H. Gender differences in pharmacokinetics and pharmacodynamics. *Int J Clin Pharmacol Ther* 1999; 37: 529-47
74. Edginton AN and Willmann S. Physiology-based simulations of a pathological condition: prediction of pharmacokinetics in patients with liver cirrhosis. *Clin Pharmacokinet* 2008; 47: 743-52. DOI: 10.2165/00003088-200847110-00005

75. Elbekai RH, Korashy HM and El-Kadi AO. The effect of liver cirrhosis on the regulation and expression of drug metabolizing enzymes. *Curr Drug Metab* 2004; 5: 157-67
76. Gandhi M, Aweeka F, Greenblatt RM and Blaschke TF. Sex differences in pharmacokinetics and pharmacodynamics. *Annu Rev Pharmacol Toxicol* 2004; 44: 499-523. DOI: 10.1146/annurev.pharmtox.44.101802.121453
77. Kinirons MT and O'Mahony MS. Drug metabolism and ageing. *Br J Clin Pharmacol* 2004; 57: 540-4. DOI: 10.1111/j.1365-2125.2004.02096.x
78. Stevens JC, Marsh SA, Zaya MJ, Regina KJ, Divakaran K, Le M and Hines RN. Developmental changes in human liver CYP2D6 expression. *Drug metabolism and disposition: the biological fate of chemicals* 2008; 36: 1587-93. DOI: 10.1124/dmd.108.021873
79. Yang X, Zhang B, Molony C, Chudin E, Hao K, Zhu J, Gaedigk A, Suver C, Zhong H, Leeder JS, Guengerich FP, Strom SC, Schuetz E, Rushmore TH, Ulrich RG, Slatter JG, Schadt EE, Kasarskis A and Lum PY. Systematic genetic and genomic analysis of cytochrome P450 enzyme activities in human liver. *Genome Res* 2010; 20: 1020-36. DOI: 10.1101/gr.103341.109
80. Thummel KE, O'Shea D, Paine MF, Shen DD, Kunze KL, Perkins JD and Wilkinson GR. Oral first-pass elimination of midazolam involves both gastrointestinal and hepatic CYP3A-mediated metabolism. *Clin Pharmacol Ther* 1996; 59: 491-502. DOI: 10.1016/S0009-9236(96)90177-0
81. Palisade C. Knowledge base and user manual. 2015.
82. Wang DG, Dong QQ, Du J, Yang S, Zhang YJ, Na GS, Ferguson SG, Wang Z and Zheng T. Using Monte Carlo simulation to assess variability and uncertainty of tobacco consumption in a city by sewage epidemiology. *BMJ Open* 2016; 6: e010583. DOI: 10.1136/bmjopen-2015-010583
83. Joshi A, Halquist M, Konsoula Z, Liu Y, Jones JP, 3rd, Heidbreder C and Gerk PM. Improving the oral bioavailability of buprenorphine: an in-vivo proof of concept. *J Pharm Pharmacol* 2017; 69: 23-31. DOI: 10.1111/jphp.12652
84. Suzuki T, Zaima C, Moriki Y, Fukami T and Tomono K. P-glycoprotein mediates brain-to-blood efflux transport of buprenorphine across the blood-brain barrier. *J Drug Target* 2007; 15: 67-74. DOI: 10.1080/10611860601141606
85. Hassan HE, Myers AL, Coop A and Eddington ND. Differential involvement of P-glycoprotein (ABCB1) in permeability, tissue distribution, and antinociceptive activity of methadone, buprenorphine, and diprenorphine: in vitro and in vivo evaluation. *J Pharm Sci* 2009; 98: 4928-40. DOI: 10.1002/jps.21770
86. Angelis ID and Turco L. Caco-2 cells as a model for intestinal absorption. *Curr Protoc Toxicol* 2011; Chapter 20: Unit20 6. DOI: 10.1002/0471140856.tx2006s47
87. Progress CBR. Caco-2 Cells and their Uses. . In *ProQuest ebrary*, Hauppauge UN (ed), 2011.
88. Polli JW, Wring SA, Humphreys JE, Huang L, Morgan JB, Webster LO and Serabjit-Singh CS. Rational use of in vitro P-glycoprotein assays in drug discovery. *J Pharmacol Exp Ther* 2001; 299: 620-8

89. Yee S. In vitro permeability across Caco-2 cells (colonic) can predict in vivo (small intestinal) absorption in man--fact or myth. *Pharm Res* 1997; 14: 763-6
90. Joshi AA, Maharao N. V. and Gerk, P. M. Simultaneous quantitation of buprenorphine and its metabolites using LC–MS. . *Current Trends in Mass Spectrometry* 2016; 14: 15–19
91. Smetanova L, Stetinova V, Kholova D, Kvetina J, Smetana J and Svoboda Z. Caco-2 cells and Biopharmaceutics Classification System (BCS) for prediction of transepithelial transport of xenobiotics (model drug: caffeine). *Neuro endocrinology letters* 2009; 30 Suppl 1: 101-5
92. Minderman H, Suvannasankha A, O'Loughlin KL, Scheffer GL, Scheper RJ, Robey RW and Baer MR. Flow cytometric analysis of breast cancer resistance protein expression and function. *Cytometry* 2002; 48: 59-65. DOI: 10.1002/cyto.10111
93. Robey RW, Honjo Y, van de Laar A, Miyake K, Regis JT, Litman T and Bates SE. A functional assay for detection of the mitoxantrone resistance protein, MXR (ABCG2). *Biochim Biophys Acta* 2001; 1512: 171-82
94. Cone EJ, Gorodetzky CW, Darwin WD and Buchwald WF. Stability of the 6,14-endo-ethanotetrahydrooripavine analgesics: acid-catalyzed rearrangement of buprenorphine. *J Pharm Sci* 1984; 73: 243-6
95. Houston JB and Kenworthy KE. In vitro-in vivo scaling of CYP kinetic data not consistent with the classical Michaelis-Menten model. *Drug metabolism and disposition: the biological fate of chemicals* 2000; 28: 246-54
96. Barsukov I, Modi S, Lian LY, Sze KH, Paine MJ, Wolf CR and Roberts GC. 1H, 15N and 13C NMR resonance assignment, secondary structure and global fold of the FMN-binding domain of human cytochrome P450 reductase. *J Biomol NMR* 1997; 10: 63-75
97. Rostami-Hodjegan A and Tucker G. 'In silico' simulations to assess the 'in vivo' consequences of 'in vitro' metabolic drug-drug interactions. *Drug Discov Today Technol* 2004; 1: 441-8. DOI: 10.1016/j.ddtec.2004.10.002
98. Bullingham RE, McQuay HJ, Porter EJ, Allen MC and Moore RA. Sublingual buprenorphine used postoperatively: ten hour plasma drug concentration analysis. *Br J Clin Pharmacol* 1982; 13: 665-73
99. Mendelson J, Upton RA, Everhart ET, Iii PJ and Jones RT. Bioavailability of Sublingual Buprenorphine. *The Journal of Clinical Pharmacology* 1997; 37: 31-37. DOI: 10.1177/009127009703700106
100. [Date Accessed Accessed].
101. Gerk JEF, Pharm D. Price of suboxone Fork Union Pharmacy, Fork Union, VA, 23055, 2017.
102. Rai S, Mukherjee K, Mal M, Wahile A, Saha BP and Mukherjee PK. Determination of 6-gingerol in ginger (Zingiber officinale) using high-performance thin-layer chromatography. *J Sep Sci* 2006; 29: 2292-5
103. van Waterschoot RA, Rooswinkel RW, Sparidans RW, van Herwaarden AE, Beijnen JH and Schinkel AH. Inhibition and stimulation of intestinal and hepatic CYP3A activity: studies in humanized CYP3A4 transgenic mice using

triazolam. *Drug metabolism and disposition: the biological fate of chemicals* 2009; 37: 2305-13. DOI: 10.1124/dmd.109.029397
104. Miners JO, Smith PA, Sorich MJ, McKinnon RA and Mackenzie PI. Predicting human drug glucuronidation parameters: application of in vitro and in silico modeling approaches. *Annu Rev Pharmacol Toxicol* 2004; 44: 1-25. DOI: 10.1146/annurev.pharmtox.44.101802.121546
105. Finel M and Kurkela M. The UDP-glucuronosyltransferases as oligomeric enzymes. *Curr Drug Metab* 2008; 9: 70-6
106. Liu J, Tawa GJ and Wallqvist A. Identifying cytochrome p450 functional networks and their allosteric regulatory elements. *PLoS One* 2013; 8: e81980. DOI: 10.1371/journal.pone.0081980
107. Hosea NA, Miller GP and Guengerich FP. Elucidation of distinct ligand binding sites for cytochrome P450 3A4. *Biochemistry* 2000; 39: 5929-39
108. Boocock DJ, Faust GE, Patel KR, Schinas AM, Brown VA, Ducharme MP, Booth TD, Crowell JA, Perloff M, Gescher AJ, Steward WP and Brenner DE. Phase I dose escalation pharmacokinetic study in healthy volunteers of resveratrol, a potential cancer chemopreventive agent. *Cancer Epidemiol Biomarkers Prev* 2007; 16: 1246-52. DOI: 10.1158/1055-9965.EPI-07-0022
109. Cheng AL, Hsu CH, Lin JK, Hsu MM, Ho YF, Shen TS, Ko JY, Lin JT, Lin BR, Ming-Shiang W, Yu HS, Jee SH, Chen GS, Chen TM, Chen CA, Lai MK, Pu YS, Pan MH, Wang YJ, Tsai CC and Hsieh CY. Phase I clinical trial of curcumin, a chemopreventive agent, in patients with high-risk or pre-malignant lesions. *Anticancer Res* 2001; 21: 2895-900
110. Erlund I, Kosonen T, Alfthan G, Maenpaa J, Perttunen K, Kenraali J, Parantainen J and Aro A. Pharmacokinetics of quercetin from quercetin aglycone and rutin in healthy volunteers. *Eur J Clin Pharmacol* 2000; 56: 545-53
111. Egert S, Wolffram S, Bosy-Westphal A, Boesch-Saadatmandi C, Wagner AE, Frank J, Rimbach G and Mueller MJ. Daily quercetin supplementation dose-dependently increases plasma quercetin concentrations in healthy humans. *J Nutr* 2008; 138: 1615-21
112. Pawar YB, Purohit H, Valicherla GR, Munjal B, Lale SV, Patel SB and Bansal AK. Novel lipid based oral formulation of curcumin: development and optimization by design of experiments approach. *Int J Pharm* 2012; 436: 617-23. DOI: 10.1016/j.ijpharm.2012.07.031
113. Ohtani M, Kotaki H, Uchino K, Sawada Y and Iga T. Pharmacokinetic analysis of enterohepatic circulation of buprenorphine and its active metabolite, norbuprenorphine, in rats. *Drug metabolism and disposition: the biological fate of chemicals* 1994; 22: 2-7
114. Walle T, Hsieh F, DeLegge MH, Oatis JE, Jr. and Walle UK. High absorption but very low bioavailability of oral resveratrol in humans. *Drug metabolism and disposition: the biological fate of chemicals* 2004; 32: 1377-82. DOI: 10.1124/dmd.104.000885
115. Anand P, Kunnumakkara AB, Newman RA and Aggarwal BB. Bioavailability of curcumin: problems and promises. *Mol Pharm* 2007; 4: 807-18. DOI: 10.1021/mp700113r

116. Li YM, Li XM, Li GM, Du WC, Zhang J, Li WX, Xu J, Hu M and Zhu Z. In vivo pharmacokinetics of hesperidin are affected by treatment with glucosidase-like BglA protein isolated from yeasts. *J Agric Food Chem* 2008; 56: 5550-7. DOI: 10.1021/jf800105c
117. Li L, Brunner I, Han AR, Hamburger M, Kinghorn AD, Frye R and Butterweck V. Pharmacokinetics of alpha-mangostin in rats after intravenous and oral application. *Mol Nutr Food Res* 2011; 55 Suppl 1: S67-74. DOI: 10.1002/mnfr.201000511
118. Li L, Han AR, Kinghorn AD, Frye RF, Derendorf H and Butterweck V. Pharmacokinetic properties of pure xanthones in comparison to a mangosteen fruit extract in rats. *Planta Med* 2013; 79: 646-53. DOI: 10.1055/s-0032-1328543
119. Moon YJ, Wang L, DiCenzo R and Morris ME. Quercetin pharmacokinetics in humans. *Biopharm Drug Dispos* 2008; 29: 205-17. DOI: 10.1002/bdd.605
120. Stingl JC, Bartels H, Viviani R, Lehmann ML and Brockmoller J. Relevance of UDP-glucuronosyltransferase polymorphisms for drug dosing: A quantitative systematic review. *Pharmacol Ther* 2014; 141: 92-116. DOI: 10.1016/j.pharmthera.2013.09.002
121. Bock KW, Lilienblum W, Fischer G, Schirmer G and Bock-Henning BS. The role of conjugation reactions in detoxication. *Arch Toxicol* 1987; 60: 22-9
122. Mulder GJ. Glucuronidation and its role in regulation of biological activity of drugs. *Annu Rev Pharmacol Toxicol* 1992; 32: 25-49. DOI: 10.1146/annurev.pa.32.040192.000325
123. Radominska-Pandya A, Czernik PJ, Little JM, Battaglia E and Mackenzie PI. Structural and functional studies of UDP-glucuronosyltransferases. *Drug Metab Rev* 1999; 31: 817-99. DOI: 10.1081/DMR-100101944
124. Tukey RH and Strassburg CP. Human UDP-glucuronosyltransferases: metabolism, expression, and disease. *Annu Rev Pharmacol Toxicol* 2000; 40: 581-616. DOI: 10.1146/annurev.pharmtox.40.1.581
125. Williams JA, Hyland R, Jones BC, Smith DA, Hurst S, Goosen TC, Peterkin V, Koup JR and Ball SE. Drug-drug interactions for UDP-glucuronosyltransferase substrates: a pharmacokinetic explanation for typically observed low exposure (AUCi/AUC) ratios. *Drug metabolism and disposition: the biological fate of chemicals* 2004; 32: 1201-8. DOI: 10.1124/dmd.104.000794
126. Kilford PJ, Stringer R, Sohal B, Houston JB and Galetin A. Prediction of drug clearance by glucuronidation from in vitro data: use of combined cytochrome P450 and UDP-glucuronosyltransferase cofactors in alamethicin-activated human liver microsomes. *Drug metabolism and disposition: the biological fate of chemicals* 2009; 37: 82-9. DOI: 10.1124/dmd.108.023853
127. Kesarwani K, Gupta R and Mukerjee A. Bioavailability enhancers of herbal origin: an overview. *Asian Pac J Trop Biomed* 2013; 3: 253-66. DOI: 10.1016/S2221-1691(13)60060-X
128. Ajazuddin, Alexander A, Qureshi A, Kumari L, Vaishnav P, Sharma M, Saraf S and Saraf S. Role of herbal bioactives as a potential bioavailability enhancer for Active Pharmaceutical Ingredients. *Fitoterapia* 2014; 97: 1-14. DOI: 10.1016/j.fitote.2014.05.005

129. Walle T, Otake Y, Brubaker JA, Walle UK and Halushka PV. Disposition and metabolism of the flavonoid chrysin in normal volunteers. *Br J Clin Pharmacol* 2001; 51: 143-6
130. Wu AG, Zeng B, Huang MQ, Li SM, Chen JN and Lai XP. The absorption and transport of magnolol in Caco-2 cell model. *Chin J Integr Med* 2013; 19: 206-11. DOI: 10.1007/s11655-012-1098-7
131. Waldmann S, Almukainzi M, Bou-Chacra NA, Amidon GL, Lee BJ, Feng J, Kanfer I, Zuo JZ, Wei H, Bolger MB and Lobenberg R. Provisional biopharmaceutical classification of some common herbs used in Western medicine. *Mol Pharm* 2012; 9: 815-22. DOI: 10.1021/mp200162b
132. Amidon GL, Lennernas H, Shah VP and Crison JR. A theoretical basis for a biopharmaceutic drug classification: the correlation of in vitro drug product dissolution and in vivo bioavailability. *Pharm Res* 1995; 12: 413-20
133. Azzolini M, La Spina M, Mattarei A, Paradisi C, Zoratti M and Biasutto L. Pharmacokinetics and tissue distribution of pterostilbene in the rat. *Mol Nutr Food Res* 2014; 58: 2122-32. DOI: 10.1002/mnfr.201400244
134. Kapetanovic IM, Muzzio M, Huang Z, Thompson TN and McCormick DL. Pharmacokinetics, oral bioavailability, and metabolic profile of resveratrol and its dimethylether analog, pterostilbene, in rats. *Cancer Chemother Pharmacol* 2011; 68: 593-601. DOI: 10.1007/s00280-010-1525-4
135. Lin HS, Yue BD and Ho PC. Determination of pterostilbene in rat plasma by a simple HPLC-UV method and its application in pre-clinical pharmacokinetic study. *Biomed Chromatogr* 2009; 23: 1308-15. DOI: 10.1002/bmc.1254
136. Galijatovic A, Otake Y, Walle UK and Walle T. Extensive metabolism of the flavonoid chrysin by human Caco-2 and Hep G2 cells. *Xenobiotica* 1999; 29: 1241-56. DOI: 10.1080/004982599237912
137. Walle UK, Galijatovic A and Walle T. Transport of the flavonoid chrysin and its conjugated metabolites by the human intestinal cell line Caco-2. *Biochem Pharmacol* 1999; 58: 431-8
138. Bethune S, Schultheiss, N. and Henck, J. Improving the Poor Aqueous Solubility of Nutraceutical Compound Pterostilbene through Cocrystal Formation. *Crystal Growth and Design* 2011; 11: 2817-2823
139. Lipert MP and Rodriguez-Hornedo N. Cocrystal Transition Points: Role of Cocrystal Solubility, Drug Solubility, and Solubilizing Agents. *Mol Pharm* 2015; 12: 3535-46. DOI: 10.1021/acs.molpharmaceut.5b00111
140. Sobers HS. Accessing the bioavailability of phytochemicals in Caco-2 cell model and developing a sensitive method for the detection and quantification of these compounds. xiii, 95 pages.
141. Zhao L, Wientjes MG and Au JL. Evaluation of combination chemotherapy: integration of nonlinear regression, curve shift, isobologram, and combination index analyses. *Clin Cancer Res* 2004; 10: 7994-8004. DOI: 10.1158/1078-0432.CCR-04-1087
142. Gruber VA and McCance-Katz EF. Methadone, buprenorphine, and street drug interactions with antiretroviral medications. *Curr HIV/AIDS Rep* 2010; 7: 152-60. DOI: 10.1007/s11904-010-0048-2

143. McCance-Katz EF, Moody DE, Morse GD, Ma Q, DiFrancesco R, Friedland G, Pade P and Rainey PM. Interaction between buprenorphine and atazanavir or atazanavir/ritonavir. *Drug Alcohol Depend* 2007; 91: 269-78. DOI: 10.1016/j.drugalcdep.2007.06.007
144. McCance-Katz EF, Moody DE, Smith PF, Morse GD, Friedland G, Pade P, Baker J, Alvanzo A, Jatlow P and Rainey PM. Interactions between buprenorphine and antiretrovirals. II. The protease inhibitors nelfinavir, lopinavir/ritonavir, and ritonavir. *Clin Infect Dis* 2006; 43 Suppl 4: S235-46. DOI: 10.1086/508188
145. Moody DE, Liu F and Fang WB. Azole antifungal inhibition of buprenorphine, methadone and oxycodone in vitro metabolism. *J Anal Toxicol* 2015; 39: 374-86. DOI: 10.1093/jat/bkv030
146. McCance-Katz EF, Sullivan LE and Nallani S. Drug interactions of clinical importance among the opioids, methadone and buprenorphine, and other frequently prescribed medications: a review. *Am J Addict* 2010; 19: 4-16. DOI: 10.1111/j.1521-0391.2009.00005.x
147. Beaulieu M, Levesque E, Hum DW and Belanger A. Isolation and characterization of a novel cDNA encoding a human UDP-glucuronosyltransferase active on C19 steroids. *J Biol Chem* 1996; 271: 22855-62
148. Ohno S and Nakajin S. Determination of mRNA expression of human UDP-glucuronosyltransferases and application for localization in various human tissues by real-time reverse transcriptase-polymerase chain reaction. *Drug metabolism and disposition: the biological fate of chemicals* 2009; 37: 32-40. DOI: 10.1124/dmd.108.023598
149. Harbourt DE, Fallon JK, Ito S, Baba T, Ritter JK, Glish GL and Smith PC. Quantification of human uridine-diphosphate glucuronosyl transferase 1A isoforms in liver, intestine, and kidney using nanobore liquid chromatography-tandem mass spectrometry. *Anal Chem* 2012; 84: 98-105. DOI: 10.1021/ac201704a
150. Sridar C, Goosen TC, Kent UM, Williams JA and Hollenberg PF. Silybin inactivates cytochromes P450 3A4 and 2C9 and inhibits major hepatic glucuronosyltransferases. *Drug metabolism and disposition: the biological fate of chemicals* 2004; 32: 587-94. DOI: 10.1124/dmd.32.6.587
151. Ottaviani G, Wendelspiess S and Alvarez-Sanchez R. Importance of critical micellar concentration for the prediction of solubility enhancement in biorelevant media. *Mol Pharm* 2015; 12: 1171-9. DOI: 10.1021/mp5006992
152. Yu JN, Zhu Y, Wang L, Peng M, Tong SS, Cao X, Qiu H and Xu XM. Enhancement of oral bioavailability of the poorly water-soluble drug silybin by sodium cholate/phospholipid-mixed micelles. *Acta Pharmacol Sin* 2010; 31: 759-64. DOI: 10.1038/aps.2010.55
153. Ulvestad M, Bjorquist P, Molden E, Asberg A and Andersson TB. OATP1B1/1B3 activity in plated primary human hepatocytes over time in culture. *Biochem Pharmacol* 2011; 82: 1219-26. DOI: 10.1016/j.bcp.2011.07.076

154. Obach RS. Prediction of human clearance of twenty-nine drugs from hepatic microsomal intrinsic clearance data: An examination of in vitro half-life approach and nonspecific binding to microsomes. *Drug metabolism and disposition: the biological fate of chemicals* 1999; 27: 1350-9
155. Stringer RA, Strain-Damerell C, Nicklin P and Houston JB. Evaluation of recombinant cytochrome P450 enzymes as an in vitro system for metabolic clearance predictions. *Drug metabolism and disposition: the biological fate of chemicals* 2009; 37: 1025-34. DOI: 10.1124/dmd.108.024810
156. Barter ZE, Perrett HF, Yeo KR, Allorge D, Lennard MS and Rostami-Hodjegan A. Determination of a quantitative relationship between hepatic CYP3A5*1/*3 and CYP3A4 expression for use in the prediction of metabolic clearance in virtual populations. *Biopharm Drug Dispos* 2010; 31: 516-32. DOI: 10.1002/bdd.732
157. Rawden HC, Carlile DJ, Tindall A, Hallifax D, Galetin A, Ito K and Houston JB. Microsomal prediction of in vivo clearance and associated interindividual variability of six benzodiazepines in humans. *Xenobiotica* 2005; 35: 603-25. DOI: 10.1080/00498250500162870
158. Peters SA, Schroeder PE, Giri N and Dolgos H. Evaluation of the use of static and dynamic models to predict drug-drug interaction and its associated variability: impact on drug discovery and early development. *Drug metabolism and disposition: the biological fate of chemicals* 2012; 40: 1495-507. DOI: 10.1124/dmd.112.044602
159. Cer RZ, Mudunuri U, Stephens R and Lebeda FJ. IC50-to-Ki: a web-based tool for converting IC50 to Ki values for inhibitors of enzyme activity and ligand binding. *Nucleic Acids Res* 2009; 37: W441-5. DOI: 10.1093/nar/gkp253
160. Basheer L and Kerem Z. Interactions between CYP3A4 and Dietary Polyphenols. *Oxid Med Cell Longev* 2015; 2015: 854015. DOI: 10.1155/2015/854015
161. Foti RS, Pearson JT, Rock DA, Wahlstrom JL and Wienkers LC. In vitro inhibition of multiple cytochrome P450 isoforms by xanthone derivatives from mangosteen extract. *Drug metabolism and disposition: the biological fate of chemicals* 2009; 37: 1848-55. DOI: 10.1124/dmd.109.028043
162. Jenkinson C, Petroczi A and Naughton DP. Red wine and component flavonoids inhibit UGT2B17 in vitro. *Nutr J* 2012; 11: 67. DOI: 10.1186/1475-2891-11-67
163. Jenkinson C, Petroczi A and Naughton DP. Effects of Dietary Components on Testosterone Metabolism via UDP-Glucuronosyltransferase. *Front Endocrinol (Lausanne)* 2013; 4: 80. DOI: 10.3389/fendo.2013.00080
164. Kimura Y, Ito H, Ohnishi R and Hatano T. Inhibitory effects of polyphenols on human cytochrome P450 3A4 and 2C9 activity. *Food Chem Toxicol* 2010; 48: 429-35. DOI: 10.1016/j.fct.2009.10.041
165. Piver B, Berthou F, Dreano Y and Lucas D. Differential inhibition of human cytochrome P450 enzymes by epsilon-viniferin, the dimer of resveratrol: comparison with resveratrol and polyphenols from alcoholized beverages. *Life Sci* 2003; 73: 1199-213

166. Regev-Shoshani G, Shoseyov O and Kerem Z. Influence of lipophilicity on the interactions of hydroxy stilbenes with cytochrome P450 3A4. *Biochem Biophys Res Commun* 2004; 323: 668-73. DOI: 10.1016/j.bbrc.2004.08.141
167. Vijayakumar TM, Kumar RM, Agrawal A, Dubey GP and Ilango K. Comparative inhibitory potential of selected dietary bioactive polyphenols, phytosterols on CYP3A4 and CYP2D6 with fluorometric high-throughput screening. *J Food Sci Technol* 2015; 52: 4537-43. DOI: 10.1007/s13197-014-1472-x
168. https://www.fda.gov/downloads/drugs/drugsafety/postmarketdrugsafetyinformationforpatientsandproviders/ucm191529.pdf. [Date Accessed Accessed].
169. Pfeiffer E, Heuschmid FF, Kranz S and Metzler M. Microsomal hydroxylation and glucuronidation of [6]-gingerol. *J Agric Food Chem* 2006; 54: 8769-74. DOI: 10.1021/jf062235l
170. Ito K, Chiba K, Horikawa M, Ishigami M, Mizuno N, Aoki J, Gotoh Y, Iwatsubo T, Kanamitsu S, Kato M, Kawahara I, Niinuma K, Nishino A, Sato N, Tsukamoto Y, Ueda K, Itoh T and Sugiyama Y. Which concentration of the inhibitor should be used to predict in vivo drug interactions from in vitro data? *AAPS PharmSci* 2002; 4: E25. DOI: 10.1208/ps040425
171. Gutierrez-Orozco F and Failla ML. Biological activities and bioavailability of mangosteen xanthones: a critical review of the current evidence. *Nutrients* 2013; 5: 3163-83. DOI: 10.3390/nu5083163
172. Wu JW, Lin LC and Tsai TH. Drug-drug interactions of silymarin on the perspective of pharmacokinetics. *J Ethnopharmacol* 2009; 121: 185-93. DOI: 10.1016/j.jep.2008.10.036
173. Paixao P, Gouveia LF and Morais JA. Prediction of the human oral bioavailability by using in vitro and in silico drug related parameters in a physiologically based absorption model. *Int J Pharm* 2012; 429: 84-98. DOI: 10.1016/j.ijpharm.2012.03.019
174. Tian S, Li Y, Wang J, Zhang J and Hou T. ADME evaluation in drug discovery. 9. Prediction of oral bioavailability in humans based on molecular properties and structural fingerprints. *Mol Pharm* 2011; 8: 841-51. DOI: 10.1021/mp100444g
175. Kumar R, Sharma A and Varadwaj PK. A prediction model for oral bioavailability of drugs using physicochemical properties by support vector machine. *J Nat Sci Biol Med* 2011; 2: 168-73. DOI: 10.4103/0976-9668.92325
176. Zheng CaW, Y. Prediction of Oral Bioavailability: Challenges and Strategies. *J Bioequiv* 2013; 6. DOI: 10.4172/jbb.10000e47
177. Hoh C, Boocock D, Marczylo T, Singh R, Berry DP, Dennison AR, Hemingway D, Miller A, West K, Euden S, Garcea G, Farmer PB, Steward WP and Gescher AJ. Pilot study of oral silibinin, a putative chemopreventive agent, in colorectal cancer patients: silibinin levels in plasma, colorectum, and liver and their pharmacodynamic consequences. *Clin Cancer Res* 2006; 12: 2944-50. DOI: 10.1158/1078-0432.CCR-05-2724
178. Dudhatra GB, Mody SK, Awale MM, Patel HB, Modi CM, Kumar A, Kamani DR and Chauhan BN. A comprehensive review on pharmacotherapeutics of

herbal bioenhancers. *ScientificWorldJournal* 2012; 2012: 637953. DOI: 10.1100/2012/637953
179. Mistry M and Houston JB. Glucuronidation in vitro and in vivo. Comparison of intestinal and hepatic conjugation of morphine, naloxone, and buprenorphine. *Drug metabolism and disposition: the biological fate of chemicals* 1987; 15: 710-7
180. Schmiedlin-Ren P, Thummel KE, Fisher JM, Paine MF and Watkins PB. Induction of CYP3A4 by 1 alpha,25-dihydroxyvitamin D3 is human cell line-specific and is unlikely to involve pregnane X receptor. *Drug metabolism and disposition: the biological fate of chemicals* 2001; 29: 1446-53
181. Chang JH, Plise E, Cheong J, Ho Q and Lin M. Evaluating the in vitro inhibition of UGT1A1, OATP1B1, OATP1B3, MRP2, and BSEP in predicting drug-induced hyperbilirubinemia. *Mol Pharm* 2013; 10: 3067-75. DOI: 10.1021/mp4001348
182. Donato MT, Montero S, Castell JV, Gomez-Lechon MJ and Lahoz A. Validated assay for studying activity profiles of human liver UGTs after drug exposure: inhibition and induction studies. *Analytical and bioanalytical chemistry* 2010; 396: 2251-63. DOI: 10.1007/s00216-009-3441-1
183. Khojasteh SC, Prabhu S, Kenny JR, Halladay JS and Lu AY. Chemical inhibitors of cytochrome P450 isoforms in human liver microsomes: a re-evaluation of P450 isoform selectivity. *Eur J Drug Metab Pharmacokinet* 2011; 36: 1-16. DOI: 10.1007/s13318-011-0024-2
184. Chou TC. Theoretical basis, experimental design, and computerized simulation of synergism and antagonism in drug combination studies. *Pharmacol Rev* 2006; 58: 621-81. DOI: 10.1124/pr.58.3.10

Appendix 1: Previous work in LS180 cells and UGT1A1

The goal of this dissertation was to explore the potential of the GRAS compounds/dietary constituents/dietary supplements to significantly inhibit the pre-systemic metabolism of BUP. Appendix 1 focuses on preliminary experimental studies conducted in LS 180 cells and recombinant UGT1A1.

A1 Methods:

A1.1 Kinetic and inhibition studies in the induced LS180 cells

The LS180 cells were treated with calcitriol (5 μM) to induce CYP3A4 expression and this induction was confirmed using P450-Glo assay (Promega, using selective CYP3A4 fluorescent probe; data not shown). Calcitriol concentration was chosen based on previously published study evaluating the effect of varying concentrations of calcitriol on CYPA4 induction in different cell lines including LS180 cells [180]. After induction (72 - 96 hours), the cells were exposed to BUP (10 μM) alone or along with certain putative inhibitors (24 μM) for two hours. The reaction was quenched with equal volume of cold acetonitrile at the end of the incubation time. The cells were then scraped followed by centrifugation at 12,500 rpm for 10 min (4ºC) to remove the protein. The supernatant (75 μL) was then analyzed using reversed phase HPLC coupled with UV spectrometric detection and Acquity QDa mass detection. The incubation time was optimized by monitoring the formation of metabolites i.e. norbuprenorphine (NBUP) and buprenorphine glucuronide (BUPG) at various time points till 2 hours. Kinetic experiments were performed by incubating increasing concentrations of buprenorphine (1 μM–160 μM) with induced LS180 cells. The Michaelis-Menten or Hill equation was fit to the resulting kinetic data, and the kinetic parameters were calculated by nonlinear regression analysis using Prism v6.0 (GraphPad

Software, Inc.; La Jolla, CA). Intrinsic clearances (Cl_{int}) were estimated using Equation 1 when the Michaelis-Menten (MM) equation was chosen and Equation 2 [95] when the Hill equation was used.

$$Cl_{int} = \frac{V_{max}}{K_m} \quad (1)$$

$$Cl_{int} = \frac{V_{max}}{K_m} \times \frac{n-1}{n(n-1)^{1/n}} \quad (2)$$

where V_{max} is the maximal velocity rate, K_m is the substrate concentration at 50% of V_{max}, and n is the Hill slope.

When present, inhibitor solutions (final concentration: 24 μM) were prepared from DMSO stock solutions (25 mM) for all pure compounds based upon their molecular weights as usual. However, since ginger extract is a mixture of mainly 6-, 8- and 10-gingerols and 6-shogaol [32], the molecular mass of 8-gingerol was chosen as an approximate representative of the mixture, and stock solutions of ginger extract were prepared to provide a final total concentration of 24 μM. Buprenorphine (17 μM) was incubated with or without 24 μM of inhibitors for 2 hours. Control reactions were carried out in the absence of inhibitors (solvent control). Significant inhibition was tested by comparing the % inhibition of norbuprenorphine or buprenorphine glucuronide formation to control reactions (no inhibition) using one-way ANOVA with Dunnett's post-hoc test ($\alpha = 0.05$; Prism v6.0). All the results are reported as mean ± SD for quadruplicate measurements.

A1.2 Kinetic and inhibition studies using recombinant UGT1A1

Linearity of BUPG formation at two recombinant UGT1A1 protein concentrations (0.2 and 0.4 mg/mL) was monitored till 1 hour (BUP = 5 μM). BUP (2 –

150μM) was incubated with 0.4 mg/mL UGT1A1 for 1 hour to establish saturable formation of the glucuronide metabolite. A typical reaction mixture (100 μL) comprised 0.4 mg/mL of recombinant UGT1A1, 50 mM Tris HCl (0.025% BSA), 2.5 mM UDPGA, 12.5 mM magnesium chloride, 8 mM saccharolactone and 31.25 μg/mL alamethicin. The reaction was quenched with equal volume of cold acetonitrile followed by centrifugation for 10 min (12,500 rpm at 4^{o}C) to precipitate protein. The supernatant was analyzed using the HPLC- UV-Acquity QDa mass spectrometric detection system. As stated earlier MM (Eq. 1) or Hill equation (Eq. 2) was fitted to the saturation data. GraphPad Prism v.6.0 was used for curve fitting and non-linear regression analysis for calculating the kinetic parameter estimates.

The inhibitors showing good inhibition of UGT metabolism of BUP in the induced LS180 cells were further tested in recombinant UGT1A1. List of tested inhibitors includes α-mangostin, 6-gingerol, hesperetin, iso-eugenol, magnolol, menthol, menthyl acetate, naringin, propyl paraben, pulegone, resveratrol and silybin. BUP (5 μM) was incubated with selected inhibitors (24 μM) for 1 hour with 0.4 mg/ml of recombinant UGT1A1 and the effect of inhibitors on BUPG formation was monitored.

A1.3 Determination of the relative contribution of the UGT and CYP isoforms in the induced LS180 cells using isoform selective inhibitors

It was of interest to estimate the relative contribution of the CYP and UGT isoforms towards formation of NBUP and BUPG, respectively in the induced LS180 cells. Hence, the formation of these metabolites in presence of certain isoform selective inhibitors was monitored in the induced LS180 cells. Same experimental procedure as explained earlier was used for performing these studies. Atazanavir (1 μM), lithocholic acid (20 μM) and amitriptyline (1 mM) were chosen as the selective inhibitors for UGT -

1A1, 1A3 and 2B7, respectively [15, 181, 182]. On the other hand, ketoconazole (1 μM), quinidine (2 μM), sulphenazole (20 μM) and montelukast (0.5 μM) were used as the selective inhibitors for CYP – 3A4, 2D6, 2C9 and 2C8, respectively [183]. These inhibitors were tested using two-fold higher concentrations than their IC_{50} or K_i values reported in the literature. [15, 181, 182]

A2 Results:

A2.1 Kinetic and inhibition studies in the induced LS180 cells

In the non-induced LS180 cells, NBUP formation appeared to be negligible (<LLOQ of NBUP, Fig. 1). After treatment with calcitriol, the NBUP formation in the induced LS180 cells increased drastically (Fig 1). Calcitriol treatment produced a two-fold increase in BUPG formation (Fig. 2), indicating possible induction of the glucuronidation pathway. Formation of both metabolites (BUP = 17 μM) was linear till two hours in the induced cells, however it explained only about ~ 50% of the disappearance of BUP (Fig. 3-4, Table 1). Non-specific binding of BUP and/or involvement of other metabolic pathways might account for the missing mass balance. The negative Y-intercept for the metabolites indicates that there is a lag time involved in the formation of metabolites. This time is most likely the time it takes for BUP to permeate and accumulate in the cells and reach the enzymes to form the metabolites. The formation of both the metabolites was saturable (Fig. 5-6); parameter estimates are reported in Table 2. MM model was chosen for both the metabolites because it had lower AIC value than the Hill model, indicating that this fit had least error. Glucuronidation appeared to be the major pathway compared to oxidation especially at BUP concentrations < 24μM. Inhibition studies indicated that 11/20 and 5/20 inhibitors,

significantly inhibited BUPG and NBUP formation respectively, while 5/20 significantly inhibited both the pathways (Figs. 7 and 8). Fig. 9 depicts the reduction in disappearance of BUP (% of control) versus inhibitor treatments. The test inhibitors that significantly reduced BUPG and/or NBUP formation seemed to reduce BUP disappearance to varying extents except hesperitin (despite showing 70 – 80% inhibition of BUPG and NBUP formation). Ginger extract and geraniol were found to significantly increase NBUP formation while showing modest (ginger extract) to no (geraniol) inhibition of BUPG formation.

Limitations:

While conducting the inhibition studies, < 20% metabolism of BUP was allowed to occur to target the linear kinetic range. The S/N ratio for BUP was relatively low; consequently the detection of BUP levels while monitoring its disappearance was not adequately sensitive. Formation rates were not normalized with protein content to account for differences in protein concentrations in different wells. The intrinsic oxidative and conjugative clearances of BUP were not corrected for protein binding shown by BUP in the LS180 cell matrix. The results of the kinetic study appeared to be in disagreement with the published studies as well as our microsomal studies, which indicate oxidation to be the dominant metabolic pathway of BUP in the intestine than glucuronidation [30, 67, 126]. In addition, the BUPG levels were higher in the induced cells than the non-induced cells, which might explain the greater conjugation of BUP than oxidation observed in the induced LS180 cells. Thus, the induced LS180 cell model was not successful in simulating the intestinal metabolic conditions of BUP in humans.

Figure 1: NBUP formation in induced vs non-induced LS180 cells

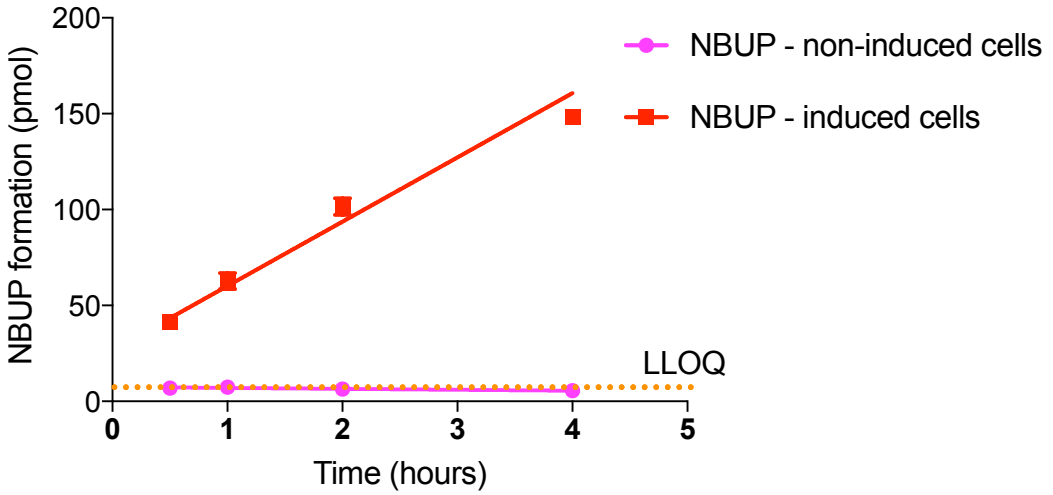

Fig 1: Kinetics of NBUP formation in induced and non-induced LS180 cells. Data shows mean ± SD values for quadruplicate measurements. Treatment with 5 µM calcitriol drastically increased the formation rate of NBUP in the induced LS180 cells.

Figure 2: Formation of BUPG in induced vs. non-induced LS180 cells

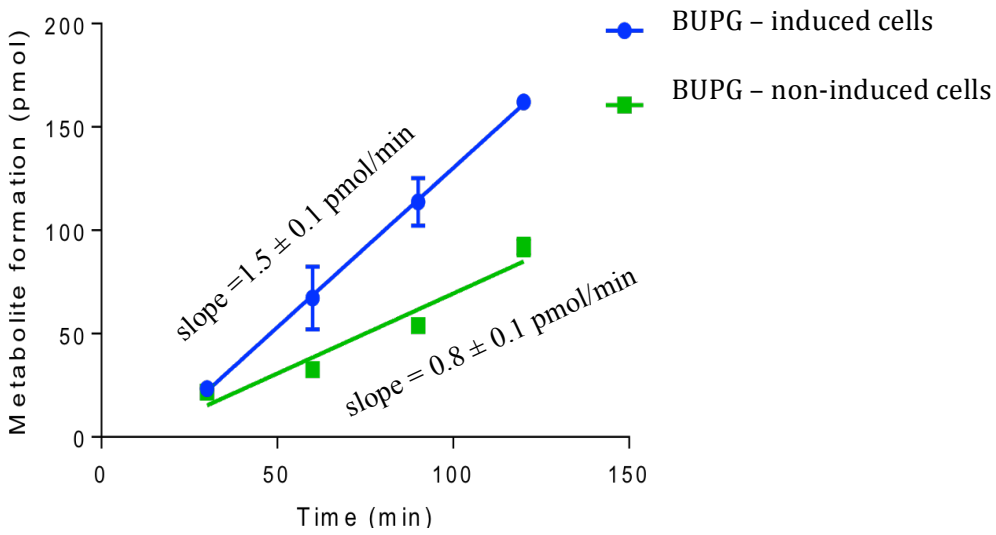

Fig 2: Kinetics of BUPG formation in induced and non-induced LS180 cells. Data shows mean ± SD values for quadruplicate measurements. Formation rate of BUPG appeared to be about two fold higher in the induced LS180 cells.

Figure 3: Linearity of metabolite formation in the induced LS180 cells

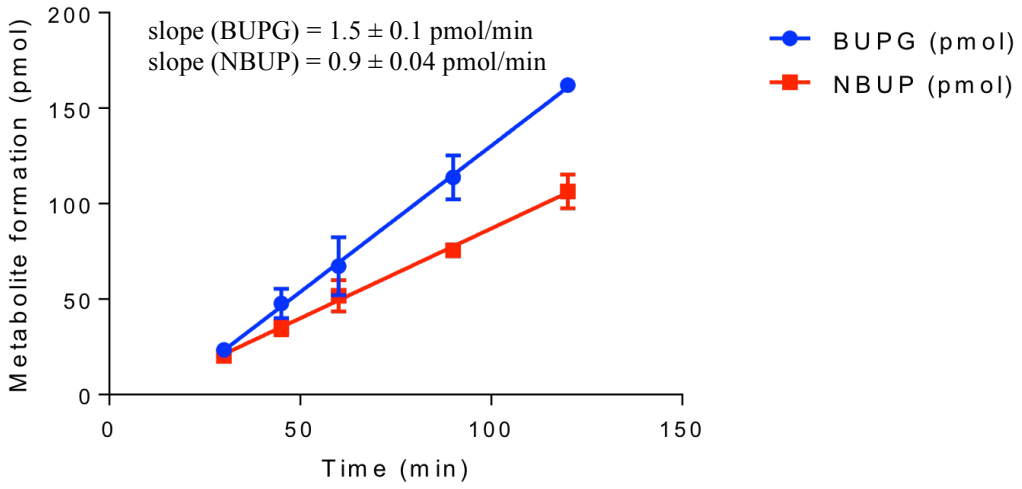

Figure 4: Disappearance of BUP and appearance of metabolites

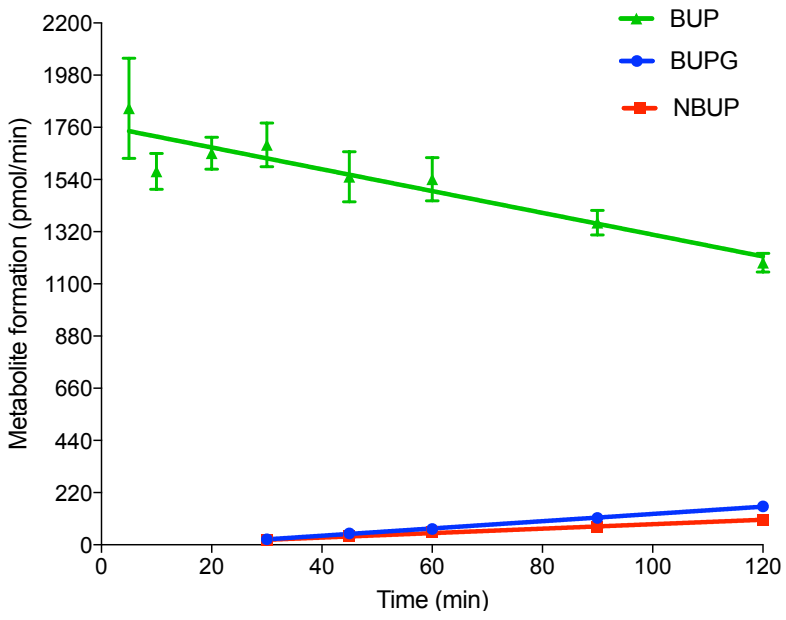

Fig 3 and 4: Formation of BUPG and NBUP (BUP=17µM) appears to be linear till two hours in LS180 cells. Rate of disappearance of BUP is faster than the formation of BUPG & NBUP.

Figure 5: Saturation of BUPG formation

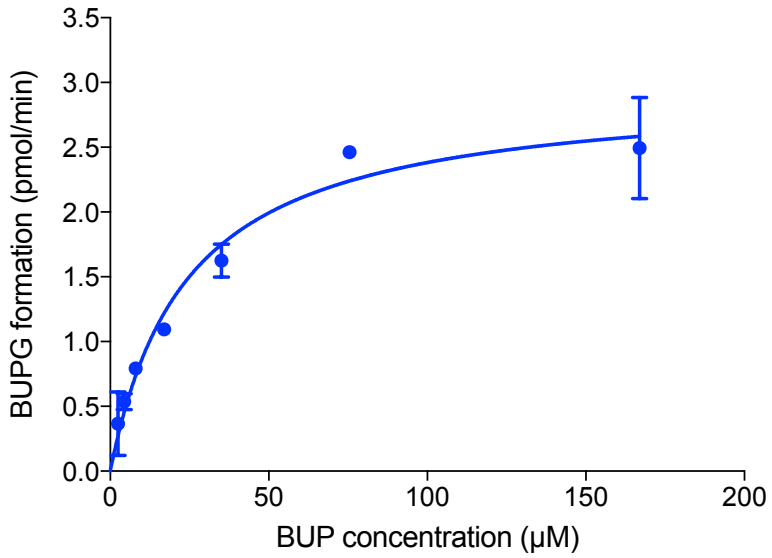

Fig 5: Saturable formation of BUPG was observed in the induced LS180 cells and it appeared to follow MM kinetics (BUP=2 –160µM). Data show mean ± SD values for quadruplicate measurements.

Figure 6: Saturation of NBUP formation

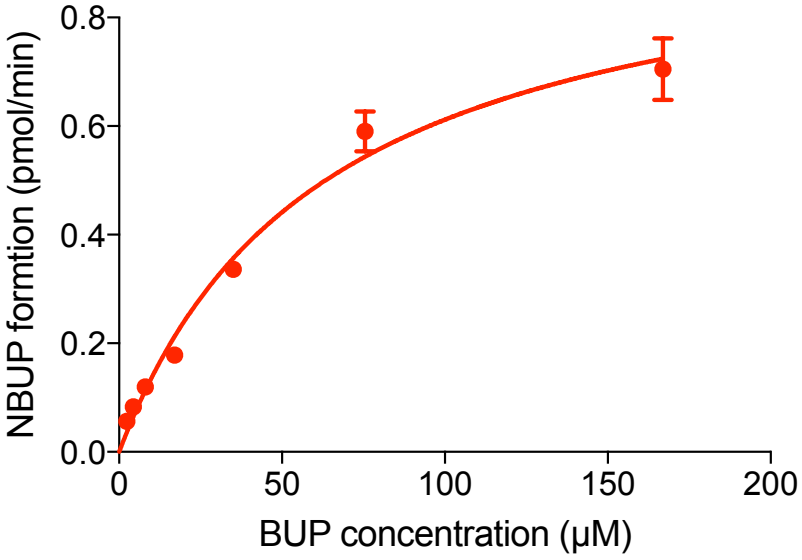

Fig 6: Saturable formation of NBUP was observed in the induced LS180 cells and it appeared to follow MM kinetics (BUP=2 – 160µM). Data show mean ± SD values for quadruplicate measurements.

Table 1: Metabolite formation and disappearance of BUP

Parameter	BUPG	NBUP
V_{max} (pmol/min)	3.0 ± 0.1	1.0 ± 0.1
K_m (µM)	24 ± 3.4	63 ± 6.9
Cl_{int} (µL/min)[a]	0.13	0.02
R^2	0.94	0.98

Table 2: Results of the saturation assay

Parameter	BUP	BUPG	NBUP
Y-intercept (pmol)	1770 ± 33.3	-23 ± 4.5	-7.0 ± 3.0
Slope (pmol/min)	-4.6 ± 0.6	1.5 ± 0.1	0.9 ± 0.04
Lag time (min)	----	14	7.5
R^2	0. 70	0.97	0.97

Figure 7: Inhibition of BUPG formation in induced LS180 cells

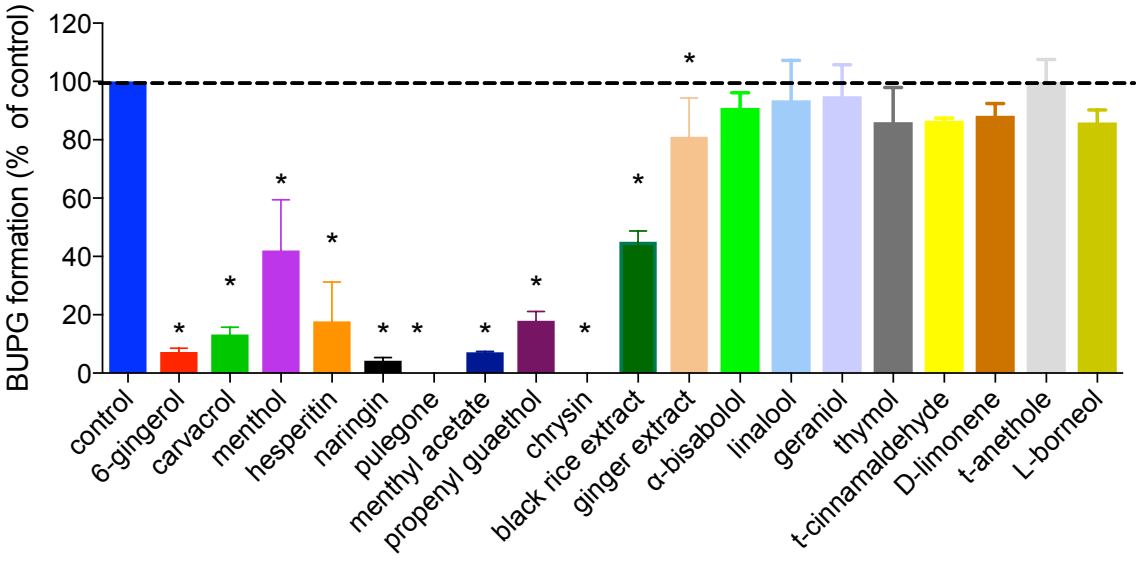

Fig 7: Inhibition of glucuronidation of BUP by various inhibitors. BUP (10µM) was incubated for 2 hours in presence and absence of test inhibitors (24µM). Results are expressed as % of control and depict mean ± SD for quadruplicate measurements. * indicates significant difference (α = 0.05) from control. BUPG formation in control was 2.99 ± 0.62 pmol/min.

Figure 8: Inhibition of NBUP formation in induced LS180 cells

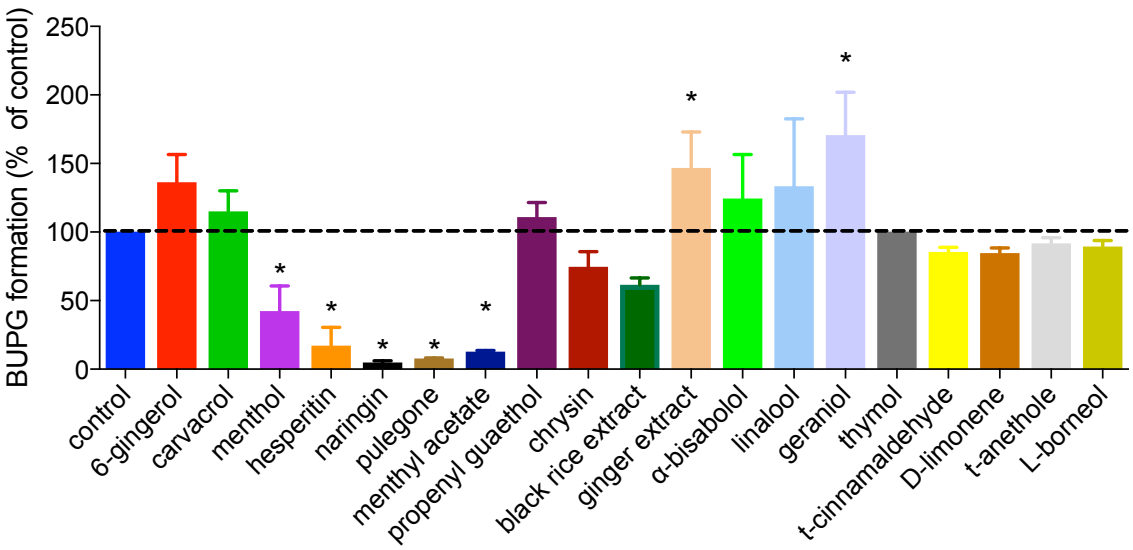

Fig 8: Inhibition of oxidation of BUP by various inhibitors. BUP (10 μM) was incubated for 2 hours in presence and absence of test inhibitors (24μM). Results are expressed as % of control and depict mean ± SD for quadruplicate measurements. * indicates significant difference (α = 0.05) from control. BUPG formation in control was 1.12 ± 0.35 pmol/min.

Figure 9: Reduction in disappearance of BUP in induced LS180 cells

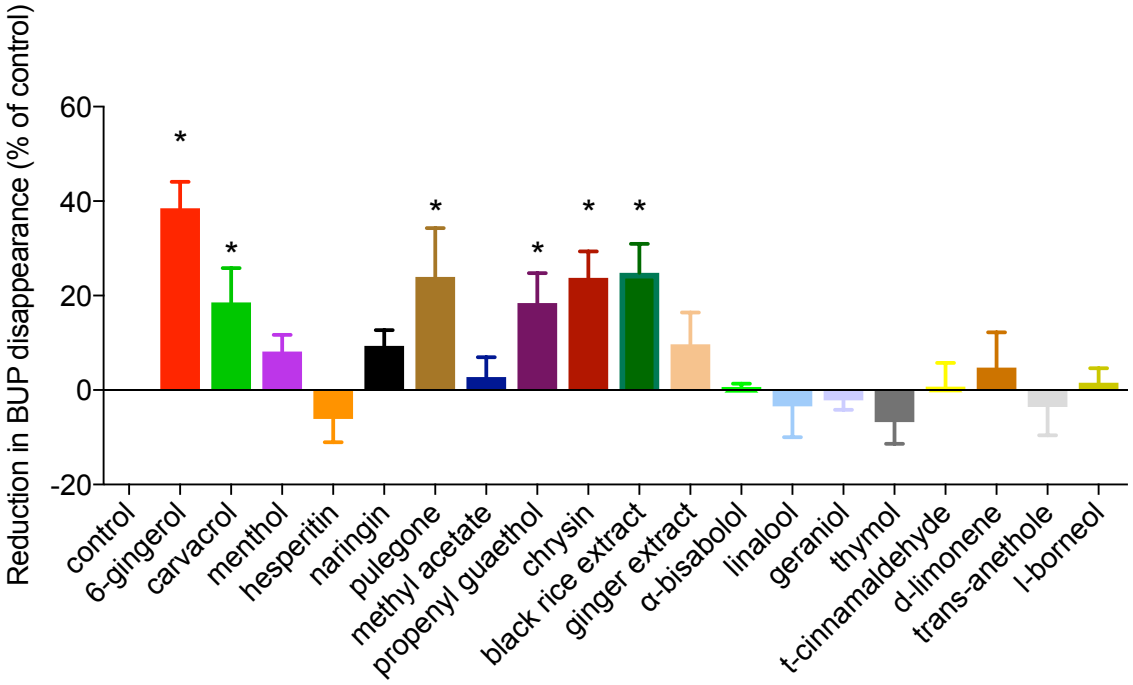

Fig 9: Reduction in the disappearance rate of BUP in induced LS180 cells. Results are expressed as % of control and depict mean ± SD for quadruplicate measurements. Control (no inhibitor) indicates no reduction in BUP disappearance. * indicates significant difference (α = 0.05) in reduction of BUP disappearance rate with respect to control.

A2.2 Kinetic and inhibition studies in recombinant UGT1A1

Formation of BUPG appeared to be linear till 1 hour and approximately proportional to protein concentration (Fig. 10). BUPG formation was saturable and the parameter estimates were in fair agreement with published values (Fig 11, Table 3). Hill model was chosen because it showed the least AIC value (difference of 23.5 in the AIC values of Hill and MM model, p-value <0.0001 for F-test). The disappearance of BUP (-1.5±0.4 pmol/min) was accounted for by formation of BUPG (1.8 ± 0.1 pmol/min) indicating achievement of mass balance in the recombinant system. Intrinsic clearance was calculated using Eq. 2. The K_m for BUPG formation appeared about two fold higher in the recombinant system than the induced LS180 cells. α-Mangostin, hesperetin, magnolol, naringin, resveratrol and silybin exhibited significant inhibition of BUPG formation (Fig. 12-13). On the other hand, compounds such as 6-gingerol, menthol, menthyl acetate and propyl paraben produced an apparent stimulation of BUPG formation (Fig. 12-13). Inhibitors that produced significant inhibition of glucuronidation of BUP in the induced LS180 cells (6-gingerol, isoeugenol, menthol, menthyl acetate, propyl paraben and pulegone) were not necessarily effective in the recombinant system. Probable reasons for such an occurrence include differences in the activity of UGT1A1 enzyme in the recombinant system versus the induced LS180 cells, significant inhibition of the other UGT isoforms involved in conjugation of BUP (UGT1A3 and/or 2B7) or inadequate inhibitor concentrations (possibility of higher K_i in the recombinant system). All the results are reported as mean ± SD for triplicate measurements.

Figure 10: Optimization of incubation time and recombinant UGT1A1 concentration

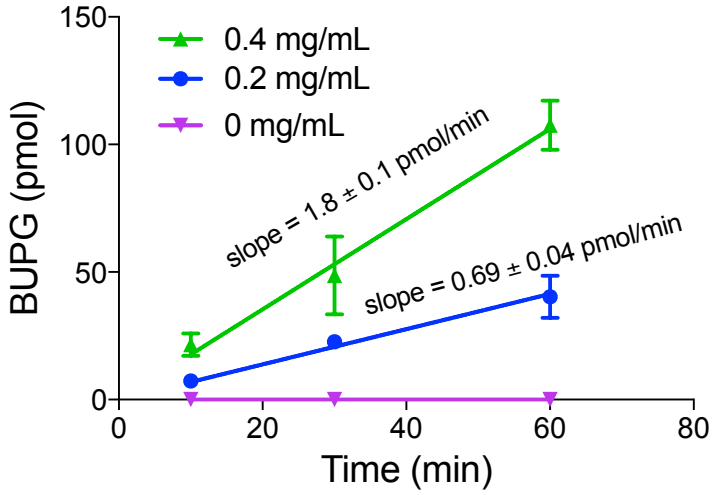

Fig 10: Formation of BUPG (BUP=5 µM) at various protein concentrations appears to be linear till 1 hour in the recombinant UGT1A1 enzyme. The R^2 values at 0.2 and 0.4 mg/ml protein concentrations were 0.90 and 0.94, respectively.

Figure 11: Saturable formation of BUPG in recombinant UGT1A1

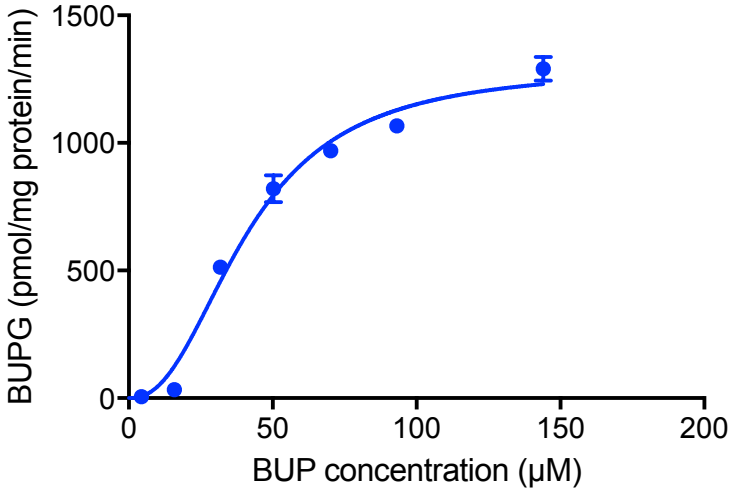

Fig 11: Saturable formation of BUPG was observed in recombinant UGT1A1 and it appeared to follow Hill equation kinetics (BUP=2–160µM). Data shows mean ± SD for triplicate measurements.

Table 3: Results of the kinetic studies for BUPG formation in recombinant UGT1A1

Parameter	Gerk lab	Picard (DMD, 2010)
V_{max} (pmol/min/mg protein)	1300 ± 56	1769 ± 240
K_m (μM)	41.3 ± 2.4	71.8 ± 12.4
h	2.3 ± 0.26	1.7 ± 0.2
Intrinsic clearance (μL/min/mg protein)	15.9	12.5
Enzyme conc (mg/ml)	0.40	0.20
LLOQ (nM)	39	2

Figure 12: Inhibition of BUPG formation in recombinant UGT1A1 (0.025% BSA)

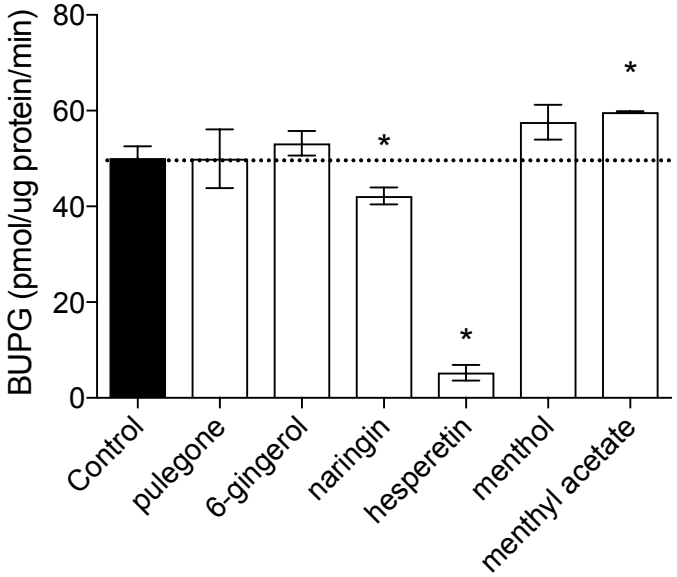

Fig 12: Inhibition of glucuronidation of BUP by various inhibitors. BUP (10 μM) was incubated for 1 hour in presence and absence of test inhibitors (24 μM). Results are expressed as mean ± SD for triplicate measurements. * indicates significant difference (α = 0.05) from control. BUPG formation is control was 50.1 ± 1.97 pmol/min/mg protein.

Figure 13: Inhibition of BUPG formation in recombinant UGT1A1 (no BSA)

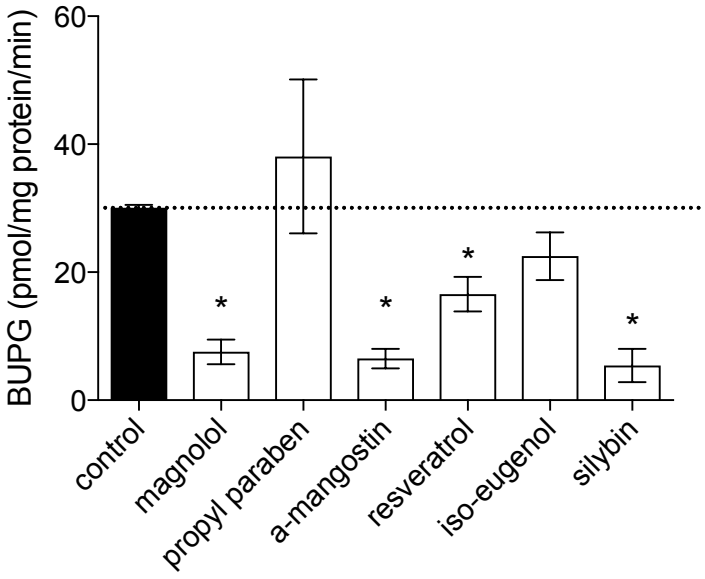

Fig 13: Inhibition of glucuronidation of BUP by various inhibitors. BUP (10 μM) was incubated for 1 hour in presence and absence of test inhibitors (24 μM). The reaction mixture lacked presence of BSA. Results are expressed as mean ± SD for triplicate measurements. * indicates significant difference (α = 0.05) from control. BUPG formation is control was 30.1 ± 0.37 pmol/min/mg protein.

A2.3 Determination of the relative contribution of the UGT and CYP isoforms in the induced LS180 cells using isoform selective inhibitors

Using atazanavir, lithocholic acid and amitriptyline as selective UGT 1A1, 1A3 and 2B7 inhibitors, BUPG formation was inhibited by 50%, 64% and 80%, respectively (Fig 14). These results suggest highest contribution of UGT2B7 towards BUPG formation followed by UGT1A3 and least contribution by UGT1A1. CYP isoform selective inhibitors did not significantly influence BUPG formation. Similarly, individual treatment with ketoconazole, quinidine, sulphenazole and montelukast resulted in inhibition of BUPG formation by 85%, 56%, 15% and 1%, respectively (Fig 15). This indicates highest contribution of CYP3A4 towards NBUP formation followed by CYP 2D6, 2C9 and lowest contribution of 2C8. Two UGT isoform selective inhibitors i.e.

lithocholic acid and amitriptyline showed a significant influence on NBUP formation. Lithocholic acid appeared to significantly increase NBUP formation (~143% of control) while amitriptyline produced a significant decrease in NBUP formation (~34% of control).

Figure 14: Effect of inhibitors on BUPG formation in induced LS180 cells

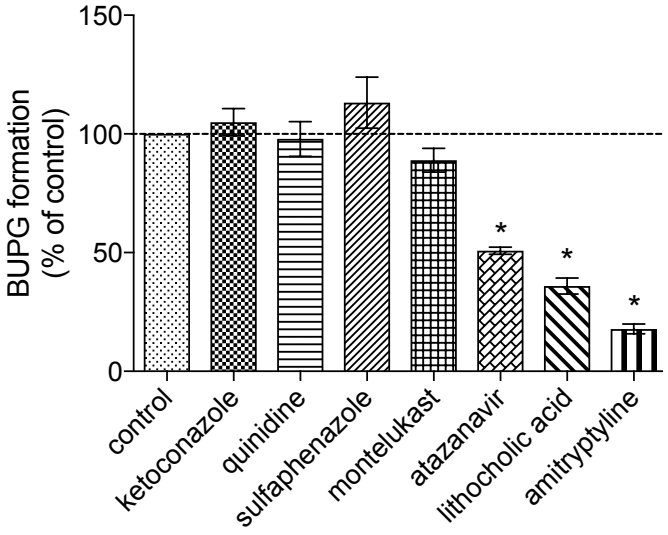

Fig 14: BUPG formation in presence of selective CYP and UGT inhibitors. BUP (10 μM) was incubated for 2 hours in presence and absence of atazanavir (1 μM), lithocholic acid (20 μM) and amitriptyline (1 mM), ketoconazole (1 μM), quinidine (2 μM), sulphenazole (20 μM) and montelukast (0.5 μM). Results are expressed as mean ± SD for quadruplicate measurements. * indicates significant difference ($\alpha = 0.05$) from control. BUPG formation is control was 3.16 ± 0.26 pmol/min. Atazanavir (1 μM), lithocholic acid (20 μM) and amitriptyline (1 mM)

Figure 15: Effect of selective inhibitors on NBUP formation in induced LS180 cells

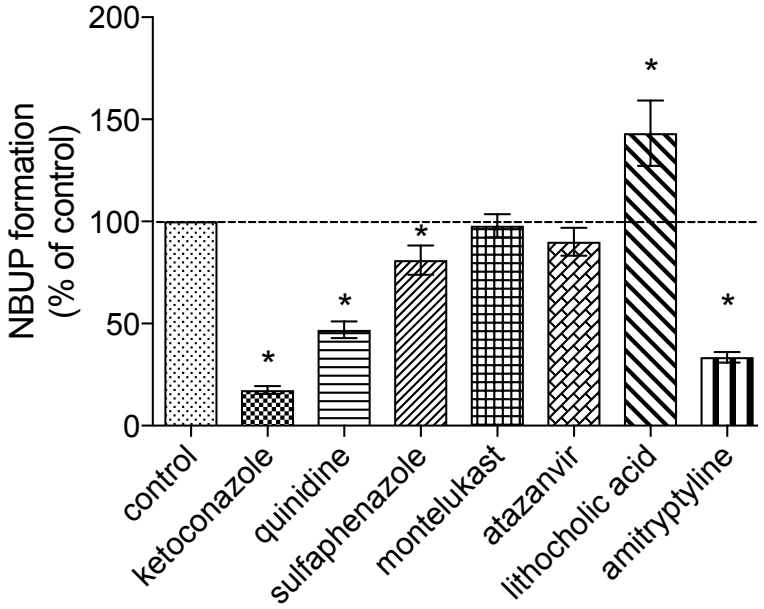

Fig 15: NBUP formation in presence of selective CYP and UGT inhibitors. BUP (10 μM) was incubated for 2 hours in presence and absence of atazanavir (1 μM), lithocholic acid (20 μM) and amitriptyline (1 mM), ketoconazole (1 μM), quinidine (2 μM), sulphenazole (20 μM) and montelukast (0.5 μM). Results are expressed as mean ± SD for quadruplicate measurements. * indicates significant difference ($\alpha = 0.05$) from control. NBUP formation is control was 0.70 ± 0.05 pmol/min.

Limitations:

The selectivity of inhibitors is quite crucial while preforming reaction phenotyping using chemical inhibition. Lithocholic acid and amitriptyline failed to produce selective inhibition of specific UGT isoforms. Also, the results suggest overlap of UGT and CYP isoform inhibition by some of the inhibitors. Hence, these results should be interpreted with caution. It is always recommended to perform reaction phenotyping studies using selective isoform substrates rather than using chemical inhibition method. The relative contribution of CYP isoforms other than CYP3A4 appears to be overestimated and is in disagreement with the published results reporting ~70 to 75% contribution of CYP3A4, ~10-15% contribution of CYP2C8, negligible/no contribution of CYP2C9 and CYP2D6

[11, 12]. Similarly, the relative contribution of UGT isoforms i.e. UGT2B7>UGT1A3 >UGT1A1 towards BUPG formation appears to be erroneous. The expression of UGT1A3 is negligible in the human intestine in comparison to the other two UGT isoforms [15, 148, 149]. Thus, in humans the contribution of UGT1A3 to the intestinal conjugation of BUP is expected to be insignificant.

The induced LS180 cells offer a theoretical advantage of simultaneously monitoring the kinetics of BUP and the effect of inhibitor treatments on both CYP and UGT metabolic pathways. However, the induced LS180 cell model was also associated with several substantial limitations and could not simulate human intestinal metabolic conditions of BUP. Hence, all the future studies were performed using pooled human intestinal and liver microsomes, which appeared to be a more clinically relevant system for BUP than the induced LS180 cells.

Appendix 2 – Combination studies

A2.1 Introduction

The final oral formulation of BUP is envisioned to comprise a combination of inhibitors for achieving maximum possible inhibition of BUP metabolism. When two or more inhibitors are combined, there is a possibility that the inhibitors might increase (additive or synergistic effect) or decrease (antagonistic effect) each other's efficiency of inhibition. Thus, it becomes important to evaluate the effect of a combination of inhibitors on the overall inhibition produced. Effect of the combination of inhibitors on the oxidation and glucuronidation metabolism of BUP was individually tested using the combination index (CI) method developed by Chou and Talalay [184].

Using the traditional Webb's method, synergy between inhibitors A and B; when each inhibits 60% of metabolism, can be calculated as follows [184]:

$$(1-0.6)(1-0.6) = 0.16 \text{ then, } (1-0.16)= 0.84.$$

Thus, the combination is expected to exhibit 84% inhibition. However, the Webb's method suffers from following disadvantages [184]:

a) limited validity because it takes into account only the potency of inhibition and ignores the shape of the "metabolite formation rate" (expressed as fraction of control) versus "inhibitor concentration" curve (e.g., hyperbolic or sigmoidal),

b) valid only when the inhibitors have hyperbolic curves (i.e., in simple Michaelis-Menten kinetics; slope h =1) and is not valid when $h \neq 1$, such as sigmoidal ($h > 1$) or flat sigmoidal ($h < 1$) curves and

c) valid only when the effects of two inhibitors are mutually non-exclusive (e.g., totally independent) and is not valid for mutually exclusive inhibitors (e.g., similar mechanisms or modes of actions, as assumed for the classic isobologram).

The CI method developed by Chou and Talalay lacks all the above limitations and is fairly universal in its application and hence was chosen for studying the combination of pterostilbene and ginger extract. In addition to the CI method, the nature of interaction in a combination was evaluated using the curve shift analysis method [141].

A2.2 Methods

A2.2.1 General description of the CI method

For testing a combination of three inhibitors (say A, B and C), a total of 7 experiments will be performed. In experiments 1 – 3 (Table 1), inhibition of BUPG formation will be monitored at a suitable BUP concentration ($\leq K_m$) and a wide range of concentrations (say 0.001 – 100 μM) of inhibitors A, B and C to get inhibition curves for each individual inhibitor. These three experiments will determine the individual potency (IC_{50}) of each of the three inhibitors. Parameters like f_a (fraction of BUPG formation inhibited), IC_{50} and h (slope) will be estimated using equation 1 (called the median effect equation) [184].

$$D_X = IC_{50} \times [f_a (1-f_a)]^{1/h} \qquad (1)$$

where D_x = inhibitor concentration, f_a = fraction of BUPG formation inhibited, h = slope of the saturation curve and IC_{50} = concentration of inhibitor or combination required to inhibit 50% of BUPG formation

The next four experiments will focus on testing equipotent combinations of A+B, B+C, A+C and A+B+C in the similar manner to get f_a, IC_{50}, and slope (h) values for each combination. Based on these experiments, CI values will then be calculated using equation 2:[184]

$$CI = \frac{D_1}{(D_X)_A} + \frac{D_2}{(D_X)_B} + \frac{D_3}{(D_X)_C} \qquad (2)$$

where D1, D2 and D3 represent different test concentrations of A, B and C and the denominators indicate the dose of each inhibitor alone required to produce same % inhibition as produced by the combination

Interpretation of the CI values: Appropriate determination of the CI value will indicate if the combination of two or more inhibitors shows an additive, synergistic or an antagonistic effect towards BUP glucuronidation. If CI = 1, then the combination will be characterized as being additive [184]. If CI < 1, then combination will be characterized as being synergistic [184]. If CI>1, the combination will be considered as antagonistic [184]. For synergy and antagonism, the extremes of CI values include 0 - 1 and 1 – ∞, respectively.

Table 1: Studying the interaction between three hypothetical inhibitors

Expt. no	Inhibitors			Parameters				
	A	B	C	f_a	h	IC_{50}	r	CI
1	D_1							
2		D_2						
3			D_3					
4	$D_1 + D_2$							
5		$D_2 + D_3$						
6	D_1	+	D_3					
7	$D_1 + D_2 + D_3$							

Table 1: D_1, D_2 and D_3 indicate range of different test concentrations of the individual inhibitors A, B and C. D_1+D_2, D_2+D_3 and D_1+D_3 indicate range of different test concentrations of a combination of two inhibitors (A+B, B+C, A+C, respectively) and D_1+D_2+D_3 represent range of different test concentrations of a combination of the three inhibitors (A+B+C). fa = fraction of BUPG formation inhibited, h = slope of the saturation curve and IC_{50} = concentration of inhibitor or combination required to inhibit 50% of BUPG formation, r = linear correlation co-efficient and CI = combination index

A2.2.2 Evaluating the combination of pterostilbene and ginger extract using CI method

As stated in the earlier section, the first step was to determine the potency of inhibition of each metabolic pathway shown by pterostilbene and ginger extract, individually using pooled human intestinal (HIM). A wide range of concentrations of pterostilbene (0.01 – 50 μM) and ginger extract (0.01 – 75 μM) was tested in pooled HIM (0.4 mg/ml). Pterostilbene and ginger extract were then combined in an equipotent manner i.e. as a ratio of their IC_{50}s and the potency of inhibition of CYP and UGT metabolism of BUP shown by the combination was determined. The two compounds were combined in the ratio of 1:11 and 2:1 (pterostilbene: ginger extract) for the CYP and UGT studies, respectively. The ratio of IC_{50}s of pterostilbene and ginger extract for inhibition of NBUP formation appeared to be between 1:15 and 1:25. However, practically these ratios could not be achieved due to solubility issues. Hence, the highest achievable ratio of pterostilbene: ginger extract of 1:11 was chosen, which is biased towards pterostilbene in its composition. The experimental procedure for determination of inhibitory potency of the individual inhibitors and the equipotent combination and subsequent data analysis has already been explained in detail in Chapter 4. The results of the IC_{50} studies are summarized in Table 2.

A2.2.3 Evaluating the combination of pterostilbene and ginger extract using curve shift analysis method (Description taken from Chapter 4)

The effect of equipotent combination of pterostilbene and ginger extract on CYP and UGT pathways was studied individually in HIM. These inhibitors were combined in an equipotent manner (as a ratio of their IC_{50} values) and a wide range of concentrations

was studied to determine the inhibitor ratio i.e. IR_{50}. IR_{50} represents the concentration of the combination that produces 50% inhibition of metabolite formation. As with earlier inhibition studies, these combination treatments were evaluated three times for their potential to inhibit oxidative metabolism and twice for inhibition of glucuronidation of BUP in pooled HIM. The nature of interaction in the combination was determined using the curve shift analysis method as previously described [141]. Briefly, the average inhibition curves of pterostilbene, ginger extract and their equipotent combination were plotted on the same graph; where X axis (I/IC_{50}) represents the IC_{50} normalized concentrations of the inhibitors and Y axis indicates the metabolite formation (NBUP or BUPG) expressed as % of control. A leftward shift in the curve of the combination with respect to the individual inhibitors would indicate a synergistic interaction whereas a rightward shift would indicate an antagonistic interaction. No significant shift in the combination curve with respect to the curves of the individual inhibitors would indicate additive interactions in the combination.

A2.3 Results:

A2.3.1 Determination of nature of interaction using CI method

The results of the IC_{50} studies for the individual inhibitor treatments are summarized in Table 2. As mentioned earlier the CI method accounts for both the potency of inhibition as well as the slope of the inhibition curve. Thus, both IC_{50} and Hill slope values were used and the CI at each concentration level of the combination was calculated using equation 1 and 2 (Table 3 and 4) individually for each metabolic pathway. For inhibition of NBUP formation, no specific pattern of interaction was observed. There appeared to be a strong apparent synergy at extremely low

concentrations of the combination and then some mild synergy at concentration 0.1 μM:1.1 μM of pterostilbene:ginger extract, respectively. CI values close to 1 were observed at three intermediate concentration levels indicating additive interactions, while an apparent antagonism was observed at the three highest concentrations (from 1.5:16.5 μM to 9:99 μM of pterostilbene:ginger extract) of the combination. For inhibition of BUPG formation a trend of decreasing CI values with increasing concentration of the combination was observed. However, at all the concentration levels except the two highest concentration (75:35 μM and 100:50 μM of pterostilbene:ginger extract), strong antagonistic interactions were observed. At the aforementioned concentrations of the combination, additive interactions were observed since CI values were close to 1.

Table 2: Summary of results of the IC_{50} studies in pooled HIM

Inhibitor	**Inhibition of NBUP formation**		**Inhibition of BUPG formation**	
	IC_{50} (μM)	Hill slope	IC_{50} (μM)	Hill slope
Ginger extract	26.9 ± 6.0	0.91 ± 0.1	47.5 ± 3.6	1.91 ± 0.3
Pterostilbene	1.30 ± 0.9	1.71 ± 0.5	24.9 ± 5.1	0.45 ± 0.03

Table 3: Effect of the combination on NBUP formation

*PT conc. (μM)	*GEX conc. (μM)	f_a	h	IC_{50}	CI
0.001	0.011	0.03 ± 0.02	0.91 (PT) + 1.71 (GEX)	26.9 (PT) + 1.30 (GEX)	0.06 ± 0.05
0.01	0.11	0.08 ± 0.00			0.13 ± 0.002
0.05	0.55	0.07 ± 0.03			1.02 ± 0.7
0.1	1.1	0.16 ± 0.03			0.61 ± 0.14
0.5	5.5	0.34 ± 0.05			1.13 ± 0.3
1.5	16.5	0.56 ± 0.04			1.46 ± 0.3
5	55	0.69 ± 0.04			2.91 ± 0.5
9	99	0.77 ± 0.06			3.69 ± 1.3

*PT and GEX refer to pterostilbene and ginger extract, respectively.

Table 4: Effect of the combination on BUPG formation

PT conc. (μM)	GEX conc. (μM)	f_a	h	IC_{50}	CI
0.01	0.005	-0.01	1.91 (PT) + 0.45 (GEX)	47.5 (PT) + 24.9 (GEX)	-
0.1	0.05	-0.03			-
1	0.5	0.05 ± 0.00			14.2 ± 1.27
10	5	0.15 ± 0.01			8.6 ± 1.54
25	12.5	0.42 ± 0.02			1.8 ± 0.31
50	25	0.64 ± 0.03			1.2 ± 0.19
70	35	0.75 ± 0.02			1.0 ± 0.11
100	50	0.87 ± 0.02			0.7 ± 0.10

A2.3.2 Determination of nature of interaction using the curve shift analysis method (taken from Chapter 4)

Reproducible IC_{50} and Hill slope values were achieved for the combination treatment for inhibition of CYP and UGT metabolism of BUP in pooled HIM with R^2 values ≥ 0.98 (Table 5 and Fig.1 (a) and (b)). The curve shift analysis method evaluates the nature of interaction based on the shift in the inhibition curve of the combination in comparison to the individual treatments. For both the pathways, the combination curve appeared to be similar to the curve of the individual inhibitor treatments, indicating additive interactions in the combination (Fig.2 (a) and (b)).

Table 5: Inhibition by combination of pterostilbene and ginger extract

Pathway	**Effect of pterostilbene and ginger extract combination**		
	IR_{50} (μM)	Hill slope	Bottom (% of control)
Oxidation	1.72 ± 0.3	0.65 ± 0.1	0
Glucuronidation	1.46 ± 0.1	1.05 ± 0.01	0

Data represents mean ± SD of IR_{50}, Hill slope and bottom values observed from separate inhibition experiments. All the determinations were performed in duplicate.

Figure 1: Inhibition of NBUP formation by pterostilbene and ginger extract combination

(a)

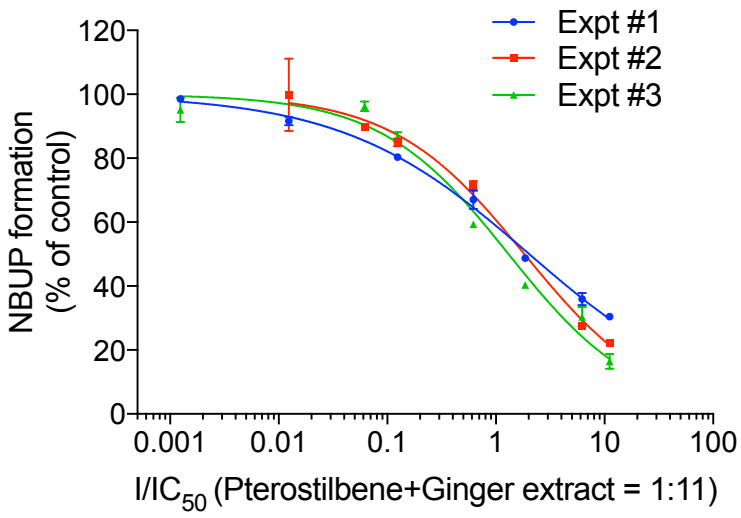

Fig 1 (a): Inhibition of NBUP formation by pterostilbene and ginger extract (1:11) combination in pooled HIM. Data represent mean ± SD of NBUP formation rate expressed as % of control. All the determinations were performed in duplicate. Each curve represents a separate experiment. In experiments 1, 2 and 3, the NBUP formation in control was 136 ± 2.17, 129 ± 5.00 and 126 ± 4.27 pmol/min/mg protein and R^2 value was 0.99, 0.98 and 0.98, respectively.

(b)

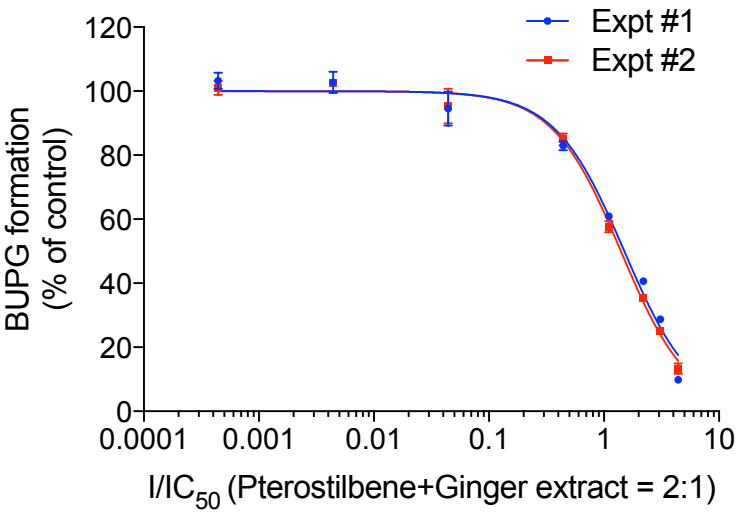

Fig 1 (b): Inhibition of BUPG formation by pterostilbene and ginger extract combination (2:1) in pooled HIM. Data represent mean ± SD of BUPG formation rate expressed as % of control. All the determinations were performed in duplicate. Each curve represents a separate experiment. In experiments 1 and 2, the NBUP formation in control was 9.33 ± 0.19 and 8.89 ± 0.11 pmol/min/mg protein and R^2 value was 0.98 and 0.99, respectively.

Figure 2: Curve shift analysis for effect on NBUP and BUPG formation in HIM

(a)

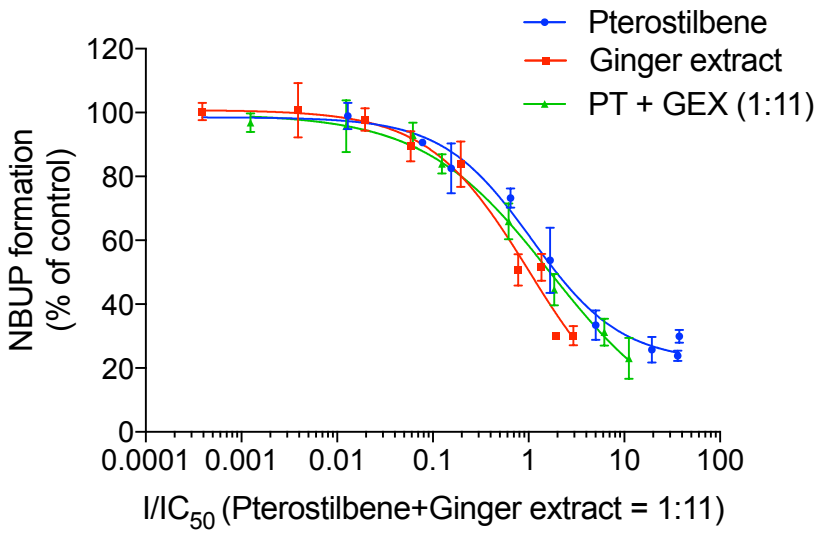

Fig 2 (a): Curve shift analysis for effect on NBUP formation in HIM. The curves represent average of three different curves for each inhibitor treatment. Data represent mean ± SD of NBUP formation rate expressed as % of control. Pterostilbene and ginger extract are combined in 1:11 ratio. No significant shift in the combination curve indicates additive interaction.

(b)

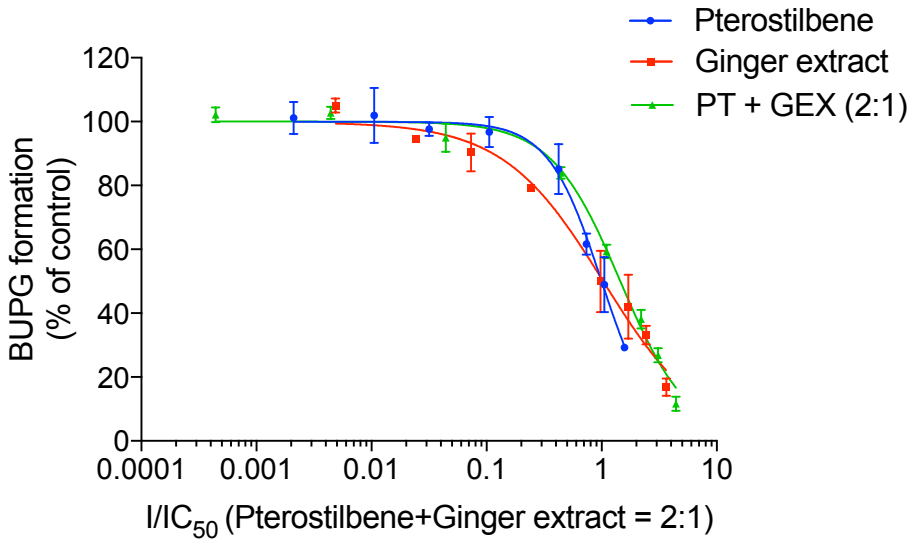

Fig 2 (b): Curve shift analysis for effect on BUPG formation in HIM. The curves represent average of two different curves for each inhibitor treatment. Data represent mean ± SD of NBUP formation rate expressed as % of control. Pterostilbene and ginger extract are combined in 2:1 ratio. No significant shift in the combination curve indicates additive interaction.

A2.4 Conclusion:

There appears to be a discrepancy in the results of the two methods, especially for the inhibition of BUPG formation. The CI method suggests strong antagonistic interactions at most of the concentrations of the combination while the curve shift analysis reveals additive interactions towards inhibition of conjugation of BUP. For inhibition of NBUP formation, the CI method reveals synergistic interactions at extremely low concentrations of the combination that are significantly lower than the IC_{50} values of individual the inhibitors. At the intermediate concentrations and high concentrations of the combination, the CI method suggests additive and antagonistic interactions, respectively. On the contrary, the curve shift analysis method indicates additive interactions throughout the concentration range of the combination. The results of the curve shift analysis method appear more logical because the graphs provide visual evidence supporting the resultant conclusions. The extreme CI values at lowest concentrations of the inhibition curve seem erroneous. At these low concentrations ($<IC_{50}$), the extent of inhibition of BUPG formation would be negligible and the predicted antagonistic or synergistic effect would lack clinical significance. Hence, the curve shift analysis method was used for evaluating the interactions in the pterostilbene-ginger extract combination.

Biography

Neha Maharao was born in Sangli, India on July 10, 1991. She received her bachelor's degree in Pharmacy from University of Mumbai in 2013. She joined the Department of Pharmaceutics at Virginia Commonwealth University (VCU, Richmond, VA) in Fall 2013, under the mentorship of Phillip M. Gerk (Pharm.D, PhD).

During her tenure as a PhD student at VCU, Neha published two manuscripts in peer-reviewed journals and has 1 additional manuscript in preparation. She has given several intramural research presentations within the department and School of Pharmacy. In addition, she has presented her research extramurally at American Association of Pharmaceutical Scientists (AAPS 2016) and at Pfizer Consumer Health (Richmond, VA).

Neha has won numerous graduate student scholarship and travel awards such as Phi Kappa Phi scholarship (2017), Dissertation assistantship ((2016-2017), Peter and Sian Byron award (2016) and VCU Graduate school award (2016). She was also nominated by two honor societies at VCU - Phi Kappa Phi (2015) and Alpha Epsilon Lambda (2014).

Neha served as the historian for the Pharmaceutics Graduate Student Association (PGSA) at VCU (2014-2015). She was the treasurer of Sigma Delta Epsilon – Graduate Women in Science, Zeta Chapter in Richmond during 2015-2016. She has been member of AAPS since 2013.